

TECHNICAL UNIVERSITY OF CRETE



DOCTORAL THESIS

Advanced Nonlinear Control Concepts for Freeway Traffic Networks

Author:
Maria KONTORINAKI

Supervisor:
Prof. Markos PAPAGEORGIU

*A thesis submitted in fulfillment of the requirements
for the degree of Doctor of Philosophy
in the*

Dynamic Systems & Simulation Laboratory
School of Production Engineering & Management

September 7, 2017

The present thesis is approved by the following jury:

Advisory Committee:

Markos Papageorgiou (Supervisor)

Professor, School of Production Engineering and Management
Technical University of Crete, Chania, Greece

Iasson Karafyllis (Member of committee in charge)

Assistant Professor, Department of Mathematics
National Technical University of Athens, Athens, Greece

Ioannis Papamichail (Member of committee in charge)

Associate Professor, School of Production Engineering and Management
Technical University of Crete, Chania, Greece

Thesis Committee:

Anargiros Delis

Associate Professor, School of Production Engineering and Management
Technical University of Crete, Chania, Greece

Elias Kosmatopoulos

Professor, Department of Electrical and Computer Engineering
Democritus University of Thrace, Xanthi, Greece

Ioannis Nikolos

Associate Professor, School of Production Engineering and Management
Technical University of Crete, Chania, Greece

Claudio Roncoli

Assistant Professor, Department of Built Environment
Aalto University, Espoo, Finland

“True stability results when presumed order and presumed disorder are balanced. A truly stable system expects the unexpected, is prepared to be disrupted, waits to be transformed.”

Tom Robbins

Technical University of Crete

Abstract

School of Production Engineering & Management

Doctor of Philosophy

Advanced Nonlinear Control Concepts for Freeway Traffic Networks

by Maria KONTORINAKI

The continuously increasing number of vehicles in industrial countries is a major problem, which triggers congestion phenomena having negative impacts such as increased travel times and fuel consumption as well as reduced safety. Useful tools for the investigation of the congestion problem are *Traffic Flow Modeling* and *Traffic Control*. Traffic Flow Modeling targets the accurate representation of the network and traffic flow characteristics, while Traffic Control aims at improving the traffic conditions of the network and mitigating the problem of traffic congestion.

Despite the continuous advances in the field of *Nonlinear Systems and Control*, the design and deployment of efficient control algorithms, originated from this field, that can be applied for Traffic Control, remains a significant objective. Literature, so far, generally lacks methods for traffic control emanated from systematic and rigorous mathematical derivations. This is mainly due to the complexity and the strong nonlinearities of traffic flow dynamics. Practical control design approaches are often based on simplified models of the system dynamics, leading to traffic systems with suboptimal performance; nevertheless, for complex control system applications, the use of more complex models is virtually unavoidable.

This thesis is one of the first attempts towards this direction. More specifically, it introduces a general class of acyclic first-order models that can be used to represent a wide variety of traffic networks, such as freeways, interconnection of freeways, urban networks and corridors; appropriate specifications on the parameter selection of these models are proposed in order to end up with models representing specific traffic networks. More specifically, the developed models correspond to large-scale discrete space-time dynamical systems that are highly nonlinear and uncertain. The assumptions surrounding the proposed modeling framework are mild enough to render the models capable of reproducing traffic flow phenomena of high interest, such as the capacity drop phenomenon and more; phenomena which cannot be represented by the classical formulation of first-order models.

As a next step, this thesis investigates potential specifications that can be accommodated within the developed models so as to be able to reproduce correctly the desired traffic pattern at an active bottleneck due to on-ramp merging and the related capacity drop phenomenon. Despite the increasing interest from the research community in integrating capacity drop in first-order models, a limited number of effective approaches have been proposed, and only a few are actually tested using real traffic data to evaluate their behavior in case a bottleneck is activated. To this end, this thesis aims to fill this gap, gathering the state-of-the-art related to capacity drop modeling within first-order models, contributing also with further insights

about their implications. The collected models are tested in calibration and validation using real traffic data from a freeway site in U.K.

Having tested the accuracy of a part of the developed model, the overall modeling framework is utilized in order to develop a general robust model-based methodology for Traffic Control. In particular, this thesis proposes a rigorous methodology that provides explicit feedback control laws for the robust global exponential stability of any selected uncongested equilibrium point of the above networks. The stabilization is achieved by means of either vector or single *Lyapunov Function* criteria and *Graph Theory* tools and exploits several important properties of the network models. The achieved stabilization is robust with respect to the overall uncertain nature of network models when congestion phenomena are present and the uncertainty stemming from the fundamental diagram selection. Potential applications of the developed control methodology include urban and peri-urban signal control, perimeter control, ramp metering and mainline metering.

Finally, by exploiting tools from the *Adaptive Control* field, this thesis proposes a general methodology for the development of generic adaptive control schemes, which have limited requirements with respect to the knowledge of system parameters. The application of the proposed control schemes guarantee the robust global exponential attractivity of the desired and unknown UEP for the closed-loop freeway systems. The proposed adaptive control schemes are then tested with respect to their ability to be used as a real-time ramp-metering control strategy. Testing this strategy with sufficiently accurate traffic flow models, different than the ones used for its design, is deemed as an indispensable step towards potential application of the proposed methodology in the field. Appropriate realistic traffic control scenarios are constructed involving local and coordination control actions.

Acknowledgements

Upon the completion of my PhD studies, I feel really thankful, and lucky as well, for being surrounded of so many important people during all this period. I want here to express my in depth gratitude to these people, in the hope that they will continue being part of my academic or personal life.

It was an honor being supervised by two excellent advisors, Prof. Markos Pappageorgiou and Prof. Iasson Karafyllis. Their academic excellence, accompanying with their constructive guidance, assisted in order to make this thesis an excellent and interesting blend of Mathematics and Engineering. I want to thank them, both separately and together, for imparting their knowledge and experience to me and for allowing me being member of the wide research community of Traffic Modeling and Control.

Besides my advisors, I am also grateful to Prof. Ioannis Papamichail. During the last five years, he assisted me in many different ways, towards and beyond academic issues. I very much appreciate the contribution and help of Prof. Ioannis Nikolos, Prof. Argiris Delis and Prof. Claudio Roncoli for their valuable feedback and stimulating discussions concerning an important part of this thesis. I thank also Prof. Elias Kosmatopoulos for accepting to be a member of my thesis committee and for his insightful comments concerning several parts of my dissertation. Of course, I want to thank all my colleagues in the Dynamic Systems and Simulation Laboratory (DSSL) for sharing thoughts and support at several issues all this period.

The completion of this thesis is also owed to my best half, Kostas Makantasis. However, his scientific and psychological contribution, during my PhD, is only a bullet in the quite large list of things for which I should thank him. A special thank goes to three very special women, Katerina, Tonia and Katerina Jr. The first for her infinite love and support; only a mother is capable to have such huge deposits. The second for being more than a sister, my best friend. And the third for being the embodiment of happiness and hope in my life.

Finally, I would like to thank the members of TRAMAN21, a European Research Council project under the European Union's Seventh Framework Programme (FP / 20072013) / ERC Grant Agreement n. 321132. Funding from TRAMAN21 is also gratefully acknowledged.



TRAMAN21
TRAffic MANagement for the 21st Century



Contents

	iii
Abstract	vii
Acknowledgements	ix
1 Introduction	1
1.1 Traffic Flow Modeling	1
1.2 Mathematical Control Theory	3
1.3 Traffic Control	6
1.4 Motivation and Objectives of this Thesis	7
1.5 Thesis Outline	8
1.6 Publications Related to this Thesis	10
2 First-Order Models: Derivation and Validation Study	11
2.1 Introduction	11
2.2 Model Derivation	15
2.2.1 Acyclic Traffic Networks with Constant Turning and Exit Rates	15
2.2.2 Some Important Consequences	19
2.2.3 Special Case: The Freeway Model	21
2.3 Capacity drop in LWR-type models	24
2.3.1 A Different Discretized LWR Formulation	24
Different shapes for the FD	25
Illustrative example	25
2.3.2 Approach 1: Switching logic for maximum flow	26
2.3.3 Approach 2: Introduction of a weaving parameter	27
2.3.4 Approach 3: Reduction of the demand function	28
2.3.5 Approach 4: Linear reduction of maximum flow	28
2.3.6 Approach 5: Increased space for vehicles entering a bottleneck	29
2.3.7 First-order model with drivers' anticipation	32
2.3.8 Second -order model METANET	32
2.4 Calibration Results	33
2.4.1 Freeway Network and Calibration Set-Up	33
2.4.2 Basic discretized-LWR formulation	35
2.4.3 Capacity drop approaches	36
3 Global Exponential Stabilization of Acyclic Traffic Networks	41
3.1 Introduction	41
3.2 Main Results	42
3.3 Proofs of Main Results	46
3.4 Illustrative Example	49

4	Global Exponential Stabilization of Freeway Models	55
4.1	Introduction	55
4.2	Main Result	56
4.3	Proofs of Main Results	58
4.4	Illustrative Example	61
5	Adaptive Stabilization of Discrete- Time Systems	69
5.1	Introduction	69
5.2	General Result	70
5.3	Main Result: Application to Freeway Traffic Control	72
5.3.1	Global Exponential Stabilization of Freeway Models	72
5.3.2	Measurements and Unknown Parameters	73
5.4	Proofs of Main Results	77
5.5	Illustrative Example	79
6	Local and Coordinated Ramp Metering using ACS	85
6.1	Introduction	85
6.2	The Adaptive Control Scheme	86
6.2.1	Nominal Feedback Law	86
	Main features of the nominal feedback law	87
	Maximization of throughput at the bottleneck	88
	Equilibrium flow	89
	Final determination of the (optimal) desired operating point	90
6.2.2	The Observer of the ACS	91
	Estimations of the uncontrollable on-ramp inflows	91
	Estimations of the mean speed	91
	Estimations of the exit rates	92
6.2.3	The Random-Location Bottleneck Case	92
6.3	Simulation Model and Set-Up	93
6.3.1	Simulation Model	93
	Simulation Set-Up	94
6.4	Local Ramp Metering	95
6.4.1	Network Description	95
6.4.2	Simulation Investigations - Non bottleneck case	96
6.4.3	Simulation Investigations - Bottleneck Cases 1 and 2	100
6.4.4	Simulation Investigations - Random-Location Bottleneck Case	103
6.5	Coordinated Ramp Metering	105
6.5.1	Network Description	105
7	Conclusions and Future Work	111
7.1	Concluding Remarks	111
7.2	Further Research	113
A	Mathematical Background	115
A.1	Nonlinear Systems and Control	115
A.2	Graph Theory	118
B	Proofs of Auxiliary Results	119
B.1	Proofs of Results of Appendix A	119
B.2	Proofs of Results of Chapter 2	120
B.3	Proofs of Results of Chapter 3	122
B.4	Proofs of Results of Chapter 4	124

B.5 Proofs of Results of Chapter 5	128
C Consistency Analysis	133
C.1 Distributed on-ramp flow	134
C.2 Concentrated on-ramp flow as a singular source	136
Bibliography	141

List of Figures

2.1	Implications of Assumption	17
2.2	Scheme of the network model	18
2.3	Scheme of the freeway model	23
2.4	The space-discretization of a freeway stretch	24
2.5	Different shapes for the FD	25
2.6	Traffic demand scenario	26
2.7	Time series of the density, speed and outflow	31
2.8	Representation of the considered freeway stretch	34
2.9	Space-time diagrams of speed	37
2.10	Time-series of the flow measurements	38
2.11	Flow-density diagram at the merge cell	39
2.12	Sensitivity investigations	40
3.1	Idea behind Theorem	44
3.2	Freeway-to-freeway network	50
3.3	Parameters of the demand and supply functions	52
3.4	Open-loop system response	52
3.5	Closed-loop system response 1	53
3.6	Closed-loop system response 2	54
4.1	Freeway stretch	62
4.2	FD of every cell	62
4.3	Open-loop system response	63
4.4	Response of the densities for the closed-loop system	64
4.5	Evolution of the Euclidean norm of the closed-loop system	65
4.6	Response of the closed-loop system under modeling errors 1	66
4.7	Response of the closed-loop system under modeling errors 2	67
5.1	Implications of Assumption (H 5.1)	72
5.2	Response of the open-loop system	80
5.3	Response of the closed-loop system	82
5.4	Response of the closed-loop system 2	82
5.5	Response of the closed-loop system 3	83
5.6	Response of the closed-loop system 4	84
5.7	Response of the closed-loop system 5	84
6.1	Space discretization of a freeway stretch	88
6.2	On-ramp cell: queue model	93
6.3	Control algorithm scheme	95
6.4	Hypothetical stretches	96
6.5	Considered FDs	96
6.6	Mainstream and on-ramp traffic demand scenarios	97
6.7	Non-bottleneck case	98

6.8	Non-bottleneck case under a stochastic demand and process noise . . .	99
6.9	Bottleneck case 1	101
6.10	Bottleneck case 1 under a stochastic demand scenario and process noise	102
6.11	Bottleneck case 2	103
6.12	Bottleneck case 2 under a stochastic demand scenario and process noise	104
6.13	Application of the ACS for the RLB case	105
6.14	Freeway for coordinated ramp metering	106
6.15	Traffic demand profiles	106
6.16	Density and flow trajectories	107
6.17	Queue lengths	107
6.18	Density and flow trajectories	109
6.19	Queue lengths for the stochastic scenario	110
C.1	Distributed on-ramp flow	136
C.2	The Rankine-Hugoniot jump conditions	137
C.3	Characteristic Riemann problems.	137
C.4	(Concentrated on-ramp flow)	139

List of Tables

2.1	Parameters of the hypothetical network.	26
2.2	Calibrated parameter values for all examined models	34
2.3	Performance indices for the calibration and validation days for all examined models	35
6.1	Parameters with common values for both scenarios of Sections 6.4 and 6.5.	94
6.2	METANET Parameters.	97
6.3	Resulting stationary flow for all bottleneck cases and for different set values of the critical density.	100
6.4	Simulation model and FD parameters (2 nd scenario).	108
6.5	Resulting stationary density and flow for the coordinated ramp metering scenario and for different set-points.	110
C.1	Speed and sign of the shock for CTM for case (A).	138
C.2	Speed and sign of the shock for Approach 5 for case (A).	138
C.3	Sign and intensity of the shock for CTM and Approach 5 for case (B).	138

List of Abbreviations

ACS	Adaptive Control Scheme
CLF	Control Lyapunov Function
CTM	Cell Transmission Model
DOP	Desired Operating Point
FD	Fundamental Diagram
FOM	First-Order Model
LWR	Lighthill Whitham Richards
NFL	Nonlinear Feedback Law
NL	Non Linear
PI	Proportional Integral
PDE	Partial Differential Equation
PWL	PieceWise Linear
RM	Ramp Metering
RGAS	Robustly Globally Asymptotically Stable
RGES	Robustly Globally Exponentially Stable
RLB	Random Located Bottleneck
RMSE	Root Mean Square Error
SLF	Single Lyapunov Function
SOM	Second-Order Model
TR	Trapping Region
UEP	Uncongested Equilibrium Point
VLF	Vector Lyapunov Function
VMS	Variable Message Signs
VSL	Variable Speed Limits

Notation & Conventions

- $S^n := \overbrace{S \times \dots \times S}^{n \text{ times}}$ for every set S and positive integer n .
- $\prod_{i=1}^n S_i := S_1 \times S_2 \times \dots \times S_n$ for certain sets S_1, S_2, \dots, S_n .
- $\mathfrak{R}_+ := [0, +\infty)$ and $\mathfrak{R}_+^n := (\mathfrak{R}_+)^n$.
- $\text{int}(S)$ denotes the interior of $S \subseteq \mathfrak{R}^n$.
- $C^0(A; \Omega)$ denotes the class of continuous functions on $A \subseteq \mathfrak{R}^n$, which take values in $\Omega \subseteq \mathfrak{R}^m$.
- $C^k(A; \Omega)$, with $k \geq 1$ integer, denotes the class of functions on $A \subseteq \mathfrak{R}^n$ with continuous derivatives of order k , which take values in $\Omega \subseteq \mathfrak{R}^m$.
- x' denotes the transpose of $x \in \mathfrak{R}^n$.
- $|x|$ denotes the Euclidean norm of $x \in \mathfrak{R}^n$.
- For $x, y \in \mathfrak{R}^n$, $x \leq y$ if $(y - x) \in \mathfrak{R}_+^n$ and $x < y$ if $(y - x) \in \text{int}(\mathfrak{R}_+^n)$.
- $[a]$ denotes the integer part of $a \in \mathfrak{R}$.
- $\Gamma \in \mathfrak{R}^{n \times n}$ denotes an $n \times n$ matrix with real entries.
- $\Gamma \in \mathfrak{R}_+^{n \times n}$ denotes an $n \times n$ matrix with nonnegative entries.
- I denotes the identity matrix.
- $1_{n \times n}$ denotes the matrix for which every entry is equal to one.
- $1_n = (1, 1, \dots, 1)' \in \mathfrak{R}^n$.
- $\rho(\Gamma)$ denotes the spectral radius of $\Gamma \in \mathfrak{R}^{n \times n}$.
- We say that $\Gamma \in \mathfrak{R}^{n \times n}$ is an upper (lower) triangular matrix if all the entries below (above) the main diagonal are zero.
- We say that the upper (lower) triangular matrix $\Gamma \in \mathfrak{R}^{n \times n}$ is strictly upper (lower) triangular if all the entries of the main diagonal are zero.
- The diagonal entries of an upper (lower) triangular matrix $\Gamma \in \mathfrak{R}^{n \times n}$ are the eigenvalues of $\Gamma \in \mathfrak{R}^{n \times n}$.
- $\text{diag}(x) \in \mathfrak{R}^{n \times n}$, denotes a diagonal matrix, for which the entries of the main diagonal are the coordinates of $x \in \mathfrak{R}^n$.
- When R is an index set, then by $(x_i; i \in R)$ we denote a vector with components all $x_i \in \mathfrak{R}$ with $i \in R$, in increasing order. For example, if $R = \{2, 5, 10\}$, then $(x_i; i \in R) = (x_2, x_5, x_{10})$.
- $\inf(S)$ ($\sup(S)$) denotes the greatest lower (least upper) bound of $S \subseteq T$, where T is a partially ordered set.
- A set $S \subset \mathfrak{R}$ is bounded from above (below) if there exists $m \in \mathfrak{R}$, called the upper (lower) bound of S , such that $x \leq m$ ($x \geq m$) for every $x \in S$.
- A set is bounded if it is bounded both from above and below.
- K_∞ denotes the class of increasing functions $\alpha \in C^0(\mathfrak{R}_+; \mathfrak{R}_+)$ with $\alpha(0) = 0$ and $\lim_{s \rightarrow +\infty} \alpha(s) = +\infty$.
- KL denotes the class of functions $a \in C^0(\mathfrak{R}_+ \times \mathfrak{R}_+; \mathfrak{R}_+)$ with the properties:
 - (i) for each $t \geq 0$ the mapping $a(\cdot, t)$ is increasing with $a(0, t) = 0$,
 - (ii) for each $s \geq 0$ the mapping $a(s, \cdot)$ is non-increasing with $\lim_{t \rightarrow +\infty} a(s, t) = 0$.

To my father...

Chapter 1

Introduction

This first chapter introduces the reader to the topic of this thesis. Sections 1.1, 1.2 and 1.3 give the background of the current thesis related with Traffic Flow Modeling, Mathematical Control Theory and Traffic Control, respectively. Sections 1.4 and 1.5 present the motivation and the objectives as well as the outline of this thesis. Finally, Section 1.6 lists the related publications.

1.1 Traffic Flow Modeling

Any scientific interest in model-based process control begins with modeling, i.e., comprehension and recording of the behavior of the process using mathematical equations. *Traffic Flow Modeling* is an independent branch of mathematics and civil engineering, which studies the interactions between drivers and their environment. Traffic flow - despite the involvement of drivers with different individual behavior - can be viewed from a macroscopic perspective as a fluid with well-defined characteristics. However, its mathematical description appears to be a more complex task than the modeling of fluids due to: i) several observed phenomena, such as traffic instability, stop-and-go traffic, but also ii) the facts that traffic flow consists of several substreams with prespecified origin-destinations and individual optimization strategies for route selection.

Traffic flow analysts approach the problem of modeling in many different ways. In terms of the considered level of detail, traffic flow models can be classified as microscopic, macroscopic or mesoscopic. Microscopic models are used to describe every vehicle as an individual and they were first proposed by Reuschel, 1950 and Pipes, 1953. Here, the models that govern the vehicle's behaviour can further be divided into car-following models, lane-change models, and route-choice models (see for example Treiber, Hennecke, and Helbing, 2000, Kesting, Treiber, and Helbing, 2007). Cellular automation models have also been used for microscopic modeling. The Nagel – Schreckenberg model (Nagel and Schreckenberg, 1992) is a simple example of such a model, which, through the vehicles' interaction, can model collective phenomena such as traffic jams. Macroscopic models, describe traffic behavior - analogous to the modeling of fluids - in terms of aggregated traffic flow variables, such as traffic density (vehicles per kilometer) and traffic volume (vehicles per hour), and make use of a conservation equation and a momentum equation. A fundamental admission related with macroscopic modeling is that under homogeneous traffic conditions in space and time, traffic density is related to traffic volume by a relationship known as the Fundamental Diagram (FD). This relationship provides maximum flow at a critical density value, while if density is further increased (e.g., due to entering traffic), traffic volume decreases and a more or less severe traffic congestion results. Finally, mesoscopic models (or hybrid models) are models of intermediate level of detail; higher than macroscopic models and less than microscopic

(see, for instance, Burghout, Koutsopoulos, and Ingmar, 2005). They often analyze transportation elements in small groups, within which, elements are considered homogeneous, e.g., vehicle platoons.

Another classification of traffic flow models is imposed by the type of the mathematical equations used, that is, whether the models are described by Partial Differential Equations (PDEs), Ordinary Differential Equations (ODEs) (see, e.g., microscopic models and Coogan and Arcaç, 2014) or Difference Equations (Discrete space-time models). Moreover, traffic flow models can also be distinguished into First-Order Models (FOMs) and Second-Order Models (SOMs) (Payne, 1971, Messmer and Papageorgiou, 1990, Aw and Rascle, 2000, Whitham, 2011, Delis, Nikolas, and Papageorgiou, 2014, Zhang and Prieur, 2017), depending on the number of dynamic variables that describe. The study of vehicular traffic flow by means of hyperbolic PDEs started in the 1950s with the well-known first-order LWR model (Lighthill and Whitham, 1955b; Richards, 1956), where the flow dynamics are described by a single PDE and the corresponding steady-state, smooth and concave FD. More details on the properties and the characteristics of this model are given below.

The kinematic wave LWR model is a scalar nonlinear conservation law of hyperbolic type and turns out to be one of the simplest nonlinear conservation laws in engineering science. A significant amount of literature proposes and extends discrete approximations of continuous LWR models applying the Godunov discretization scheme (Godunov, 1959), where the FD is transformed into two flux functions known as the demand (flow that can be sent from upstream) and the supply (flow that can be received downstream) functions (Lebacque, 1996). The most cited among these discretized models is the Cell Transmission Model (CTM) (Daganzo, 1994), where the flow is expressed as a function of density via the definition of a triangular FD, and the space and time increments are selected according to the free speed. Other FOMs, which are not of LWR-type and do not utilize the demand-supply method, have been introduced so as to represent the diffusion of kinematic waves. Continuous and discrete-time models of this type have been proposed by Lighthill and Whitham, 1955b and Papageorgiou, Blosseville, and Hadj-Salem, 1989, respectively.

LWR-type models represent a valuable tool for the study of traffic behavior, as they are simple, yet effective in reproducing not only free-flow conditions, but also wave formation and propagation under congested conditions. Remarkably, CTM realistically predicts shockwave propagations, while all the parameters have a physical interpretation, implying that they can be easily calibrated using real traffic data (Muñoz et al., 2004). Furthermore, CTM is characterized by low computational requirements (Gomes and Horowitz, 2006; Lo, 2001) and it can be easily extended for large-scale freeway and urban networks (Lebacque et al., 1996). Finally, it has been employed for the study of different applications, such as dynamic traffic assignment (Lebacque et al., 1996; Ziliaskopoulos, 2000), traffic prediction, signal control and ramp metering (Alecsandru et al., 2011; Gomes and Horowitz, 2006; Zhang, Ritchie, and Recker, 1996). However, neither LWR nor CTM can reproduce more complex traffic phenomena such stop-and-go waves and the capacity drop.

In order to avoid the weaknesses of LWR-type FOMs, various second-order macroscopic traffic flow models have been proposed which contain an additional dynamic equation to describe the speed evolution. Payne, 1971 and later Whitham, 2011 derived a so-called "momentum equation" from a car-following argument, while several modifications of these models (called hereafter PW-like models) were subsequently proposed (Zhang, 1998). PW-like models are also of hyperbolic type.

Although SOMs are capable to reproduce traffic instabilities, such as stop-and-go waves, as well as the capacity drop phenomenon at active bottlenecks, they also present some drawbacks: (i) they may (under rare circumstances, as shown by Helbing and Johansson, 2009) produce negative speeds or flows (also known as *wrong-way travel* phenomenon, see the work by Daganzo, 1995a); (ii) they usually include a high number of parameters (some of which without clear physical significance), that need to be appropriately calibrated; and (iii) any optimization problem built upon SOMs is characterized by a nonlinear formulation, which implies a rather high computation effort and the impossibility to guarantee convergence to a global optimum (Kotsialos and Papageorgiou, 2004). With respect to the last drawback, also FOMs include non-linearities, which however may be more efficiently tackled while defining an optimization problem, by using computationally-efficient mixed-integer linear formulations (Ferrara, Sacone, and Siri, 2015) or, under specific assumptions, by using only linear constraints (Ziliaskopoulos, 2000; Roncoli, Papageorgiou, and Papamichail, 2015c).

Traffic flow models can also be separated into those which preserve the anisotropic property, i.e., what happens behind a vehicle generally does not affect the behavior of that vehicle, and those that do not. In contrast to the LWR model which assumes smooth and concave FDs, other kinematic wave models can be produced with more general FDs, e.g., continuous, piecewise smooth, and not necessarily concave. However, there exist specific choice for the FD where the anisotropic property is not preserved (see e.g. Zhang, 2001), therefore whether a first-order kinematic wave model is anisotropic or not depends on the kind of the FD it adopts. SOMs that do not preserve the anisotropic property have been proposed by Payne, 1971 and later Whitham, 2011, while SOMs that preserve it have been proposed by Zhang, 2002, Aw and Rascle, 2000 and Karafyllis, Bekiari-Liberis, and Papageorgiou, 2017.

Recently, researchers have also developed another class of traffic flow models, the two phase models (see Monamy, Haj-Salem, and Lebacque, 2012, Colombo, 2003), based on the admission of the existence of two distinct behaviors of traffic flow (free or congested). These models are concerned with *phase transitions* in hyperbolic systems of conservation laws, i.e., free boundary separating two different models and whose evolution is determined by the solution on both of its sides.

Important aspects of Traffic flow Modeling are model Calibration and Validation procedures. Specifically, freeway traffic flow models include a set of parameters, whose values may differ for different freeway sites and depend on factors such as network topology, drivers' behavior, percentage of trucks, weather conditions and more. Thus, before employing a traffic flow model in practice, it is important first to calibrate it against real traffic data. The calibration procedure aims to appropriately specify the model parameter values, so that the representation of the network and traffic flow characteristics is as accurate as the model structure allows and this is achieved by using appropriate optimization algorithms.

1.2 Mathematical Control Theory

Mathematical Control Theory is the area of applied mathematics that deals with the basic principles underlying the analysis and design of control systems (Sontag, 1998). One of the main lines of work in Control Theory deals with the uncertainties, which are imposed either by the model describing the system or by the environment in which the object to be controlled operates. In order to handle deviations from a desired system behavior, the main tool is the use of *feedback*. Feedback control theory

involves the analysis and synthesis of feedback controllers that manipulate system inputs to obtain a desired effect on the output of the system in the face of system uncertainty and system disturbances. Feedback control systems are also used in order to compensate for errors from a precomputed and potentially optimal trajectory. Here, Dynamical Systems Theory and Stability Theory have played an important role towards feedback design. *Dynamical Systems Theory* provides a paradigm for modeling and studying phenomena that undergo spatial and temporal evolution. *Stability Theory* concerns the behavior of the system trajectories of a dynamical system when the system initial state is near an equilibrium state; its importance is emphasized since exogenous disturbances and system component uncertainty are always present.

More often than not, physical and engineering systems are inherently nonlinear and therefore the use of linear techniques for controlling such systems is not effective. Although local analysis and control design in general can be carried out satisfactorily using linear or linearized models, global analysis requires more powerful methods. During the last years, the area of *Nonlinear Systems and Control* has made significant progresses with the *Lyapunov Stability Theory* giving rise both to the study of the behavior of nonlinear dynamical systems but also to the design of feedback controllers for their stabilization (Haddad and Chellaboina, 2008). The main idea behind Lyapunov function methods is the existence of some sort of "energy" measure for the states which diminishes along suitably chosen paths. Then, the system can be forced to follow these paths leading to a minimal-energy configuration, without any requirement to explicitly compute the solutions of the system. However, there does not exist a unified procedure for finding such a measure (Lyapunov function) for general nonlinear systems; to do so a certain amount of physical intuition and experience is needed.

The question of existence of a smooth and more generally continuous feedback law in the nonlinear case is the subject of much current research and it is closely related to the existence of Lyapunov functions. Lyapunov-based methods were inspired by Jurdevic and Quinn, 1978, who give sufficient conditions for smooth stabilization based on the ability to construct a Lyapunov function for the closed-loop system. Artstein, 1983 and Coron and Rosier, 1994 introduced and exploited the notion of the *Control Lyapunov Function* (CLF) whose existence guarantees a feedback control law, which globally stabilizes a nonlinear dynamical system. Advances in Lyapunov-based methods have been developed for analysis and control design for numerous classes of nonlinear dynamical systems and Lyapunov's direct method has become one of the cornerstones of systems and control theory. In particular, we can distinguish three different techniques which are helpful to construct Lyapunov-function based feedback and which have found wide applicability, both for local and global stabilization: *backstepping*, *damping control* and *universal formulas* (Sontag, 1998). Backstepping (also called "adding an integrator") (Tsinias, 1989; Coron and Praly, 1991; Krstic, Kanellakopoulos, and Kokotovic, 1995; Tsinias, 2000), which has received a great deal of attention in the literature, allows one to recursively design controllers for certain complex systems by a step-by-step procedure, starting with a simpler system and adding at each stage an integrator "in front" (at the input) of the simpler system (Sepulchre, Jankovic, and Kokotovic, 1997). The popularity of this method lies on the fact that it provides a systematic procedure for finding a Lyapunov function for nonlinear closed-loop cascade systems. Damping control allows the construction of feedback that is smooth at the origin, while universal formulas, typically guarantees smoothness only away from the equilibrium of interest.

Recently, many researchers have addressed the stabilization of equilibrium points

of large-scale discrete-time systems. However, the verification of stability for large-scale systems still remains a challenging problem on its own. To this purpose, many tools have been proposed in the literature such as *Vector Lyapunov Functions* (VLFs) that are very useful for large-scale discrete-time systems. Sufficient stability conditions by means of VLFs have been proposed by Haddad and Chellaboina, 2008, p. 792-798. In addition, small-gain conditions have been proposed by Jiang, Teel, and Praly, 1994 and Liu, Hill, and Jiang, 2012, which can be expressed by means of a VLF formulation (as shown by Karafyllis and Jiang, 2011, Chapter 5). Recently, sufficient conditions have been provided by Karafyllis and Papageorgiou, 2015 for the Robust Global Exponential Stability (RGES) of nonlinear large-scale uncertain networks by means of VLFs.

A significant amount of research is also made in the area of *Adaptive Control*. Adaptive control deals with the control of linear and nonlinear systems with unknown parameters and typically make use of identification techniques to produce estimates of the system parameters for use by controllers (Krstic, Kanellakopoulos, and Kokotovic, 1995; Ioannou and Kosmatopoulos, 2006). Intuitively, an adaptive controller is a controller that can modify its behavior in response to changes in the dynamics of the process and the character of the disturbances. This can be made by a controller with adjustable parameters and a mechanism for adjusting the parameters. An important feature of adaptive control is its reliance on "certainty equivalence" controllers. This means that a controller is first designed as if all the plant parameters were known, and the controller parameters are calculated as functions of the plant parameters, by solving design equations. When the actual plant parameters are not known, the controller parameters are either estimated directly (direct schemes) or computed by solving the same design equations with plant parameter estimates (indirect schemes). The resulting controller is called a certainty equivalence controller (Karafyllis and Krstic, 2016).

Identification techniques include among others the construction of *observers*, which deal with obtaining estimates of the internal unmeasured state variables from the measurable output. Observer-based control is a way to solve the output feedback control problem, that implies a restriction in the possibility to use all the states directly for feedback. Relevant general theorems guarantee the existence of observers, which achieve stabilization of many linear and nonlinear systems using controllers that are itself a linear system (Gauthier and Kupka, 1994; Gauthier and Kupka, 2001; Khalil and Praly, 2014). Such a controller is said to incorporate integral or *dynamic feedback*, and it includes a differential (or difference) equation, driven by the observations, that calculates the necessary estimate. Moreover, observer-based adaptive control schemes, i.e., combination of a time-varying controller, a state observer and a parameter tuning mechanism, have been proposed by Calugi, 2002, which solve the control problem of a plant with uncertain parameters whose state is only partially available by the measurements. Although only for linear systems it is ensured the possibility of decomposing the problem in two or three sub-problems (thanks to the separation principle), there exist adaptive schemes which allow a separation of the controller, the parameter update law and the state observer also for some classes of nonlinear systems (Krstic, Kanellakopoulos, and Kokotovic, 1995; Ahmed-Ali, Giri, and Krstic, 2017).

1.3 Traffic Control

Traffic Control aims to tackle congestion phenomena observed at traffic networks. Of particular interest in this thesis is the problem of traffic congestion observed in freeway networks. Modern freeways, in most urban areas, are seriously congested on a daily basis during rush hours leading the drivers to experience excessive delays and reduced traffic safety, affecting also the environment with increased fuel consumption and consequently air pollution. Congestion on freeways appears a paradox to people who are not familiar with traffic flow characteristics; drivers often spend several hours in long freeway queues although there is no apparent reason for a breakdown (no accident, no traffic lights). The answer to this paradox lies partially in keeping a safe distance between cars and partially in the dynamic driver behavior when acting as distance regulators.

Extensive research has been conducted to investigate and develop traffic control measures, which can tackle this phenomenon. Freeway traffic control measures aimed at increasing the efficiency and safety of the traffic system can be distinguished into the following three classes:

- **Variable Message Signs (VMS)**, such as speed limitation or harmonization via Variable Speed Limits (VSL), no overtaking and congestion warning, which aim at homogenizing traffic flow on a freeway axis. This usually leads to more stable behavior of the traffic flow and may increase traffic throughput as well as the critical density value. Recent studies have demonstrated that VSL may be used as a mainstream metering device as well (Carlson et al., 2010b).
- **Ramp Metering (RM)** which, by the use of traffic lights positioned at on-ramps, aims at regulating the entering traffic flow and operating traffic flow near its maximum value, avoiding overload due to excessive demands (Papageorgiou and Kotsialos, 2000). Although some delay may be caused at waiting ramp queues, the overall time may be decreased due to the optimal operation of the existing infrastructure.
- **Variable Route Recommendation Signs (VRRS)**, which aim at distributing traffic flow in a freeway network so as to minimize delays and to optimally utilize the existing infrastructure.

To achieve their goal, these control measures must be driven by appropriate control strategies (Papageorgiou and Kotsialos, 2000). For instance, ramp metering control strategies have as an ultimate goal to determine, in the most efficient way, the inflows from the on-ramps, when congestion phenomena are present or imminent at the corresponding mainstream region, so as to maximize the freeway throughput.

Control strategies can be classified into *fixed-time* and *traffic-responsive* strategies, with the latter being classified into *local* or *coordinated* strategies (Papageorgiou and Kotsialos, 2000). Fixed-time control strategies use historical data in order to specify optimal, time-of-day-dependent plans, while traffic-responsive (real-time) strategies use current traffic data, provided by sensors installed in the freeway network and the on-ramps, in order to appropriately specify the values of the control variables in order to minimize the extent of congestion. The latter strategies are considered to be the most robust and efficient approach in this context. Moreover, real-time local ramp metering strategies make use of measurements from the vicinity (or further downstream) of a single ramp, while coordinated ramp metering strategies make use of measurements from an entire region of the network to control all metered ramps included therein.

The most important traffic control strategies include *Nonlinear Optimal Control*, *Model Predictive Control* and *Explicit Feedback Control*. The first two control approaches can be used as a network-wide freeway traffic control approach (see, e.g. Burger et al., 2013; Carlson et al., 2010a; Gomes and Horowitz, 2006; Hegyi, De Schutter, and Hellendoorn, 2005) and they are very efficient. However, none of these proposed methods has advanced to a field-operational tool since they are highly demanding from the computational point of view. Other proposed local control strategies include feedforward control approaches, such as the demand-capacity strategy and its variations (Masher et al., 1975), neural network (Zhang and Ritchie, 1997) and fuzzy logic based (Vukanovic and Ernhof, 2006) approaches. On the other hand, optimal control strategies (Bellemans, De Schutter, and De Moor, 2002; Chen, Hotz, and Ben-Akiva, 1997; Gomes and Horowitz, 2006; Hegyi, De Schutter, and Hellendoorn, 2003; Kotsialos, Papageorgiou, and Middelham, 2001; Papageorgiou and Mayr, 1982; Zhang and Recker, 1999; Zhang and Levinson, 2004), linear multivariable control strategies (Diakaki and Papageorgiou, 1994; Papageorgiou, Blosseville, and Hadj-Salem, 1990), and rule-based algorithms (Hourdakis and Michalopoulos, 2002; Jacobson, Henry, and Mehyar, 1989) belong to the coordinated ramp metering strategies.

Explicit feedback control approaches has been shown to enhance the efficiency of traffic operations without undue computational requirements. A pioneering development in this direction was the I-type local feedback ramp metering regulator ALINEA (Papageorgiou, Hadj-Salem, and Blosseville, 1991) and its extensions (Wang and Papageorgiou, 2006; Wang et al., 2010), which has been used in hundreds of successful field implementations around the world (see, e.g. Papageorgiou, Hadj-Salem, and Middelham, 1997; Papamichail et al., 2010). ALINEA controls the traffic entering from an on-ramp and targets a critical density in the mainstream merging segment so as to maximize the freeway throughput. Other proposed local feedback control algorithms for ramp metering include (Hou, Xu, and Yan, 2008; Kachroo and Ozbay, 2011; Shlayan and Kachroo, 2013; Sun and Horowitz, 2006), to mention just a few. Feedback control approaches for mainstream traffic control by use of VSL have been rather sparse (see Carlson, Papamichail, and Papageorgiou, 2011 and Iordanidou et al., 2015 for a recent extension to the multiple bottleneck case). Furthermore, local and coordinated feedback control strategies can also be combined, e.g., as in the work by Papamichail and Papageorgiou, 2008.

1.4 Motivation and Objectives of this Thesis

To adequately address the increasing freeway traffic congestion problems, it is essential to investigate, develop and deploy the potentially most efficient methods, and recent advances in the field of Nonlinear Systems and Control should be appropriately exploited to this end. So far, literature generally lacks of studies that provide rigorous methods, which simultaneously guarantee strong theoretical properties and are easily applicable for real traffic control.

This thesis aims to commence such an promising approach for developing control strategies in order to produce more efficient and robust traffic control. In particular, this thesis utilizes mathematical tools originated from the field of Nonlinear Systems and Control for the stabilization of nonlinear systems that describe general traffic systems and freeways. To the best of the author's knowledge this is the first time that such an approach is adopted for control of traffic systems. Moreover, this thesis focuses on space-time discretized traffic flow models with nice analytical

properties (e.g., explicit state-space form, involvement of continuous and differential functions) and which provide, from an engineering application point of view, easy applicability for producing codes in a computer environment for simulations purposes, short computation times and convenient discretization intervals. Since the original PDEs are largely empirical, it may not be necessary to apply special effort and employ complex numerical schemes for their accurate discretization. Instead, an approximate, but explicit and analytical space-time discretized model may first be derived from the PDEs; to be used eventually as a self-contained modeling tool for practical applications (rather than the original PDEs).

Specifically, the main objective of this thesis is threefold:

- First, to develop general discrete space-time models for traffic networks, specific instances of which are well-known and established traffic flow models proposed in the literature so far. Particular emphasis is given in this first aspect of the present thesis to freeway models that are able to reproduce the right traffic pattern and the capacity drop phenomenon observed in freeway networks. To this end, appropriate specifications on the developed models are proposed so as to account with the capacity drop phenomenon. An extended literature review of other proposed enhanced LWR-type models incorporating capacity drop is performed and appropriate comparisons are made through simulation and calibration/validation procedure.
- Second, the present thesis aims to provide a rigorous methodology for the construction of explicit feedback laws that are able to guarantee the RGES of the Uncongested Equilibrium Point (UEP) of the developed general traffic flow models. The stability of the closed-loop systems is checked in terms of VLF and SLF criteria and appropriate theorems are constructed. The stabilization is achieved by regulating an appropriate set of inflows; for freeway models, sufficient conditions for the specification of such a set are also provided. All the provided sufficient conditions can be easily checked and give to the traffic engineer the ability to design easily an opportune feedback controller. Moreover, for freeway networks and in case limited information is provided regarding the system parameters, this thesis also provides a methodology for the construction of adaptive control schemes, the application of which guarantee the robust global exponential convergence to any selected unknown UEP.
- As a final step, the developed control schemes are tested in a realistic freeway traffic control scenario in order to investigate potential application of the scheme to the real field. Here, appropriate hypothetical scenarios are constructed and the developed schemes are tested with respect to their ability to stabilize the system when bottlenecks exist far downstream of a metered on-ramp.

1.5 Thesis Outline

The thesis is organized in a series of self-contained chapters. This first introductory chapter presents some prerequisite notions on Traffic Flow Modeling and Control, the motivation and the objectives of this thesis. The outline of the rest of the document is as follows:

- Chapter 2 introduces the reader to the basis of this work, i.e., modeling. First, the model derivation of the general proposed acyclic traffic network and its

special case of a freeway model are presented along with all the accompanying discussion on their properties and the related assumptions. Then, specific cases of the developed freeway models are introduced, which are able to incorporate the capacity drop phenomenon. Finally the proposed freeway models are tested in terms of calibration and validation using real-data from a network in UK.

- Chapter 3 presents the control methodology developed for the acyclic traffic flow models developed in Chapter 2. The application of the proposed methodology, which guarantees the RGES of the UEP of the aforementioned models, and the proofs of the corresponding results are extensively presented. Moreover, this chapter demonstrates the applicability of the obtained results by means of simulation using a realistic hypothetical network.
- Chapter 4 presents a methodology for constructing explicit feedback laws for a special case of the acyclic traffic flow models, that is, freeway networks. The application of this control methodology renders the UEP robustly globally exponentially stable and the importance behind its development lies on the fact that a SLF is constructed. The proof of the main result as well as illustrative examples are also presented.
- Chapter 5 extends the results presented in Chapter 4 and provides a methodology for the development of Adaptive Control Schemes (ACSs) which are able to guarantee the robust global exponential attractivity of the UEP of the developed freeway models. The ACS is composed by the nominal feedback presented in Chapter 4 as well as a nonlinear dead-beat observer which performs the exact identification of the unknown parameters after a transient period.
- Chapter 6 provides insights into the practical properties and performance of the methodology developed in Chapter 5, under realistic and customary traffic scenarios occurring in freeway networks. Testing this strategy with sufficiently accurate traffic flow models, different than the ones used for its design, is deemed as an indispensable step towards potential application of the proposed methodology in the field. More specifically, the ACS presented in Chapter 5 is tested in simulation in terms of its ability to control a bottleneck far downstream of a metered on-ramp. Moreover, the ACS is tested under scenarios which call for coordinated control measures by exploiting the corresponding inherent feature of the ACS.
- The thesis is concluded in Chapter 7, which summarizes its findings and results. Future perspectives are also presented here, which can help to the extension of these results.
- The present thesis contains also a number of Appendices. Appendix A presents the related mathematical background accompanying with some important definitions, lemmas and theorems. The reader is encouraged to first read this chapter before proceeding to the main core of this study, i.e., Chapters 3, 4 and 5). Appendix B contains the proofs of some important auxiliary results used in the proofs of the main results. Finally, Appendix C presents a study that links a proposed discrete space-time FOM incorporating capacity drop with the continuous space-time LWR model.

1.6 Publications Related to this Thesis

The research findings of this thesis have contributed to the following publications:

Journals

1. Karafyllis, I., Kontorinaki, M., Papageorgiou, M.: "Global Exponential Stabilization of Freeway Models", *International Journal of Robust and Nonlinear Control*, 2016, vol. 26, pp. 1184-1210.
2. Karafyllis, I., Kontorinaki, M., Papageorgiou, M.: "Robust Global Adaptive Exponential Stabilization of Discrete-Time Systems with Application to Freeway Traffic Control", *IEEE Transactions on Automatic Control*, doi: 10.1109/TAC.2017.2699125.
3. Kontorinaki, M., Karafyllis, I., Papageorgiou, M.: "Global Exponential Stabilization of Acyclic Traffic Networks", *International Journal of Control*, doi: 10.1080/00207179.2017.1362114.
4. Kontorinaki, M., Karafyllis, I., Papageorgiou, M.: "Local and Coordinated Ramp Metering within a Unifying Framework of an Adaptive Control Scheme", submitted to the *Transportation Science*.
5. Kontorinaki, M., Spiliopoulou, A., Roncoli, C., Papageorgiou, M.: "First-order models incorporating Capacity Drop: Overview and Real-data Validation", submitted to the *Transportation Research Part B: Methodological*.

Conferences

1. Karafyllis, I., Kontorinaki, M., Papageorgiou, M.: "Global Exponential Stabilization of Freeway Models", *International Journal of Robust and Nonlinear Control, Proceedings of the 14th annual European Control Conference (ECC 2015)*, Linz, Austria, 15-17 July 2015, pp. 2645-2650.
2. Karafyllis, I., Kontorinaki, M., Papageorgiou, M.: "Nonlinear Adaptive Control Scheme for Discrete-Time Systems with Application to Freeway Traffic Flow Networks.", *Proceedings of the 15th Annual European Control Conference (ECC 2016)*, Aalborg, Denmark, June 29 - July 1, 2016, pp. 275-282.
3. Kontorinaki, M., Karafyllis, I., Papageorgiou, M.: "Nonlinear Feedback Control for General Acyclic Traffic Networks", *Proceedings of the IFAC World Congress 2017*, Toulouse, France, 9-14 July, 2017, pp. 5448-5455.
4. Kontorinaki, M., Karafyllis, I., Papageorgiou, M.: "Local and Coordinated Ramp Metering within a Unifying Framework of an Adaptive Control Scheme", to appear in *Proceedings of the IEEE 20th International Conference on Intelligent Transportation Systems (ITSC 2017)*, Yokohama, Japan, 16-19 October, 2017.
5. Kontorinaki, M., Spiliopoulou, A., Roncoli, C., Papageorgiou, M.: "Capacity Drop in First-Order Traffic Flow Models: Overview and Real-Data Validation", *Proceedings of the 95th Annual Meeting of the Transportation Research Board (TRB)*, Washington, D.C., USA, 10-14 January, 2016, paper no. 16-3541.

Chapter 2

First-Order Models: Derivation and Validation Study

2.1 Introduction

Networks are large-scale entities representing different types of physical or cyber-physical systems such as fluid flow networks, communication networks, smart grids, etc. (Ahmed, Akhtar, and Aziz, 2015; Marinaki and Papageorgiou, 2005; Moarref and Rodrigues, 2016; Shahid, 2016). In this thesis, particular emphasis is given to traffic networks for which a plethora of diverse infrastructures can be addressed on the basis of a unifying modeling approach (see, for example, Coogan and Arcaç, 2014; Fermo and Tosin, 2013; Pisarski and Wit, 2012). More specifically, traffic networks may constitute urban road networks consisting of interconnected links which are modelled as store-and-forward components (Aboudolas, Papageorgiou, and Kosmatopoulos, 2009) or cell-transmission links (Buisson, Lebacque, and Lesort, 1996); large urban networks consisting of homogeneous subnetworks (Aboudolas and Geroliminis, 2013); freeway networks consisting of series of links, which are modelled, e.g., via general discretized LWR models (Lebacque, 1996; Lighthill and Whitham, 1955b) or its simplified CTM version (Daganzo, 1994); large mixed (corridor) networks consisting of urban and freeway links (Papageorgiou, 1995).

A general class of highly nonlinear and uncertain discrete space-time dynamical systems is presented in this chapter. The developed FOM represents general acyclic networks consisting of an arbitrary number of elementary components with constant turning and exit rates. The components can be interconnected to form any two-dimensional structure with no cycles for the overall network. The requirement regarding the absence of cycles is utterly necessary for reasons that will be apparent in the subsequent chapters of this thesis. It is important to note that specific instances of the proposed general model may result in all the traffic network structures mentioned above; however, in this thesis, particular emphasis is given in the case of freeway models.

Regarding freeways, this chapter proposes appropriate specifications on the developed freeway models so as to account with the capacity drop phenomenon. Despite the increasing interest from the research community in integrating capacity drop in FOMs, a limited number of effective approaches have been proposed, and only a few are actually tested using real traffic data to evaluate their behavior in case a bottleneck is activated. This chapter aims to fill this gap, gathering the state-of-the-art related to capacity drop modeling within discretized LWR-type models, contributing with further insights about their implications, and testing their capability to reproduce correctly the desired traffic pattern at an active bottleneck due to on-ramp merging. The selection criteria for the approaches that are described and analyzed in this chapter are two: first, the selected models should include a

low number of parameters, which implies a limited effort in calibration and easier application; second, the selected models should be capable of reproducing the capacity drop for a typical on-ramp merge scenario. In addition, based on the above considerations, a new modeling approach is introduced, which is, among others, a special case of the developed and proposed freeway models. An analysis that links this model with the continuous LWR model is also provided in Appendix C. Several modeling ideas have been proposed by the research community in order to incorporate the capacity drop phenomenon into LWR-type models using different assumptions. The rest of this section is devoted to a comprehensive literature review of the proposed approaches, along with an attempt to categorize them according to their underlying basic ideas.

Capacity drop is one of the most known and puzzling phenomena characterizing traffic flow behavior. Empirical observations show that, whenever a bottleneck is activated, the maximum outflow that materializes (also called discharge flow) may be some 5 to 20 % lower than the nominal bottleneck capacity. The capacity drop is then defined as the difference between these two values of flow, i.e., the capacity and the discharge flow. Certainly, the capacity drop reflects infrastructure performance degradation, leading to increased congestion space-time extent and longer vehicle delays. To avoid or delay the activation of a bottleneck, and the related capacity drop phenomenon, various traffic control measures have been proposed and applied (Cassidy and Rudjanakanoknad, 2005; Papageorgiou, Hadj-Salem, and Blosseville, 1991; Papageorgiou et al., 2003).

Since the pioneering work by Edie, 1961, it has been observed that the flow-density relation can be discontinuous, featuring a sharp speed drop within a small density range, when a critical density value is exceeded. Specifically, this discontinuity in the FD generally arises when congestion appears in the area of an active bottleneck and reflects the capacity drop phenomenon. The resulting particular shape of the FD has sometimes been referred as "inverse lambda", see Koshi, Iwasaki, and Ohkura, 1983. This behavior can be theoretically modeled via definition of two flow values for a specific range of densities around the critical density, where the different flows appear in dependence of the current and past traffic conditions. Nevertheless, some research works suggested that it is more appropriate to employ a continuous FD rather than a discontinuous one, since the latter may cause infinite shock-wave and characteristic wave speeds, as discussed by Jin, Gan, and Lebacque, 2015; moreover such a discontinuity differs from observations in the field (Cassidy, 1998).

Various approaches to enable the description of the aforementioned behavior have been proposed in different works. Muralidharan and Horowitz, 2015 and Li et al., 2015 proposed to reduce the outflow of a cell to a fixed value (lower than its nominal capacity) by modifying the demand function when the density of the cell becomes overcritical, leading to a FD of the "inverse lambda" shape. More specifically, Muralidharan and Horowitz, 2015 proposed an augmented Link-Node Cell Transmission Model (LN-CTM), which is utilized in the formulation of an optimization problem; while Li et al., 2015 utilized a CTM variation accompanied with a stochastic component (added in order to reproduce stop-and-go waves) and proposed a methodology to reduce crash risks via Variable Speed Limits (VSL). Furthermore, Jin, 2010 proposed a model that takes into account lateral and longitudinal movements of vehicles, in order to study the aggregated traffic dynamics of a freeway, including lane-changing effects. More specifically, a modified FD using an "inverse-lambda" shape is proposed by adding a parameter, which captures the intensity of lane-changing effects.

Other works considered the capacity drop mechanism being produced as a consequence of microscopic phenomena, such as lane-changing maneuvers, slow vehicles entering a merge cell, and heterogeneous lane behavior due to the variations of traffic states at merges, which prevent the system to reach the full freeway capacity before the breakdown (Cassidy and Ahn, 2005; Laval and Daganzo, 2006; Treiber, Kesting, and Helbing, 2006). Again, Muralidharan and Horowitz, 2015 proposed the inclusion of an additional weaving parameter affecting the supply function within the LN-CTM in order to capture the intensity of lane changing maneuvers. As previously mentioned, a similar feature is also present in the model proposed by Jin, 2010.

Other studies incorporated the ability of reproducing capacity drop into LWR-type models by considering explicitly its phenomenological aspects, i.e., the appearance of the capacity drop immediately after queues are forming upstream of the bottleneck location. This can be achieved by letting the downstream supply be smaller than the upstream demand. Torné, Soriguera, and Geroliminis, 2014 proposed a modeling approach, within a so-called Capacity-Lagged CTM (CL-CTM), which modifies the FD from a triangular to a trapezoidal shape in case VSL are applied. This is materialized via definition of appropriate rules to switch from capacity to a reduced discharge flow, where the two flow values (capacity and discharge flow) are chosen a priori. Similarly, Jin, Gan, and Lebacque, 2015 modifies the supply function by introducing an exogenously specified reduced capacity, which is activated when the demand of the cell is lower than its supply. Han et al., 2016 employed a similarly modified FD, with the difference that the capacity of the bottleneck cell reduces (linearly) as the density of the upstream cell (the congested one) increases. Furthermore, Landman, Hegyi, and Hoogendoorn, 2015 employed the macroscopic multilane FOM proposed by Van Lint, Hoogendoorn, and Schreuder, 2008, which enables capacity drop by decreasing the supply function of the cells located downstream of a congested one, using a pre-specified factor. Srivastava and Geroliminis, 2013 proposed a memory-based methodology, where two different values of density are chosen in order to determine whether a cell is in free-flow or congested state; whenever a cell is congested, the corresponding supply function is bounded by a pre-specified flow lower than its capacity. Thus, in this formulation, (at least) two additional parameters need to be specified: one (or two) density threshold(s), characterizing the interval where flow capacity drop is appearing, and the discharge flow. The main disadvantage of this approach is the generation of high-frequency fluctuations between congested and uncongested states that does not allow a cell to remain in congested state for a long period. The authors suggest using moving averages to smooth the density variations while applying the switching logic; however, this may not be sufficient to eliminate the aforementioned problem, since fluctuations with lower frequency and larger amplitude may be still observed.

Other researchers have tried to incorporate capacity drop within the LWR framework by accounting for the bounded acceleration of vehicles entering a bottleneck location. For instance, Lebacque, 2003 proposed a two-phase traffic flow model, where the first phase corresponds to the LWR model, while in the second phase the acceleration of vehicles is constant and equal to a maximum value; moreover, also a simplified approach that proposes only a modification of the FD is presented. Similar assumptions have been made by Monamy, Haj-Salem, and Lebacque, 2012 for a link-node model that has been also partially validated with real data for a merging scenario. Both the simplified model proposed by Lebacque, 2003 and the model proposed by Monamy, Haj-Salem, and Lebacque, 2012 utilize a decreasing demand

function for densities beyond a critical value to reflect bounded acceleration of vehicles, while the supply function remains the same. However, this model is capable to reproduce the capacity drop phenomenon in on-ramp merges only for specific cases; in fact, if the flow, that the merge cell can receive, is smaller than its capacity (due to the unchanged supply function), the desired effect is cancelled, because the merge cell cannot become congested and continues operating at capacity. The concept of the simplified model proposed by Lebacque, 2003 can also be followed by the proposed general modeling framework of Section 2.2, which allows for a wide range of demand functions to be taken into account, where the capacity drop can be included through the definition of linearly decreasing or even discontinuous demand functions for overcritical densities; while Roncoli, Papageorgiou, and Papamichail, 2015c included the possibility of capacity drop into a multi-lane FOM in order to define a quadratic programming optimization problem (Roncoli, Papageorgiou, and Papamichail, 2015b); a modified FD is used, similar to the one proposed by Lebacque, 2003, and the capacity drop is triggered by lateral and on-ramp flows.

Furthermore, Leclercq, Laval, and Chiabaut, 2011 proposed to quantify capacity drop as a consequence of bounded acceleration of merging vehicles. The capacity drop is defined as a function of the on-ramp demand considering two possible demand scenarios (low/high demand) and a set of different model parameters. The basis of this work is the Newell-Daganzo (ND) model (Newell, 1982; Daganzo, 1995b), enhanced by the introduction of different formulas and rules to compute the capacity of the merge cell depending on the on-ramp and mainstream demands. However, this approach focuses mainly on determining the value of the capacity drop, without advising on any methodology for its implementation into discretized LWR-type models.

Last but not least, some researchers have tried to incorporate the capacity drop phenomenon into LWR-type models through the hysteresis phenomenon of traffic flow (see, e.g. Alvarez-Icaza and Islas, 2013; Yuan et al., 2015), which was first reported by Treiterer and Myers, 1974 and derives from the fact that the acceleration and the deceleration of vehicles are not symmetric procedures. This means, that, whenever the traffic is moving from free-flow to congested regime, the observed flow reaches the bottleneck capacity; while, the transition from congested regime to free-flow occurs via a maximum flow, which is lower than the capacity. Thus, two different branches may exist in the FD, whereby the deceleration branch lies above the acceleration branch. It is worth noting that SOMs employing a continuous FD may naturally produce the hysteresis behavior of traffic flow and the capacity drop, thanks to the included dynamic speed equation (see e.g. Papageorgiou, Blosseville, and Hadj-Salem, 1990, Figure 14).

Several of the proposed approaches are tested in the following sections in order to provide further insights about their implications and their capability to reproduce correctly the desired traffic patterns at an active bottleneck due to on-ramp merging. The selected modeling approaches are those that are simple in terms of the number of parameters and can be formulated within a simple general LWR model framework. In particular, the following modeling approaches are selected to be tested in the next section: i) the "inverse lambda" shape FD modeling approach proposed by Muralidharan and Horowitz, 2015 and Li et al., 2015; ii) the model, which introduces a weaving parameter for lane-changing effects, proposed by Muralidharan and Horowitz, 2015; iii) the modeling approach proposed by Torné, Soriguera, and Geroliminis, 2014 with appropriate modifications for the case of an on-ramp merge; iv) a similar modeling approach with the one proposed by Han et al., 2016 which utilizes linearly decreasing capacity for the downstream supply; and finally, v) a new

modeling approach extending the ones proposed by Lebacque, 2003 and Monamy, Haj-Salem, and Lebacque, 2012.

The rest of this chapter is structured as follows: Section 2.2 presents the model derivation of the developed acyclic traffic networks as well as the related assumptions and consequences which are relevant to the proposed modeling framework. Section 2.3 is devoted to the study of the capacity drop phenomenon observed in freeways and the related specifications on the developed models needed for its incorporation. The selected approaches are analyzed and compared; in addition, a FOM that is not of LWR-type is included for comparison. Finally, Section 2.4 presents a calibration/validation study of the first-order capacity drop modeling approaches using real traffic data from a freeway network in UK.

2.2 Model Derivation

2.2.1 Acyclic Traffic Networks with Constant Turning and Exit Rates

We consider a general traffic network which consists of n components (cells). Each cell may have an external (controllable) inflow (e.g., from corresponding on-ramps), located near the cell's upstream boundary; and an external outflow (e.g., via corresponding off-ramps), located near the cell's downstream boundary. The density of vehicles at time $t \geq 0$ in cell $i \in \{1, \dots, n\}$ is denoted by $x_i(t)$. The total outflow and the total inflow of cell $i \in \{1, \dots, n\}$ at time $t \geq 0$ are denoted by $F_i^{out}(t) \geq 0$ and $F_i^{in}(t) \geq 0$, respectively. All flows during a time interval are measured in [veh]. Consequently, the conservation equation (balance of mass) for each component $i \in \{1, \dots, n\}$ is given by:

$$x_i(t+1) = x_i(t) - F_i^{out}(t) + F_i^{in}(t), i = 1, \dots, n, t \geq 0. \quad (2.1)$$

Each component of the network has storage capacity $\rho_i^{max} > 0$, ($i = 1, \dots, n$); therefore, we define the set of the states, i.e., $x \in S$, as:

$$S = [0, \rho_1^{max}] \times \dots \times [0, \rho_n^{max}]. \quad (2.2)$$

Our first assumption is dealing with the outflows. We assume that there exist functions $f_{D,i} : D \times [0, \rho_i^{max}] \rightarrow \mathbb{R}_+$, $s_i : D \times S \times \mathbb{R}_+^n \rightarrow [0, 1]$ with $f_{D,i}(d, x_i) \leq x_i$ for all $(d, x_i) \in D \times [0, \rho_i^{max}]$, where $D \subseteq \mathbb{R}^l$ is a non-empty compact set, constants $b_{i,j} \geq 0$, $i, j = 1, \dots, n$, with $b_{i,i} = 0$, for $i = 1, \dots, n$, and constants $p_i \geq 0$, $i = 1, \dots, n$ so that:

$$\left(\begin{array}{c} \text{flow of vehicles} \\ \text{from cell } i \text{ to cell } j \end{array} \right) = b_{i,j} s_i(d, x, v) f_{D,i}(d, x_i), \text{ for } i, j = 1, \dots, n, \quad (2.3)$$

$$\left(\begin{array}{c} \text{flow of vehicles} \\ \text{from cell } i \text{ to} \\ \text{regions out of the freeway} \end{array} \right) = p_i s_i(d, x, v) f_{D,i}(d, x_i), \text{ for } i = 1, \dots, n. \quad (2.4)$$

We also assume that:

$$\sum_{j=1}^n b_{i,j} + p_i = 1, \text{ for } i = 1, \dots, n. \quad (2.5)$$

Some explanations are needed at this point. The functions $f_{D,i} : D \times [0, \rho_i^{max}] \rightarrow \mathbb{R}_+$ ($i = 1, \dots, n$) denote, the attempted outflow from the i -th cell, i.e., the outflow that will exit the cell if there is sufficient space in the downstream cells. Particularly, the functions $f_{D,i}$ remind, what in the specialized literature of Traffic Engineering is called, the demand-part of the FD of the i -th cell. Notice that, the functions $f_{D,i}$ are allowed to be uncertain (by introducing the time-varying variable $d \in D$). In addition, $b_{i,j}$ are turning rates and p_i are exit rates, i.e., portions of $F_i^{out}(t)$ that are bound for the off-ramp of the i -th cell. The functions $s_i : D \times S \times \mathbb{R}_+^n \rightarrow [0, 1]$ ($i = 1, \dots, n$) are introduced in order to accommodate congestion phenomena. Specifically, these functions assume the value of 1 if the downstream cells can accommodate the whole attempted outflow of the upstream cell; they are less than 1 if the downstream cells cannot accommodate the full attempted outflow, e.g., because they are congested, as it will also explained in more detail later.

Combining (2.2), (2.3), (2.4), we obtain:

$$F_i^{out} = s_i(d, x, v) f_{D,i}(d, x_i), \text{ for } i = 1, \dots, n. \quad (2.6)$$

Next, we make the following assumption for the functions $f_{D,i} : D \times [0, \rho_i^{max}] \rightarrow \mathbb{R}_+$ ($i = 1, \dots, n$):

H 2.1

For each $d \in D$, the function $f_{D,i}(d, \cdot) : [0, \rho_i^{max}] \rightarrow \mathbb{R}_+$ satisfies $0 < f_{D,i}(d, z) < z$ for all $z \in (0, \rho_i^{max}]$. There exists $\rho_i^{cr} \in (0, \rho_i^{max}]$ such that for each $d \in D$, the function $f_{D,i}(d, \cdot)$ is continuous and increasing on $[0, \rho_i^{cr}]$. Moreover, there exist constants $L_i \in (0, 1)$, $G_i \in (0, 1]$, $\tilde{\rho}_i^{cr} \in (0, \rho_i^{cr}]$ such that $|f_{D,i}(d, z) - f_{D,i}(d, y)| \geq L_i |z - y|$ for each $d \in D$ and $y, z \in [0, \tilde{\rho}_i^{cr}]$ and $|f_{D,i}(d, z) - f_{D,i}(d, y)| \leq G_i |z - y|$ for each $d \in D$ and $y, z \in [0, \rho_i^{cr}]$. Finally, there exists a positive constant $f_i^{min} > 0$ such that for each $d \in D$ it holds that $f_{D,i}(d, z) \geq f_i^{min}$, for all $z \in [\rho_i^{cr}, \rho_i^{max}]$.

Remark 2.1: Assumption (H 2.1) is a technical assumption that allows a very general class of functions $f_{D,i} : D \times [0, \rho_i^{max}] \rightarrow \mathbb{R}_+$ to be taken into account. The implications of Assumption (H 2.1) are illustrated in Figure 2.1. Assumption (H 2.1) includes the basic properties of the so-called *demand function* (Daganzo, 1995b; Gomes and Horowitz, 2006; Gomes et al., 2008; Lebacque and Khoshyaran, 2002; Lebacque, 1996) in the Godunov discretization; whereby ρ_i^{cr} is the critical density, where $f_{D,i}$ achieves a maximum value (capacity flow). Assumption (H 2.1) allows the demand function $f_{D,i}$: (i) to be uncertain (due to the dependence on $d \in D$); (ii) to be non-differentiable on $(0, \rho_i^{cr})$; and (iii) not to have a strict upper bound for $z \in [\rho_i^{cr}, \rho_i^{max}]$. In fact, Assumption (H 2.1) allows the demand function $f_{D,i}$ to be any arbitrary function (discontinuous or decreasing or, even, increasing), taking any values within the bounds mentioned by (H 2.1) (corresponding to the right grey area in Figure 2.1), for $z \in (\rho_i^{cr}, \rho_i^{max}]$. The possibility of reduced demand flow for over-critical densities (i.e., when $x_i(t) \geq \rho_i^{cr}$) could be used to reflect the capacity drop phenomenon, as it will be shown in the next section.

Our second assumption is dealing with the inflows. Let $v_i \geq 0$ ($i = 1, \dots, n$) denote the attempted external inflow to cell $i \in \{1, \dots, n\}$ from the region out of the network and set $v = (v_1, \dots, v_n)' \in \mathbb{R}_+^n$. Typically, v_i , $i = 1, \dots, n$, correspond to external on-ramp flows, which may be determined by a ramp metering control

strategy. We assume also that there exist functions $f_{S,i} \in C^0(D \times S; \mathbb{R}_+)$, $\bar{s}_i : D \times S \times \mathbb{R}_+^n \rightarrow [0, 1]$ ($i = 1, \dots, n$) with $0 < f_{S,i}(d, x) \leq \rho_i^{max} - x_i$, for all $(d, x) \in D \times S$ with $x_i < \rho_i^{max}$ and $i = 1, \dots, n$, so that:

$$F_i^{in} = \bar{s}_i(d, x, v)v_i + \sum_{j=1}^n b_{j,i}s_j(d, x, v)f_{D,j}(d, x_j) \leq f_{S,i}(d, x), \quad (2.7)$$

for all $i = 1, \dots, n$ and $(d, x, v) \in D \times S \times \mathbb{R}_+^n$.

$$\text{if } v_i + \sum_{j=1}^n b_{j,i}f_{D,j}(d, x_j) \leq f_{S,i}(d, x), \text{ for all } i = 1, \dots, n, \quad (2.8)$$

then $\bar{s}_i(d, x, v) = s_i(d, x, v) = 1$, for $i = 1, \dots, n$.

Again, the functions $f_{S,i} : D \times S \rightarrow \mathbb{R}_+$ ($i = 1, \dots, n$) remind, what in the specialized literature of Traffic Engineering is called, the *supply function* of the i -th cell. When $\bar{s}_i(d, x, v) + \sum_{j=1}^n b_{j,i}s_j(d, x, v) < 1 + \sum_{j=1}^n b_{j,i}$ then we say that the i -th cell is *congested*, because in this case the total attempted inflow to the i -th cell (the demand flow, i.e., $v_i + \sum_{j=1}^n b_{j,i}f_{D,j}(d, x_j)$) is strictly greater than the actual inflow (F_i^{in}) to the i -th cell, i.e., the i -th cell cannot accommodate that demand. The functions $s_i, \bar{s}_i : D \times S \times \mathbb{R}_+^n \rightarrow [0, 1]$ ($i = 1, \dots, n$) are introduced so that for each cell: (i) the demand is always less than the supply (this is inequality (2.7)), and (ii) when the maximum value of all demands can be accommodated then no congestion phenomena are present (this is implication (2.8)). Priority rules for each junction can be expressed by means of the functions $s_i, \bar{s}_i : D \times S \times \mathbb{R}_+^n \rightarrow [0, 1]$ ($i = 1, \dots, n$), (see Section 2.2.3, definition (2.16)).

The supply function is usually given by the function $f_{S,i}(d, x) = \min(Q_i, c_i(\rho_i^{max} - x_i))$, where Q_i represents the maximum admissible inflow of the i -th cell and $c_i \in (0, 1]$ represents the normalized congestion wave speed. Then, the FD of cell i is composed by the increasing function $f_{D,i}(d, x_i)$, for $x_i \in [0, \rho_i^{cr}]$ and by the non-increasing function $f_{S,i}(d, x) = \min(Q_i, c_i(\rho_i^{max} - x_i))$, for $x_i \in [\rho_i^{cr}, \rho_i^{max}]$. Notice here that the uncertainty $d \in D$ has been introduced in order to accommodate the uncertain nature of the FD.

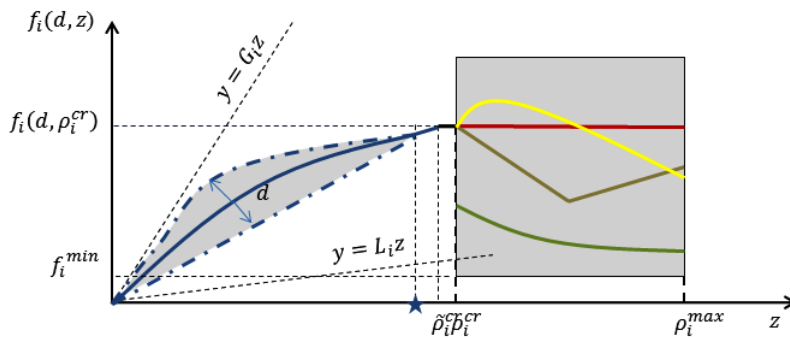


FIGURE 2.1: Implications of Assumption (H 2.1).

Combining equations (2.1), (2.6) and (2.7) we obtain the following nonlinear uncertain discrete space-time system for $i = 1, \dots, n$:

$$x_i^+ = x_i + \bar{s}_i(d, x, v)v_i - s_i(d, x, v)f_{D,i}(d, x_i) + \sum_{j=1}^n b_{j,i}s_j(d, x, v)f_{D,j}(d, x_j), \quad (2.9)$$

Figure 2.2 illustrates schematically the network described by the model (2.9). For physical reasons, we would expect a network of the form (2.9) under Assumption (H 2.1) to satisfy the following three properties:

- (P1) If the attempted external inflows $v_i \geq 0$ ($i = 1, \dots, n$) are "small" for a sufficiently large time period then the network densities will eventually be "small".
- (P2) If $x_i \neq 0$, for some $i = 1, \dots, n$, then there is at least one non-zero outflow.
- (P3) If the attempted external inflows $v_i \geq 0$ ($i = 1, \dots, n$) and the $x_i \geq 0$ ($i = 1, \dots, n$) are "small", then no congestion phenomena are present in the network.

Indeed, consider a traffic network with zero external inflows. If the network does not satisfy Property (P1) above, then it is possible that the network retains a certain amount of density (i.e., the vehicles do not exit). The same situation would occur in the case where Property (P2) above does not hold. Of course, there are "special" cases (e.g., a gridlock around a cycle) where vehicles are trapped in the network and do not exit, but it is clear that in such situations one cannot deal with congestion phenomena via inflow control, i.e., by making the external inflows sufficiently small. Property (P3) is another empirical fact that should be verified to enable inflow control: congestion phenomena are present only when the attempted external inflows $v_i \geq 0$ ($i = 1, \dots, n$) and the network densities $x_i \geq 0$ ($i = 1, \dots, n$) are "sufficiently large".

Since we intend to study network models with the above properties, we consider only acyclic networks, which satisfy the following assumption:

H 2.2

The matrix $B = \{b_{i,j} : i, j = 1, \dots, n\} \in [0, 1]^{n \times n}$ which contains the turning rates of the acyclic network (2.9) is strictly upper triangular.

Remark 2.2: Assumption (H 2.2) is a consequence of our goal for global stabilization of the network (excluding cases that are not controllable via inflow control, see

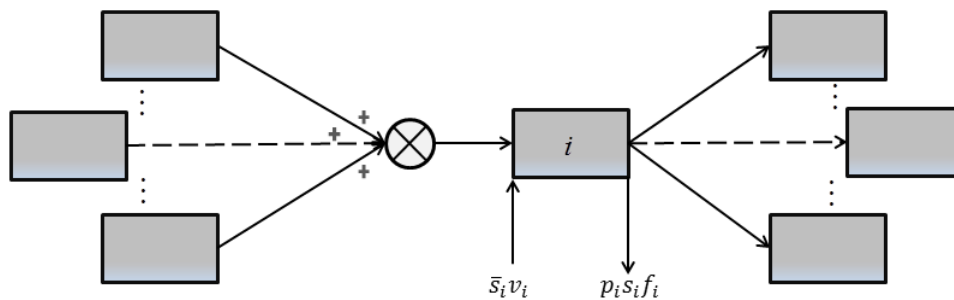


FIGURE 2.2: Scheme of the network model (2.9).

Chapter 3). Specifically, Proposition 3.2 in the following chapter shows that the existence of cycles is incompatible with the existence of a globally stabilizing feedback.

H 2.3

There exist functions $\tilde{s}_i \in C^0(D \times S \times \mathbb{R}_+^n; [0, 1])$ with $s_i(d, x, v) \geq \tilde{s}_i(d, x, v)$, for all $(d, x, v) \in D \times S \times \mathbb{R}_+^n$, $i = 1, \dots, n$, and constants $v_i^{max} > 0$ ($i = 1, \dots, n$) such that the following implication holds:

$$\text{if } x_i \tilde{s}_i(d, x, v) = 0 \text{ and } v_i < v_i^{max}, i = 1, \dots, n, \text{ then } x = 0. \quad (2.10)$$

Remark 2.3: Assumption (H 2.3) is a technical assumption related to Property (P2) and guarantees that the functions s_i should admit a continuous and positive definite lower bound for some $i = 1, \dots, n$. Implication (2.10) guarantees that if the outflow of every cell of the network is zero, then the density of every cell should be zero (P2). To see this, notice that if $0 = F_i^{out} = s_i(d, x, v)f_{D,i}(d, x_i)$ (recall (2.6)), then we obtain $\tilde{s}_i(d, x, v)f_{D,i}(d, x_i) = 0$, for $i = 1, \dots, n$. Since $f_{D,i}(d, x_i) = 0 \Leftrightarrow x_i = 0$ (recall (H 2.1)), the condition $\tilde{s}_i(d, x, v)f_{D,i}(d, x_i) = 0$ is equivalent to $\tilde{s}_i(d, x, v)x_i = 0$. Therefore, Assumption (H 2.3) guarantees the following implication: "if $F_i^{out} = 0$ and $v_i < v_i^{max}$, $i = 1, \dots, n$, then $x = 0$ ".

H 2.4

There exist constants $\mu_i \in (0, \tilde{\rho}_i^{cr})$, $v_i^{max} > 0$ ($i = 1, \dots, n$), such that

$$v_i^{max} + \sum_{j=1}^n b_{j,i} f_{D,j}(d, x_j) \leq f_{S,i}(d, x), \text{ for all } (d, x) \in D \times S \text{ with } x \leq \mu, \quad (2.11)$$

for every $i = 1, \dots, n$, where $\mu = (\mu_1, \dots, \mu_n)'$.

Remark 2.4: Property (P3) is a direct consequence of Assumption (H 2.4) and (2.8): if the network densities are small (here below μ_i) and the attempted external inflows are small (below v_i^{max}), then the total attempted inflow should be accommodated by the i -th cell. It should be noted that for $v_i \in [0, v_i^{max}]$, the left hand side of inequality (2.11) is an upper bound of the total inflow of the i -th cell (recall (2.7) where $F_i^{in} = \bar{s}_i(d, x, v)v_i + \sum_{j=1}^n b_{j,i}s_j(d, x, v)f_{D,j}(d, x_j)$ and $\bar{s}_i(d, x, v) \leq 1$, $s_i(d, x, v) \leq 1$ for all $i = 1, \dots, n$). Consequently, inequality (2.11) guarantees that the inflows are less than the supplies, provided that $x \leq \mu$ and $v_i \in [0, v_i^{max}]$, for all $i = 1, \dots, n$.

2.2.2 Some Important Consequences

Assumptions (H 2.1), (H 2.2), (H 2.3) and (H 2.4) have important consequences. A list of these is given below, while the rest are presented in the next (control) chapters where they are exploited in the proofs of the main results.

C1

For each $d \in D$, the mappings $[0, \rho_i^{cr}] \ni z \rightarrow (z - f_{D,i}(d, z)) \geq 0$ are non-decreasing for $i = 1, \dots, n$.

Consequence (C1) is a direct consequence of the facts that: (a) $|f_{D,i}(d, z_1) - f_{D,i}(d, z_2)| \leq G_i |z_1 - z_2|$ for all $z \in (0, \rho_i^{cr})$ and $d \in D$, (b) $f_{D,i}(\cdot, z)$ are increasing function in $[0, \rho_i^{cr}]$ and (c) $0 < f_i(d, z) < z$ for all $z \in (0, \rho_i^{max}]$ and $d \in D$.

C2

For each $i = 1, \dots, n$ there exist constants $\lambda_i \in (0, 1)$ such that:

$$|x_i - x_i^* - f_{D,i}(d, x_i) + f_{D,i}(d, x_i^*)| \leq \lambda_i |x_i - x_i^*|, \text{ for all } x_i, x_i^* \in [0, \tilde{\rho}_i^{cr}], d \in D \quad (2.12)$$

Consequence (C2) is a direct consequence of the facts that: (a) there exist constants $L_i \in (0, 1)$, $\tilde{\rho}_i^{cr} \in (0, \rho_i^{cr}]$ such that $|f_{D,i}(d, z_1) - f_{D,i}(d, z_2)| \geq L_i |z_1 - z_2|$ for all $z_1, z_2 \in [0, \tilde{\rho}_i^{cr}]$ and $d \in D$ and (b) Property (C1). We conclude that (2.12) holds with $\lambda_i = (1 - L_i) \in (0, 1)$.

C3

There exist constants $\theta_i > 0$ ($i = 1, \dots, n$) and $\Theta > 0$ such that $f_{D,i}(d, z) \geq \theta_i z$ and $f_{D,i}(d, z) \geq \Theta z$ for all $z \in [0, \rho_i^{max}]$, $d \in D$ and $i = 1, \dots, n$.

Consequence (C3) is a direct consequence of the facts that: (a) $f_{D,i}(d, z) \geq L_i z$ for all $z \in [0, \tilde{\rho}_i^{cr}]$, $d \in D$ and $i = 1, \dots, n$, (b) Assumption (H 2.1) in conjunction with the previous inequality guarantees that $f_{D,i}(d, x_i) \geq \min(f_i^{min}, L_i \tilde{\rho}_i^{cr})$ for all $x_i \in [\tilde{\rho}_i^{cr}, \rho_i^{max}]$, $d \in D$ and $i = 1, \dots, n$. Combining (a) and (b), we obtain $f_{D,i}(d, x_i) \geq \theta_i x_i$ for all $x_i \in [0, \rho_i^{max}]$, $d \in D$ and $i = 1, \dots, n$, where $\theta_i := \min(L_i, (\rho_i^{max})^{-1} f_i^{min}, (\rho_i^{max})^{-1} L_i \tilde{\rho}_i^{cr})$. Notice that $\theta_i > 0$ for $i = 1, \dots, n$ and define $\Theta := \min_{i=1, \dots, n}(\theta_i)$.

C4 : Proposition 2.1

Consider the network (2.9) under Assumptions (H 2.1), (H 2.2), (H 2.3). Then for all the constants $r_i > 0$ ($i = 1, \dots, n$), involved in Lemma (A.7), and for every family of constants $\tilde{\varepsilon}_i \in (0, \min(v_i^{max}, \min\{f_{S,i}(d, 0) : d \in D\}))$ ($i = 1, \dots, n$), there exists a constant $C > 0$ such that:

$$\left(\sum_{i=1}^n r_i x_i \right)^+ \leq (1 - C) \sum_{i=1}^n r_i x_i + \sum_{i=1}^n r_i v_i, \quad (2.13)$$

for all $(d, x) \in D \times S$ and for all $v_i \geq 0$ with $v_i \leq \min(v_i^{max}, \min\{f_{S,i}(d, 0) : d \in D\}) - \tilde{\varepsilon}_i$ ($i = 1, \dots, n$).

Remark 2.5: Inequality (2.13) and induction allows us to show that for every $\omega > 0$ and for sufficiently small external inflows ($0 \leq v_i(t) \leq \min(v_i^{max}, \min\{f_{S,i}(d, 0) : d \in D\}) - \tilde{\varepsilon}_i$ for all $t \geq 0$) there exists $T > 0$ sufficiently large such that the following estimate holds for all $t \geq T$, for every initial condition $x(0) \in S$ and for every input $\{d(t) \in D\}_{t=0}^\infty$:

$$\sum_{i=1}^n r_i x_i(t) \leq \omega + C^{-1} \max_{i=1, \dots, n} (\sup \{v_i(t) : t \geq 0\}) \sum_{i=1}^n r_i.$$

The above inequality shows that if the attempted external inflows $v_i \geq 0$ ($i = 1, \dots, n$) are "small" for a sufficiently large time period then the network densities will eventually be "small" (Property (P1)). The proof of Proposition 2.1 is provided in Appendix B.

2.2.3 Special Case: The Freeway Model

In this section, a special case of the acyclic network (2.9) will be derived: the freeway model. To this end, we make the following specifications:

(S1) The freeway cells are ordered with an increasing index (see for example Figure 2.3). Then, we assume that the entries of the matrix B which contains the turning rates of the network (2.9) and the corresponding exit rates p_i to regions out of the freeway are selected as follows:

$$\begin{aligned} b_{i,j} &= 0 \text{ for every } j \neq i + 1 \text{ with } i = 1, \dots, n \text{ and } j = 1, \dots, n, \\ b_{i,j} &= 1 - p_i > 0 \text{ for } j = i + 1 \text{ with } i = 1, \dots, n - 1 \text{ and } j = 1, \dots, n. \end{aligned} \quad (2.14)$$

We consider the n -th cell to be the last freeway cell; therefore $p_n = 1$. We also assume that $p_i < 1$ for $i = 1, \dots, n - 1$, and that all exits to regions out of the network can accommodate the respective exit flows. Notice that with these specifications Assumption (H 2.2) is satisfied.

(S2) For the first cell 1, there is just one external inflow, $v_1 > 0$.

(S3) The considered demand functions for the freeway models are assumed not to be uncertain, i.e., $f_{D,i}(d, z) = f_{D,i}(z)$, for every $i = 1, \dots, n$, and therefore Assumption (H 2.1) admits as special case the following assumption:

H 2.1*

The function $f_{D,i}(\cdot) : [0, \rho_i^{max}] \rightarrow \mathfrak{R}_+$ satisfies $0 < f_{D,i}(z) < z$ for all $z \in (0, \rho_i^{max}]$ and for each $i = 1, \dots, n$. There exists $\rho_i^{cr} \in (0, \rho_i^{max}]$ such that the function $f_{D,i}(\cdot)$ is continuous and increasing on $[0, \rho_i^{cr}]$ for each $i = 1, \dots, n$. Moreover, there exist constants $L_i \in (0, 1)$, $G_i \in (0, 1]$, $\tilde{\rho}_i^{cr} \in (0, \rho_i^{cr}]$ such that $|f_{D,i}(z) - f_{D,i}(y)| \geq L_i |z - y|$ for each $y, z \in [0, \tilde{\rho}_i^{cr}]$ and $|f_{D,i}(z) - f_{D,i}(y)| \leq G_i |z - y|$ for each $y, z \in [0, \rho_i^{cr}]$ for each $i = 1, \dots, n$. Finally, there exists a positive constant $f_i^{min} > 0$ such that $f_{D,i}(z) \geq f_i^{min}$, for all $z \in [\rho_i^{cr}, \rho_i^{max}]$ and for each $i = 1, \dots, n$.

(S4) The considered supply functions for the freeway models are assumed not to be uncertain and they are given by:

$$f_{S,i}(x_i) = \min(Q_i, c_i(\rho_i^{max} - x_i)), \quad (2.15)$$

where $Q_i > 0$, $c_i \in (0, 1]$ ($i = 1, \dots, n$) denote the maximum received flow (capacity inflow) and the congestion wave speed, respectively, of the i -th cell.

(S5) The functions $s_i : D \times S \times \mathfrak{R}_+^n \rightarrow [0, 1]$, which have been introduced in order to accommodate congestion phenomena in the model (2.9), are selected as follows:

$$s_i = (1 - d_i) \min \left(1, \max \left(0, \frac{f_{S,i+1}(x_{i+1}) - v_{i+1}}{(1 - p_i)f_{D,i}(x_i)} \right) \right) + d_i \min \left(1, \frac{f_{S,i+1}(x_{i+1})}{(1 - p_i)f_{D,i}(x_i)} \right), \quad (2.16)$$

for $i = 1, \dots, n - 1$, where $f_{S,i}(x_i)$ are given by (2.15) and

$$d_i(t) \in [0, 1], i = 2, \dots, n, t \geq 0, \quad (2.17)$$

denote time-varying priority rules. Then $d = (d_1, \dots, d_{n-1}) \in D = [0, 1]^{n-1}$. For the last cell we assume that $s_n(d, x, v) = 1$ for every $(d, x, v) \in D \times S \times \mathfrak{R}_+^n$. Note that, if the supply is higher than the total demand, then (2.16) yields $s_i = 1$, irrespective of the value of d_i , since the total demand flow can be accommodated by the downstream cell. Thus, the parameter d_i determines the relative inflow priorities, when the downstream supply prevails. Specifically, when $d_i(t) = 0$, then the on-ramp inflow has absolute priority over the internal inflow; on the other hand, when $d_i(t) = 1$, then the internal inflow has absolute priority over the on-ramp inflow; while intermediate values of d_i reflect intermediate priority cases. The parameters $d_i(t) \in [0, 1]$ are treated as unknown parameters (disturbances). Notice that by introducing the parameters $d_i(t) \in [0, 1]$ (and by allowing them to be time-varying), we have taken into account all possible cases for the relative priorities of the inflows (and we also allow the priority rules to be time-varying); see (Coogan and Arcak, 2014; Daganzo, 1995b) for freeway models with specific priority rules, which are special cases of the proposed general approach.

Taking into account the above considerations, the network model (2.9) admits the following "freeway" form:

$$\begin{aligned} x_1^+ &= x_1 - s_1(d, x, v)f_{D,1}(x_1) + \min(f_{S,1}(x_1), v_1) \\ &= x_1 - s_1(d, x, v)f_{D,1}(x_1) + \bar{s}_1(d, x, v)v_1, \end{aligned} \quad (2.18)$$

$$\begin{aligned} x_i^+ &= x_i - s_i(d, x, v)f_{D,i}(x_i) + \min(f_{S,i}(x_i), v_i + (1 - p_{i-1})f_{D,i-1}(x_{i-1})) \\ &= x_i - s_i(d, x, v)f_{D,i}(x_i) + \bar{s}_i(d, x, v)v_i + s_{i-1}(d, x, v)(1 - p_{i-1})f_{D,i-1}(x_{i-1}), \end{aligned} \quad (2.19)$$

for $i = 2, \dots, n - 1$,

$$\begin{aligned} x_n^+ &= x_n - f_{D,n}(x_n) + \min(f_{S,n}(x_n), v_n + (1 - p_{n-1})f_{D,n-1}(x_{n-1})) \\ &= x_n - f_{D,n}(x_n) + \bar{s}_n(d, x, v)v_n + s_{n-1}(d, x, v)(1 - p_{n-1})f_{D,n-1}(x_{n-1}), \end{aligned} \quad (2.20)$$

where $f_{S,i}(x_i)$ and $s_i(d, x, v)$ are given by (2.15) and (2.16), respectively. The values of $\bar{s}_i \in [0, 1]$, $i = 1, \dots, n$, may also be similarly derived from (2.7), when $v_i > 0$, but they are not needed in what follows. Since the functions $f_{D,i} : [0, \rho_i^{max}] \rightarrow \mathfrak{R}_+$ satisfy $0 < f_{D,i}(x_i) < x_i$ for all $x_i \in (0, \rho_i^{max}]$, it follows that (2.18)-(2.20) is an uncertain control system on S (i.e., $x = (x_1, \dots, x_n)' \in S$) with inputs $v = (v_1, \dots, v_n)' \in (0, +\infty) \times \mathfrak{R}_+^{n-1}$ and disturbances $d = (d_1, \dots, d_{n-1}) \in D = [0, 1]^{n-1}$. We emphasize that the uncertainty $d \in D$ appears in the equations (2.18)-(2.20) only when the supply function prevails, i.e., only when $v_i(t) + (1 - p_{i-1})f_{D,i-1}(x_{i-1}(t)) > f_{S,i}(x_i(t))$ for some $i \in \{2, \dots, n\}$.

Remark 3.1: The freeway model (2.18)-(2.20) with (2.15) and (2.16) under Assumption (H 2.1*), satisfies Assumptions (H 2.3) and (H 2.4). More specifically:

- Assumption (H 2.4) is satisfied with $v_i^{max} > 0$, $\mu_i \in (0, \tilde{\rho}_i^{cr})$, $i = 1, \dots, n$, given by the following recursive formulas:

$$\mu_n = \tilde{\rho}_n^{cr}/2, \mu_i = \min\left(\frac{\tilde{\rho}_i^{cr}}{2}, \frac{1}{2}f_{S,i+1}(\mu_{i+1})\right), \quad (2.21)$$

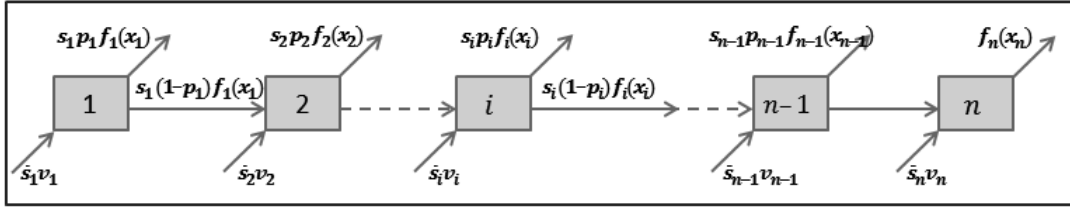


FIGURE 2.3: Scheme of the freeway model.

for $i = 1, \dots, n-1$ and

$$v_i^{max} = \frac{1}{2} f_{S,i}(\mu_i), \quad (2.22)$$

for $i = 1, \dots, n$.

- Assumption (H 2.3) holds with $v_i^{max} > 0$ ($i = 1, \dots, n$) given by (2.22) and the continuous functions $\tilde{s}_i(d, x, v)$ ($i = 1, \dots, n$) given by:

$$\tilde{s}_i(d, x, v) := \min \left(1, \frac{\max(0, f_{S,i+1}(x_{i+1}) - v_{i+1})}{(1-p_i)\rho_i^{max}} \right) \quad (2.23)$$

for $i = 1, \dots, n-1$ and $\tilde{s}_n := 1$.

In conclusion, specifications (S1)-(S5), definitions (2.15), (2.16) and Remark 3.1 allow us to conclude that the freeway model (2.18)-(2.20) is a special case of the network model (2.9). Furthermore, we have to note that the model (2.18)-(2.20) with (2.15) and (2.16) is also a generalized version of the known first-order discrete Godunov approximation to the kinematic-wave partial differential equation of the LWR-model (see (Lighthill and Whitham, 1955a; Lighthill and Whitham, 1955b; Richards, 1956)) with nonlinear ((Lebacque, 1996)) or piecewise linear (Cell Transmission Model - CTM, (Daganzo, 1994; Daganzo, 1995b) FD. However, the presented framework can also accommodate recent modifications of the LWR-model as in (Lebacque, 2003; Muralidharan, Horowitz, and Varaiya, 2012; Roncoli, Papageorgiou, and Papamichail, 2015a) to reflect the so-called capacity drop phenomenon (see the following sections). Notice that the piecewise smooth selections $f_{D,i}(z) = Q_i \rho_i^{cr-1} z$ for $z \in [0, \rho_i^{cr}]$ and $f_{D,i}(z) = Q_i$ for $z \in (\rho_i^{cr}, \rho_i^{max}]$ ($i = 1, \dots, n$) with $\rho_i^{max} \geq \rho_i^{cr} + c_i^{-1} Q_i$ allow us to obtain the standard CTM with: (i) triangular-FD (if $\rho_i^{max} = \rho_i^{cr} + c_i^{-1} Q_i$); and (ii) trapezoidal-FD (if $\rho_i^{max} > \rho_i^{cr} + c_i^{-1} Q_i$) (see also Section 2.3.1). In the latter case, Assumption (H 2.1*) holds with arbitrary $\tilde{\rho}_i^{cr} \in (0, \rho_i^{cr}]$.

For the subsequent description and testing of different capacity-drop approaches, a simple formulation of a discretized LWR model is utilized. Despite the fact that some of the considered approaches are originally introduced for more sophisticated models, here, their implementation is based on a common formulation, which also permits a clearer understanding and a fairer result comparison. The notation is kept consistent for all the described approaches. Moreover, a simple illustrative example is constructed, which demonstrates the qualitative behavior of the different approaches that are tested hereafter.

2.3 Capacity drop in LWR-type models

2.3.1 A Different Discretized LWR Formulation

The freeway model (2.18)-(2.20) can also admit the following specific form, where the involved variables are measured in the common traffic units and which indicates the basic discretized LWR-model formulation:

$$\begin{aligned} x_1^+ &= x_1 + \frac{T}{l_1 \bar{L}_1} \left(-\max \left(0, \frac{f_1(x_1, x_2, v_2)}{1 - p_1} \right) + \min \left(v_1(k), f_{S,1}(\rho_1) \right) \right) \\ x_i^+ &= x_i + \frac{T}{l_i \bar{L}_i} \left(-\max \left(0, \frac{f_i(x_i, x_{i+1}, v_{i+1})}{1 - p_i} \right) + f_{i-1}(x_{i-1}, x_i, v_i) + v_i \right), i = 2, \dots, n \end{aligned} \quad (2.24)$$

$$\begin{aligned} f_i(x_i, x_{i+1}, v_{i+1}) &= \min \{ (1 - p_i) f_{D,i}(x_i), f_{S,i+1}(x_{i+1}) - v_{i+1} \}, i = 1, \dots, n - 1, \\ f_n(x_n) &= f_{D,n}(x_n) \end{aligned} \quad (2.25)$$

$$f_{D,i}(x_i) = \min \{ g_i(x_i), Q_i \}, \text{ for } i = 1, \dots, n \quad (2.26)$$

$$f_{S,i+1}(x_{i+1}) = \min \{ Q_{i+1}, c_{i+1}(\rho_{i+1}^{max} - x_{i+1}) l_{i+1} \} \text{ for } i = 1, \dots, n - 1. \quad (2.27)$$

where T denotes the simulation time step measured in [h], l_i denotes the number of lanes in the i^{th} cell, \bar{L}_i denotes the length of the i^{th} cell, f_i denotes the actual out-flow from the i^{th} cell to the $(i + 1)^{th}$ cell and g_i denotes any general non-decreasing function. Figure 2.4 illustrates schematically the freeway model (2.24)-(2.27). The density of vehicles here is measured in [veh/km/lane], any flow variable is measured in [veh/h] and speed is measured [km/h]. As it has already been mentioned, the FD is a relation between density and flow and is characterized by its concave branches, where the demand part and the supply part reflect, respectively, its increasing and decreasing branches (Godunov, 1959; Lebacque, 1996). The density value (unimodal FDs) or values (multimodal FDs), for which the maximum flow is attained, is defined as the critical density of the cell.

Notice that in (2.26) and (2.27), the demand and supply functions, are completed by assuming capacity flow values Q_i for overcritical and undercritical densities, respectively. Consequently, the model predicts capacity flow even when congestion is created (no capacity drop), in accordance with the non-discretised LWR model.

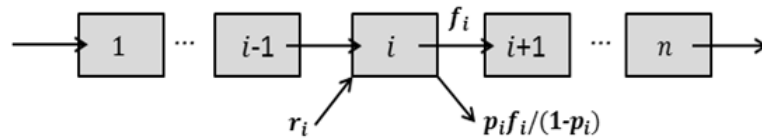


FIGURE 2.4: The space-discretization of a hypothetical freeway stretch.

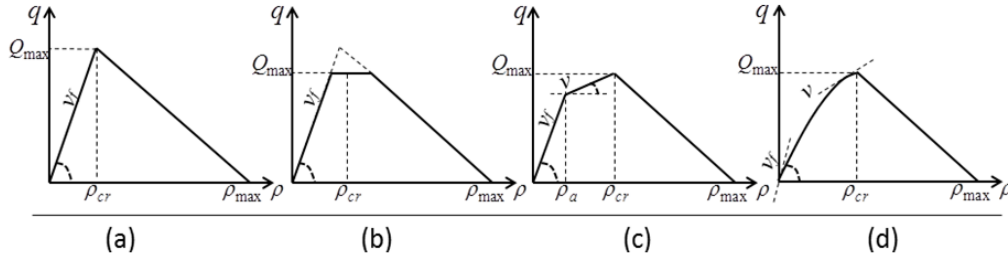


FIGURE 2.5: Different choices for the left-hand side of the FD corresponding to: (a) a triangular FD (CTM), (b) a trapezoidal FD, (c) a piecewise linear FD and (d) a nonlinear FD.

Note also, that the right-hand side of the FD in (2.27) is described by a linear function (with a negative slope c_i); while the left-hand side of the FD in (2.26) is assumed to be a non-decreasing function $g_i(x_i)$.

Different shapes for the FD

Different functions $g_i(x_i)$ can be used for the demand function in (2.26). The original CTM formulation by Daganzo, 1994 considers a triangular-shaped FD (Figure 2.5(a)), where $g_i(x_i) = v_{f,i}x_i l_i$, $g_i(\rho_i^{cr}) = Q_i$ and $c_i = Q_i/(\rho_i^{max} - \rho_i^{cr})l_i$ (with $c_i < v_{f,i}$ and $v_{f,i} < \bar{L}_i/T$). This formulation has two main drawbacks: first, when using realistic free-flow and congestion-wave speeds, it may lead to high (and sometimes unrealistic) capacity flow; second, only one speed value is considered for all under-critical densities, which is often not compatible with traffic observations. To overcome the first issue, a trapezoidal FD can be used, where $g_i(x_i) = v_{f,i}x_i l_i$, $g_i(\rho_i^{cr}) \geq Q_i$ and $c_i \geq Q_i/(\rho_i^{max} - \rho_i^{cr})l_i$, as illustrated in Figure 2.5(b). In this case, the critical density, instead of being unique for both the FD parts, can be selected within an interval of densities, thus increasing also the degree of freedom for model calibration. Nevertheless, in real traffic, the observed speed may be characterized by a decreasing-behavior also for undercritical densities, which can be reflected by using a nonlinear concave function g_i (Figure 2.5(d)), where $g_i(\rho_i^{cr}) = Q_i$ and $c_i = Q_i/(\rho_i^{max} - \rho_i^{cr})l_i$. An opportune calibration of such function may lead to more realistic results. As an example, a nonlinear exponential function, as proposed by Messmer and Papageorgiou, 1990, can be employed (see (2.44)). A similar behavior can also be obtained, with similar accuracy, considering a piecewise-linear approximation of the nonlinear function (Figure 2.5(c)), which is helpful, for instance, in case linear constraints are needed for the formulation of an optimization problem (see e.g., Ziliaskopoulos, 2000; Roncoli, Papageorgiou, and Papamichail, 2015c).

Illustrative example

In order to illustrate the behavior of each approach, a simple hypothetical freeway stretch is considered, consisting of $n = 15$ homogeneous cells (common FD) of equal length (500 m). The freeway stretch includes an on-ramp located at the upstream boundary of the cell $i = 13$. The parameters that characterize the network are shown in Table 2.1. For the sake of simplicity, in all the following tests, the function g_i utilized in (2.26) is selected to be $g_i(x_i) = v_{f,i}x_i l_i$ (for $i = 1, \dots, 15$), leading to triangular-shaped FD (Figure 2.5(a)). A hypothetical trapezoidal traffic demand

TABLE 2.1: Parameters of the hypothetical network.

T sec	n	\bar{L}_i km	l_i	ρ_i^{cr} veh/km/lane	$v_{f,i}$ km/h	ρ_i^{max} veh/km/lane	Q_i veh/h	c_i km/h
5/3600	15	0.5	3	20	100	120	6000	20

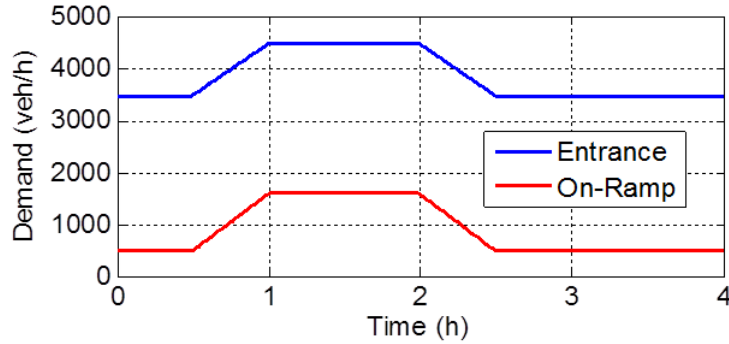


FIGURE 2.6: Demand scenario: entrance (blue), on-ramp (red).

scenario is applied to the network (see Figure 2.6), which, for some time period, generates a flow higher than the capacity at the merge area, thus generating congestion that spills back for some cells, however without reaching the network origin. The system is initialized from a steady state, that is $x_i(0) = 11.7$ [veh/km/lane], for $i = 1, \dots, 12$, and $x_i(0) = 13.3$ [veh/km/lane], for $i = 13, 14, 15$. The simulation time horizon is $T^{hor} = 4$ h for all the following tests.

Figure 2.7(a), (b), (c) illustrates some significant characteristics of the CTM in case congestion is created at an on-ramp merge. Once the total demand (sum of mainstream and factual ramp flows) exceeds the bottleneck's capacity, only a portion of the available mainstream flow is allowed to access the 13th cell. This causes an increase of density in the upstream cell (the 12th cell) (see Figure 2.7(a), red line), which eventually enters into a congested state, generating a congestion wave that propagates to further upstream cells. During this period, the density in the merge cell remains at its critical value (see Figure 2.7(a), blue line), allowing an outflow equal to capacity (Figure 2.7(c)). As a consequence of the observations above, the speed at the 12th cell decreases (Figure 2.7(b), red line), while the speed at the merge cell (13th) remains constant and equal to the free speed. Note that, in contrast to this modeled behavior, the merge cell is typically congested in real traffic; while the exit flow is reduced upon the onset of congestion due to capacity drop.

2.3.2 Approach 1: Switching logic for maximum flow

One effective way to implement a FD characterized by the inverse-lambda shape is via the definition of an opportune switching logic to define dynamically the current maximum flow. An example can be found in the study proposed by Torné, Soriguera, and Geroliminis, 2014, where a set of rules is proposed to impose capacity drop in case VSL are applied in a certain area of the network. The concept is based on the coexistence of two FDs for the same location: a triangular-shaped one, active in case VSL are not applied (and, thus, no congestion is present); and a trapezoidal-shaped one, characterized by lower capacity that materializes in case congestion is

present. This method can be extended straightforwardly to the case of bottlenecks due to lane drops, tunnels, etc.; in addition, it is shown here that it is also effective in case congestion is generated because of a merging on-ramp. The formulation is described by (2.24), (2.25), and:

$$f_{D,i}(x_i(k)) = \min\{g_i(x_i(k)), R_i(k)\}, \text{ for } i = 1, \dots, n, \quad (2.28)$$

$$f_{S,i+1}(x_{i+1}(k)) = \min\{R_{i+1}(k), c_{i+1}(\rho_{i+1}^{max} - x_{i+1}(k))l_{i+1}\}, \text{ for } i = 1, \dots, n-1, \quad (2.29)$$

where

$$R_1(k) = Q_1, R_2(k) = Q_2, \quad (2.30)$$

$$R_{i+1}(k+1) = \begin{cases} \bar{Q}_{i+1} & \text{if } c_i(\rho_i^{max} - x_i(k))l_i < \min(f_{D,i-1}(x_{i-1}(k)), R_i(k)) \\ Q_{i+1} & \text{otherwise} \end{cases}, \quad (2.31)$$

for $i = 2, \dots, n-1$. R_i are auxiliary variables that define the maximum flow for cell i , and \bar{Q}_i corresponds, for this modeling approach, to the queue discharge flow observed after the congestion onset. The queue discharge flow \bar{Q}_i can also be viewed as $\bar{Q}_i = \alpha Q_i$, i.e., a portion $\alpha < 1$ of the capacity flow. For this simulation test, this portion is constant and equal to $\alpha = 0.95$. Equation (2.30) reflects the assumption that the backspilling congestion does not reach the entrance of the network. Moreover, all cells are initially uncongested, thus $R_i(0) = Q_i$, for every $i = 1, \dots, n$.

Figure 2.7(d), (e), (f), illustrates the behavior resulting from the application of this approach. The main idea lies in decreasing the capacity of the cell located immediately downstream of a congested one. More specifically, when the total flow (on-ramp and mainstream) exceeds the capacity of the merge cell, the density of the upstream cell starts increasing (see Figure 2.7(d), red line), while at the same time its speed starts decreasing (see Figure 2.7(e), red line); consequently, after some time, its supply function becomes smaller than the demand function of the upstream cell; this, according to (2.31), triggers a reduction of the maximum flow for the downstream cell (see Figure 2.7(f)), which persists until the overall demand is sufficiently decreased. As a drawback, the flow reduction appears with some delay after the congestion starts, since this reduction materializes only when both the demand flow of the 11th cell and the maximum flow of the 12th cell become higher than the supply of the 12th cell. Furthermore, it is interesting to point out that, despite the flow-drop, there is no congestion, i.e. no over-critical density (Figure 2.7(d), blue line), and therefore also no speed-drop (Figure 2.7(e), blue line), at the merge cell.

2.3.3 Approach 2: Introduction of a weaving parameter

Another option to achieve a reduced outflow at a merge cell is via the introduction of a weaving parameter that essentially affects the supply function at the merge cell, as proposed by Muralidharan and Horowitz, 2015. The purpose of this parameter is to take into account the ‘‘intensity’’ of lane changing maneuvers performed by vehicles just entered from the on-ramp, imposing a reduction of the available space for vehicles coming from upstream. The mathematical formulation consists of (2.24), (2.32), (2.26), and (2.27) where

$$f_i(x_i, x_{i+1}, v_{i+1}) = \min\{(1 - p_i)f_{D,i}(x_i), f_{S,i+1}(x_{i+1}) - \eta_r v_{i+1}\} \quad (2.32)$$

for $i = 1, \dots, n - 1$, where $\eta_r > 1$ is the weaving parameter that aims to reduce the available space at the merge cell, thus limiting farther the mainstream flow entering the cell. For a given η_r , the resulting outflow from the merge cell, namely the queue discharge flow, is a function of the on-ramp flow. It can be seen from Figure 2.7(i) (where $\eta_r = 1.2$ is used), that the capacity flow is never reached even in case of low factual on-ramp flow; for this reason, the flow reduction is barely visible. Notice also that, similarly to Approach 1, the merge cell is not congested (Figure 2.7(g), (h), blue line).

2.3.4 Approach 3: Reduction of the demand function

Another formulation, also utilized by Muralidharan and Horowitz, 2015 and Li et al., 2015, consists of the definition of a discontinuous demand part of the FD at bottleneck locations. More specifically, a flow lower than the capacity is defined, which materializes once the density of the cell becomes overcritical. In particular, the model can be described by (2.24), (2.25), (2.27), and:

$$f_{D,i}(x_i) = \begin{cases} g_i(x_i) & \text{if } x_i \leq \rho_i^{cr} \\ \bar{Q}_i & \text{otherwise} \end{cases}, \text{ for } i = 1, \dots, n. \quad (2.33)$$

This approach produces the normal behavior of LWR model when the density of the upstream of the merge cell (here the 12th cell) is undercritical (Figure 2.7(j)), leading the merge cell to reach properly capacity flow; then, whenever the density becomes overcritical, the outflow from the upstream of the merge cell drops to a value corresponding to \bar{Q}_i which in turn leads the outflow from the merge cell (discharge flow) to a value equal to $\bar{Q}_i + v_{i+1}(k)$ (Figure 2.7(l)); in this case, $\bar{Q}_i = \alpha Q_i$, and $\alpha = 0.7$ are employed. The flow drop can be observed only if the value of the parameter *alpha* is selected to ensure that $\bar{Q}_i + v_{i+1}(k) < Q_{i+1}$. The main drawback of this approach is that traffic congestion persists longer than in the other cases, because, once formed, its disappearance can only be triggered by a sufficient decrease of the arriving demand (that must become smaller than \bar{Q}_i), irrespectively of any variation of the ramp inflow. Again, no congestion appears at the merge cell (Figure 2.7(k), (j), blue line).

2.3.5 Approach 4: Linear reduction of maximum flow

As previously mentioned, the presence of capacity drop within traffic flow models plays a key role for the design and testing of freeway traffic control strategies. Among others, model-based control problems have been widely exploited in recent years because of the possibility to explicitly consider system dynamics and physical constraints. In some works, the classic formulation of FOMs was implemented via use of integer variables and opportune switching rules; see, e.g., Ferrara, Sacone, and Siri, 2015; Muralidharan and Horowitz, 2015; Sun and Horowitz, 2005. In other works, (see, e.g., Roncoli, Papageorgiou, and Papamichail, 2015c; Ziliaskopoulos, 2000), linear inequalities (derived from the piecewise linear FD) were considered as constraints in the optimization problem; hereafter, some variants of these models are presented, which allow to define linearly constrained formulations for corresponding optimization problems. Here, a similar formulation as the one proposed by Han et al., 2016 is presented.

A concept similar to Approach 1 is considered, albeit with the introduction of an additional linear term that reduces the supply function of a downstream cell.

Specifically, when congestion starts in cell i ($x_i > \rho_i^{cr}$), the maximum flow materialized within the supply term of the downstream cell $i + 1$ is linearly decreased as a function of x_i , according to the following equations:

$$f_{S,i+1}(x_{i+1}) = \min\{F_{i+1}(x_i), c_{i+1}(\rho_{i+1}^{max} - x_{i+1})l_{i+1}\} \quad (2.34)$$

for $i = 1, \dots, n - 1$, where $F_{i+1}(x_i)$ is given by:

$$F_{i+1}(x_i) = \begin{cases} Q_{i+1} & \text{if } x_i \leq \rho_i^{cr} \\ \bar{Q}_{i+1} + \frac{Q_{i+1} - \bar{Q}_{i+1}}{\rho_i^{cr} - \rho_i^{max}}(x_i - \rho_i^{max}) & \text{otherwise} \end{cases}, \quad (2.35)$$

for $i = 1, \dots, n - 1$, with $\bar{Q}_i = \alpha Q_i$; where in the illustrative example $\alpha = 0.9$. The proposed formulation is thus given by (2.24), (2.25), (2.26), (2.34), and (2.35). For under-critical densities, F_i is constant and equal to the capacity flow; however, in case the density of the i^{th} cell increases beyond its critical value (Figure 2.7(m), red line), the maximum flow of the supply function of the $(i + 1)^{th}$ cell is reduced linearly (Figure 2.7(o)). Therefore, the queue discharge flow from the bottleneck's cell depends on the factual on-ramp flow which imposes higher density values for the upstream cells. It should be mentioned here that in case there is no particular need for linear formulations, other functions can also be considered for the above reduction of the maximum flow. This approach appears to work appropriately also for bottlenecks due to capacity reduction (e.g., lane drops, tunnels). Differently from Approach 2, the model is capable of reaching capacity before congestion starts, and the capacity drop appears with a shorter delay with respect to the one observed in Approach 1. On the other hand, the merge cell remains uncongested, similarly to all previous approaches.

2.3.6 Approach 5: Increased space for vehicles entering a bottleneck

Yet another approach may be conceived, which, in contrast to all previous approaches, allows for the bottleneck (e.g., merge) cell to become congested (as in real traffic observations), while producing a reduced outflow from the merge cell as well. Two different mechanisms are employed in order to achieve this behavior. The first one is activated in case of high on-ramp flow and imposes that the merge cell is able to receive more flow than its nominal capacity. To this end, in case a cell contains an external on-ramp, the flux function f_i is modified via the introduction of the parameter $\theta_r < 1$. In the basic discretized LWR formulation, the supply function of a cell becomes active (smaller than the demand function of the previous cell), when the density of this cell is equal or exceeds its critical value. The introduction of θ_r acts as a delay in the activation of the supply function by reducing it, in terms of the on-ramp flow, less than the real on-ramp flow would otherwise impose (in contrast to Approach 2, where the parameter η_r hastens the activation of the supply function). Essentially, this contributes to the increase of the available space for the upstream mainstream flow entering the merge cell. As a result, the density at merge cell is allowed to increase beyond the critical ($x_i > \rho_i^{cr}$), and therefore become congested. Notice that the inflow of the merge cell can exceed its nominal capacity, but the same does not hold for its outflow, since the latter is determined by its demand function. However, this cannot produce any reduced outflow (capacity drop) by itself. The second mechanism consists in the introduction of a decreasing demand function for overcritical densities, similar to the one proposed by Lebacque, 2003 and Monamy, Haj-Salem, and Lebacque, 2012. Due to the fact that the density of the merge cell

can now be overcritical (thanks to the application of the first mechanism), the decreasing demand function imposes smaller outflow, i.e. a capacity drop. There is a large range of decreasing functions that can be considered. Here, for simplicity, a linearly decreasing function is selected. Notice that the proposed demand functions are continuous, in contrast with the demand functions employed in Approach 3. The mathematical formulation consists of (2.24), (2.36), (2.37), and (2.27) where:

$$f_i(x_i, x_{i+1}, v_{i+1}) = \min\{(1 - p_i)f_{D,i}(x_i), f_{S,i+1}(x_{i+1}) - \theta_r v_{i+1}\}, \quad (2.36)$$

for $i = 1, \dots, n - 1$,

$$f_{D,i}(x_i) = \begin{cases} g_i(x_i) & \text{if } x_i \leq \rho_i^{cr} \\ Q_i + \bar{Q}_i \frac{x_i(k) - \rho_i^{cr}}{\rho_i^{cr} - \rho_i^{max}} & \text{otherwise} \end{cases}, \quad (2.37)$$

for $i = 1, \dots, n$. In the illustrative example, $\theta_r = 0.7$ and $\bar{Q}_i = \alpha Q_i$ are used, where $\alpha = 0.4$. Figure 2.7(p), (q), (r) illustrates the above considerations. Specifically, by the time the merge cell becomes congested (Figure 2.7(p), blue line), producing also the corresponding speed drop (Figure 2.7(q), blue line), and the corresponding capacity drop is observed for the flow exiting the merge cell (Figure 2.7(r)). The magnitude of this drop and the resulting queue discharge flow are determined by the combination of the values of parameters a , θ_r and the on-ramp flow. At the same time, θ_r affects also the magnitude of the increase of the density at the merge cell, i.e., reducing θ_r produces a higher density increase at the merge cell, resulting in a higher speed. Finally, it is interesting to point out that the congestion is first created at the merge cell and the flow drop occurs immediately after the maximum flow is reached, in accordance with real traffic observations.

This behavior can be alternatively obtained with different formulations (instead of using the parameter θ_r). For instance, such an effect can be also obtained by considering an increased upper bound (capacity) in (2.27) for undercritical densities, e.g. increasing capacity by 5% and increasing accordingly the resulting from the common FD wave speed (e.g. increased similarly by 5%) (Kontorinaki et al., 2016). Again, a decreasing demand function for over-critical densities (2.37) has to be considered so as to achieve the desired capacity drop. This alternative modeling approach acts in the same way as parameter θ_r does (delay the activation of the supply function), but it may also be applied for bottlenecks due to lane drops, tunnels etc., and not only for on-ramp merges.

This new modeling approach has also been examined regarding its relation and consistency with the PDE of the LWR model (see Appendix C). Among others, this analysis enables to assess how the introduced parameters of Approach 5 affect the solution of the discretized model when the discretization parameters (cell length and simulation time step) tend to zero. However, in order to conduct such an analysis, it is important to determine the two ways the on-ramp flow term may be treated within the discretization: first by assuming that the on-ramp flow term is distributed flow within specific space bounds (Section C.1 of the Appendix); second by assuming the on-ramp flow is a concentrated (Dirac function) flow at a given space point of the freeway (Section C.2 of the Appendix). From the analysis it follows that, when treating the on-ramp via the first way, the proposed discretized model is consistent with the LWR PDE, while simulation results reveal that in some cases the solution of the discretized model converges (as the discretization parameters tend to zero) to the solution of the CTM (which in turn converges to the LWR PDE solution). However, following the second way for treating the on-ramp flow, one can only define

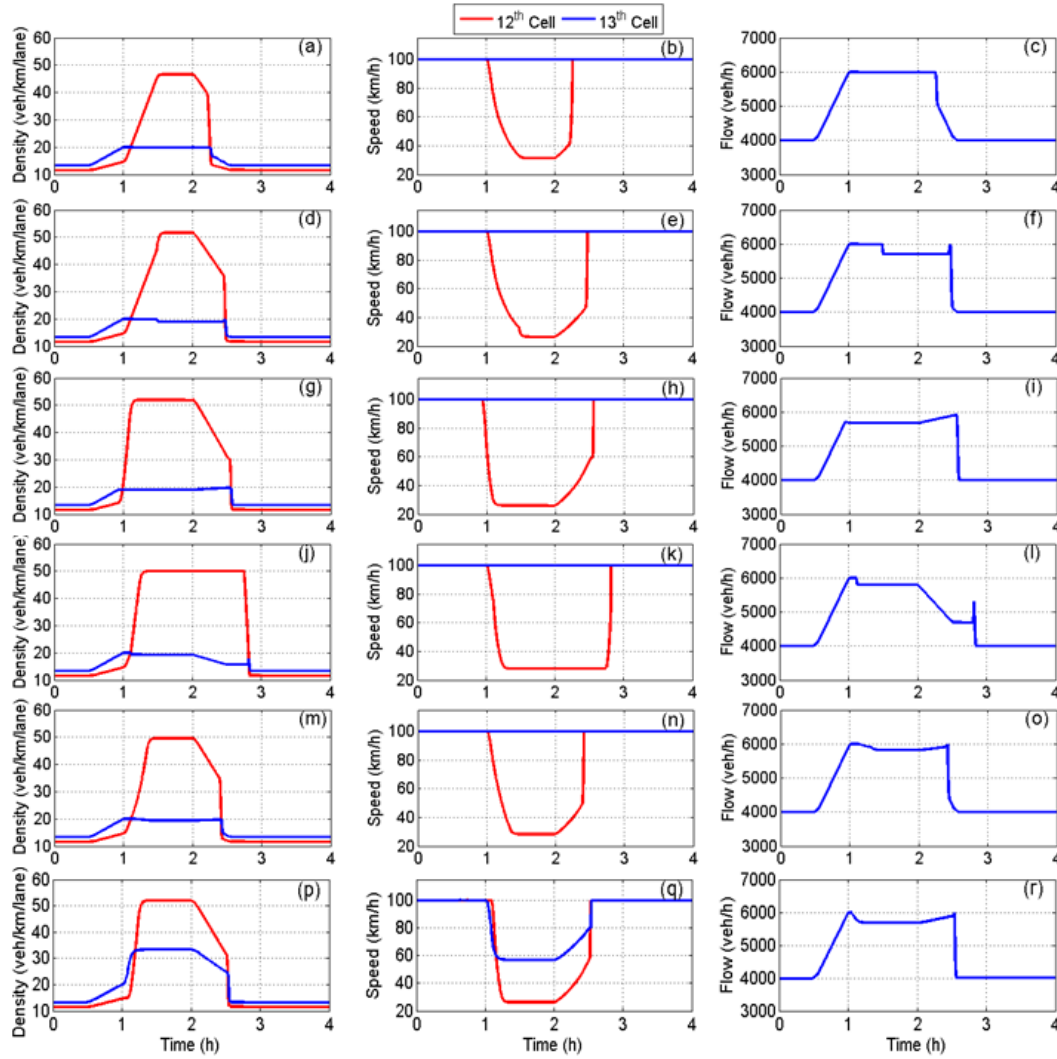


FIGURE 2.7: The time-series of the density of the 12th and 13th cell, the speed of the 12th and 13th cell and the outflow from the 13th cell for the application of (a),(b),(c) CTM, (d),(e),(f) Approach 1, (g),(h),(i) Approach 2, (j),(k),(l) Approach 3, (m),(n),(o) Approach 4, (p),(q),(r) Approach 5.

the integral form of the PDE at the point where the on-ramp is implemented (due to the apparent singularity introduced by the Dirac function). The analysis is then performed by means of the resulting shock speed of the proposed model (following from the Rankine-Hugoniot condition) and by comparing it with the shock speed of the CTM following the methodology described by (LeVeque, 2002). In this case, the analysis indicates that the solution of the discretized model converges (as the discretization parameters tend to zero) to a different solution with a different shock speed from the one imposed by CTM. However, the model is still consistent with the PDE of LWR everywhere else except the point where the on-ramp is implemented. The reader should be transferred to Appendix C for a more detailed justification of the above analysis.

2.3.7 First-order model with drivers' anticipation

Other FOMs, which are not of LWR-type and do not utilize the demand-supply method, have been proposed in the past. For comparison purposes in the calibration procedure of the next section, an alternative FOM, which was first proposed by Lighthill and Whitham, 1955b in order to represent the diffusion of kinematic waves, is introduced. The following discretized formulation is a variation of *Model E* presented and tested in Papageorgiou, Blosseville, and Hadj-Salem, 1989, with the difference that the model is formulated here in terms of flow, instead of speed. The complete model is described by (2.24), (2.38), (2.39) and (2.44):

$$\begin{aligned} f_i(x_i, x_{i+1}, x_{i+2}) &= \beta(1 - p_i)q_i(x_i, x_{i+1}) + (1 - \beta)(q_{i+1}(x_{i+1}, x_{i+2}) - v_{i+1}), \\ f_{n-1}(x_{n-1}, x_n) &= (1 - p_{n-1})q_{n-1}(x_{n-1}, x_n), f_n(x_n(k)) = Q_n^e(x_n), \end{aligned} \quad (2.38)$$

$$q_i(x_i, x_{i+1}) = Q_i^e(x_i) - \frac{\tilde{v}l_i}{\bar{L}_i}(x_{i+1} - x_i), i = 1, \dots, n - 1, q_n(x_n) = Q_n^e(x_n), \quad (2.39)$$

where $0 < \beta \leq 1$ and \tilde{v} are model parameters, q_i represents the total outflow from the i^{th} cell and Q_i^e represents the FD of the i^{th} cell. This model includes an anticipation term that influences the total outflow from a cell according to the downstream prevailing conditions. This mechanism, included in (2.39), suggests that drivers adjust their speed, by also taking into account the downstream density. Moreover, in the space-discretised version, the traffic volume from a cell to another is a convex combination of the total traffic volume of the current and the next cells (2.38). Thanks to the anticipation term, this model is capable to reproduce the capacity drop phenomenon. The utilized mathematical formula for the FD for the calibration test below is given by (2.44). However, it should be noted that in case, for some specific reasons (e.g., the formulation of an optimization problem), linear constraints are needed, this formula may be replaced by a piecewise-linear concave function.

2.3.8 Second-order model METANET

In the calibration tests of the following sections, the SOM METANET (Messmer and Papageorgiou, 1990) is used for comparison purposes (also used in the simulation tests of Chapter 6). For a specific cell $i \in \{1, \dots, n\}$ with length \bar{L}_i and l_i lanes, the nonlinear difference equations of the METANET model are:

$$x_i^+ = x_i + \frac{T}{\bar{L}_i l_i} (-q_i^{int} - q_i^{ext} + q_{i-1}^{int} + \bar{r}_i), \quad (2.40)$$

$$q_i(k) = x_i(k)v_i(k)l_i, q_i^{int}(k) = (1 - p_i)q_i(k), q_i^{ext}(k) = p_i q_i(k), \quad (2.41)$$

$$V_i^e(x_i) = x_i v_{f,i} \exp((-1/a_i)(x_i/\rho_i^{cr})^{a_i}), \quad (2.42)$$

$$v_i^+ = v_i + \underbrace{\frac{T}{\bar{L}_i} v_i (v_{i-1} - v_i)}_{convection} + \underbrace{\frac{T}{\tau} (V_i^e(x_i) - v_i)}_{relaxation} - \underbrace{\frac{\nu T}{\tau^m \bar{L}_i} \left(\frac{x_{i+1} - x_i}{x_i + \kappa} \right)}_{anticipation} - \underbrace{\frac{\delta T}{\bar{L}_i l_i} \left(\frac{\bar{r}_i v_i}{x_i(k) + \kappa} \right)}_{on-ramp}, \quad (2.43)$$

where v_i (in [km/h]) denotes the mean speed of the i^{th} cell, $q_i(k)$ (in [veh/h]) is the total outflow of vehicles leaving cell i during the time period $(kT, (k+1)T]$, \bar{r}_i (in [veh/h]) denotes the actual inflow from the on-ramp i during the time period $(kT, (k+1)T]$. As one can notice, here, for convenience (see Chapter 6), another formulation for the conservation equation is used. It should be emphasized here that METANET allows for very high on-ramp flows to be entered and therefore appropriate bounds should be taken into account for \bar{r}_i (see Chapter 6). Notice also that \bar{r}_i is not necessarily the same with the previously used variable v_i for on-ramp inflows. Moreover, τ^m , ν , δ and κ are model parameters. Moreover, V_i^e denotes the steady-state speed-density relationship that represents the so-called FD of traffic flow, whereby $v_{f,i}$, as previously, is the free-flow speed and $a_i > 0$ is a parameter.

2.4 Calibration Results

In this section the approaches described in Section 2.3 are validated and compared regarding the accuracy of reproducing traffic conditions in a real freeway stretch with particular emphasis on the reproduction of the capacity drop phenomenon.

2.4.1 Freeway Network and Calibration Set-Up

The considered freeway stretch of 9.5 km in length is part of the M56 freeway in the United Kingdom, direction from Chester to Manchester. This 3-lane freeway stretch includes an off-ramp and a two-lane on-ramp, which, before entering the freeway, is divided into two separate lanes. The corresponding on-ramp flows of each lane enter the freeway at two different locations, as shown in Figure 2.8. Figure 2.8 displays the locations of the on-ramps and off-ramp and the locations of the available detector stations. In order to apply the selected traffic flow models, the examined freeway stretch is divided into 38 model cells of about 250 m each, as shown in Figure 2.8. Using this representation, the freeway cells are well-defined, and the model equations presented in the previous section are directly applicable.

The real traffic data used in this study were obtained from the MIDAS database¹. The traffic data include flow and speed measurements at each detector location, with a time resolution of 60 s. The traffic data analysis showed that, within this freeway stretch, recurrent congestion is created during the morning peak hours due to the high on-ramp flow. In particular, Figure 2.9(a) displays the space-time diagram of the real speed measurements for 03/06/2014. It is observed that congestion is created upstream of the second on-ramp during 7–8 a.m. which spills back several kilometers. Moreover, downstream of the second on-ramp, there is an area characterized by low speed, due to the acceleration of vehicles exiting the congestion area. Figure 2.10 presents the time-series of the flow measurements (black line) from detector station D 8180 which is located downstream of the congestion creation area (see, also, Figure 2.8). It is observed that a capacity drop is present there, as the merge area outflow drops visibly when congestion sets in (between 7:10 a.m. and 8:10 a.m.).

In order to apply the examined models to this freeway stretch and achieve a fair comparison, it is important to first calibrate the models using the available real traffic data. The model calibration procedure aims to specify the model parameter values, so that the representation of the network traffic conditions is as accurate as

¹Highways Agency, 2007. Motorway Incident Detection and Automatic Signalling (MIDAS) Design Standard. (No. 1st ed.). Bristol, UK.

TABLE 2.2: Calibrated parameter values for all examined models

Model	v_f	ρ^{cr}	c	ρ^{max}	Q	ρ^a	α	η_r	θ_r
Triang. FD	112	18.7	21.2	117.4	6282	-	-	-	-
Trapez. FD	112	-	21.8	145	6192	-	-	-	-
PWL FD	110.5	24.7	14.8	165.5	6258	14.4	-	-	-
NL FD	113.5	25.3	12.2	195.4	6225	-	-	-	-
Approach 1	123.2	36.4	25.9	124.9	6900	-	0.89	-	-
Approach 2	123.4	35.9	21.9	139.2	6900	-	-	1.56	-
Approach 3	122.8	33.5	21.4	149.1	6900	-	0.72	-	-
Approach 4	123	35.6	25.9	131.2	6900	-	0.63	-	-
Approach 5	122.8	35.6	33.4	104.5	6900	-	0.34	-	0.71
FOM-Ant	119.7	29.4	-	-	6402	-	-	-	-
METANET	114.2	28.9	-	-	6525	-	-	-	-

the model structure allows. This can be achieved by employing a suitable optimization methodology which aims at minimizing the discrepancy between the model estimations and the real traffic data. More details on the utilized model calibration procedure are provided by Spiliopoulou et al., 2014.

In the current study, the Nelder-Mead optimization method is employed for the calibration of the examined traffic flow models. The models are fed with boundary data (inflows at the upstream boundary and the on-ramps and exit rates at the off-ramp) and produce the stretch-internal traffic states according to the respective equations and parameter values. The utilized performance index (PI) under minimization is the Root-Mean-Square Error (RMSE) of the real versus the model-predicted speed values at all detector locations. The models are calibrated using real traffic data from 03/06/2014 and a simulation time step equal to $T = 5$ s. It should be stressed that all cells of the modeled freeway stretch are characterized by the same parameters of the FD for each model. After the calibration procedure, the accuracy and robustness of the resulted models is evaluated by validating the produced models with different traffic data (from the same freeway site) than the data used for their calibration. In this study, the models are validated using real traffic data from 19/06/2014.

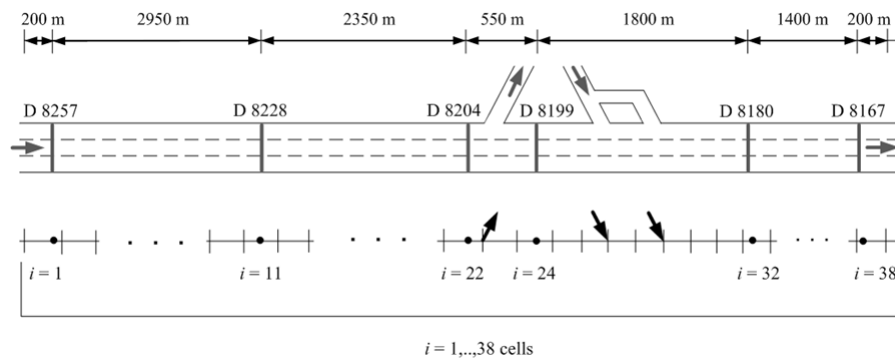


FIGURE 2.8: Representation of the considered freeway stretch in UK.

TABLE 2.3: Performance indices for the calibration and validation days for all examined models

Model	Speed Error	Flow Error	Speed Error	Flow Error
	03/06/2014	03/06/2014	19/06/2014	19/06/2014
Triang. FD	18	625.7	23.4	477.8
Trapez. FD	18	651.8	24.2	473.9
PWL FD	12.6	626.6	19	479.9
NL FD	12.6	653.4	19	487.8
Approach 1	11.6	603	19	425.8
Approach 2	11.9	606.7	18.9	485.8
Approach 3	12.8	685.1	18.9	439.3
Approach 4	11.3	584.3	18.6	425.9
Approach 5	10.9	576	18.4	431.4
FOM-Ant	9.9	598.6	17.2	446.2
METANET	7.9	471.2	14.8	420.6

2.4.2 Basic discretized-LWR formulation

As mentioned before, the investigated capacity drop approaches are based on the discretized LWR model. This basic FOM cannot reflect the capacity drop phenomenon; however, different shapes of the FD may improve the model's accuracy. To investigate this, four different shapes of the FD are examined, all applied to the basic discretized LWR model, i.e. triangular FD, trapezoidal FD, piecewise linear FD, and nonlinear exponential FD (see, Figure 2.5).

Table 2.2 includes the calibrated model parameter values and Table 2.3 the corresponding PI values for the calibration and the validation datasets. It is interesting to see that all four variations (Triang. FD, Trapez. FD, PWL FD, NL FD) produced a similar value for the Q (capacity) parameter. Moreover, as it was expected, the use of a triangular FD results in a low ρ^{cr} value, lower than in the other formulations. Figure 2.9(a)-(e) displays the space-time diagrams of the real speed measurements and the corresponding models' predictions of speed for the calibration date. It is observed that the models using a triangular or a trapezoidal FD predict free flow conditions at all areas outside congestion. In contrast, the use of a piecewise linear or non-linear FD allows for mean speed variations also outside of the congestion area, thus achieving higher accuracy at lower densities, compared to the first two formulations. Considering the above results, LWR-type FOMs with nonlinear FD are used in the subsequent investigations of capacity drop approaches, i.e., the function g , used in the demand function, is an exponential increasing function. More specifically, function g is defined as

$$g(x_i) = v_{f,i} x_i l_i \exp\left(-\frac{1}{a_i} \left(\frac{x_i}{\rho_i^{cr}}\right)^{a_i}\right) \quad (2.44)$$

where $a_i = -1/\ln(Q_i/(l_i v_{f,i} \rho_i^{cr}))$.

2.4.3 Capacity drop approaches

Five capacity drop approaches, which were described in Section 2.3, are implemented for this simple, but typical, freeway stretch. Table 2.2 includes the estimated model parameter values for all five approaches. It should be mentioned that in all examined approaches the maximum capacity flow Q was fixed at 6900 veh/h, which is close to the highest flows observed in the network. This was done in order to achieve a fair comparison of the models regarding the reproduction of the capacity drop phenomenon.

Table 2.2 shows that in all five approaches similar values were estimated for the v_f and ρ^{cr} parameters, while quite different values were obtained for the parameters c and ρ^{max} due to the different formulations adopted for the reproduction of the capacity drop phenomenon. Moreover, it should be noted that, although in all approaches the parameter α is related to the magnitude of the capacity drop, the impact on the resulting capacity drop is substantially different, and for this reason the value of α varies in the different approaches. Table 2.3 presents the PI values for the calibration and the validation datasets. It is observed that the models achieve similar PI values, which implies that they are all able to reproduce the traffic conditions in this network with reasonable and comparable accuracy. More specifically, all approaches, except for Approach 3, improve the PI value compared to the basic LWR model with non-linear FD.

Table 2.2 and Table 2.3 also include the calibration results for the FOM with anticipation (presented in Section 2.3.7) and the SOM METANET (presented in Section 2.3.8), which are applied to this freeway stretch for comparison purposes. Note that Table 2.2 presents only some of the estimated parameters of these two models while the rest parameters were estimated equal to: $\tilde{v}=6.4 \text{ km}^2/\text{h}$ and $\beta=0.76$ for the FOM with anticipation and $\tau=26.8 \text{ s}$, $\nu=45.6 \text{ km}^2/\text{h}$, $\delta=0.1 \text{ h/km}$, $\kappa=10 \text{ veh/km/lane}$, $v_{min}=7 \text{ km/h}$ for METANET model.

Figure 2.9(f)-(j) presents the space-time diagrams of the corresponding speed estimations for all five capacity-drop approaches for the calibration date. It is observed that the estimations of all five approaches are close to the real speed data and are actually similar to each other. Figure 2.9(k)-(l) displays the corresponding speed estimations of the FOM with anticipation and the SOM METANET. It is shown here that the FOM with anticipation achieves a remarkably high accuracy in representing the prevailing traffic conditions thanks to the included anticipation term (Eq. (2.39)). On the other hand, METANET model produces, as expected, the most realistic representation of the traffic characteristics, thanks to the fact that it accounts also the vehicle acceleration capabilities and the driver reaction time.

Regarding the reproduction of the capacity drop phenomenon, Figure 2.10 displays the time-series of the real flow measurements and the corresponding models' estimations at the location of detector station D 8180 (see, Figure 2.8), which is placed about 800 m downstream of the merge area. It is observed that, except for the basic LWR model with nonlinear FD, all five approaches produce a reduced merge area outflow during the congestion period. Moreover, all approaches, except for Approach 2, are capable to estimate a high merge area outflow (close to capacity) just before the onset of congestion, which is in accordance with the real flow values observed. Figure 2.10(g) shows that the FOM with anticipation also produces a reduced merge area outflow, however with a smaller flow drop than the real observed flow drop. Finally, Figure 2.10(h) presents the flow estimations of the SOM METANET which are very close to the real traffic measurements.

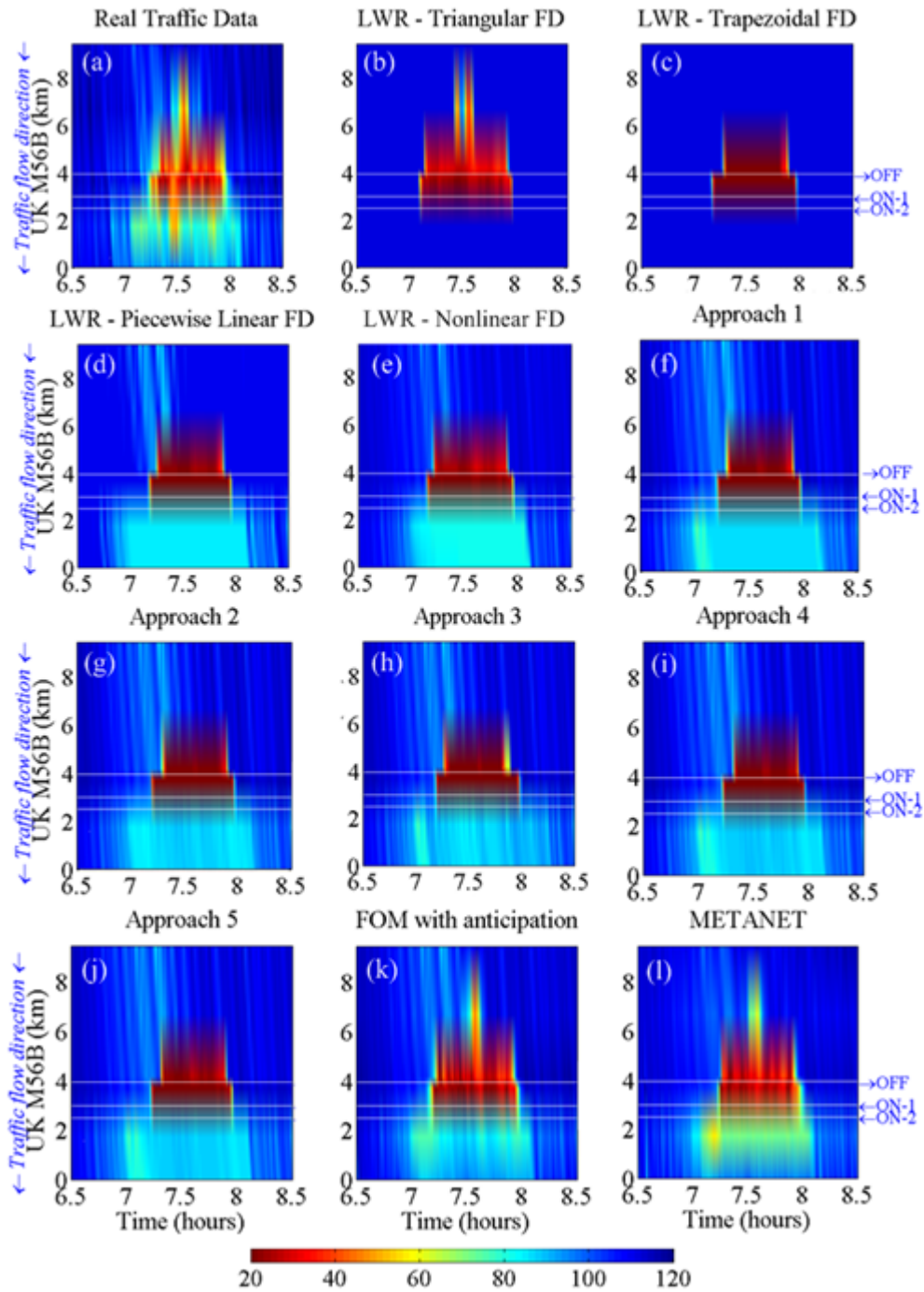


FIGURE 2.9: Space-time diagrams of speed for (a) the real traffic data; (b) the LWR model with triangular FD; (c) the LWR model with trapezoidal FD; (d) the LWR model with piecewise linear FD; and (e) the LWR model with nonlinear FD; (f) Approach 1; (g) Approach 2; (h) Approach 3; (i) Approach 4; (j) Approach 5; (k) FOM with anticipation; and (l) METANET model for 03/06/2014.

In order to evaluate quantitatively the accuracy of the five approaches in reproducing the capacity drop phenomenon, the RMSE of the real flow measurements and the corresponding model estimations of flow is calculated, for the freeway cell where the detector station D 8180 is located and for a time window around the time

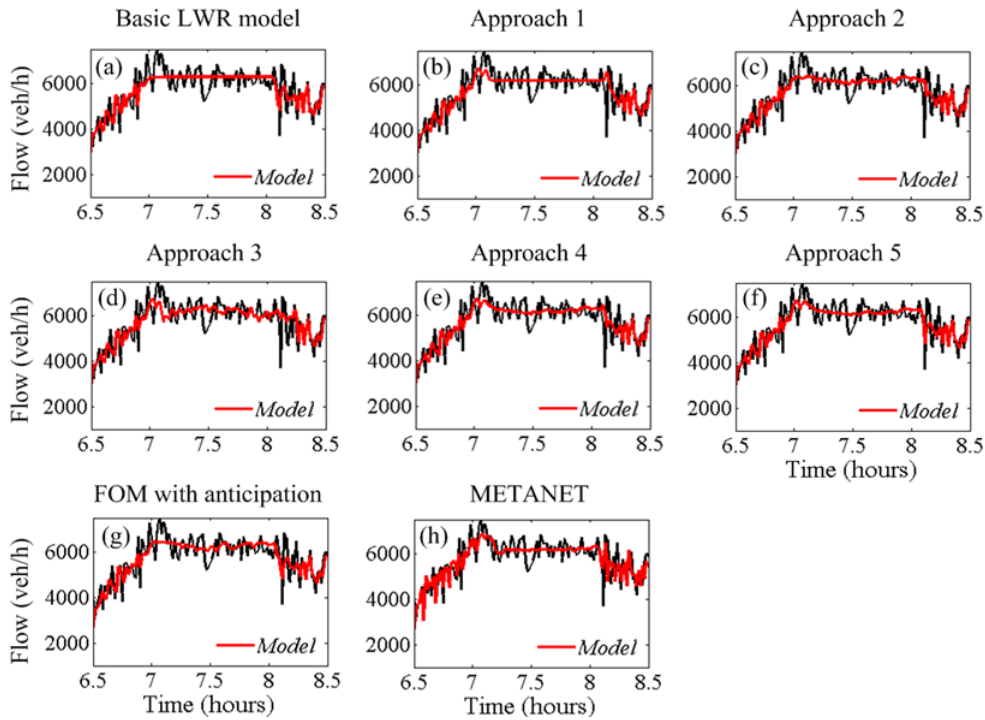


FIGURE 2.10: Time-series of the real flow measurements at the location of detector station D 8180 and the corresponding flow estimations of (a) the basic LWR model; (b) Approach 1; (c) Approach 2; (d) Approach 3; (e) Approach 4; (f) Approach 5; (g) FOM with anticipation; and (h) METANET model; for 03/06/2014.

when capacity drop appears (i.e. between 7–7:15 a.m.). Table 2.3 includes the corresponding flow error for all examined models for the calibration and the validation datasets. It is observed that all approaches, except for Approach 3, for the calibration day, and Approach 2, for the validation day, achieve a lower error compared to the basic LWR formulation without capacity drop. Furthermore, the FOM with anticipation, although reproducing correctly the propagation of congestion (as it can be also deduced from the low PI value), seems less capable to create a satisfactory capacity drop. As Table 2.3 shows, the flow error in Approach 4 and Approach 5 is noticeably smaller than the flow error of the FOM with anticipation. Finally, it is noted that the SOM METANET achieves the highest accuracy in reproducing the capacity drop compared to all employed FOMs.

Figure 2.11 displays the flow versus density diagram (i.e., the FD) at the merge cell (cell 29th, Figure 2.8) for the basic LWR model (again, using a nonlinear demand part of the FD) and all five approaches. It is observed that, as expected, the basic LWR model is not able to reproduce the capacity drop phenomenon (see Figure 2.10(a) and Figure 2.11(a)). Comparing the five examined approaches, it is observed that actually only Approach 1, Approach 4 and Approach 5 produce a capacity drop at the merge cell, resulting though in different FD shapes (due to their different formulations).

In particular, in Approach 1 the merge area discharge flow corresponds exactly to the pre-specified value $\bar{Q} = aQ = 6141 \text{ veh/h}$ (see Figure 2.11(b)). In Approach 4 (see Figure 2.11(e)), the magnitude of the observed capacity drop varies according to the density of the upstream cell; i.e. in case of stronger congestion, characterized by a

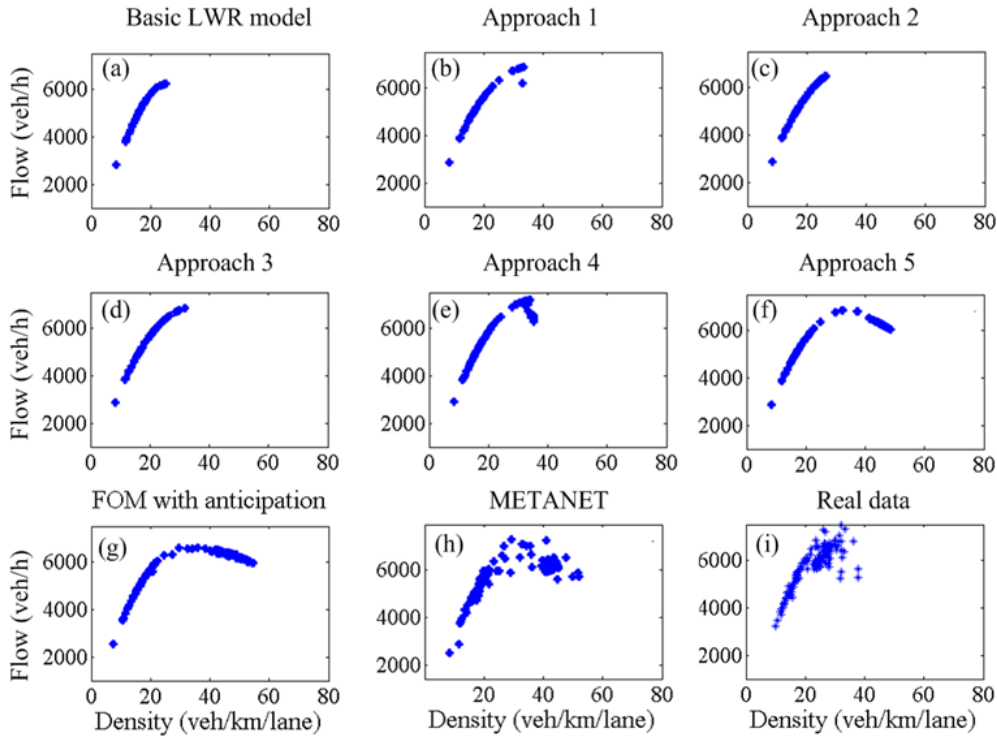


FIGURE 2.11: Flow-density diagram at the merge cell using (a) the basic LWR model; (b) Approach 1; (c) Approach 2; (d) Approach 3; (e) Approach 4; (f) Approach 5; (g) FOM with anticipation; (h) METANET model; and (i) real data at detector D 8180, for 03/06/2014.

lower speed, a stronger capacity drop is observed, which is in accordance with some traffic observations. Finally, in Approach 5, the capacity drop observed follows the shape of the demand function of the merge cell while the magnitude of the observed capacity drop also depends on the magnitude of the applied on-ramp volume (see Figure 2.11(f)). On the other hand, Approach 2 and Approach 3 do not produce a capacity drop at the merge cell (see Figure 2.11(c) and Figure 2.11(d)) although they manage to produce a reduced outflow from the merge area during congestion period (see Figure 2.10(c) and Figure 2.10(d)). In particular, in Approach 2 the observed merge area outflow never reaches capacity, even before the onset of congestion, in accordance with the behavior described in Section 3. Moreover, regarding Approach 3, the discharge flow that materializes is also dependent on the on-ramp flow entering the merge cell (which causes the fluctuations that can be observed in the corresponding plot), whereas the mainstream flow exiting the cell upstream of the merge cell, during the congestion period, is constantly equal to $\bar{Q} = aQ = 4968 \text{ veh/h}$. Figure 2.11 also includes, for comparison, the flow versus density diagram at the merge cell for the FOM with anticipation (Figure 2.11(g)) and the SOM METANET (Figure 2.11(h)); as well as the corresponding real-data diagram at the location of the detector station D 8180, which is about 800 m downstream of the merge area (Figure 2.11(i)). As a result, Figure 2.11(i) cannot be directly compared to the other plots, but it is included here as it corresponds to the closest measurement point downstream of the bottleneck location. Notice that the density in Figure 2.11(i) has been estimated from flow and speed measurements by $x(t) = q(t)/v(t)$.

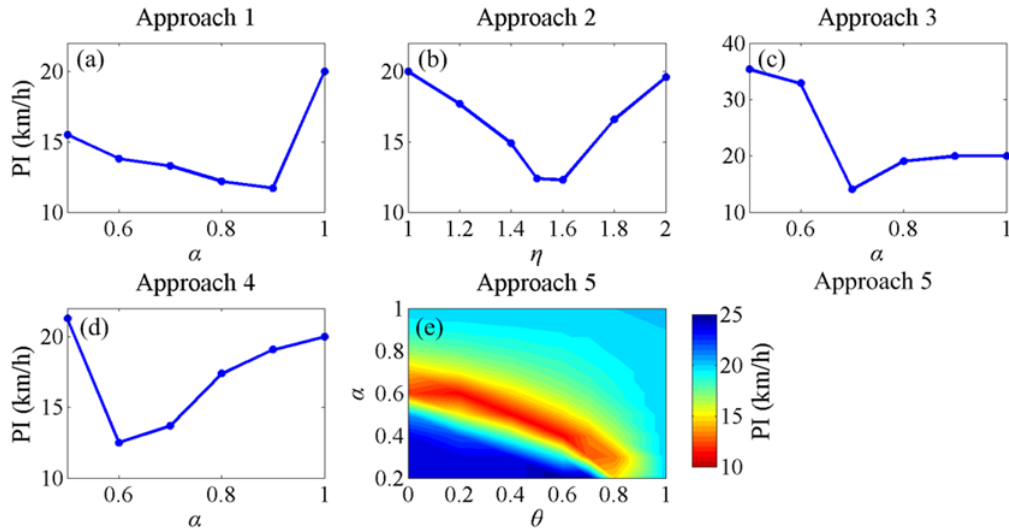


FIGURE 2.12: Sensitivity investigations in changes to the models' parameters related to the capacity drop, in terms of PI value for (a) Approach 1; (b) Approach 2; (c) Approach 3; (d) Approach 4; and (e) Approach 5 for 03/06/2014.

While examining the presented five approaches, a question was raised regarding the sensitivity of the models to variations of the parameters α or η_r and/or θ_r (depending on the approach) which are involved in the reproduction of the capacity drop phenomenon. To investigate this issue, different values were fixed for these parameters and the models were calibrated again (with respect to the rest parameters) for each examined value. Figure 2.12 displays all the related results. As an example, Figure 2.12(a) presents the best obtained PI values after calibrating Approach 1 for different fixed values of the parameter α within the range [0.5, 1]. It is observed that the model achieves lowest PI values for α close to 0.9. Similarly, in Approach 2 the PI is minimized for η_r in the range [1.4, 1.5] (Figure 2.12(b)), in Approach 3 for α close to 0.7 (Figure 2.12(c)) and in Approach 4 for α close to 0.6 (Figure 2.12(d)). Regarding Approach 5, which includes two parameters related to the capacity drop, α and θ_r , the investigations include different coupled values of these two parameters and the model was calibrated again for each one of these couples. Figure 2.12(e) presents the best obtained PI value for each investigated couple. It may be seen that different coupled values of the two parameters lead to equally low PI values. This means that these two parameters are strongly correlated. Considering the above investigations, it is concluded that the models are sensitive to the value of the parameters related to the capacity drop. Finally, note that for $\alpha = 1$, in Approach 1, 3 and 4, and for $\eta_r = 1$ and $\theta_r = 1$, in Approach 2 and Approach 5, respectively, the basic LWR model is obtained.

Chapter 3

Global Exponential Stabilization of Acyclic Traffic Networks

3.1 Introduction

This chapter presents a rigorous methodology for the construction of explicit feedback laws that guarantee the RGES of the UEP for the general nonlinear discrete-time acyclic traffic networks presented in Section 2.2.1. Traffic networks, satisfying specific assumptions, have been studied by Coogan and Arcak, 2014, where sufficient conditions for the local stability of the UEP are provided; while Gomes et al., 2008 analyze the equilibriums of the CTM based on monotone systems theory. There are several other works that address stability issues within more specific modeling frameworks for traffic networks. For example, Haddad and Geroliminis, 2012 derive necessary and sufficient conditions for stable equilibrium accumulations in the undersaturated regimes of macroscopic FDs; while Smith, 1984 studies the stability of equilibriums of a traffic assignment model. However, studies that address rigorously stabilization issues are quite rare. Stability results for simple traffic control systems have been considered by Karafyllis and Papageorgiou, 2014, where sufficient conditions for the local and global ISS property of vehicular-traffic networks are provided under the effect of PI regulators. Moreover, Li et al., 1997 propose link layer feedback (velocity) control laws that stabilize simple, multi-lane and two-dimensional freeway models.

Based on the proposed general modeling framework presented in Section 2.2.1, the results provided by Karafyllis and Papageorgiou, 2015, and specifically Theorem A.5 (see Appendix A), are utilized for the developed uncertain models of acyclic networks. More specifically, this chapter provides a parameterized family of explicit feedback control laws which can robustly globally exponentially stabilize the desired UEP of a given acyclic traffic network. The achieved stabilization is robust with respect to: i) any uncertainty related to the FD of traffic flow; as well as ii) the overall uncertain nature of the developed model when congestion phenomena are present. In fact, in the latter case, the model which describes the time evolution of the network variables is almost completely uncertain (besides the requirement of known and constant turning and exit rates). Furthermore, the assumptions that surround the proposed methodology are weak enough to render the methodology applicable to other kinds of acyclic networks instead of traffic networks. Finally, we emphasize that, as it is proved herein (Proposition 3.2), the requirement regarding the absence of cycles inside the network is utterly necessary for the existence of a robust global exponential stabilizer of the UEP of the network. The present methodology can also be used as perimeter control strategy as well as for arterial (or corridor) networks with arbitrary topology that contain no cycles. To the best of the author's knowledge, this is the first study that addresses rigorously global stabilization issues for

such problems.

The structure of the present chapter is as follows: Section 3.2 presents the main results of this chapter, while the proofs of the main results can be found in Section 3.3. An illustrative example of a freeway-to-freeway network is presented in Section 3.4.

3.2 Main Results

The acyclic traffic model presented in Section 2.2.1 is considered in this chapter. For convenience reasons, here the corresponding model is rewritten. Consider the following nonlinear uncertain discrete space-time system for $i = 1, \dots, n$:

$$x_i^+ = x_i + \bar{s}_i(d, x, v)v_i - s_i(d, x, v)f_{D,i}(d, x_i) + \sum_{j=1}^n b_{j,i}s_j(d, x, v)f_{D,j}(d, x_j), \quad (3.1)$$

under Assumptions (H 2.1), (H 2.2), (H 2.3), (H 2.4). We next assume the existence of a point $x^* = (x_1^*, \dots, x_n^*)' \in S$ with $x_i^* \in (0, \mu_i)$ for $i = 1, \dots, n$ and a vector $v^* = (v_1^*, \dots, v_n^*)' \in \mathfrak{R}_+^n$ with $v_i^* < v_i^{max}$ for $i = 1, \dots, n$, that satisfy the following equations:

$$f_{D,i}(d, x_i^*) = v_i^* + \sum_{j=1}^n b_{j,i}f_{D,j}(d, x_j^*), \text{ for all } i = 1, \dots, n, d \in D. \quad (3.2)$$

Since $x_i^* \in (0, \mu_i)$, $v_i^* < v_i^{max}$, for $i = 1, \dots, n$, it follows from Assumption (H 2.4) that the following inequalities hold:

$$v_i^* + \sum_{j=1}^n b_{j,i}f_{D,j}(d, x_j^*) < f_{S,i}(d, x^*), \text{ for all } i = 1, \dots, n, d \in D. \quad (3.3)$$

The point $x^* = (x_1^*, \dots, x_n^*)' \in S$ is called the UEP of the network corresponding to the vector of external inflows $v^* = (v_1^*, \dots, v_n^*)' \in \mathfrak{R}_+^n$. Notice that the input $d \in D$ is a vanishing perturbation for system (3.1) with $v(t) \equiv v^*$. This is also illustrated in Figure 2.1, which shows that the input $d \in D$ does not change the position of the equilibrium point (denoted by a star).

Proposition 3.2

Consider the network (3.1) under Assumptions (H 2.1), (H 2.4). Assume the existence of a point $x^* = (x_1^*, \dots, x_n^*)' \in S$ with $x_i^* \in (0, \mu_i)$ for $i = 1, \dots, n$ and a vector $v^* = (v_1^*, \dots, v_n^*)' \in \mathfrak{R}_+^n$ with $v_i^* < \min(v_i^{max}, \min\{f_{S,i}(d, 0) : d \in D\})$ for $i = 1, \dots, n$, that satisfy equations (3.2). Assume that the network contains at least one cycle. Then, system (3.1) with input $(v, d) \in \mathfrak{R}_+^n \times D$ is not globally asymptotically controllable to the equilibrium point $x^* = (x_1^*, \dots, x_n^*)' \in S$.

Proposition 3.2 is one of the most important consequences of the existence of an UEP and Assumptions (H 2.1), (H 2.2), (H 2.3), (H 2.4). More specifically, the Proposition 3.2 reveals the reason for studying acyclic networks (explicitly guaranteed by (H 2.2)) and shows that if the network contains cycles, then the system is not globally asymptotically controllable to the UEP. That means that Assumption (H 2.2) is utterly necessary in order to proceed to the study of the stabilization of the network (3.1) because otherwise there is no feedback control law which can render the UEP globally exponentially stable.

We next assume that some of the external inflows may be controlled. Let $v^{min} \in \mathbb{R}_+^n$ be a vector with $v^{min} \leq v^*$, let $K \in \mathbb{R}_+^{n \times n}$ be a non-negative, constant matrix and let $\tau > 0$ be a constant. We set:

$$v = v^* - \text{diag}(v^* - v^{min}) (1_n - h(1_n - \tau^{-1}Kh(x - x^*))), \quad (3.4)$$

where $h : \mathbb{R}^n \rightarrow \mathbb{R}_+^n$ is the mapping defined by:

$$h(x) = (\max(0, x_1), \dots, \max(0, x_n))' \in \mathbb{R}_+^n \quad (3.5)$$

for all $x \in \mathbb{R}^n$. Notice that if $v_i^{min} = v_i^*$ for some $i \in \{1, 2, \dots, n\}$ then it follows from (3.4) that $v_i = v_i^*$, i.e., the external inflow v_i is uncontrolled. Therefore, by assuming (3.4), we have taken into account all possible cases for the control of external inflows. We intend to prove the following theorem, which shows that the UEP can be robustly, globally, exponentially stabilized by the continuous feedback law (3.4), which regulates certain or all the external inflows.

Theorem 3.3

Consider the network (3.1) under Assumptions (H 2.1), (H 2.2), (H 2.3), (H 2.4). Assume the existence of a point $x^* = (x_1^*, \dots, x_n^*)' \in S$ with $x_i^* \in (0, \mu_i)$ for $i = 1, \dots, n$ and a vector $v^* = (v_1^*, \dots, v_n^*)' \in \mathbb{R}_+^n$ with $v_i^* < \min(v_i^{max}, \min\{f_{S,i}(d, 0) : d \in D\})$ for $i = 1, \dots, n$, that satisfy equations (3.4). Then there exists an index set $R \subseteq \{i \in \{1, \dots, n\} : v_i^* > 0\}$, a matrix $K \in \mathbb{R}_+^{n \times n}$ and a vector $v^{min} \in \mathbb{R}_+^n$ with $0 < v_i^{min} < v_i^*$ for $i \in R$, $v_i^{min} = v_i^*$ for $i \notin R$ such that for every $\tau \in (0, 1)$, $x^* = (x_1^*, \dots, x_n^*)' \in S$ is RGES for the closed-loop system (3.1) with (3.4).

Theorem 3.3 is an existence result. However, its proof is constructive and provides formulae (or sufficient conditions) for all constants and for the index set R . Notice that the index set R is the set of all inflows that must be controlled in order to be able to guarantee that the UEP is RGES. The importance of Theorem 3.3 lies on the following facts:

1. It provides a family of robust, global, exponential stabilizers (parameterized by $\tau \in (0, 1)$) and an explicit feedback law (formula (3.4)).
2. The achieved stabilization is robust with respect to:
 - (a) The uncertain nature (introduced by $d \in D$) of the FD of traffic flow (by considering uncertain $f_{D,i}(d, \cdot)$ and $f_{S,i}(d, \cdot)$, respectively).
 - (b) The overall uncertain nature of the model (3.1) when congestion phenomena are present (by considering uncertain functions $s_i(d, \cdot, \cdot)$ and $\bar{s}_i(d, \cdot, \cdot)$).

Notice here, that the only requirements regarding the functions s_i (and \bar{s}_i , respectively) are summarized within the implication (2.8) and Assumption (H 2.3). However, implication (2.8) is not a strict requirement since it allows the functions s_i (for $i = 1, \dots, n$) to take any value within $[0, 1]$, when at least one cell is congested. One possibility for the uncertainty within the functions s_i (for $i = 1, \dots, n$) is to be represented with respect to unknown and even time-varying priority rules as presented in Section 2.2.3 (formula (2.16)); however, here, this type of uncertainty may be enhanced by considering priority rules for all the internal inflows of the network. Notice also, that the only requirements regarding the functions $f_i(d, \cdot)$ and $f_{S,i}(d, \cdot)$ are summarized within Assumption (H 2.1) and the inequality $f_{S,i}(d, x) \leq \rho_i^{max} - x_i$

which again allow for a large variety of FDs to be considered (see the illustrative example in the following section).

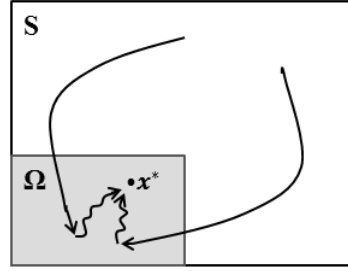


FIGURE 3.1: Idea behind Theorem 3.3.

The main idea behind the proof of Theorem 3.3 is the construction of a VLF for the closed-loop system. The construction of the VLF is based on the existence of a Trapping Region (TR) Ω for the system (3.1) in which no congestion phenomena are present. The appropriate selection of the gain matrix $K \in \mathbb{R}_+^{n \times n}$ in (3.4) forces the selected control action to lead the state in the set Ω (see Figure 3.1). In other words, the control action will first eliminate all congestion phenomena and then will drive the state to the desired equilibrium.

Proposition 3.4

Consider the network (3.1) under Assumptions (H 2.1), (H 2.2), (H 2.3), (H 2.4). Assume the existence of a point $x^* = (x_1^*, \dots, x_n^*)' \in S$ with $x_i^* \in (0, \mu_i)$ for $i = 1, \dots, n$ and a vector $v^* = (v_1^*, \dots, v_n^*)' \in \mathbb{R}_+^n$ with $v_i^* < v_i^{max}$ for $i = 1, \dots, n$, that satisfy equations (3.2). Then there exist constants $\beta_i \in (x_i^*, \mu_i]$ ($i = 1, \dots, n$) such that for every $v^{min} \in \mathbb{R}_+^n$ with $v^{min} \leq v^*$, $K \in \mathbb{R}_+^{n \times n}$ and $\tau > 0$ it holds that:

$$x \in \Omega, d \in D \Rightarrow x^+ \in \Omega, \quad (3.6)$$

where $\Omega = [0, \beta_1] \times \dots \times [0, \beta_n]$, $h : \mathbb{R}^n \rightarrow \mathbb{R}_+^n$ is the mapping defined by (3.5) and x^+ is given by (3.1) with (3.4).

Proposition 3.4 shows the existence of a positively invariant region for (3.1). Implication (3.6) shows that $\Omega \subset S$ is a positively invariant region for inputs that satisfy $d(t) \in D$ and $0 \leq v(t) \leq v^* - \text{diag}(v^* - v^{min})(1_n - h(1_n - \tau^{-1}Kh(x(t) - x^*)))$ for all $t \geq 0$. It should be noticed that $x^* \in \text{int}(\Omega)$, i.e., the UEP is in the interior of the positively invariant region. In order to study the stability properties of the UEP of the network (3.1), we need the technical lemmas below.

More specifically, Lemma 3.7 shows the existence of a TR for system (3.1) and Theorem 3.8 shows that the UEP is RGES for the system (3.1) under the proposed feedback regulator (3.4). The proof of Theorem 3.8 is based on Theorem A.5 and therefore on the construction of a VLF. Theorem 3.8 is utilized in order to prove the main result of this section, i.e., Theorem 3.3. The proofs of the lemmas below are provided in the Appendix B.

Lemma 3.5

Consider the network (3.1) under Assumptions (H 2.1), (H 2.2), (H 2.3), (H 2.4). Assume the existence of a point $x^* = (x_1^*, \dots, x_n^*)' \in S$ with $x_i^* \in (0, \mu_i)$ and a vector $v^* = (v_1^*, \dots, v_n^*)' \in \mathbb{R}_+^n$ with $v_i^* < v_i^{max}$ ($i = 1, \dots, n$), that satisfy equations (3.2). Then there exist constants $\beta_i \in (x_i^*, \mu_i]$ ($i = 1, \dots, n$) such that for every $b \in \mathbb{R}_+^n$ with $b \leq v^*$, $K \in \mathbb{R}_+^{n \times n}$ and $\tau > 0$, implication (3.6) holds and such that:

$$\begin{aligned} x \in \Omega, d \in D \Rightarrow \\ h(x^+ - x^*) \leq (I + B' \text{diag}(G) - \text{diag}(L))h(x - x^*), \end{aligned} \quad (3.7)$$

$$\begin{aligned} x \in \Omega, d \in D \Rightarrow \\ h(x^* - x^+) \leq (I + B' \text{diag}(G) - \text{diag}(L))h(x^* - x) + \text{diag}(v^* - b)\tau^{-1}Kh(x - x^*), \end{aligned} \quad (3.8)$$

where $\Omega = [0, \beta_1] \times \dots \times [0, \beta_n]$, $h : \mathbb{R}^n \rightarrow \mathbb{R}_+^n$ is the mapping defined by (3.5), $L = (L_1, \dots, L_n)' \in \mathbb{R}^n$, $G = (G_1, \dots, G_n)' \in \mathbb{R}^n$, $B \in \mathbb{R}^{n \times n}$ is the matrix $B = \{b_{i,j} : i, j = 1, \dots, n\}$ and x^+ is given by (3.1) with (3.4).

Lemma 3.6

Consider the network (3.1) under Assumptions (H 2.1), (H 2.2), (H 2.3), (H 2.4). Assume the existence of a point $x^* = (x_1^*, \dots, x_n^*)' \in S$ with $x_i^* \in (0, \mu_i)$ and a vector $v^* = (v_1^*, \dots, v_n^*)' \in \mathbb{R}_+^n$ with $v_i^* < v_i^{max}$ ($i = 1, \dots, n$), that satisfy equations (3.2). Then there exist constants $\beta_i \in (x_i^*, \mu_i]$ ($i = 1, \dots, n$) such that for every $v^{min} \in \mathbb{R}_+^n$ with $v^{min} \leq v^*$, $K \in \mathbb{R}_+^{n \times n}$ and $\tau > 0$, implications (3.6), (3.7), (3.8) hold and there exists a constant $M > 0$ (depending on $b \in \mathbb{R}_+^n$, $K \in \mathbb{R}_+^{n \times n}$ and $\tau > 0$), which satisfies the following property:

$$x \in S, d \in D \Rightarrow |x^+ - x^*| \leq M|x - x^*|, \quad (3.9)$$

where x^+ is given by (3.1) with (3.4).

Lemma 3.7

Consider the network (3.1) under Assumptions (H 2.1), (H 2.2), (H 2.3), (H 2.4). Assume the existence of a point $x^* = (x_1^*, \dots, x_n^*)' \in S$ with $x_i^* \in (0, \mu_i)$ and a vector $v^* = (v_1^*, \dots, v_n^*)' \in \mathbb{R}_+^n$ with $v_i^* < \min(v_i^{max}, \min\{f_{S,i}(d, 0) : d \in D\})$ ($i = 1, \dots, n$), that satisfy equations (3.2). Let $r = (r_1, \dots, r_n)' \in \text{int}(\mathbb{R}_+^n)$ be the constants involved in Lemma A.7 and let $C > 0$ be the corresponding constant for which inequality (2.13) holds for all $(d, x) \in D \times S$ and for all $v_i \geq 0$ with $v_i \leq v_i^*$ ($i = 1, \dots, n$). Assume that there exist $v^{min} \in \mathbb{R}_+^n$ with $v^{min} \leq v^*$ such that:

$$r'v^{min} \leq C \min_{i=1, \dots, n} (r_i x_i^*). \quad (3.10)$$

Then there exist constants $\beta_i \in (x_i^*, \mu_i]$ ($i = 1, \dots, n$) and a matrix $K \in \mathbb{R}_+^{n \times n}$ such that for every $\tau \in (0, 1)$ implications (3.6), (3.7), (3.8) hold and the set $\Omega = [0, \beta_1] \times \dots \times [0, \beta_n]$ is a TR for the closed-loop system (3.1) with (3.4).

Theorem 3.8

Consider the network (3.1) under Assumptions (H 2.1), (H 2.2), (H 2.3), (H 2.4). Assume the existence of a point $x^* = (x_1^*, \dots, x_n^*)' \in S$ with $x_i^* \in (0, \mu_i)$ for $i = 1, \dots, n$ and a vector $v^* = (v_1^*, \dots, v_n^*)' \in \mathbb{R}_+^n$ with $v_i^* < \min(v_i^{max}, \min\{g_i(d, 0) : d \in D\})$, for $i = 1, \dots, n$, that satisfy equations (3.2). Let $r = (r_1, \dots, r_n)' \in \text{int}(\mathbb{R}_+^n)$ be the constants involved in Lemma A.7 and let $C > 0$ be the corresponding constant for which inequality (2.13) holds for all $(d, x) \in D \times S$ and for all $v_i \geq 0$ with $v_i \leq v_i^*$ ($i = 1, \dots, n$). Assume that there exist $v^{min} \in \mathbb{R}_+^n$ with $v^{min} \leq v^*$ such that (3.10) holds. Then there exist constants $\beta_i \in (x_i^*, \mu_i]$ ($i = 1, \dots, n$) and a matrix $K \in \mathbb{R}_+^{n \times n}$ such that for every $\tau \in (0, 1)$, implications (3.6), (3.7), (3.8) hold and the equilibrium point $x^* = (x_1^*, \dots, x_n^*)' \in S$ is RGES for the closed-loop system (3.1) with (3.4).

Finally, the following corollary provides sufficient conditions for the RGES of the UEP for the open-loop system (3.1) with $v = v^*$. The sufficient conditions are given by means of the selection of UEP. Its proof is provided in the next section.

Corollary 3.9

Consider the network (3.1) under Assumptions (H 2.1), (H 2.2), (H 2.3), (H 2.4). Assume the existence of a point $x^* = (x_1^*, \dots, x_n^*)' \in S$ with $x_i^* \in (0, \mu_i)$ and a vector $v^* = (v_1^*, \dots, v_n^*)' \in \mathbb{R}_+^n$ with $v_i^* < \min(v_i^{max}, \min\{f_{S,i}(d, 0) : d \in D\})$, for $i = 1, \dots, n$, that satisfy equations (3.2). Let $r = (r_1, \dots, r_n)' \in \text{int}(\mathbb{R}_+^n)$ be the constants involved in Lemma A.7 and let $C > 0$ be the corresponding constant for which inequality (2.13) holds for all $(d, x) \in D \times S$ and for all $v_i = v_i^*$ ($i = 1, \dots, n$). Assume that

$$r'v^* \leq \min_{i=1, \dots, n} (r_i x_i^*). \quad (3.11)$$

Then the equilibrium point $x^* = (x_1^*, \dots, x_n^*)' \in S$ is RGES for the open-loop system (3.1) with $v = v^*$.

3.3 Proofs of Main Results

Proof of Proposition 3.2: Let the index set $E \subseteq \{1, \dots, n\}$ be the set of all the indices of the cells that are in one of the cycles in the network (3.1). Let also $e \leq n$ be the cardinality of the set E . Then, we define $E := \{i_1, i_2, \dots, i_e\}$ so that $b_{i_1, i_2}, b_{i_2, i_3}, \dots, b_{i_{e-1}, i_e}, b_{i_e, i_1} \neq 0$. Moreover, consider an initial condition $x(0)$ for which $x_{i_k}(0) = a_{i_k}$ for every $k = 1, \dots, e$ (but otherwise arbitrary) and let $\{d(t) \in D\}_{t=0}^\infty$ and $\{v(t) \in U\}_{t=0}^\infty$ be arbitrary sequences. Due to the fact that $g_{i_k}(d, x) = 0$ if $x_{i_k} = a_{i_k}$ (direct consequence of continuity of $g_i(d, x)$ and the fact that $0 < g_i(d, x) \leq \rho_i^{max} - x_i$ for every $i = 1, \dots, n$) for every $k = 1, \dots, e$, we have from (2.7) that for $k = 1$:

$$F_{i_1}^{in}(0) = 0 \Rightarrow \bar{s}_{i_1}(d(0), x(0), v(0))v_{i_1}(0) + \sum_{j=1}^n b_{j, i_1} s_j(d(0), x(0), v(0))f_j(d(0), x_j(0)) = 0 \Rightarrow$$

$$\begin{aligned} \bar{s}_{i_1}(d(0), x(0), v(0))v_{i_1}(0) + \sum_{j=1}^n b_{j,i_1} s_j(d(0), x(0), v(0)) f_j(d(0), x_j(0)) &= 0 \\ \text{and } \sum_{j=1}^n b_{j,i_1} s_j(d(0), x(0), v(0)) f_j(d(0), x_j(0)) &= 0. \end{aligned}$$

But the fact that $\sum_{j=1}^n b_{j,i_1} s_j(d(0), x(0), v(0)) f_j(d(0), x_j(0)) = 0$ implies that:

$$\begin{aligned} b_{i_e, i_1} s_{i_e}(d(0), x(0), v(0)) f_{i_e}(d(0), x_{i_e-1}(0)) &= b_{i_e, i_1} s_{i_e}(d(0), x(0), v(0)) f_{i_e}(d(0), a_{i_e}) \\ &= b_{i_e, i_1} s_{i_e}(d(0), x(0), v(0)) f_{i_e}^{min} = 0 \Rightarrow s_{i_e}(d(0), x(0), v(0)) = 0. \end{aligned}$$

Repeating the above process for every $k = 1, \dots, e$, we obtain that $\bar{s}_{i_k}(d(0), x(0), v(0)) = 0$ and $s_{i_k}(d(0), x(0), v(0)) = 0$ for every $k = 1, \dots, e$. Therefore, we conclude from (3.1) that $x_{i_k}(1) = x_{i_k}(0) = a_{i_k}$. Using induction, it follows that $x_{i_k}(t) = a_{i_k}$ for every $t \geq 0$. The proof is complete. \triangleleft

Proof of Proposition 3.4: Lemma A.8 guarantees that there exists $\xi \in \text{int}(\mathfrak{R}_+^n)$ such that $\sum_{j=1}^n b_{j,i} G_j \xi_j < L_i \xi_i$, for $i = 1, \dots, n$. Using (A.7) and the fact that $h(x) \leq \xi$ for all $x \in \mathfrak{R}^n$ with $x \leq \xi$, we have that:

$$(I + B' \text{diag}(G) - \text{diag}(L)) h(x) < \xi. \quad (3.12)$$

Since $x_i^* \in (0, \mu_i)$, for $i = 1, \dots, n$, there exists a constant $\varepsilon^* > 0$, sufficiently small, such that $x^* + \varepsilon^* \xi \leq \mu$, where $\mu = (\mu_1, \dots, \mu_n)' \in \text{int}(\mathfrak{R}_+^n)$. We define:

$$\beta := x^* + \varepsilon^* \xi. \quad (3.13)$$

Let arbitrary $x \in \Omega, d \in D, v \in \mathfrak{R}_+^n$ with $v \leq v^* - \text{diag}(v^* - b)(1_n - h(1_n - \tau^{-1} K h(x - x^*)))$ be given. Since $x_i \leq \beta_i \leq \mu_i$ and $v_i \leq v_i^* < v_i^{max}$, for $i = 1, \dots, n$, it follows from (2.8) and (2.11) that:

$$x_i^+ = x_i + v_i - f_{D,i}(d, x_i) + \sum_{j=1}^n b_{j,i} f_{D,j}(d, x_j), \text{ for } i = 1, \dots, n. \quad (3.14)$$

Using the fact that $v_i \leq v_i^* - (v_i^* - v_i^{min})(1 - \max(0, 1 - \tau^{-1} \sum_{j=1}^n K_{i,j} \max(0, x_j - x_j^*)))$, for $i = 1, \dots, n$, in conjunction with (3.2), we obtain from (3.14):

$$\begin{aligned} x_i^+ &\leq x_i - (v_i^* - v_i^{min}) + (v_i^* - v_i^{min}) \max \left(0, 1 - \tau^{-1} \sum_{j=1}^n K_{i,j} \max(0, x_j - x_j^*) \right) \\ &\quad + f_{D,i}(d, x_i^*) - f_{D,i}(d, x_i) + \sum_{j=1}^n b_{j,i} (f_{D,j}(d, x_j) - f_{D,j}(d, x_j^*)), \end{aligned} \quad (3.15)$$

for $i = 1, \dots, n$. Using Assumption (H 2.1), we get $L_i(x_i - x_i^*) \leq f_{D,i}(d, x_i) - f_{D,i}(d, x_i^*) \leq G_i(x_i - x_i^*)$ for $i = 1, \dots, n$ and $x_i \geq x_i^*$. Using Property (C2) and

the above inequality, it follows that:

$$\begin{aligned} f_{D,i}(d, x_i) - f_{D,i}(d, x_i^*) &\leq G_i \max(0, x_i - x_i^*), \\ x_i - x_i^* + f_{D,i}(d, x_i^*) - f_{D,i}(d, x_i) &\leq (1 - L_i) \max(0, x_i - x_i^*) \end{aligned} \quad (3.16)$$

for $x_i \in [0, \beta_i]$, $i = 1, \dots, n$. Combining (3.15), (3.16) we obtain for $i = 1, \dots, n$:

$$\begin{aligned} x_i^+ &\leq x_i^* - (v_i^* - v_i^{\min}) + (v_i^* - v_i^{\min}) \max \left(0, 1 - \tau^{-1} \sum_{j=1}^n K_{i,j} \max(0, x_j - x_j^*) \right) \\ &\quad + (1 - L_i) \max(0, x_i - x_i^*) + \sum_{j=1}^n b_{j,i} G_j \max(0, x_j - x_j^*). \end{aligned} \quad (3.17)$$

Using vector notation and definition (3.5), we are in a position to write inequalities (3.17) in the following form:

$$\begin{aligned} x^+ &\leq x^* - v^* + v^{\min} + \text{diag}(v^* - v^{\min})h(1_n - \tau^{-1}Kh(x - x^*)) \\ &\quad + (I + B' \text{diag}(G) - \text{diag}(L))h(x - x^*). \end{aligned} \quad (3.18)$$

In order to show (3.6), it suffices to show that:

$$\begin{aligned} x^* - v^* + v^{\min} + \text{diag}(v^* - v^{\min})h(1_n - \tau^{-1}Kh(x - x^*)) \\ + (I + B' \text{diag}(G) - \text{diag}(L))h(x - x^*) \leq \beta \end{aligned}$$

for all $x \in \mathfrak{R}_+^n$ with $x \leq \beta$ or equivalently, using (3.13),

$$\begin{aligned} \text{diag}(v^* - v^{\min})h(1_n - \tau^{-1}Kh(x - x^*)) + \\ (I + B' \text{diag}(G) - \text{diag}(L))h(x - x^*) \leq \varepsilon^* \xi + v^* - v^{\min} \end{aligned} \quad (3.19)$$

for all $x \in \mathfrak{R}_+^n$ with $x \leq x^* + \varepsilon^* \xi$. Setting $x = x^* + \varepsilon^* \zeta$, where $\zeta \in \mathfrak{R}^n$, and using the fact that $h(\varepsilon^* \zeta) = \varepsilon^* h(\zeta)$ for all $\zeta \in \mathfrak{R}^n$ (a direct consequence of definition (3.5)), it follows that (3.19) holds provided that:

$$\text{diag}(v^* - v^{\min})h(1_n - \varepsilon^* \tau^{-1}Kh(\zeta)) + \varepsilon^* (I + B' \text{diag}(G) - \text{diag}(L))h(\zeta) \leq \varepsilon^* \xi + v^* - v^{\min} \quad (3.20)$$

for all $\zeta \in \mathfrak{R}^n$ with $\zeta \leq \xi$. However, inequality (3.12) and the fact that $h(1_n - \varepsilon^* \tau^{-1}Kh(\zeta)) \leq 1_n$ imply (3.20). The proof is complete. \triangleleft

Proof of Theorem 3.8: A direct application of Theorem A.5. Indeed, Lemma 3.6 and Lemma 3.7 guarantee that all assumptions of Theorem A.5 hold for the closed-loop system (3.1), (3.4) with

$$\begin{aligned} V_i(x) &:= \max(0, x_i - x_i^*) \text{ for } i = 1, \dots, n \text{ and} \\ V_i(x) &:= \max(0, x_{i-n}^* - x_{i-n}) \text{ for } i = n + 1, \dots, 2n. \end{aligned} \quad (3.21)$$

Notice that definitions (3.21) guarantee the inequality

$$\frac{1}{\sqrt{n}} |x - x^*| \leq \max_{i=1, \dots, 2n} (V_i(x)) = \max_{i=1, \dots, n} (|x_i - x_i^*|) \leq |x - x^*|, \quad (3.22)$$

for all $x \in S$, while (3.7), (3.8) and (3.21) imply the inequality:

$$V(x^+) \leq \Gamma V(x) \text{ for all } (d, x) \in D \times \Omega, \quad (3.23)$$

where $V(x) = (V_1(x), \dots, V_{2n}(x))' \mathfrak{R}^{2n}$ and

$$\Gamma := \begin{bmatrix} I + B' \text{diag}(G) - \text{diag}(L) & 0 \\ \text{diag}(v^* - v^{\min}) \tau^{-1} K & I + B' \text{diag}(G) - \text{diag}(L) \end{bmatrix}. \quad (3.24)$$

Lemma A.9 guarantees that the matrix $I + B' \text{diag}(G) - \text{diag}(L)$ is a lower triangular matrix with $\rho(I + B' \text{diag}(G) - \text{diag}(L)) < 1$. Then, it follows that the matrix Γ , as defined by (3.24), is a lower triangular matrix with its diagonal entries being the same with the diagonal entries of the matrix $I + B' \text{diag}(G) - \text{diag}(L)$. Therefore, $\rho(\Gamma) < 1$. The proof is complete. \triangleleft

Proof of Theorem 3.3: Without loss of generality, by virtue of Theorem 3.8, it suffices to show the existence of $v^{\min} \in \mathfrak{R}_+^n$ with $v^{\min} \leq v^*$ such that (3.10) hold. We set:

$$R := \{i \in \{1, \dots, n\} : v_i^* > 0\}, v^{\min} := \lambda v^*, \lambda := \min \left(\frac{1}{2}, \frac{C \min_{i=1, \dots, n} (r_i x_i^*)}{r' v^*} \right). \quad (3.25)$$

Definitions (3.25) guarantee that (3.10) holds. The proof is complete. \triangleleft

Proof of Corollary 3.9: Again a direct application of Theorem A.5. Selecting $m \in \{1, 2, \dots\}$ so that:

$$m := \left\lceil \frac{\ln(C \min_{i=1, \dots, n} (r_i \beta_i) - r' v^*) - \ln(C r' \rho^{\max})}{\ln(1 - C)} \right\rceil + 1, \quad (3.26)$$

and following the same procedure as in the proof of Lemma 3.7, we conclude that the UEP is RGES for the open-loop system (3.1) with $v = v^*$ satisfying (3.11). The proof is complete. \triangleleft

3.4 Illustrative Example

Consider a 3-lane freeway-to-freeway traffic network of the form (3.1) with $n = 8$ cells. The traffic network consists of two smaller freeways, 2 km each; the first is composed by the cells $i = 1, 2, 3, 4$, and the second is composed by the cells $i = 5, 6, 7, 8$ (see, Figure 3.2). The cells are homogeneous, each cell being 0.5 km in length. The whole network admits two external inflows; one external inflow at the upstream boundary of the first cell and one external inflow at the upstream boundary of the fifth cell, while there are no intermediate external inflows ($v_2 = v_3 = v_4 = v_6 = v_7 = v_8 = 0$ and $v_1, v_5 \neq 0$). At the end of the first freeway (4th cell) there is an off-ramp joining the second freeway which becomes an on-ramp for the second freeway at the upstream boundary of the 7th cell (see Figure 3.2). According to this configuration, the exit and turning rates of the freeway are defined as follows

$$p_i = 0 \text{ for } i = 1, 2, 3, 5, 6, 7, p_4 = 0.5, p_8 = 1 \text{ and} \\ b_{i,j} = \begin{cases} 1 & \text{if } j = i + 1 \text{ and } i \in \{1, \dots, 7\} \setminus \{4\} \\ 0.5 & \text{if } i = 4 \text{ and } j = 7 \\ 0 & \text{if otherwise} \end{cases}, i, j = 1, \dots, 8. \quad (3.27)$$

Consequently, the only control possibilities are the inflows v_1, v_5 . It should be noted here that the 7th cell is a bottleneck for the overall network due to the ramp that joins both freeways. Congestion may be created in the 7th cell, due to high on-ramp demand from the 1st and the 5th cells, and spill back to both freeways depending on the priority rules.

All the following simulation tests have been conducted using the following form of the model (3.1), which is expressed by means of the supply function $f_{S,i}$ ($i = 1, \dots, n$):

$$x_i^+ = x_i - s_i(d, x, v) f_{D,i}(d, x, v) + \min \left(f_{S,i}(d, x), v_i + \sum_{j=1}^n b_{j,i} f_{D,j}(d, x_j) \right), \quad (3.28)$$

$$s_i(d, x, v) = \begin{cases} \min \left(1, \max \left(0, \frac{f_{S,i+1}(d, x) - v_{i+1}}{b_{i,i+1} f_{D,i}(d, x_i)} \right) \right) & \text{if } x_i > 0 \\ 1 & \text{if } x_i = 0 \end{cases}, \text{ for } i \neq 4, 8,$$

$$s_4(d, x, v) = \begin{cases} \min \left(1, \max \left(0, \frac{f_{S,7}(d, x) - b_{6,7} f_{D,6}(d, x_6)}{b_{4,7} f_{D,4}(d, x_4)} \right) \right) & \text{if } x_4 > 0 \\ 1 & \text{if } x_4 = 0 \end{cases},$$

$$s_8(d, x, v) = 1 \quad (3.29)$$

Notice that, according to (3.29), constant priority rules for the junctions have been taken into account by assuming a full priority rate for the external inflows and by assuming that the mainstream flow coming from the 6th cell has full priority over the mainstream flow coming from the 4th cell (see also (2.16) and the related discussion). Furthermore, we assume that the simulation time step is $T=15$ s. However, since all flows and densities are measured in [veh] (as imposed by the form of the model (2.9) and (3.28), (3.29)), the cell length, the time step and the number of lanes do not appear explicitly, but they are only reflected implicitly in the values of every variable and every constant (e.g. critical density, jam density, flow capacity, wave speed etc.) corresponding to density or flow. Appropriate transformations in common traffic units are given for the most critical variables wherever it is needed.

The demand and the supply functions have been defined so as to reflect the uncertainty, d , derived from the FD of traffic flow. More specifically, we assume that the demand functions are given as a convex combination of several functions ϕ_i (e.g., linear or quadratic) satisfying Assumption (H 2.1). Furthermore, it should be noted that the functions ϕ_i should guarantee that the uncertainty d is a vanishing perturbation for the system (3.28), (3.29), i.e., it does not change the position of the UEP (see Figures 2.1 and 3.3). Here, six different functions are used to represent the uncertainty in the demand functions. Specifically, the functions ϕ_i , for $i = 1, \dots, 6$ are

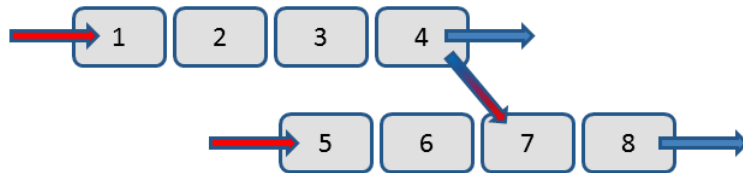


FIGURE 3.2: The scheme of the freeway-to-freeway network.

given by:

$$\begin{aligned}
\phi_1(z) &= \frac{5}{11}z, \phi_2(z) = -(13.5/3025)z^2 + 0.7z, \phi_3(z) = (14/3025)z^2 + 0.2z, \\
\phi_4(z) &= \begin{cases} (-49/3025)z^2 + 0.9z & \text{if } z \in [0, 27.5] \\ (-38/3025)z^2 + 82/55z - 19 & \text{if } z \in (27.5, 55] \end{cases} \\
\phi_5(z) &= \begin{cases} (7/756.25)z^2 + 0.2z & \text{if } z \in [0, 27.5] \\ (21/6050)z^2 + 71.5/1210z + 8.25 & \text{if } z \in (27.5, 55] \end{cases} \\
\phi_6(z) &= -\frac{3}{23}z + \frac{740}{23}, \phi_7(z) = (83/52900)z^2 - (4471/10580)z + 46019/1058.
\end{aligned} \tag{3.30}$$

Then, the demand functions are given by:

$$f_{D,i}(d, x_i) = \begin{cases} d_1\phi_1(x_i) + d_2(1 - d_1)\phi_2(x_i) + (1 - d_2)(1 - d_1)\phi_3(x_i) & \text{if } x_i \in [0, 55 + 2\varepsilon] \\ d_3\phi_6(x_i) + (1 - d_3)\phi_7(x_i) & \text{if } x_i \in (55 + 2\varepsilon, 170] \end{cases}, \tag{3.31}$$

for $i = 1, 2, 3, 4, 7, 8$,

$$f_{D,i}(d, x_i) = \begin{cases} d_1\phi_1(x_i) + d_2(1 - d_1)\phi_4(x_i) + (1 - d_2)(1 - d_1)\phi_5(x_i) & \text{if } x_i \in [0, 55 + 2\varepsilon] \\ d_3\phi_6(x_i) + (1 - d_3)\phi_7(x_i) & \text{if } x_i \in (55 + 2\varepsilon, 170] \end{cases}, \tag{3.32}$$

for $i = 5, 6$, where $d_i \in [0, 1]$, for $i = 1, 2, 3$, correspond to time-varying weight parameters and $\varepsilon = 10^{-5}$. According to (3.31), (3.32), each cell has the same critical density $\rho_i^{cr} = 55 + 2\varepsilon[\text{veh}]$ ($i = 1, \dots, 8$) (corresponding to 36.7 [veh/km/lane] with the above settings) and the same jam density $\rho_i^{max} = 170$ [veh] ($i = 1, \dots, 8$) (corresponding to 113.3 [veh/km/lane]). Notice also that, according to (3.31), (3.32), decreasing functions have been considered for overcritical densities (see Chapter 6), so as to incorporate into the model (3.28), (3.29) the capacity drop phenomenon.

As it has already been mentioned, for traffic flow networks the supply functions are usually described by the functions $f_{S,i}(d, x) = \min(Q_i, c_i(\rho_i^{max} - x_i))$, where $Q_i > 0$ represents the maximum inflow for the i^{th} cell and $c_i \in (0, 1]$ represents the normalized congestion wave speed. Here, in order to consider the uncertainty of the supply functions, we assume that

$$f_{S,i}(d, x_i) = d_4 \min(115, \tilde{\rho}_i^{max} - x_i), \tag{3.33}$$

where $d_4 \in [0.22, 0.30]$ is a time-varying parameter resulting to a congestion wave speed within approximately 26 to 36 [km/h] and a maximum inflow approximately between 2000 to 2750 [veh\h\lane]. For the overall system (3.28), (3.29), the uncertainty $d(t) = (d_1(t), \dots, d_4(t)) \in D$ is a time-varying parameter taking values from a uniform distribution within $D = [0, 1]^3 \times [0.22, 0.3]$. Figure 3.3 visualizes a grey area which includes any possible demand and supply functions.

Assumption (H 2.1) is satisfied for $\rho_i^{cr} = \tilde{\rho}_i^{cr} = 55 + 2\varepsilon[\text{veh}]$, $f_i^{min} = 10[\text{veh}]$ ($i = 1, \dots, 8$), $L_i = 0.2$, $G_i = 0.71$ for $i = 1, 2, 3, 4, 7, 8$ and $L_i = 0.009$, $G_i = 0.9$ for $i = 5, 6$. The cell flow capacities are approximately $f_{D,i}(d, \rho_i^{cr}) = 25[\text{veh}]$ ($i = 1, \dots, 8$),

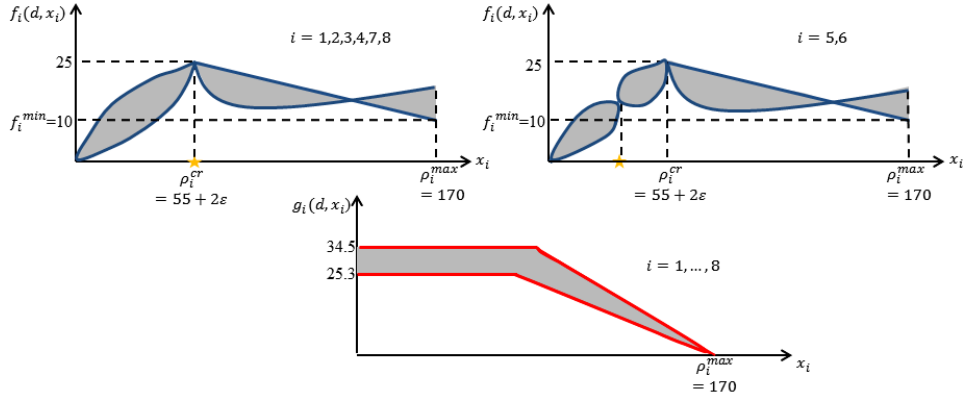


FIGURE 3.3: Specification of the parameters of the demand and supply functions of every cell.

corresponding to 2000 [veh/h/lane]. Notice also that the matrix B , given by (3.27), satisfies Assumption (H 2.2). Assumption (H 2.4) holds for $\mu_i = 55 + \varepsilon$ for $i \neq 5, 6$ and $\mu_i = 27.5 + \varepsilon$ for $i = 5, 6$, where $\varepsilon = 10^{-5}$ and $v_i^{max} = 0.3$ for $i \neq 1, 5$ and $v_1^{max} = v_5^{max} = 25$. Finally, Assumption (H 2.3) holds for

$$\begin{aligned} \tilde{s}_i(d, x, v) &:= \min \left(1, \frac{\max(0, f_{S,i+1}(d, x) - v_{i+1})}{b_{i,i+1}\rho_i^{max}} \right), \text{ for } i \neq 4, 8, \\ \tilde{s}_4(d, x, v) &:= \min \left(1, \frac{\max(0, f_{S,7}(d, x) - v_7 - b_{6,7}f_{D,6}(d, x_6))}{b_{4,7}a_4} \right), \\ &\text{and } \tilde{s}_8(d, x, v) := 1 \end{aligned} \quad (3.34)$$

and v_i^{max} (for $i = 1, \dots, 8$) as previous.

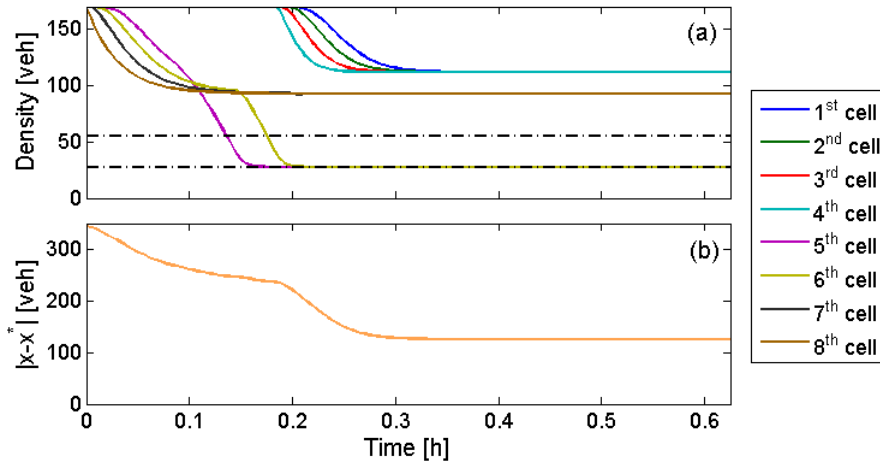


FIGURE 3.4: (a) The response of the density of every cell and (b) the evolution of the Euclidean norm of the deviation $x(t) - x^*$ of the state from the UEP, that is $|x(t) - x^*|$, for the open-loop system, for initial condition $x_0 = [170, \dots, 170]$, $v = v^*$ and $d(t) \equiv (1, 0, 1, 0.26)$.

Here, $R = \{1, 5\}$ and therefore we select $v_1^{min} = v_5^{min} = 0.5$ while $v_i^{min} = 0$ for every $i \neq 1, 5$. Our goal is to globally exponentially stabilize the system at an UEP which is as close as possible to the critical density (due to the fact that the flow value

at the critical density is the largest). Equation (3.2) and inequality (3.3) are satisfied by selecting $v^* = (25, 0, 0, 0, 12.5, 0, 0, 0)$ and $x^* = (55, 55, 55, 55, 27.5, 27.5, 55, 55)$. The above UEP is not open-loop RGES due to the existence of additional (congested) equilibria. This is shown in Figure 3.4, where the solution of the open-loop system, with constant inflows $v^* = (25, 0, 0, 0, 12.5, 0, 0, 0)$, constant $d(t) \equiv (1, 0, 0, 1, 0.5)$ and $x_0 = [\rho_1^{max}, \dots, \rho_8^{max}]$, is attracted by the congested equilibrium $(111.8, 111.8, 111.8, 111.8, 27.5, 27.5, 92.82, 92.82)'$ (Figure 3.4(a)) leading to outflow, which is 7.4 [veh] lower than the capacity flow of the 4th cell and 4.9 [veh] lower than the capacity flow of the 8th cell and a constant deviation of 125.5 [veh] for the Euclidean norm (Figure 3.4(b)). Therefore, if the objective is the operation of the freeway with largest possible outflow, then a control strategy will be needed.

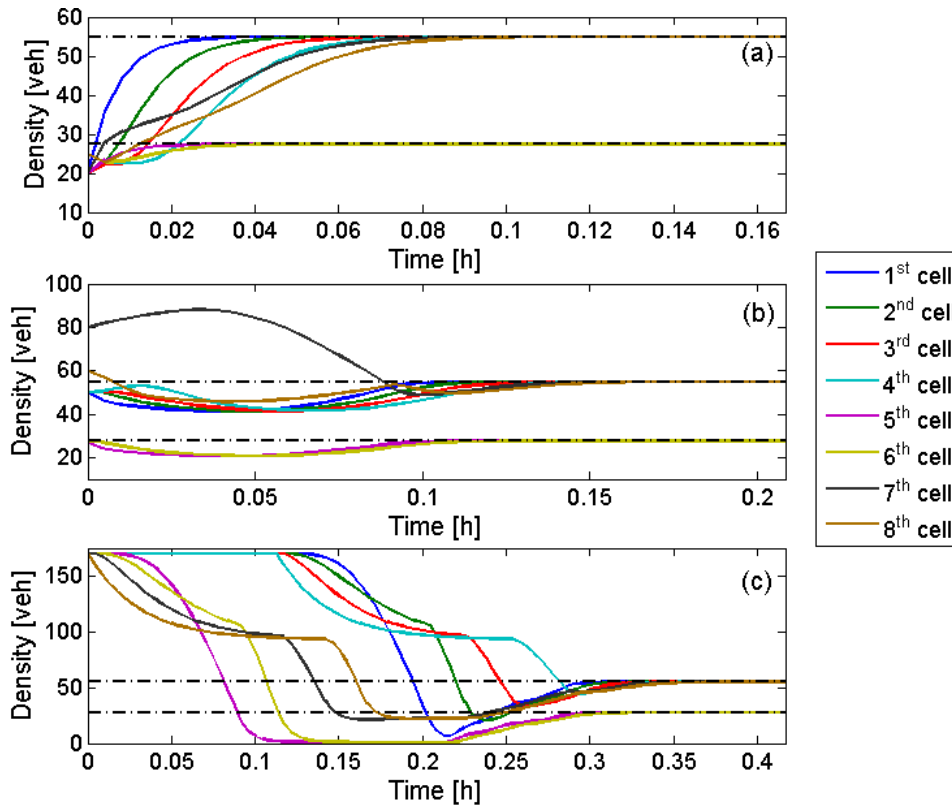


FIGURE 3.5: The response of the density of every cell for the closed-loop system, under the proposed feedback regulator, for different initial conditions; (a) $x_0 = [20, 25, 20, 25, 20, 25, 20, 25]'$, (b) $x_0 = [50, 50, 50, 50, 27, 27, 80, 60]'$ and (c) $x_0 = [170, \dots, 170]$ and for $d(t) \equiv (1, 0, 1, 0.26)$.

We constructed the matrix K and the constant τ using the sufficient conditions provided from the proofs of the technical lemmas and propositions. Here, we simply used $K = 0.001 \cdot 1_{n \times n}$ and $\tau = 1/2$ which satisfy those conditions and allow for a good control performance with respect to overshooting effects. Figure 3.5 shows the response of the density of every cell for the closed-loop system (3.28), (3.29), (3.4) and three different initial conditions for constant $d(t) \equiv (1, 0, 1, 0.26)$; Figure 3.5(a) is with $x_0 = (20, 25, 20, 25, 20, 25, 20, 25)'$ corresponding to very low densities; Figure 3.5(b) is with $x_0 = (50, 50, 50, 50, 27, 27, 80, 60)'$ corresponding to a more realistic traffic situation for which a sudden incident created congestion in a small part of the second freeway; and Figure 3.5(c) is with $x_0 = (\rho_1^{max}, \dots, \rho_8^{max})'$ corresponding to a

fully congested network. The feedback regulator is seen to respond very satisfactorily in these tests, exhibiting a fast convergence to the UEP for each one of the initial conditions.

Figure 3.6 shows again the response of the density of every cell for the closed-loop system (3.28), (3.29), (3.4) and three different initial conditions (same as those of Figure 3.5) for time-varying $d(t) = (d_1(t), \dots, d_4(t)) \in D$ taking values from a uniform distribution within $D = [0, 1]^3 \times [0.22, 0.3]$. In this case, although small oscillations exist, the rate of convergence to the UEP is similar to the previous test. This demonstrates the robustness of the feedback regulator (3.4) with respect to the uncertainties derived from the FD (3.31), (3.32), (3.33).

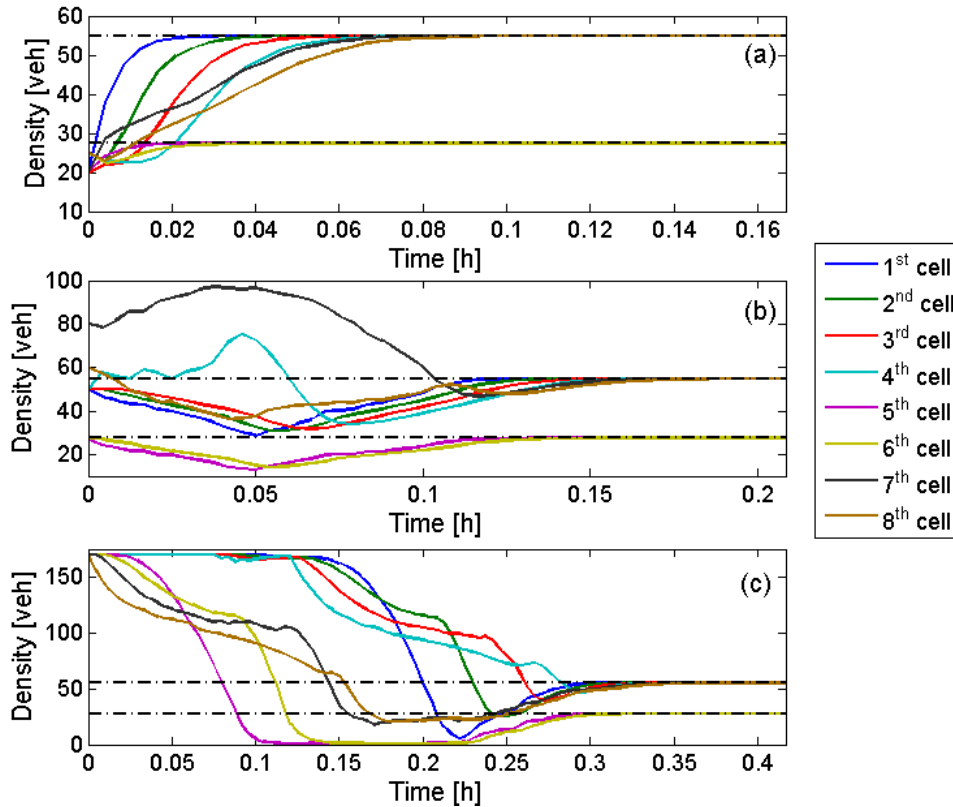


FIGURE 3.6: The response of the density of every cell for the closed-loop system, under the proposed feedback regulator, for different initial conditions; (a) $x_0 = [20, 25, 20, 25, 20, 25, 20, 25]'$, (b) $x_0 = [50, 50, 50, 50, 27, 27, 80, 60]'$ and (c) $x_0 = [170, \dots, 170]$ and for time-varying $d(t)$.

Chapter 4

Global Exponential Stabilization of Freeway Models

4.1 Introduction

In this chapter, we provide a rigorous methodology for the construction of explicit feedback laws that guarantee the RGES of the UEP of the general nonlinear discrete-time freeway models presented in Section 2.2.3 (instead of the general traffic networks of Section 2.2.1, which were studied in Chapter 3). The considered discrete-time freeway models, presented in Section 2.2.3, are generalized versions of the known first-order discrete Godunov approximations (Godunov, 1959) to the kinematic-wave partial differential equation of the LWR-model (see (Lighthill and Whitham, 1955a; Lighthill and Whitham, 1955b; Richards, 1956)) with nonlinear ((Lebacque, 1996)) or piecewise linear (CTM, (Daganzo, 1994; Daganzo, 1995b; Gomes et al., 2008) outflow functions (FDs), and which are special case of the proposed general acyclic network model (2.9).

In contrast to the results provided in Chapter 3, in this chapter, the construction of the robust global exponential feedback stabilizer is based on a SLF approach (see Karafyllis and Jiang, 2011). In fact, the constructed SLF acts as a CLF for the open-loop system and is given by an explicit formula (see formulas (4.8), (4.9), (4.10)). Clearly, the availability of a SLF is very crucial (and can be used in a straightforward way for various purposes) due to the existence of several important results which concern the study of robustness properties of nonlinear systems with a SLF (Artstein, 1983; Coron and Rosier, 1994). Here, the availability of a SLF allowed the formation of sufficient conditions for the construction of the index set R which, as previous, contains the indices of the inflows that must be controlled in order to guarantee the RGES of the UEP of the closed-loop system. Again, the proposed methodology provides a parameterized family of robust global exponential feedback stabilizers for the UEP of freeway models, while the achieved stabilization is robust with respect to all priority rules that can be used for the inflows.

The structure of the present chapter is as follows: Section 4.2 includes the main results of this chapter, while the proofs of the main results can be found in Section 4.3. A comparison is made, by means of simulation, with an existing feedback law, for freeway traffic control, proposed in the literature and employed in practice. More specifically, we consider the RLB PI-type regulator which was proposed in (Wang et al., 2010) and is the most sophisticated of the very few comparable feedback regulators that have been employed in field operations (Papamichail et al., 2010). The corresponding results are presented in Section 4.4, accompanying with a study of the performance of the corresponding closed-loop systems and its robustness under the effect of measurement errors.

4.2 Main Result

The freeway model presented in Section 2.2.3 is considered in this chapter. For convenience reasons, here the corresponding model is rewritten. Consider the following nonlinear uncertain discrete space-time system:

$$\begin{aligned} x_1^+ &= x_1 - s_1(d, x, v)f_{D,1}(x_1) + \min(f_{S,1}(x_1), v_1) \\ &= x_1 - s_1(d, x, v)f_{D,1}(x_1) + \bar{s}_1(d, x, v)v_1, \end{aligned} \quad (4.1)$$

$$\begin{aligned} x_i^+ &= x_i - s_i(d, x, v)f_{D,i}(x_i) + \min(f_{S,i}(x_i), v_i + (1 - p_{i-1})f_{D,i-1}(x_{i-1})) \\ &= x_i - s_i(d, x, v)f_{D,i}(x_i) + \bar{s}_i(d, x, v)v_i + s_{i-1}(d, x, v)(1 - p_{i-1})f_{D,i-1}(x_{i-1}), \end{aligned} \quad (4.2)$$

for $i = 2, \dots, n - 1$,

$$\begin{aligned} x_n^+ &= x_n - f_{D,n}(x_n) + \min(f_{S,n}(x_n), v_n + (1 - p_{n-1})f_{D,n-1}(x_{n-1})) \\ &= x_n - f_{D,n}(x_n) + \bar{s}_n(d, x, v)v_n + s_{n-1}(d, x, v)(1 - p_{n-1})f_{D,n-1}(x_{n-1}), \end{aligned} \quad (4.3)$$

and define the vector field $\tilde{F} : [0, 1]^{n-1} \times S \times (0, +\infty) \times \mathfrak{R}_+^{n-1} \rightarrow S$ for all $x \in S$, $d = (d_1, \dots, d_{n-1}) \in D = [0, 1]^{n-1}$ and $v = (v_1, \dots, v_n) \in (0, +\infty) \times \mathfrak{R}_+^{n-1}$: $\tilde{F}(d, x, v) = (\tilde{F}_1(d, x, v), \dots, \tilde{F}_n(d, x, v))' \in \mathfrak{R}^n$, where $\tilde{F}_1(d, x, v)$, $\tilde{F}_i(d, x, v)$, for $i = 2, \dots, n - 1$, and $\tilde{F}_n(d, x, v)$ are given by the right hand side of (4.1), (4.2), (4.3) (with (2.15) and (2.16)), respectively. Notice that, using this definition, the control system (4.1), (4.2), (4.3) can be written in the following vector form:

$$\begin{aligned} x^+ &= \tilde{F}(d, x, v), \\ x \in S, d \in D, v \in (0, +\infty) \times \mathfrak{R}_+^{n-1}. \end{aligned} \quad (4.4)$$

Section 2.2.3 revealed that the freeway model (4.4) under Assumption (H 2.1*) is special case of the network (2.9) under (H 2.1), (H 2.2), (H 2.3), (H 2.4). Moreover, the definition of the UEP for the freeway model (4.4) under Assumption (H 2.1*) remains the same with its definition in Chapter 3. Therefore, definitions (3.2) and (3.3) take the following form under (2.14) and Assumption (H 2.1*):

There exist $x^* = (x_1^*, \dots, x_n^*) \in S$ with $x_i^* \in (0, \mu_i)$, for $i = 1, \dots, n$, and a vector $v^* = (v_1^*, \dots, v_n^*)' \in (0, +\infty) \times \mathfrak{R}_+^{n-1}$ with $v_i^* < v_i^{max}$ ($i = 1, \dots, n$), for $i = 1, \dots, n$, that satisfy the following equations:

$$f_{D,1}(x_1^*) = v_1^*, f_{D,i}(x_i^*) = v_i^* + (1 - p_{i-1})f_{D,i-1}(x_{i-1}^*) = v_i^* + \sum_{j=1}^{i-1} \left(\prod_{k=j}^{i-1} (1 - p_k) \right) v_j^*, \quad (4.5)$$

for $i = 2, \dots, n$. Since $x_i^* \in (0, \mu_i)$, $v_i^* < v_i^{max}$, it follows from Assumption (H 2.4) that the following inequalities hold:

$$v_1^* < f_{S,1}(x_1^*), v_i^* + (1 - p_{i-1})f_{D,i-1}(x_{i-1}^*) < f_{S,i}(x_i^*), i = 2, \dots, n. \quad (4.6)$$

The above UEP is not RGES for arbitrary $v_1^* > 0$, $v_i^* \geq 0$ ($i = 2, \dots, n$); indeed, for relatively large values of external demands $v_1^* > 0$, $v_i^* \geq 0$ ($i = 2, \dots, n$) other equilibria for model (4.4) (congested equilibria) may appear, for which the cell densities are large and can attract the solution of (4.4) (see the illustrative example in Section 4.4).

The following result is our main result in feedback design. The result shows that a continuous, robust, global exponential stabilizer exists for every freeway model of the form (4.4) under Assumption (H 2.1*).

Theorem 4.1

Consider system (4.4) with $n \geq 3$ under Assumption (H 2.1*). Then there exist a subset $R \subseteq \{1, \dots, n\}$ of the set of all indices $i \in \{1, \dots, n\}$ with $v_i^* > 0$, constants $\sigma \in (0, 1]$, $v_i^{min} \in (0, v_i^*)$ for $i \in R$ and a constant $\tau^* > 0$ such that for every $\tau \in (0, \tau^*)$ the feedback law $k : S \rightarrow \mathfrak{R}_+^n$ defined by:

$$\begin{aligned} k(x) &:= (k_1(x), \dots, k_n(x))' \in \mathfrak{R}^n \text{ with} \\ k_i(x) &:= \max(v_i^* - \gamma_i \Xi(x), v_i^{min}), \text{ for all } x \in S, i \in R, \\ k_i(x) &:= v_i^*, \text{ for all } x \in S, i \notin R, \end{aligned} \quad (4.7)$$

$$\Xi(x) := \sum_{i=1}^n \sigma^i \max(0, x_i - x_i^*) \text{ for all } x \in S, \quad (4.8)$$

where $\gamma_i := \tau^{-1}(v_i^* - v_i^{min})$ and achieves RGES of the UEP x^* of system (4.4), i.e., x^* is RGES for the closed-loop system (4.4) with $u = k(x)$. Moreover, for every $\tau \in (0, \tau^*)$, there exist constants $h, \bar{\theta}, A, \tilde{M}, K > 0$ so that the function $V : S \rightarrow \mathfrak{R}_+$ defined by:

$$V(x) := \sum_{i=1}^n \sigma^i |x_i - x_i^*| + A\Xi(x) + K \max\left(0, \sum_{i=1}^n I_i(x) - P(x)\right), \quad (4.9)$$

for all $x \in S$, where $I_j(x) := \sum_{i=1}^j x_i$ for $j = 1, \dots, n$, and

$$P(x) := \tilde{M} - \bar{\theta} \min(h, \Xi(x)), \quad (4.10)$$

is a Lyapunov function with exponent 1 for the closed-loop system (4.4) with $v = k(x)$.

Although Theorem 4.1 is an existence result, its proof is constructive and provides formulae for all constants and for the index set R (see following sections). Notice that the index set R is the set of all inflows that must be controlled in order to be able to guarantee that the UEP is RGES; consequently, the knowledge of the index set R is critical.

The importance of Theorem 4.1 lies on the facts that:

1. Theorem 4.1 provides a family of robust global exponential stabilizers (parameterized by the parameter $\tau \in (0, \tau^*)$) and an explicit formula for the feedback law (formula (4.7));
2. The achieved stabilization result is robust for all possible (and even time varying) priority rules for the junctions that may apply at specific freeways; thus, there is no need to know or estimate the applied priority rules;
3. Theorem 4.1 provides an explicit formula for the SLF of the closed-loop system. This is important, because the knowledge of the SLF allows the study of the

robustness of the closed-loop system to various disturbances (measurement errors, modeling errors, etc.) as well the study of the effect of interconnections of freeways (by means of the small-gain theorem; see (Karafyllis and Jiang, 2011)).

The main idea behind the proof of Theorem 4.1 is the construction of the SLF of the closed-loop system, which acts as a CLF (see Karafyllis and Jiang, 2011) for the open-loop system. The construction of the SLF is based on the observation that there are no congestion phenomena when the cell densities are sufficiently small, i.e.,

"There exists a set $\tilde{\Omega} \subset S$ such that no congestion phenomena are present when $x \in \tilde{\Omega}$."

The existence of the set $\tilde{\Omega} \subset S$ is important because, when no congestion phenomena are present, then the freeway model admits the simple (cascade) form:

$$\begin{aligned} x_1^+ &= x_1 - f_{D,1}(x_1) + v_1 \\ x_i^+ &= x_i - f_{D,i}(x_i) + (1 - p_{i-1})f_{D,i-1}(x_{i-1}) + v_{i+1}, i = 2, \dots, n, x \in \tilde{\Omega} \end{aligned}$$

and a Lyapunov function for the above form can be a function of the form $V_1(x) := \sum_{i=1}^n \sigma^i |x_i - x_i^*| + A\Xi(x)$, where $\Xi(x) := \sum_{i=1}^n \sigma^i \max(0, x_i - x_i^*)$; and $\sigma \in (0, 1]$ and $A > 0$ are appropriate constants. The SLF for the freeway model is the linear combination of the "Lyapunov function" for the uncongested model (i.e., $V_1(x) := \sum_{i=1}^n \sigma^i |x_i - x_i^*| + A\Xi(x)$) and a penalty term, i.e., the term $\max(0, \sum_{i=1}^n I_i(x) - P(x))$, that penalizes large cell densities (and thus penalizes the possibility of the state being out of the set $\tilde{\Omega} \subset S$).

The appropriate selection of the weight of the penalty term $K > 0$ forces the selected control action to lead the state in the set $\tilde{\Omega} \subset S$ (see Figure 3.1). In other words, the construction of the SLF guarantees that the control action will first eliminate all congestion phenomena and then will drive the state to the desired equilibrium.

Remark 4.1: It is important also to note that the feedback stabilizer defined by (4.7) is special case of the feedback law proposed in (3.4). This can be shown by selecting the matrix $K \in \mathfrak{R}_+^{n \times n}$ as $K_{i,j} = \sigma^j$, for every $i, j = 1, \dots, n$, where $\sigma \in (0, 1]$ is the parameter involved in (4.8). Therefore, clearly, the results of this chapter are special case of the results provided in Chapter 2.

4.3 Proofs of Main Results

Proof of Theorem 4.1 Inequalities (2.8) and Assumption (H 2.4) allow us to define the set $\tilde{\Omega} := [0, \mu_1] \times \dots \times [0, \mu_n]$ for which it holds that:

$$\begin{aligned} x_1^+ &= x_1 - f_{D,1}(x_1) + v_1, \\ x_i^+ &= x_i - f_{D,i}(x_i) + (1 - p_{i-1})f_{D,i-1}(x_{i-1}) + v_i, i = 2, \dots, n. \end{aligned} \tag{4.11}$$

for every $x \in \tilde{\Omega}$ and $v_i \in [0, v_i^*]$ ($i = 1, \dots, n$).

Let $\lambda_i \in (0, 1)$, $G_i \in [0, 1]$ ($i = 1, \dots, n$), be the constants involved in Consequence (C2) and Assumption (H 2.1*) respectively. Let $\sigma \in (0, 1]$ be a constant so that:

$$L := \max \left(\lambda_n, \max_{i=1, \dots, n-1} (\lambda_i + \sigma G_i (1 - p_i)) \right) < 1. \tag{4.12}$$

Notice that $L < 1$ for all $\sigma \in (0, 1)$ due to the fact that $1 - \lambda_i = L_i \leq G_i$. In what follows, we have $p_n = 1 = s_n$. Let $C > 0$ be the constant involved in (2.13) and let $R \subseteq \{1, \dots, n\}$ be a subset of the set of all indices $i \in \{1, \dots, n\}$ for which $v_i^* > 0$ and such that:

$$\begin{aligned} \sum_{i \notin R} (n+1-i)v_i^* &< \min_{i=1, \dots, n} (((n-i)p_i + 1)f_{D,i}(x_i^*)), \\ \sum_{i \notin R} (n+1-i)v_i^* &< C \min_{i=1, \dots, n} ((n+1-i)\mu_i), \end{aligned} \quad (4.13)$$

where $\mu_i > x_i^*$ for $i = 1, \dots, n$ are the constants defined by (2.11). Such a set $R \subseteq \{1, \dots, n\}$ always exists (for example, $R \subseteq \{1, \dots, n\}$ can be the set of all indices $i \in \{1, \dots, n\}$ for which $v_i^* > 0$). Inequalities (4.13) imply that there exist constants $\varepsilon \in (0, 1)$ and $v_i^{min} \in (0, v_i^*)$ for $i \in R$ such that:

$$\begin{aligned} \sum_{i \in R} (n+1-i)v_i^{min} + \sum_{i \notin R} (n+1-i)v_i^* &\leq \min_{i=1, \dots, n} (((n-i)p_i + 1)f_{D,i}(x_i^*)) \\ &\text{and} \\ \sum_{i \in R} (n+1-i)v_i^{min} + \sum_{i \notin R} (n+1-i)v_i^* &\leq \varepsilon C \min_{i=1, \dots, n} ((n+1-i)\mu_i). \end{aligned} \quad (4.14)$$

We define the following parameters:

- $h := \min_{i=1, \dots, n} (\sigma^i (\mu_i - x_i^*)),$
- $\tilde{M} := \max(\min_{i=1, \dots, n} (\mu_i (n+1-i)), (1-C) \sum_{i=1}^n I_i(x^*) + (1-C)h \max_{i=1, \dots, n} ((n+1-i)\sigma^{-i}) + \sum_{i=1}^n (n+1-i)v_i^*),$
- $\bar{\theta} := h^{-1}(\tilde{M} - \varepsilon \min_{i=1, \dots, n} ((n+1-i)\mu_i)),$
- $\tau^* := \min(h, (\bar{\theta}L)^{-1} \sum_{i \in R} (n+1-i)(v_i^* - v_i^{min}))$ and let $\tau \in (0, \tau^*),$
- $A := 1 + (1-L)^{-1} \sum_{i \in R} \sigma^i \gamma_i,$ where $\gamma_i := \tau^{-1}(v_i^* - v_i^{min})$ for $i \in R,$
- $K := \frac{\sum_{i=1}^n \sigma^i \max(\rho_i^{max} - x_i^*, x_i^*) + A \sum_{i=1}^n \sigma^i (\rho_i^{max} - x_i^*) - (A+L)h}{(1-\varepsilon)C \min_{i=1, \dots, n} ((n+1-i)\mu_i)}.$

We next prove the implication:

$$\text{if } x \in \tilde{\Omega}, d \in [0, 1]^{n-1} \text{ and } v \in [0, v_1^*] \times \dots \times [0, v_n^*] \text{ then } \Xi(x^+) \leq L\Xi(x) \quad (4.15)$$

where $L \in (0, 1)$ is defined by (4.12) and $x^+ = \tilde{F}(d, x, u)$. Indeed, using (4.11) and definition (4.8), we get for all $x \in \tilde{\Omega}, d \in [0, 1]^{n-1}$ and $v \in [0, v_1^*] \times \dots \times [0, v_n^*]:$

$$\begin{aligned} \Xi(x^+) &= \sum_{i=2}^n \sigma^i \max(0, x_i - f_{D,i}(x_i) + (1-p_{i-1})f_{D,i-1}(x_{i-1}) + v_i - x_i^*) \\ &+ \sigma \max(0, x_1 - f_{D,1}(x_1) + v_1 - x_1^*) \leq \sum_{i=1}^n \sigma^i \max(0, x_i - f_{D,i}(x_i) + f_{D,i}(x_i^*) - x_i^*) \\ &+ \sum_{i=2}^n \sigma^i (1-p_{i-1}) \max(0, f_{D,i-1}(x_{i-1}) - f_{D,i-1}(x_{i-1}^*)) \end{aligned} \quad (4.16)$$

Using Assumption (H 2.1*), Consequences (C1), (C2), the fact that $\mu_i \leq \tilde{\rho}_i^{cr}$, for $i = 1, \dots, n$, and the fact that $f_{D,i}$ is increasing on $[0, \tilde{\rho}_i^{cr}]$, for $i = 1, \dots, n$, we get:

$$\begin{aligned} \max(0, f_{D,i}(x_i) - f_{D,i}(x_i^*)) &\leq G_i \max(0, x_i - x_i^*), \\ \max(0, x_i - f_{D,i}(x_i) + f_{D,i}(x_i^*) - x_i^*) &\leq \lambda_i \max(0, x_i - x_i^*), \\ \text{for all } x_i &\in [0, \mu_i], i = 1, \dots, n. \end{aligned} \quad (4.17)$$

Combining (4.12), (4.16), (4.17), we obtain implication (4.15). Next, we show the implication:

$$\text{if } x \in S, d \in [0, 1]^{n-1} \text{ and } v \in [0, v_1^*] \times \dots \times [0, v_n^*] \text{ then } P(x^+) \geq P(x), \quad (4.18)$$

where $x^+ = \tilde{F}(d, x, u)$. Indeed, (4.18) is a direct consequence of (4.15) and definition (4.10) when $x \in \tilde{\Omega}$. On the other hand, when $x \in S \setminus \tilde{\Omega}$ there exists at least one $i \in \{1, \dots, n\}$ for which $x_i > \mu_i$. Therefore, definition (4.8) implies $\Xi(x) > \min_{i=1, \dots, n} (\sigma^i (\mu_i - x_i^*))$, and consequently definition (4.10) gives $P(x) = \tilde{M} - \bar{\theta}h$ (a consequence of the fact that $h = \min_{i=1, \dots, n} (\sigma^i (\mu_i - x_i^*))$). Since $P(x) \geq \tilde{M} - \bar{\theta}h$ for all $x \in S$ (a consequence of (4.10)), we get $P(x^+) \geq \tilde{M} - \bar{\theta}h = P(x)$ when $x \in S \setminus \tilde{\Omega}$.

In what follows, we have $x^+ = \tilde{F}(d, x, k(x))$. Next we make the following claims. Their proofs are provided in the Appendix B.

(Claim 1): For all $x \in S, d \in [0, 1]^{n-1}$, the following inequality holds:

$$V(x^+) \leq V(x) - (1 - L) \sum_{i=1}^n \sigma^i |x_i - x_i^*|. \quad (4.19)$$

(Claim 2): There exist constants $K_2 \geq K_1 > 0$ such that the following inequality holds.

$$K_1 |x - x^*| \leq V(x) \leq K_2 |x - x^*| \text{ for all } x \in S. \quad (4.20)$$

Using (4.19), the fact that $\sigma \in (0, 1]$, and (4.20), we get for all $x \in S, d \in [0, 1]^{n-1}$:

$$\begin{aligned} V(x^+) &\leq V(x) - (1 - L) \sum_{i=1}^n \sigma^i |x_i - x_i^*| \\ &\leq V(x) - (1 - L) \sigma^n |x - x^*| \leq (1 - (1 - L) \sigma^n K_2^{-1}) V(x). \end{aligned}$$

The above inequality implies that the inequality

$$V(\tilde{F}(d, x, k(x))) \leq \tilde{L} V(x) \text{ for all } x \in S, d \in [0, 1]^{n-1} \quad (4.21)$$

holds with $\tilde{L} := 1 - (1 - L) \sigma^n K_2^{-1}$. Notice that $\tilde{L} \in (0, 1)$. Inequalities (4.20) and (4.21) show that the function $V : S \rightarrow \mathfrak{R}_+$ is a Lyapunov function with exponent $\kappa = 1$ for the closed-loop system (4.4) with $v = k(x)$. Remark A.1 guarantees that x^* is RGES for the closed-loop system (4.4) with $v = k(x)$. The proof is complete. \triangleleft

Remark 4.2: The proof of Theorem 4.1 provides a methodology for obtaining an estimation of the set $R \subseteq \{1, \dots, n\}$, the constant $\sigma \in (0, 1]$ and the critical constant $\tau^* > 0$. Let $C > 0$ be the constant involved in (2.13). Select $R \subseteq \{1, \dots, n\}$ to be a subset of the set of all indices $i \in \{1, \dots, n\}$, for which $v_i^* > 0$ and for which there

exist $v_i^{min} \in (0, v_i^*)$ such that:

$$\begin{aligned} \sum_{i \in R} (n+1-i) v_i^{min} + \sum_{i \notin R} (n+1-i) v_i^* &\leq \min_{i=1, \dots, n} ((n-i) p_i + 1) f_{D,i}(x_i^*) \\ \sum_{i \in R} (n+1-i) v_i^{min} + \sum_{i \notin R} (n+1-i) v_i^* &< C \min_{i=1, \dots, n} ((n+1-i) \mu_i) \end{aligned}$$

where $\mu_i > x_i^*$, for $i = 1, \dots, n$, are the constants defined by (2.11). Let $\varepsilon \in (0, 1)$ be a constant which satisfies $\sum_{i \in R} (n+1-i) v_i^{min} + \sum_{i \notin R} (n+1-i) v_i^* \leq \varepsilon C \min_{i=1, \dots, n} ((n+1-i) \mu_i)$. The estimation of the critical constant $\tau^* > 0$ may be done in the following way:

- Select $\sigma \in (0, 1]$ so that $L = \max(\lambda_n, \max_{i=1, \dots, n-1} (\lambda_i + \sigma G_i(1 - p_i))) < 1$,
Define:
- $h := \min_{i=1, \dots, n} (\sigma^i (\mu_i - x_i^*))$.
- $\tilde{M} := \max(\min_{i=1, \dots, n} (\mu_i (n+1-i)), (1-C) \sum_{i=1}^n I_i(x_i^*) + (1-C) h \max_{i=1, \dots, n} ((n+1-i) \sigma^{-i}) + \sum_{i=1}^n (n+1-i) v_i^*)$,
- $\bar{\theta} := h^{-1} (\tilde{M} - \varepsilon, \min_{i=1, \dots, n} ((n+1-i) \mu_i))$,

where $\lambda_i \in (0, 1)$, $G_i \in [0, 1]$ ($i = 1, \dots, n$), are the constants involved in Consequence (C2) and $I_j(x) := \sum_{i=1}^j x_i$ for $j = 1, \dots, n$. The estimated value of $\tau^* > 0$ is given by $\tau^* := \min(h, (\bar{\theta} L)^{-1} \sum_{i \in R} (n+1-i) (v_i^* - v_i^{min}))$. However, the estimated value of $\tau^* > 0$, which is obtained by applying the above methodology, may be conservative (significantly smaller than the actual value).

4.4 Illustrative Example

Consider a freeway model of the form (4.1), (4.2), (4.3), (2.16) with $n = 5$ cells. The freeway stretch considered for the simulation test is 2.5 km long and has three lanes. The cells are homogeneous, thus each cell is 0.5 km and it has no intermediate on/off-ramps (i.e., $v_i(t) \equiv v_i^* = 0$ for $i = 2, 3, 4, 5$ and $p_i = 0$ for $i = 1, \dots, 4$) (Figure 4.1). Consequently, the only control possibility is the inflow v_1 of the first cell. The simulation time step is set to $T = 15$ s. Each cell has the same critical density $\rho_i^{cr} = 55$ [veh] ($i = 1, \dots, 5$) (corresponding to 36.7 [veh/km/lane] with the above settings) and the same jam density $\rho_i^{max} = 170$ [veh] ($i = 1, \dots, 5$) (corresponding to 113.3 [veh/km/lane]). We also suppose that the cell flow capacities are $Q_i = 25$ [veh] $i = 1, 2, 3, 4$ and $Q_5 = 20$ [veh] (corresponding to 2000 [veh/h/lane] and 1600 [veh/h/lane], respectively). Note that the last cell has 20% lower flow capacity (e.g. due to grade or curvature or tunnel or bridge etc.) than the first four cells and is therefore a potential bottleneck for the freeway. Furthermore, the congestion wave speed is $c_i = 25/115$ ($i = 1, \dots, 4$) and $c_5 = 20/115$ (corresponding to 26 [km/h] and 20.9 [km/h], respectively).

Figure 4.2 depicts the triangular FDs for the above model. The dash-dotted line corresponds to the demand function, while the solid line corresponds to the supply function. More precisely, the demand part for every cell is given by the following functions:

$$f_{D,i}(z) = \begin{cases} (5/11)z & z \in [0, 55] \\ (25/115)(170 - z) & z \in (55, 87.2] \\ 18 & z \in (87.2, 170] \end{cases} \quad (i = 1, \dots, 4),$$

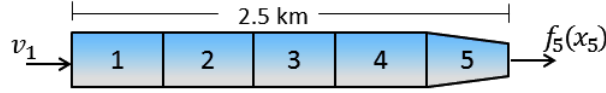


FIGURE 4.1: Freeway stretch.

$$f_{D,5}(z) = \begin{cases} (4/11)z & z \in [0, 55] \\ (20/115)(170 - z) & z \in (55, 72.25] \\ 17 & z \in (72.25, 170] \end{cases}$$

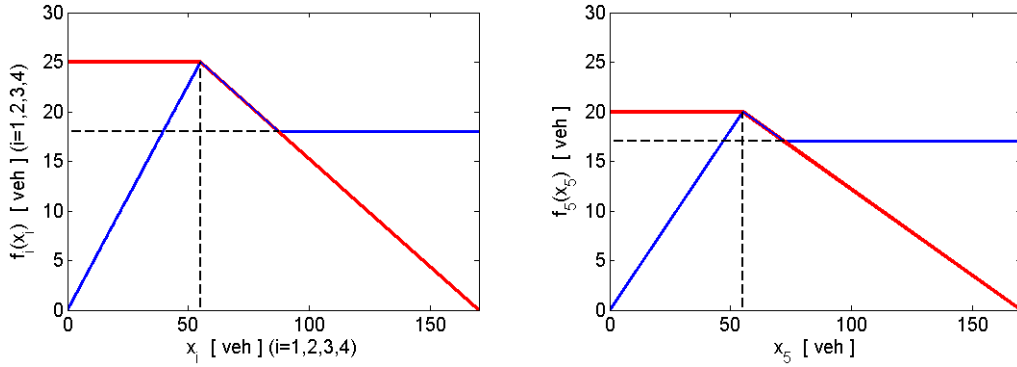


FIGURE 4.2: FD of every cell.

Notice that the capacity drop phenomenon has been taken into account by considering a partly decreasing demand function for over-critical densities $x_i \in (55, 170]$.

Assumption (H 2.1*) holds with $\rho_i^{cr} = \tilde{\rho}_i^{cr} = 55[\text{veh}]$ ($i = 1, \dots, 5$), $L_i = 6/11$ ($i = 1, \dots, 4$), $L_5 = 7/11$. The UEP $x_i^* = 11v_1^*/5[\text{veh}]$ ($i = 1, \dots, 4$), $x_5^* = 11v_1^*/4[\text{veh}]$, exists for $v_1^* < 20[\text{veh}]$. Simulations showed that the open-loop system converges to an UEP for main inflow v_1^* less than 17 [veh]. For higher values of the main inflow, the UEP is not globally exponentially stable due to the existence of additional (congested) equilibria. This is shown in Figure 4.3, where the evolution of the Euclidean norm of the deviation of the solution of the open-loop system, with constant inflow $v_1^* = 19.99[\text{veh}]$, from the UEP is depicted. In this test, the solution is attracted by the congested equilibrium $(91.8, 91.8, 91.8, 91.8, 72.25)'$ [veh] for which the value of the Euclidean norm of its deviation from the UEP is 97,19 [veh]. The components of the UEP for $v_1^* = 19.99[\text{veh}]$, are $x_i^* = 43.978[\text{veh}]$ ($i = 1, \dots, 4$) and $x_5^* = 54.9725[\text{veh}]$. Therefore, if the objective is the operation of the freeway with large flows, then a control strategy will be needed.

We next notice that Consequence (C2) holds with $\lambda_i = 6/11$, $G_i = 5/11$ ($i = 1, \dots, 4$), $\lambda_5 = 7/11$ and $G_5 = 4/11$. Therefore, we are in a position to achieve global exponential stabilization of the UEP for model (4.1)-(4.3) by using Theorem 4.1. Indeed, Theorem 4.1 guarantees that for every $\sigma \in (0, 1]$ there exists a constant $v_1^{\min} \in (0, v_1^*)$ and a constant $\gamma > 0$ such that, the feedback law $k : (0, 10]^5 \rightarrow \mathfrak{R}_+$ defined by:

$$v_1 = \max \left(v_1^* - \gamma \sum_{i=1}^5 \sigma^i \max(0, x_i - x_i^*), v_1^{\min} \right) \quad (4.22)$$

achieves RGES of the UEP $x^* = (x_1^*, \dots, x_5^*)' \in (0, 55)^5$ for the closed-loop system.

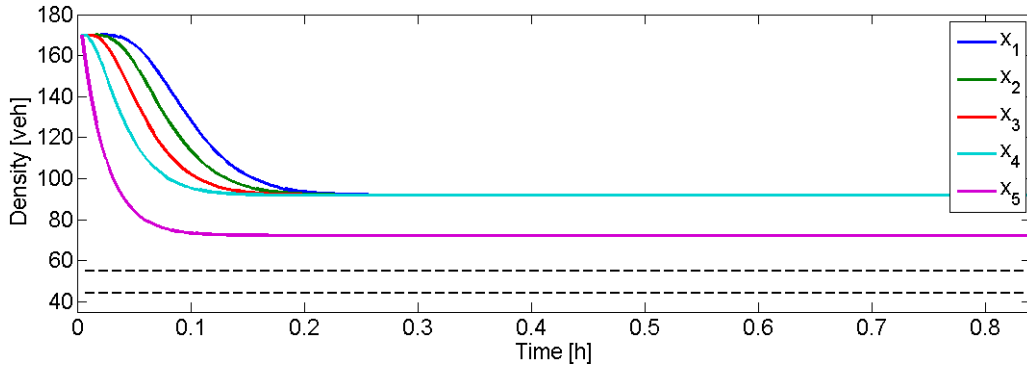


FIGURE 4.3: The response of the densities, for the open-loop system with constant inflow $v_1^* = 19.99$ [veh] and with fully congested initial condition.

We selected $v_1^* = 19.99$ [veh], which is very close to 20[veh], the capacity flow of cell 5. The value of the constant $v_1^{min} \in (0, v_1^*)$ was chosen to be 0.2 [veh]; this is a rather low minimum flow value in practice, but allows us here to study the dynamic properties of the regulators in a broader feasible control area. Various values of the constants $\sigma \in (0, 1]$ and $\gamma > 0$ were tested by performing a simulation study with respect to various initial conditions. Low values for $\sigma \in (0, 1]$ require large values for $\gamma > 0$ in order to have global exponential stability for the closed-loop system.

Moreover, in order to evaluate the performance of the controller, we used as a performance criterion the total number of Vehicles Exiting the Freeway (VEF) on the interval $[0, N]$, i.e.,

$$VEF_N = \sum_{k=0}^N f_{D,5}(x_5(k \cdot T)). \quad (4.23)$$

Notice that the freeway performs best (and total delays are minimised) if VEF is maximized; the maximum theoretical value for VEF is $20 \cdot (N + 1)$, which is achieved if cell 5 is operating at capacity flow ($Q_5 = 20$ [veh]) at all times. For $N = 200$, the maximum theoretical value of VEF is 4020 [veh].

All following tests of the proposed regulator (4.22) were conducted with the same values $\sigma = 0.7$ and $\gamma = 0.6$. The response of the density of all the cells for the closed-loop system with the proposed feedback regulator (4.22) and initial condition $x_0 = (60, 57, 58, 60, 62)'$ is shown in Figure 4.4(a). Notice that all initial cell density values are slightly overcritical (slightly congested). For this case, we had $VEF_{200} = 3979.8$ [veh]. The feedback regulator is seen to respond very satisfactorily in this test and achieves an accordingly high performance.

A detailed comparison of the proposed feedback regulator (4.22) was made with the Random Located Bottleneck (RLB) PI regulator, which was proposed in (Wang et al., 2010). The RLB PI regulator for the present system is implemented as follows:

$$z_i(t) = \min(z_{max}, \min(Q_1, c_1(\rho_1^{max} - x_1(t-1)), v_1(t-1)) + \psi, \max(z_{min}, P_i(t))), \quad (4.24)$$

$$P_i(t) = z_i(t-1) - K_p(x_i(t) - x_i(t-1)) + K_I(\rho_i^{ct} - x_i(t)) \quad (4.25)$$

$$z_i^{sm}(t) = \vartheta z_i(t) + (1 - \vartheta) z_i^{sm}(t-1) \quad (4.26)$$

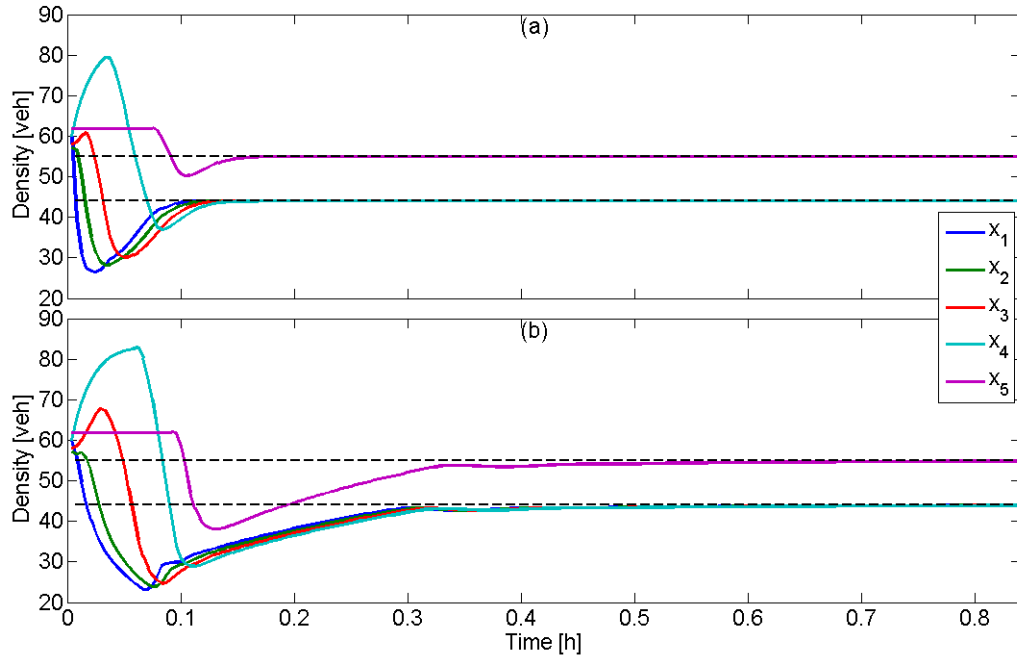


FIGURE 4.4: The response of the densities for the closed-loop system with initial condition $x_0 = (60, 57, 58, 60, 62)$ using (a) the proposed feedback regulator and (b) the RLB PI regulator.

$$j(t) = \min \left\{ l \in \{1, 2, 3, 4, 5\} : z_l^{sm}(t) = \min_{i=1, \dots, 5} (z_i^{sm}(t)) \right\} \quad (4.27)$$

$$v_1(t) = z_{j(t)}(t). \quad (4.28)$$

for $i = 1, \dots, 5$, where $\psi, K_p, K_I > 0$ and $\vartheta \in (0, 1)$ are constant parameters. Essentially, (4.24) reflects the parallel (independent) operation of five bounded PI-type regulators, one for each cell; while (4.26) performs an exponential smoothing of the respective obtained inflows (with smoothing parameter ϑ). Eventually, the smoothed inflow values are compared in (4.27) in order to pick the currently most conservative regulator; whose (unsmoothed) inflow is finally actually activated as a control input in (4.28), see (Wang et al., 2010) for the background and detailed reasoning for this approach. The parameters for the RLB PI regulators are set (as proposed in (Wang et al., 2010) - with the suitable transformation in the current units) to be $K_p = 5/18$, $K_I = 1/90$, while $\psi = 4[\text{veh}]$, $\vartheta = 0.5$, $u_{\min} = 0.2[\text{veh}]$ and $u_{\max} = 25[\text{veh}]$. These values were indeed tested, before being adopted, and were indeed found to be near optimal. Notice that all PI regulators were given the same gain values for simplicity and convenience, as suggested by Wang et al., 2010. In all reported tests, the initial condition for the RLB PI regulator was $z_i(-1) = z_i^{sm}(-1) = z_1(-1) = 20[\text{veh}]$, for $i = 1, \dots, 5$, and $x(-1) = x(0) = x_0$, where x_0 is the vector of the initial values for the densities of every cell.

When applied to the same initial condition $x_0 = (60, 57, 58, 60, 62)'$, the RLB PI regulator (Figures 4.4(b)), led to slower convergence compared with the proposed regulator (4.22). This is also reflected in the computed value of $VEF_{200} = 3785.9[\text{veh}]$ for RLB PI regulator. In general, conducting a simulation study with

various levels of initial conditions, the proposed regulator (4.22) exhibited faster performance than the RLB PI regulator. For example, Figure 4.5 shows the evolution of the Euclidean norm $|x(t) - x^*|$ for the closed-loop system with the proposed feedback regulator (4.22) (blue) and for the closed-loop system with the RLB PI regulator (4.24)-(4.28) (red), when starting from the initial condition $x_0 = (\rho_1^{max}, \dots, \rho_5^{max})'$, reflecting a fully congested original state. It is again clear that the proposed feedback regulator (4.22) achieves faster convergence and higher performance of $VEF_{200} = 3845.2[\text{veh}]$ compared to $VEF_{200} = 3007.8[\text{veh}]$, which is resulted for the RLB PI regulator.

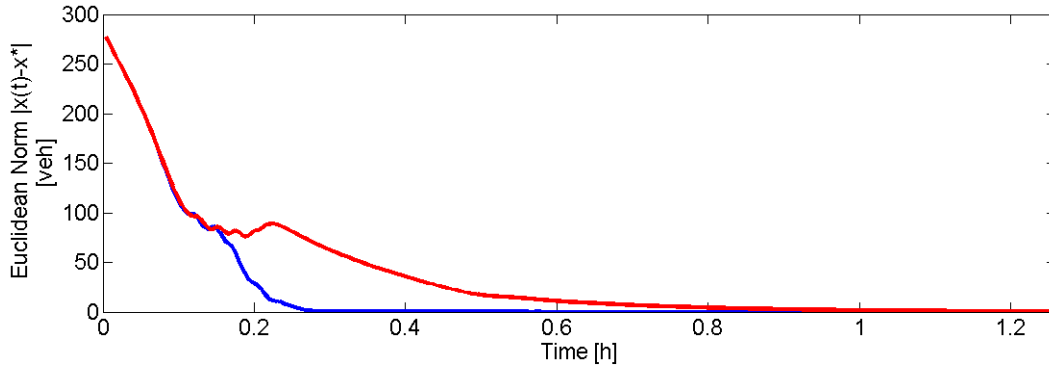


FIGURE 4.5: The evolution of the Euclidean norm $|x(t) - x^*|$ of the closed-loop system with a fully congested using the proposed feedback regulator (blue line) and the RLB PI regulator (red line).

We next investigated the robustness of the proposed feedback regulator with respect to measurement errors. The applied formula for the measurements is:

$$\tilde{x}(t) = PR(x(t) + Ae(t)), \quad (4.29)$$

where PR is the projection operator on the closure of S , $e(t)$ is a normalized vector, and $A \geq 0$ is the magnitude of the measurement error. In this case, the feedback law (4.22) was implemented based on the state measurement $\tilde{x}(t)$ given by (4.29), i.e.,

$$v_1(t) = \max \left(v_1^* - \gamma \sum_{i=1}^5 \sigma^i \max(0, \tilde{x}_i(t) - x_i^*), v_1^{min} \right). \quad (4.30)$$

For comparison purposes, we also present the performance of the RLB PI regulator for the same system, under the same measurement errors. In this case, equation (4.25) is replaced by the equation :

$$P_i(t) = z_i(t-1) - K_p(\tilde{x}_i(t) - \tilde{x}_i(t-1)) + K_I(\rho_i^{ct} - \tilde{x}_i(t)), \quad (4.31)$$

for $i = 1, \dots, 5$, where the state measurement $\tilde{x}(t)$ is given by (4.29).

Figure 4.6 shows the response of the cell densities for two cases: (a) for the closed-loop system with the proposed feedback regulator (4.30) and (b) for the closed-loop system with the RLB PI regulator (4.24), (4.31), (4.26)-(4.28), where the state measurement in both cases is given by (4.29) with $A = 10[\text{veh}]$, $e(t) = \frac{\cos(\omega t)}{\sqrt{5}}(1, 1, \dots, 1)$, $\omega = \pi$. The initial condition is the UEP.

In this test, the RLB PI regulator is less sensitive to measurement errors than the proposed feedback regulator (4.30), the latter producing a higher offset (Figure

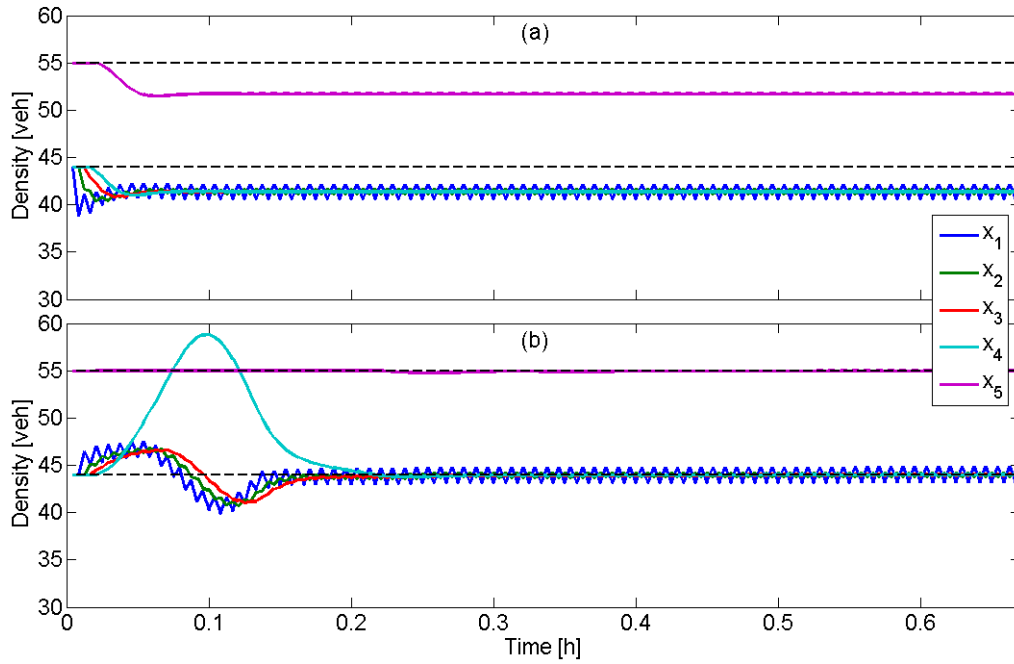


FIGURE 4.6: The response of the densities of the closed-loop system with initial condition $x_0 = x^*$ under (a) the proposed feedback regulator and (b) the RLB PI regulator. In both cases the state measurement is given by (4.29) with $A = 10[\text{veh}]$, $e(t) = (\cos(\omega t)/\sqrt{5})(1, \dots, 1)$ and $\omega = \pi$.

4.6(a)). This is also reflected in the computed values of $VEF_{200} = 3789[\text{veh}]$ for the proposed feedback regulator (4.30) (which is 6% less than the maximum value of VEF_{200}) and $VEF_{200} = 4016.8[\text{veh}]$ for the RLB PI regulator (which is 0.8% less than the maximum value of VEF_{200}) due to the measurement error. The ultimate mean values of the states are much closer to the equilibrium values for the RLB PI regulator than for the proposed feedback regulator (4.30), indicating that the RLB PI regulator achieves a much smaller mean offset in this case. It should be noted at this point that various frequencies ω were tested for measurement errors. While Figure 4.6 is typical for medium and high frequencies (the RLB PI regulator achieves a smaller mean offset than the proposed feedback regulator (4.30)), the results indicate higher sensitivity of the RLB PI regulator with respect to measurement errors at low frequencies (Figure 4.7). For low frequency measurement errors, the proposed feedback regulator (4.30) achieves a smaller mean offset than the RLB PI regulator, as shown in Figure 4.7(a) and (b), respectively. Figure 4.7 shows the response of the densities (a) for the closed-loop system with the proposed feedback regulator (4.30), and (b) for the closed-loop system with the RLB PI regulator (4.24), (4.31), (4.26)-(4.28), where the state measurement in both cases is given by (4.29) with $A = 10[\text{veh}]$, $e(t) = (\cos(\omega t)/\sqrt{5})(1, 1, \dots, 1)$, $\omega = 0.1$. The initial condition is the UEP.

The conclusions of this simulation study are: 1) the proposed feedback regulator (4.22) can achieve a faster convergence of the state to the equilibrium compared to the RLB PI regulator in the absence of measurement errors, and 2) the proposed feedback regulator (4.30) is quite robust to measurement errors. However, it is more sensitive to measurement errors with high frequency than the RLB PI regulator; but it is less sensitive to low-frequency measurement errors than the RLB PI regulator. Intended future extensions are expected to improve the properties of the proposed

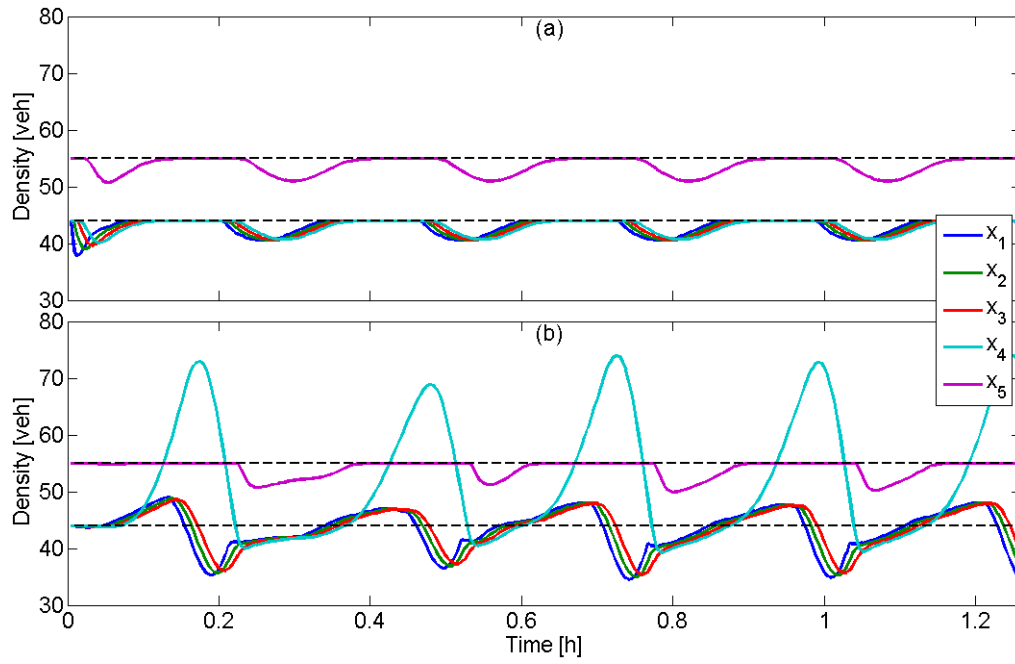


FIGURE 4.7: The response of the densities of the closed-loop system with initial condition $x_0 = x^*$ under (a) the proposed feedback regulator and (b) the RLB PI regulator. In both cases the state measurement is given by (4.29) with $A = 10[\text{veh}]$, $e(t) = (\cos(\omega t)/\sqrt{5})(1, \dots, 1)$ and $\omega = 0.1$.

feedback regulator in this respect, as well as in cases of modelling errors or persisting disturbances.

Chapter 5

Adaptive Stabilization of Discrete-Time Systems with Application to Freeway Traffic Control

5.1 Introduction

Adaptive control for discrete-time systems has been studied in many works (see for instance (Hayakawa, Haddad, and Leonessa, 2004; Zhang, Wen, and Soh, 1999; Zhang, Wen, and Soh, 2001; Zhao and Kanellakopoulos, 1997) and in many cases it is a direct extension of ACSs for continuous-time systems (see (Krstic, Kokotovic, and Kanelakopoulos, 1995)). The limitations of ACSs for discrete-time systems have been studied in (Xie and Guo, 1999). The major shortcoming of many adaptive control methodologies is that the closed-loop system does not exhibit an exponential convergence rate to the desired equilibrium point of the system, even if the nominal feedback law achieves global exponential stability properties when the parameters are precisely known.

This work is devoted to the development of ACSs for general uncertain discrete-time systems, with unknown constant parameters, which guarantee robust global exponential convergence to the desired equilibrium point. The idea is simple: use a nominal feedback law, which achieves RGES properties when the vector of the parameters is known, in conjunction with a nonlinear, dead-beat observer. The dead-beat observer (designed using an extension of the methodology described in (Karafyllis and Kravaris, 2007)) achieves the precise knowledge of the vector of unknown parameters after a transient period; then the states of the closed-loop system are robustly led to the desired equilibrium point with an exponential rate by the nominal feedback law. The proposed ACS does not require the knowledge of a Lyapunov function for the closed-loop system under the action of the nominal feedback stabilizer. The applicability of the obtained results is demonstrated by the rigorous application of the proposed ACS to the freeway models developed and presented in Section 2.2.3 of Chapter 2.

A Lyapunov approach was adopted in Chapter 4, which led to the RGES of the UEP of general nonlinear freeway models. However, the nonlinear feedback stabilizer demands the knowledge of several model parameters, which are usually unknown. The present chapter proposes an ACS, based on the existence of the nominal feedback law developed in Chapter 4 and a nonlinear dead-beat observer. The proposed ACS guarantees the robust global exponential convergence rate to the desired UEP of the freeway model (2.18)-(2.20).

The structure of the present chapter is as follows: Section 5.2 is devoted to the development of the robust global exponential ACSs for general nonlinear uncertain

discrete-time systems. The obtained results are applied rigorously, in Section 5.3, to the general uncertain freeway model (2.18)-(2.20) of Section 2.2.3, while the proofs of the main results can be found in Section 5.4. An illustrating example is presented in Section 5.5.

5.2 General Result

Consider the discrete-time system:

$$x^+ = f(d, \theta^*, x, u), x \in S, d \in D, u \in U, \theta^* \in \Theta, \quad (5.1)$$

where $S \subseteq \mathbb{R}^n$, $D \subseteq \mathbb{R}^l$, $U \subseteq \mathbb{R}^m$, $\Theta \subseteq \mathbb{R}^q$ are non-empty sets and $f : D \times \Theta \times S \times U \rightarrow S$ is a locally bounded mapping. In this setting, $x \in S$ denotes the state of the system (5.1), $d \in D$ is an unknown, time-varying input, $u \in U$ is the control input and $\theta^* \in \Theta$ denotes the vector of unknown, constant parameters. The measured output of the system is given by:

$$y(t) = h(d(t), \theta^*, x(t)), \quad (5.2)$$

where $h : D \times \Theta \times S \rightarrow \mathbb{R}^k$ is a locally bounded mapping. Let $Y \subseteq \mathbb{R}^k$ be a set with $h(D \times \Theta \times S) \subseteq Y$. We assume that $x^* \in S$ is an equilibrium point for system (5.1) and $d \in D$ is a vanishing perturbation, i.e., there exist vectors $y^* \in h(D \times \{\theta^*\} \times S)$ and $u^* \in U$ such that $f(d, \theta^*, x^*, u^*) = x^*$, $y^* = h(d, \theta^*, x^*)$ for all $d \in D$. Notice that $y^* \in Y$. By $y^{(\kappa)}(t) = (y(t-1), y(t-2), \dots, y(t-\kappa))$ for certain positive integer $\kappa > 0$, we denote the " κ -history" of the signal $y(t)$ (defined for all $t \geq \kappa$). By (y^*, \dots, y^*) we mean the vector in $\mathbb{R}^{k\kappa}$ which is formed by combining the vector $y^* \in \mathbb{R}^k$ κ times. Since $y^* \in Y$, it follows that $(y^*, \dots, y^*) \in Y^\kappa$.

The main result of this chapter provides sufficient conditions for dynamic RGES of the equilibrium point $x^* \in S$. The stabilizer is constructed under the following assumptions for system (5.1), (5.2):

J1

Suppose that there exists a mapping $K : \Theta \times Y \rightarrow U$ such that $x^* \in S$ is RGES for the closed-loop system (5.1), (5.2) with $u = K(\theta^*, y)$.

J2

Suppose that there exist a positive integer $\kappa > 0$, a set $A \subseteq Y^\kappa$ which contains all $w \in Y^\kappa$ in a neighborhood of (y^*, \dots, y^*) and a mapping $\Psi : Y \times A \rightarrow \Theta$, such that for every sequence $\{(d(t), \hat{\theta}(t)) \in D \times \Theta\}_{t=0}^\infty$ and for every $x_0 \in S$, the solution $x(t)$ of (5.1), (5.2) with $u = K(\hat{\theta}, y)$, initial condition $x(0) = x_0$ corresponding to inputs $\{(d(t), \hat{\theta}(t)) \in D \times \Theta\}_{t=0}^\infty$ satisfies $\theta^* = \Psi(y(t), y^{(\kappa)}(t))$ for all $t \geq \kappa$ with $y^{(\kappa)}(t) \in A$.

J3

(J3) There exists a positive integer $m > 0$, such that for every sequence $\{(d(t), \hat{\theta}(t)) \in D \times \Theta\}_{t=0}^\infty$ and for every $x_0 \in S$, the solution $x(t)$ of (5.1), (5.2) with $u = K(\hat{\theta}, y)$, initial condition $x(0) = x_0$ corresponding to inputs $\{(d(t), \hat{\theta}(t)) \in D \times \Theta\}_{t=0}^\infty$ satisfies $y^{(\kappa)}(t - i(t)) \in A$ for some $i(t) \in \{0, 1, \dots, m\}$ and for all $t \geq m + \kappa$.

Assumption (J1) is a standard assumption, which guarantees the existence of a robust global exponential stabilizer when the vector of the parameters $\theta^* \in \Theta$ is known. Assumptions (J2)-(J3) are equivalent to complete, robust observability of θ^* from the output given by (5.2) (see, also Karafyllis and Kravaris, 2007). More specifically, Assumption (J2) guarantees the existence of a function Ψ (the reconstruction map, see Karafyllis and Kravaris, 2007), which gives the exact value of θ^* , provided that the κ -history of the output signal belongs to a specific set A . Assumption (J3) guarantees that the κ -history of the output signal is bound to enter the set A , every m time units.

The following result combines a certainty equivalence type controller with a finite-time identifier and guarantees exponential convergence both of the state $x(t)$ and the estimate $\hat{\theta}(t)$ to x^* and θ^* , respectively, for every disturbance $d(t)$.

Theorem 5.1

Consider system (5.1) with output given by (5.2) under Assumptions (J1), (J2), (J3). Moreover, suppose that the sets $f(D \times \Theta \times S \times U)$, Y , Θ are bounded. Finally, assume that there exist a constant $L \geq 0$, neighborhoods $N_1 \subseteq \mathbb{R}^n$ of x^* , $N_2 \subseteq \mathbb{R}^k$ of y^* , $N_3 \subseteq \mathbb{R}^q$ of θ^* , such that the inequalities $|f(d, \theta^*, x, K(\hat{\theta}, h(d, \theta^*, x))) - x^*| + |h(d, \theta^*, x) - y^*| \leq L|x - x^*| + L|\hat{\theta} - \theta^*|$ and $|\Psi(h(d, \theta^*, x), w) - \theta^*| \leq L|x - x^*| + L \sum_{i=1}^{\kappa} |w_i - y^*|$ hold for all $x \in N_1 \cap S$, $d \in D$, $\hat{\theta} \in N_3 \cap \Theta$, $w_i \in N_2 \cap Y$ ($i = 1, \dots, p$) with $w = (w_1, \dots, w_p)$.

Then, the dynamic feedback stabilizer

$$\begin{aligned} w_1^+ &= y \\ w_2^+ &= w_1 \\ &\vdots \\ w_{\kappa}^+ &= w_{\kappa-1} \\ \hat{\theta}^+ &= \begin{cases} \hat{\theta} & \text{if } w \notin A \\ \Psi(y, w) & \text{if } w \in A \end{cases} \\ u &= K(\hat{\theta}, y) \end{aligned} \quad (5.3)$$

where $w = (w_1, \dots, w_{\kappa}) \in Y^{\kappa}$, $\hat{\theta} \in \Theta$ achieves the following:

1) There exist constants $M, \sigma > 0$ such that for every sequence $\{d(t) \in D\}_{t=0}^{\infty}$ and for every $(x_0, w_0, \hat{\theta}_0) \in S \times Y^{\kappa} \times \Theta$, the solution $(x(t), w(t), \hat{\theta}(t))$ of the closed-loop system (5.1), (5.2) with (5.3), initial condition $(x(0), w(0), \hat{\theta}(0)) = (x_0, w_0, \hat{\theta}_0)$ corresponding to input $\{d(t) \in D\}_{t=0}^{\infty}$ satisfies

$$\begin{aligned} |x(t) - x^*| + \sum_{i=1}^{\kappa} |w_i(t) - y^*| + |\hat{\theta}(t) - \theta^*| \leq \\ M \exp(-\sigma t) \left(|x(0) - x^*| + \sum_{i=1}^{\kappa} |w_i(0) - y^*| + |\hat{\theta}(0) - \theta^*| \right) \end{aligned} \quad (5.4)$$

for all $t \geq 0$.

2) For every sequence $\{d(t) \in D\}_{t=0}^{\infty}$ and for every $(x_0, w_0, \hat{\theta}_0) \in S \times Y^{\kappa} \times \Theta$ the solution $(x(t), w(t), \hat{\theta}(t))$ of the closed-loop system (5.1), (5.2) with (5.3), initial condition $(x(0), w(0), \hat{\theta}(0)) = (x_0, w_0, \hat{\theta}_0)$ corresponding to input $\{d(t) \in D\}_{t=0}^{\infty}$ satisfies $\hat{\theta}(t) = \theta^*$, for all $t \geq m + \kappa + 1$.

Remark 5.1: The dynamic feedback stabilizer (5.3) achieves dead-beat estimation (provided by the variable $\hat{\theta} \in \Theta$) of the vector of unknown constant parameters $\theta^* \in \Theta$. Due to the dead-beat estimation, the exponential convergence property for the closed-loop system is preserved, as estimate (5.4) shows.

5.3 Main Result: Application to Freeway Traffic Control

5.3.1 Global Exponential Stabilization of Freeway Models

Consider the freeway model (2.18)-(2.20) with (2.15) and (2.16). We make the following assumption for the functions $f_{D,i} : [0, \rho_i^{max}] \rightarrow \mathfrak{R}_+$, ($i = 1, \dots, n$):

H 5.1

There exist constants $\rho_i^{cr} \in (0, \rho_i^{max})$ and $v_{f,i} \in (0, 1)$ such that $f_{D,i}(z) = v_{f,i}z$ for $z \in [0, \rho_i^{cr}]$. Moreover, there exists a positive constant $f_i^{min} > 0$ such that $f_{D,i}(\rho_i^{cr}) = v_{f,i}\rho_i^{cr} \geq f_{D,i}(z) \geq f_i^{min}$ for all $z \in [\rho_i^{cr}, \rho_i^{max}]$.

Remark 5.2: The implications of Assumption (H 5.1) for the demand function are illustrated in Figure 5.1. Assumption (H 2.1*), related with the freeway models of Section 2.2.3, is more general than Assumption (H 5.1); however, for the development of the methodology of Chapter 4, it was assumed that all parameters of the model were known. More specifically, for Assumption (H 2.1*), it was not necessary the demand functions $f_{D,i} : [0, \rho_i^{max}] \rightarrow \mathfrak{R}_+$, ($i = 1, \dots, n$) to be linear on the corresponding intervals $[0, \rho_i^{cr}]$; however, this is the only difference between (H 2.1*) and (H 5.1). The linearity of the demand functions on the interval $[0, \rho_i^{cr}]$ is a consequence of the consideration of constant free flow speed for under-critical densities (here, represented by the dimensionless variable $v_{f,i} \in (0, 1)$), which is suggested in many studies in the literature (see, for example, Daganzo, 1995b).

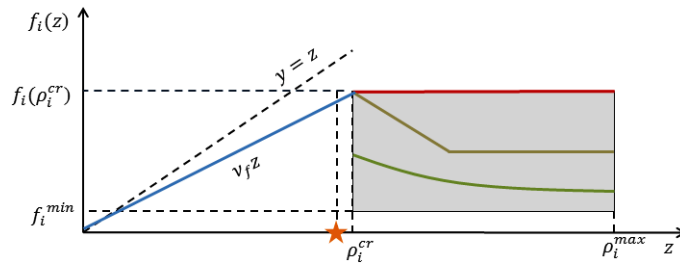


FIGURE 5.1: Implications of Assumption (H 5.1).

Consider the freeway model (4.4) under Assumption (H 5.1). Let $v^* = (v_1^*, \dots, v_n^*)' \in (0, +\infty) \times \mathfrak{R}_+^{n-1}$ be a vector that satisfies (4.6). Any inflow vector that satisfies (4.6), defines an UEP $x^* = (x_1^*, \dots, x_n^*) \in \prod_{i=1}^n (0, \rho_i^{cr})$ for the freeway model, which satisfies (4.5) and can be written in the following form under Assumption (H 5.1):

$$x_1^* = v_{f,1}^{-1} v_1^* \quad , \quad x_i^* = v_{f,i}^{-1} \left(v_i^* + \sum_{j=1}^{i-1} v_j^* \prod_{k=j}^{i-1} (1 - p_k) \right), \quad i = 2, \dots, n \quad (5.5)$$

As discussed in the previous chapters, the UEP is not globally exponentially stable for arbitrary $v_1^* > 0, v_i^* \geq 0$ ($i = 2, \dots, n$). Indeed, simulations show that there are critical values of inflows, so that if the inflows $v_i^* \geq 0$ ($i = 1, \dots, n$) are larger than the critical values, then other equilibria for model (2.18)-(2.20) (congested equilibria) appear. These congested equilibria have large cell densities and attract the solution of (2.18)-(2.20).

The nominal feedback for the ACS that we intend to use is provided by Theorem 4.1. Theorem 4.1 is based on the construction of a CLF approach for system (2.18)-(2.20) under a more general assumption than Assumption (H 5.1) (see Assumption (H 2.1*)). The feedback law provides values for the controllable inflows ($v_i, i \in R$), in the interval $[v_i^{min}, v_i^*]$ for all $i \in R$, where $v_i^{min} \in (0, v_i^*)$, for $i \in R$, are the minimum allowable inflows. Since the proof of Theorem 4.1 is constructive, criteria for the selection of the index set $R \subseteq \{1, \dots, n\}$ and the constants $\sigma \in (0, 1]$, $v_i^{min} \in (0, v_i^*)$ for $i \in R$ and $\tau^* > 0$ are provided. Without loss of generality, we will assume, in what follows, that $R \neq \emptyset$ (because otherwise the UEP is open-loop RGES).

Let $\mu_i \in (0, \rho_i^{cr}), v_i^{max} < (0, +\infty)$ ($i = 1, \dots, n$) be constants such that:

$$\begin{aligned} v_1^{max} &< f_{S,1}(\mu_1), \\ v_i^{max} + (1 - p_{i-1})v_{f,i-1}\mu_{i-1} &< f_{S,i}(\mu_i), i = 2, \dots, n. \end{aligned} \quad (5.6)$$

It follows that if $x \in \Omega = \prod_{i=1}^n (0, \mu_i)$ and $v \in (0, v_1^{max}] \times \prod_{i=1}^n [0, v_i^{max}]$:

$$\bar{s}_i = 1, \text{ for } i = 1, \dots, n \text{ and } s_i = 1 \text{ for } i = 2, \dots, n, \quad (5.7)$$

$$\begin{aligned} x_1^+ &= x_1 - f_{D,1}(x_1) + v_1 \\ x_i^+ &= x_i - f_{D,i}(x_i) + v_i + (1 - p_{i-1})f_{D,i-1}(x_{i-1}), i = 2, \dots, n \end{aligned} \quad (5.8)$$

In what follows, we assume that $x^* = (x_1^*, \dots, x_n^*) \in \prod_{i=1}^n (0, \mu_i - \varepsilon]$, $v_i^* \in [v_i^{min} + \varepsilon, v_i^{max}]$ for $i \in R$ and for some $\varepsilon \in (0, 1/2)$ and $v^* \in (0, v_1^{max}] \times \prod_{i=2}^n [0, v_i^{max}]$. Moreover, we assume that $p_i \in [0, 1 - \varepsilon]$, for $i = 1, \dots, n - 1$ and $v_{f,i} \in [\varepsilon, 1 - \varepsilon]$, for $i = 1, \dots, n$.

Another feature of the present problem is that the selection of the UEP may be made in an implicit way. For example, we may want the UEP that guarantees the maximum outflow from the freeway. In such cases, the equilibrium position of the controllable inflows is determined as a function of the nominal values of the uncontrollable inflows and the parameters of the freeway, i.e., there exists a smooth function:

$$g : [0, 1 - \varepsilon]^{n-1} \times \prod_{i \notin R} [0, v_i^{max}] \times [\varepsilon, 1 - \varepsilon]^n \rightarrow \prod_{i \in R} [v_i^{min} + \varepsilon, v_i^{max}]$$

such that

$$(v_i^*; i \in R) = g(p, v_i^*; i \notin R, v_f) \quad (5.9)$$

where $p = (p_1, \dots, p_{n-1})' \in [0, 1 - \varepsilon]^{n-1}$ and $v_f = (v_{f,1}, \dots, v_{f,n})' \in [\varepsilon, 1 - \varepsilon]^n$.

5.3.2 Measurements and Unknown Parameters

Let $m \in \{1, \dots, n\}$ be the cardinal number of the set R and let $u \in U = \prod_{i \in R} [v_i^{min}, v_i^{max}] \subseteq (0, +\infty)^m$ be the vector of all controllable inflows v_i with $i \in R$. The model parameters which are (usually) unknown or uncertain are: the exit rates $p_i \in [0, 1)$,

for $i = 1, \dots, n-1$, the uncontrollable inflows $v_i^* \in \mathfrak{R}_+$ for $i \notin R$ and the demand coefficients $v_{f,i} \in (0, 1)$, for $i = 1, \dots, n$. All these parameters will be denoted by $\theta^* = (p, v_i^*; i \notin R, v_f)$ and are assumed to take values in a compact set $\Theta := [0, 1 - \varepsilon]^{n-1} \times \prod_{i \notin R} [0, v_i^{max}] \times [\varepsilon, 1 - \varepsilon]^n$, for some $\varepsilon \in (0, 1/2)$. Therefore, the control system (2.18)-(2.20) can be written in the following vector form:

$$\begin{aligned} x^+ &= \bar{F}(d, \theta^*, x, u), \\ x \in S, d \in D, \theta^* \in \Theta, u \in U &= \prod_{i \in R} [v_i^{min}, v_i^{max}]. \end{aligned} \quad (5.10)$$

Notice that the feedback law defined by (4.7) is a feedback law of the form $u = K(\theta^*, x)$: the feedback law depends on the unknown parameters through x^* and $(v_i^*; i \in R)$ (recall (5.5) and (5.9)). It follows that Assumption (J1) holds for system (5.10). An explicit definition of the feedback law $K : \Theta \times S \rightarrow U$ is given by the following equations for all $\hat{\theta} = (\hat{p}, \hat{v}_i^*; i \notin R, \hat{v}_f) \in \Theta$, $x \in S$ with $\hat{v}_f = (\hat{v}_{f,1}, \dots, \hat{v}_{f,n})' \in [\varepsilon, 1 - \varepsilon]^n$, $\hat{p} = (\hat{p}_1, \dots, \hat{p}_{n-1})' \in [0, 1 - \varepsilon]^{n-1}$:

$$(\hat{v}_i^*; i \in R) = g(\hat{p}, \hat{v}_i^*; i \notin R, \hat{v}_f), \quad (5.11)$$

$$\begin{aligned} \hat{x}_1^* &= \min(\hat{v}_{f,1}^{-1} \hat{v}_1^*, \mu_1 - \varepsilon), \\ \hat{x}_i^* &= \min \left(\hat{v}_{f,i}^{-1} \left(\hat{v}_i^* + \sum_{j=1}^{i-1} \hat{v}_j^* \prod_{k=j}^{i-1} (1 - \hat{p}_k) \right), \mu_i - \varepsilon \right), \quad i = 2, \dots, n, \end{aligned} \quad (5.12)$$

$$\begin{aligned} u &= K(\hat{\theta}, x) \text{ with} \\ K_i(\hat{\theta}, x) &= \max(v_i^{min}, \hat{v}_i^* - \tau^{-1}(\hat{v}_i^* - v_i^{min})\Xi(\hat{\theta}, x)), \quad x \in S, i \in R, \end{aligned} \quad (5.13)$$

$$\Xi(\hat{\theta}, x) := \sum_{i=1}^n \sigma^i \max(0, x_i - \hat{x}_i^*), \quad x \in S. \quad (5.14)$$

The measured quantities are the cell densities $x \in S$ and the outflows from each cell. We have two kinds of outflows from each cell: the outflow to regions out of the freeway

$$\begin{aligned} q^{ext} &= (q_1^{ext}, \dots, q_n^{ext})' \in \mathfrak{R}_+^n, \\ q_i^{ext} &= p_i s_{i+1} f_{D,i}(x_i), \quad i = 1, \dots, n-1, q_n^{ext} = f_{D,n}(x_n), \end{aligned} \quad (5.15)$$

and the outflows from one cell to the next cell

$$\begin{aligned} q^{int} &= (q_1^{int}, \dots, q_{n-1}^{int})' \in \mathfrak{R}_+^{n-1}, \\ q_i^{int} &= (1 - p_i) s_{i+1} f_{D,i}(x_i), \quad i = 1, \dots, n-1. \end{aligned} \quad (5.16)$$

Therefore, the measured output is given by:

$$y = h(d, \theta^*, x) = (x, q^{ext}, q^{int}) \in S \times \mathfrak{R}_+^n \times \mathfrak{R}_+^{n-1}. \quad (5.17)$$

Assumption (H5.1) guarantees that $h(D \times \Theta \times S) \subseteq Y$, where $Y := S \times \prod_{i=1}^n [0, \rho_i^{max}] \times \prod_{i=1}^{n-1} [0, \rho_i^{max}]$ is a bounded set. It follows from (5.7), (5.8), (5.15), (5.16), Assumption (H5.1) and the fact that $\mu_i \in (0, \rho_i^{er})$ ($i = 1, \dots, n$), that if $x(t-1) \in \Omega = \prod_{i=1}^n (0, \mu_i)$,

$t \geq 1$, then the following equations hold:

$$p_i = \frac{q_i^{ext}(t-1)}{q_i^{ext}(t-1) + q_i^{int}(t-1)}, i = 1, \dots, n-1, \quad (5.18)$$

$$v_i^* = x_i(t) - x_i(t-1) + q_i^{int}(t-1) + q_i^{ext}(t-1) - q_{i-1}^{int}(t-1), i \in \{2, \dots, n\} \setminus R, \quad (5.19)$$

$$v_n^* = x_n(t) - x_n(t-1) + q_n^{ext}(t-1) - q_{n-1}^{int}(t-1), \text{ if } n \notin R, \quad (5.20)$$

$$v_1^* = x_1(t) - x_1(t-1) + q_1^{int}(t-1) + q_1^{ext}(t-1), \text{ if } 1 \notin R, \quad (5.21)$$

$$v_{f,i} = \frac{q_i^{ext}(t-1) + q_i^{int}(t-1)}{x_i(t-1)}, i = 1, \dots, n-1, v_{f,n} = \frac{q_n^{ext}(t-1)}{x_n(t-1)} \quad (5.22)$$

Equations (5.18)-(5.22), (5.17) allow us to define a mapping $\Psi : h(D \times \Theta \times S) \times Y \rightarrow \Theta$ for which $\theta^* = (p_1, \dots, p_{n-1}, v_i^*; i \notin R, v_{f,1}, \dots, v_{f,n})' = \Psi(y(t), y(t-1))$ for all $t \geq 1$ with $y(t-1) \in A$, where $A \subseteq Y$ is the set for which:

$$A := \{w = (w_1, w_2, w_3) \in Y | w_1 \in \Omega \text{ and } w_{2,i} + w_{3,i} > 0 \text{ for } i = 1, \dots, n-1\}, \quad (5.23)$$

where $\Omega = \prod_{i=1}^n (0, \mu_i)$. The mapping $\Psi : h(D \times \Theta \times S) \times Y \rightarrow \Theta$ is defined by:

$$\hat{\theta} = (\hat{p}_1, \dots, \hat{p}_{n-1}, \hat{v}_i^*; i \notin R, \hat{v}_{f,1}, \dots, \hat{v}_{f,n})' = \Psi(y, w), \quad (5.24)$$

with

$$\hat{p}_i = \min \left(1 - \varepsilon, \frac{w_{2,i}}{w_{2,i} + w_{3,i}} \right), i = 1, \dots, n-1, \quad (5.25)$$

$$\hat{v}_i^* = \max(0, \min(v_i^{max}, x_i - w_{1,i} + w_{3,i} + w_{2,i} - w_{3,i-1})), i \in \{2, \dots, n-1\} \setminus R \quad (5.26)$$

$$\hat{v}_n^* = \max(0, \min(v_n^{max}, x_n - w_{1,n} + w_{2,n} - w_{3,n-1})), \text{ if } n \notin R, \quad (5.27)$$

$$\hat{v}_1^* = \max(0, \min(v_1^{max}, x_1 - w_{1,1} + w_{3,1} + w_{2,1})), \text{ if } 1 \notin R, \quad (5.28)$$

$$\hat{v}_{f,i} = \max \left(\varepsilon, \min \left(1 - \varepsilon, \frac{w_{2,i} + w_{3,i}}{w_{1,i}} \right) \right), i = 1, \dots, n-1, \quad (5.29)$$

$$\hat{v}_{f,n} = \max \left(\varepsilon, \min \left(1 - \varepsilon, \frac{w_{2,n}}{w_{1,n}} \right) \right). \quad (5.30)$$

Using Assumption (H 5.1), (4.6), (5.5) and (5.17), it follows that there exists $y^* \in Y$ with $y^* = h(d, \theta^*, x^*)$, for all $d \in D$. By virtue of our assumption $x^* = (x_1^*, \dots, x_n^*) \in \prod_{i=1}^n (0, \mu_i)$ and $v^* \in (0, v_1^{max}] \times \prod_{i=2}^n [0, v_i^{max}]$, (5.23), we conclude that the set A contains all $w \in Y$ in a neighborhood of y^* . It follows that Assumption (J2) holds with $\kappa = 1$ for system (5.10) with output given by (5.15), (5.16), (5.17).

The following proposition (which is a consequence of Consequence (C4) and

(5.6)) guarantees that Assumption (J3) holds for system (5.10) with output (5.15), (5.16), (5.17). Its proof is provided in the Appendix B.

Proposition 5.2

Suppose that $v_i^{min} > 0$ ($i \in R$) and v_i^{max} ($i \notin R$) are sufficiently small and that $\tau > 0$ is sufficiently small ($\tau \leq \epsilon^2 \sigma^n \min_{i \in R} ((v_i^{max} - v_i^{min})^{-1})$). Then there exists an integer $m \geq 1$ such that for every sequence $\{(d(t), \hat{\theta}(t)) \in D \times \Theta\}_{t=0}^{\infty}$ and for every $x_0 \in S$, the solution $x(t)$ of (5.10), (5.17) with $u = K(\hat{\theta}, x)$, initial condition $x(0) = x_0$ corresponding to inputs $\{(d(t), \hat{\theta}(t)) \in D \times \Theta\}_{t=0}^{\infty}$ satisfies $y(t-1-i(t)) \in A$ for some $i(t) \in \{0, 1, \dots, m\}$ and for all $t \geq m+1$.

The main result for the freeway model is a consequence of Theorem 5.1 and the fact that all functions are sufficiently smooth in a neighborhood of the equilibrium.

Corollary 5.3

Consider system (5.10) with output given by (5.15), (5.16), (5.17). Suppose that $v_i^{min} > 0$ ($i \in R$) and v_i^{max} ($i \notin R$) are sufficiently small and that $\tau > 0$ is sufficiently small. Then the dynamic feedback law given by:

$$w_1^+ = x, w_2^+ = q^{ext}, w_3^+ = q^{int} \quad (5.31)$$

$$\hat{p}_i^+ = \begin{cases} \hat{p}_i & \text{if } w \notin A \\ \min\left(1 - \epsilon, \frac{w_{2,i}}{w_{2,i} + w_{3,i}}\right) & \text{if } w \in A \end{cases} \quad (5.32)$$

$$(\hat{v}_i^*)^+ = \begin{cases} \hat{v}_i^* & \text{if } w \notin A \\ \max(0, \min(v_i^{max}, x_i - w_{1,i} + w_{3,i} + w_{2,i} - w_{3,i-1})) & \text{if } w \in A \end{cases} \quad (5.33)$$

$$(\hat{v}_n^*)^+ = \begin{cases} \hat{v}_n^* & \text{if } w \notin A \\ \max(0, \min(v_n^{max}, x_n - w_{1,n} + w_{2,n} - w_{3,n-1})) & \text{if } w \in A \end{cases} \quad (5.34)$$

$$(\hat{v}_1^*)^+ = \begin{cases} \hat{v}_1^* & \text{if } w \notin A \\ \max(0, \min(v_1^{max}, x_n - w_{1,1} + w_{3,1} + w_{2,1})) & \text{if } w \in A \end{cases} \quad (5.35)$$

$$\hat{v}_{f,i}^+ = \begin{cases} \hat{v}_{f,i} & \text{if } w \notin A \\ \max\left(\epsilon, \min\left(1 - \epsilon, \frac{w_{2,i} + w_{3,i}}{w_{1,i}}\right)\right) & \text{if } w \in A \end{cases} \quad (5.36)$$

$$\hat{v}_{f,n}^+ = \begin{cases} \hat{v}_{f,n} & \text{if } w \notin A \\ \max\left(\epsilon, \min\left(1 - \epsilon, \frac{w_{2,n}}{w_{1,n}}\right)\right) & \text{if } w \in A \end{cases} \quad (5.37)$$

with (5.11), (5.12), (5.13), (5.14), $\hat{p} = (\hat{p}_1, \dots, \hat{p}_{n-1})$, $p = (p_1, \dots, p_{n-1})$, $\hat{v}_f = (\hat{v}_{f,1}, \dots, \hat{v}_{f,n})$, $v_f = (v_{f,1}, \dots, v_{f,n})$, $w = (w_1, w_2, w_3)$, $\hat{v}^* = (\hat{v}_1^*, \dots, \hat{v}_n^*)$, achieves the following:

1) There exist constants $M, \sigma > 0$ such that for every sequence $\{d(t) \in D\}_{t=0}^{\infty}$ and for every $(x_0, w_0, \hat{p}_0, \hat{v}_{j,0}^*; j \notin R, \hat{v}_{f,0}) \in S \times Y \times \Theta$, the solution of the closed-loop system (5.10), (5.17) with (5.31)-(5.37), (5.11)-(5.14), initial condition $(x(0), w(0), \hat{p}(0), \hat{v}_j^*(0); j \notin R, \hat{v}_f(0)) = (x_0, w_0, \hat{p}_0, \hat{v}_{j,0}^*; j \notin R, \hat{v}_{f,0})$ corresponding to input $\{d(t) \in D\}_{t=0}^{\infty}$ satisfies:

$$\begin{aligned} |x(t) - x^*| + |w(t) - y^*| + |\hat{v}_f(t) - v_f| + |\hat{p}(t) - p| + |\hat{v}^*(t) - v^*| \leq \\ M \exp(-\sigma t) (|x(0) - x^*| + |w(0) - y^*| + \\ |\hat{v}_f(0) - v_f| + |\hat{p}(0) - p| + \sum_{i \notin R} |\hat{v}_i^*(0) - v_i^*|), \end{aligned} \quad (5.38)$$

for all $t \geq 0$.

2) There exists an integer $N \geq 1$ such that for every sequence $\{d(t) \in D\}_{t=0}^{\infty}$ and for every $(x_0, w_0, \hat{p}_0, \hat{v}_{j,0}^*; j \notin R, \hat{v}_{f,0}) \in S \times Y \times \Theta$, the solution of the closed-loop system (5.10), (5.17) with (5.31)-(5.37), (5.11)-(5.14), initial condition $(x(0), w(0), \hat{p}(0), \hat{v}_j^*(0); j \notin R, \hat{v}_f(0)) = (x_0, w_0, \hat{p}_0, \hat{v}_{j,0}^*; j \notin R, \hat{v}_{f,0})$ corresponding to input $\{d(t) \in D\}_{t=0}^{\infty}$ satisfies $\hat{p}(t) = p$, $\hat{v}_f(t) = v_f$, $\hat{v}^*(t) = v^*$, for all $t \geq N$.

It is important to notice, that Theorem 4.1 provides a state feedback law, which guarantees the robust, global, exponential stabilization of the freeway model (5.10) when the parameters of the freeway model are known. On the other hand, Corollary 5.3 provides a dynamic feedback law, under which the states of the freeway model (5.10) converge to the UEP, even when the vector of parameters is unknown.

5.4 Proofs of Main Results

Proof of the Corollary 5.3: Let $N_1 \subseteq \Omega$ be a neighborhood of x^* , $N_2 \subseteq A$ be a neighborhood of y^* , and let $N_3 \subseteq \mathfrak{R}^{3n-1-m}$ be a neighborhood of θ^* . Since $\Omega = \prod_{i=1}^n (0, \mu_i)$, it follows from Assumption (H 5.1) and the fact that $\mu_i \in (0, \rho_i^{cr})$ for $i = 1, \dots, n$ that $f_i(x_i) = v_{f,i} x_i$ for $i = 1, \dots, n$. Definitions (5.15), (5.16), (5.17) in conjunction with (5.7) and the fact that $p_i \in [0, 1)$ for $i = 1, \dots, n-1$, $v_{f,i} \in (0, 1)$ for $i = 1, \dots, n-1$, imply that the following inequality holds for all $x \in \Omega$ and $d = (d_2, \dots, d_n) \in D = [0, 1]^{n-1}$:

$$\begin{aligned} |h(d, \theta^*, x) - y^*| &\leq |x - x^*| + |q^{ext} - q^{ext^*}| + |q^{int} - q^{int^*}| \leq \\ |x - x^*| + \sum_{i=1}^{n-1} |p_i f_{D,i}(x_i) - p_i f_{D,i}(x_i^*)| + |f_{D,n}(x_n) - f_{D,n}(x_n^*)| + \\ \sum_{i=1}^{n-1} |(1-p_i) f_{D,i}(x_i) - (1-p_i) f_{D,i}(x_i^*)| & \\ \leq |x - x^*| + \sum_{i=1}^n v_{f,i} |x_i - x_i^*| &\leq \left(1 + \sum_{i=1}^n v_{f,i}\right) |x - x^*| \end{aligned} \quad (5.39)$$

Next, we notice that by virtue of (5.8) and the facts that $p_i \in [0, 1)$ for $i = 1, \dots, n-1$, $\mathbf{v}_{f,i} \in (0, 1)$, for $i = 1, \dots, n$, $f_{D,i}(x_i^*) = v_i^* + (1 - p_{i-1})f_{D,i-1}(x_{i-1}^*)$, for $i = 2, \dots, n$, $f_{D,1}(x_1^*) = v_1^*$, it follows that the following holds for all $x \in \Omega$, $d \in D$ and $u \in \mathfrak{R}^m$:

$$\begin{aligned}
& |\bar{F}(d, \theta^*, x, u) - x^*| \leq \\
& |x_1 - f_{D,1}(x_1) + v_1 - x_1^*| + \sum_{i=2}^n |x_i - f_{D,i}(x_i) + v_i + (1 - p_{i-1})f_{D,i-1}(x_{i-1}) - x_i^*| \\
& \leq \sum_{i=2}^n |x_i - f_{D,i}(x_i) + f_{D,i}(x_i^*) + (1 - p_{i-1})f_{D,i-1}(x_{i-1}) - (1 - p_{i-1})f_{D,i-1}(x_{i-1}^*) - x_i^*| \\
& + m|u - u^*| + |x_1 - f_{D,1}(x_1) + v_1 - x_1^*| \leq \\
& (1 - \mathbf{v}_{f,1})|x_1 - x_1^*| + \sum_{i=2}^n (1 - \mathbf{v}_{f,i})|x_i - x_i^*| + \\
& \sum_{i=2}^n (1 - p_{i-1})\mathbf{v}_{f,i-1}|x_{i-1} - x_{i-1}^*| + m|u - u^*| \\
& \leq \left(n - \sum_{i=1}^n \mathbf{v}_{f,i} + \sum_{i=2}^n (1 - p_{i-1})\mathbf{v}_{f,i-1} \right) |x - x^*| + m|u - u^*|,
\end{aligned} \tag{5.40}$$

where $u^* = (v_i^*; i \in R)$. Using (5.13) and (5.14), it is straightforward to show that there exists a constant $\tilde{L} > 0$ such that the following inequality holds for all $x, \hat{x}^* \in S$ and $\hat{v}^* \in \prod_{i=1}^n [0, v_i^{max}]$:

$$|u - u^*| \leq \tilde{L}|x - x^*| + \tilde{L}|\hat{x}^* - x^*| + \tilde{L}|\hat{v}^* - v^*|. \tag{5.41}$$

Using (5.11), (5.12) and the fact that the function $g : [0, 1 - \varepsilon]^{n-1} \times \prod_{i \notin R} [0, v_i^{max}] \times [\varepsilon, 1 - \varepsilon]^n \rightarrow \prod_{i \in R} [v_i^{min} + \varepsilon, v_i^{max}]$ is a smooth function, it follows that the following inequality holds for all $\hat{\theta} \in N_3 \cap \Theta$:

$$|\hat{x}^* - x^*| + |\hat{v}^* - v^*| \leq M|\hat{\theta} - \theta^*|. \tag{5.42}$$

Finally, using definitions (5.24)-(5.30) in conjunction with the fact that $N_2 \subseteq A$, it follows that there exists a constant $\bar{L} > 0$ such that:

$$|\Psi(h(d, \theta^*, x), w) - \theta^*| \leq \bar{L}|x - x^*| + \bar{L} \sum_{i=1}^{\kappa} |w_i - y^*|, \tag{5.43}$$

for all $x \in N_1 \cap S$, $d \in D$, $\hat{\theta} \in N_3 \cap \Theta$, $w_i \in N_2 \cap Y$ ($i = 1, \dots, p$), with $w = (w_1, \dots, w_p)$.

Since, we have already proved that Assumptions (J1), (J2), (J3) hold for the closed-loop system (5.10), (5.17) with (5.31)-(5.37), (5.11)-(5.14), it follows from (5.39), (5.40), (5.41), (5.42) and (5.43) that all assumptions of Theorem 5.1 hold. Therefore, Corollary 5.3 is a direct application of Theorem 5.1 to the closed-loop system (5.10), (5.17) with (5.31)-(5.37), (5.11)-(5.14). The proof is complete. \triangleleft

5.5 Illustrative Example

The following example illustrates the application of the results of the previous section to a specific freeway model. The selected values for the parameters have physical interpretation and the example demonstrates the efficiency of the proposed control scheme, even in the case of modeling errors.

Consider a freeway model of the form (2.18)-(2.20) with (2.15) and (2.16) and with $n = 5$ cells. The freeway stretch considered for the simulation test is 2.5 km long and has three lanes. Each cell is 0.5 km long and has an on-ramp and off-ramp. The first and the third on-ramp are assumed to be controllable, hence $R = \{1, 3\}$, and the vector of the controllable inflows is $u = (v_1, v_3)$. The inflows from the rest of the on-ramps are assumed to be unknown and therefore they will have to be estimated. Regarding the priority rules, we assume that $d_i(t) \equiv 0$ for the whole simulation horizon, which means that the on-ramp inflows have absolute priority over the internal inflows. The simulation time step is set to be $T = 15s$ and the cell capacities are $\rho_i^{max} = 170$ [veh], for $i = 1, \dots, 5$. Note that, since all flows and densities are measured in [veh], the cell length, the time step and the number of lanes do not appear explicitly, but they are only involved implicitly in the value of every variable and every constant (e.g. critical density, jam density, flow capacity, wave speed etc.) corresponding to density or flow.

The formulas of the demand functions are given by the following equations:

$$f_{D,i}(z) = \begin{cases} \left(\frac{5}{11}\right)z & z \in [0, 55] \\ 25 - \left(\frac{7}{115}\right)(z - 55) & z \in (55, 170] \end{cases} \quad (i = 1, \dots, 4),$$

$$f_{D,5}(z) = \begin{cases} \left(\frac{4}{11}\right)z & z \in [0, 55] \\ 20 - \left(\frac{3}{115}\right)(z - 55) & z \in (55, 170] \end{cases}. \quad (5.44)$$

Assumption (H 5.1) holds with $\rho_i^{cr} = 55$ [veh], $\rho_i^{max} = 170$ [veh] for $i = 1, \dots, 5$, $v_{f,i} = 5/11$, $f_i^{min} = 18$ for $i = 1, \dots, 4$, $v_{f,5} = 4/11$ and $f_5^{min} = 17$. Thus, every cell has the same critical and jam density which correspond to 36.7 [veh/km/lane] and 113.3 [veh/km/lane], respectively, in common traffic units with the above settings. Definitions (5.44) guarantee that the demand functions for $i = 1, \dots, 4$ lead to 20% higher flow capacity ($f_{D,i}(\rho_i^{cr}) = 25$ [veh] for $i = 1, \dots, 4$, corresponding to 2000 [veh/h/lane]) than the flow capacity of the fifth cell ($f_{D,5}(\rho_5^{cr}) = 20$ [veh], corresponding to 1600 [veh/h/lane]) and therefore the last cell is a strong bottleneck for the freeway (e.g., due to grade or curvature or tunnel or bridge etc.). Notice also, that the capacity drop phenomenon has been taken into account by considering a linearly decreasing demand function for over-critical densities $x_i \in (55, 170]$ (as discussed in Section 2.3.6). Furthermore, the congestion wave speeds are $c_i = 0.22$ for $i = 1, \dots, 5$ corresponding to 26.4 [km/h]. Finally, we suppose that the cell flow capacities Q_i , for $i = 1, \dots, 5$, satisfy the inequalities $Q_i \geq c_i \rho_i^{max}$, for $i = 1, \dots, 5$, and therefore, they play no role in the model (2.18)-(2.20).

Our goal is to globally exponentially stabilize the system at an UEP which is as close as possible to the critical density (due to the fact that the flow value at the critical density is largest). Therefore, we selected as the upper bound for the equilibrium densities and for each cell to be the $\mu_i = \rho_i^{cr} - \epsilon$ ($i = 1, \dots, 5$), where $\epsilon = 10^{-4}$. The exit rates are set to be $p_1 = 0.04$, $p_2 = 0.15$, $p_3 = 0.08$, $p_4 = 0.1$ and we selected $v_1^{max} = 25$, $v_2^{max} = 1.3$, $v_3^{max} = 4$, $v_4^{max} = 2.3$ and $v_5^{max} = 2.8$, so that inequalities (5.6) hold. The uncontrollable inflows are $v_2^* = 1$, $v_4^* = 2$ and $v_5^* = 2.5$. Summarizing, the vector

of the parameters θ^* consists of the exit rates $p = [p_1, p_2, p_3, p_4]'$, the unknown external uncontrollable inflows v_i^* ($i = 2, 4, 5$) and the slopes $v_f = [v_{f,1}, \dots, v_{f,5}]'$ of the demand functions. Hence, $\theta^* = [p_1, \dots, p_4, v_2^*, v_4^*, v_5^*, v_{f,1}, \dots, v_{f,5}]$.

The function

$$g : [0, 1 - \epsilon]^4 \times \prod_{i=2,4,5} [0, v_i^{max}] \times [\epsilon, 1 - \epsilon]^5 \rightarrow \prod_{i=1,3} [v_i^{min} + \epsilon, v_i^{max}]$$

with $v_1^{min} = v_3^{min} = 0.2$ involved in (5.9) has been selected in such a way that the outflow from the last (fifth) cell is approximately maximized:

$$g(p, v_2^*, v_4^*, v_5^*, r) = (v_1^*, v_3^*) = (\hat{g}(p, v_2^*, v_4^*, v_5^*, v_f), 4) \quad (5.45)$$

where

$$\hat{g}(z) = \begin{cases} v_1^{min} + \epsilon & z \in (-\infty, v_1^{min}] \\ 50^2 z^2 - 10^3 z + 100.2001 & z \in (v_1^{min}, v_1^{min} + 2\epsilon] \\ z & z \in (v_1^{min} + 2\epsilon, v_1^{max} - 1] \\ \frac{-1}{4} z^2 + 13z - 144 & z \in (v_1^{max} - 1, v_1^{max} + 1] \\ v_1^{max} & z \in (v_1^{max}, \infty) \end{cases} \quad (5.46)$$

where $z = (v_{f,5}x_5^* - (v_5^* + (1 - p_4)v_4^* + (1 - p_3)(1 - p_4)v_3^* + (1 - p_2)(1 - p_3)(1 - p_4)v_2^*)) / ((1 - p_1)(1 - p_2)(1 - p_3)(1 - p_4))$ and $x_5^* = \mu_5 - 2\epsilon$.

The UEP is $x^* = [38.045, 38.723, 41.715, 42.778, 54.9997]$ for $v^* = [17.29316, 1, 4, 2, 2.5]$, $p = [0.04, 0.15, 0.08, 0.1]$ and $v_f = [5/11, 5/11, 5/11, 5/11, 4/11]$. The above UEP is not globally exponentially stable due to the existence of additional (congested) equilibria. This is shown in Figure 5.2, where the solution of the open-loop system, with constant inflows $v^* = [17.29316, 1, 4, 2, 2.5]$, is attracted by the congested equilibrium $[96.19, 94.6, 87.73, 85.22, 82.33]'$ leading to outflow, which is 0.72 [veh] lower than the capacity flow of the last cell. Therefore, if the objective is the operation of the freeway with largest outflow, then a control strategy will be needed.

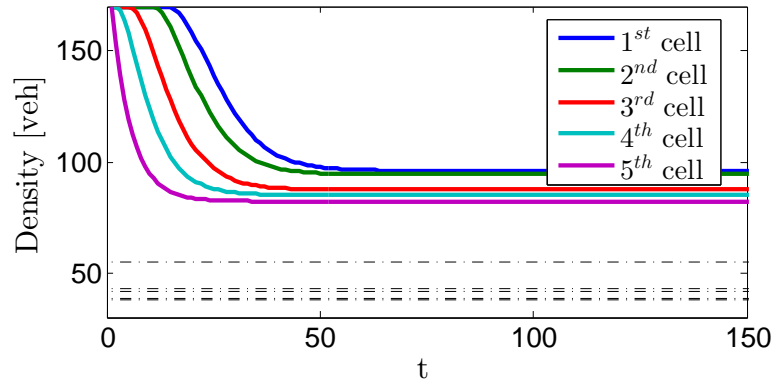


FIGURE 5.2: Time evolution of the states of the open-loop system with a fully congested initial condition.

We are in a position to guarantee global exponential attractivity of the UEP for the freeway model that was described above by using Corollary 5.3. Indeed, Corollary 5.3 guarantees that there exist constants $\sigma \in (0, 1]$, $v_1^{min}, v_3^{min} > 0$ and $\tau > 0$

such that, the feedback law $K : \Theta \times S \rightarrow U$ defined by:

$$K_1(\hat{\theta}, x) = \max \left(v_1^{min}, \hat{v}_1^* - \tau^{-1}(\hat{v}_1^* - v_1^{min}) \sum_{i=1}^5 \sigma^i \max(0, x_i - \hat{x}_i^*) \right), \quad (5.47)$$

$$K_3(\hat{\theta}, x) = \max \left(v_3^{min}, \hat{v}_3^* - \tau^{-1}(\hat{v}_3^* - v_3^{min}) \sum_{i=1}^5 \sigma^i \max(0, x_i - \hat{x}_i^*) \right),$$

$$(\hat{v}_1^*, \hat{v}_3^*) = g(\hat{p}, \hat{v}_i^*; i \notin R, \hat{v}_f), \quad (5.48)$$

for the closed-loop system (5.10), (5.15), (5.16), (5.17) with (5.31)-(5.37), (5.47), (5.48), (5.12) and (5.14), achieves global exponential attractivity of the UEP $x^* = [38.045, 38.723, 41.715, 42.778, 54.9997]$.

It is important here to note that the feedback law (5.47) aims to maximize the outflow from the fifth cell without assuming knowledge of the cell's capacity flow. The maximization is achieved by implicitly estimating the capacity flow of the fifth cell in real time, using the estimation of the slope of the demand function ($\hat{v}_{f,5}(t)$) and the (given) critical density of the same cell. Empirical traffic engineering investigations have shown that the capacity is stochastic, in the sense that traffic breakdown on different days may occur at different flow values. In contrast, the critical density, at which capacity flow occurs, is deemed more stable from day to day. This is the very practical reason why it is assumed in this work that the critical density is constant and known, while capacity flow is estimated in real time. Note that, this is in full accordance with simpler but proven (in many field installations) control laws like ALINEA (Papageorgiou, Hadj-Salem, and Blosseville, 1991), which also considers a given density set-point.

Selecting $v_1^{min} = v_3^{min} = 0.2$, we tested various values of the constants $\sigma \in (0, 1]$ and $\tau > 0$ by performing a simulation study with respect to many initial conditions. Low values for $\sigma \in (0, 1]$ require small values for $\tau > 0$ in order to guarantee global exponential stability for the closed-loop system. All the following tests of the proposed regulator were conducted with the same values $\sigma = 0.7$ and $\tau = 10$. Moreover, all the following simulation tests were conducted with the same initial conditions for the observer states $w_{1,i}(0) = 100$ [veh], $w_{2,i}(0) = 20$ [veh], $w_{3,i}(0) = 20$ [veh] for $i = 1, \dots, 5$, $\hat{p}_i(0) = 0$ for $i = 1, \dots, 4$, $\hat{v}_i^*(0) = 0$ for $i = 2, 4, 5$ and $\hat{v}_{f,i}(0) = 0.7$ for $i = 1, \dots, 5$.

Figure 5.3 shows the evolution of the density of every cell and Figure 5.4(a) shows the evolution of the Euclidean norm of the deviation $x(t) - x^*$ of the state from the UEP, i.e., $|x(t) - x^*|$, for the closed-loop system with the proposed feedback regulator (5.31)-(5.37), (5.47), (5.48), (5.12) and (5.14) for three different initial conditions. The first condition corresponds to very low densities ($x_0 = (10, 15, 10, 15, 10)'$), the second initial condition corresponds to congested states with high deviations between each other ($x_0 = (70, 85, 65, 120, 100)'$), while the third initial condition corresponds to the state where the density of every cell has its maximum value, i.e. ρ_i^{max} ($i = 1, \dots, 5$), which also corresponds to the initial condition for Figure 5.3. Indeed, both Figure 5.3 and 5.4 show that the proposed feedback stabilizer (5.31)-(5.37), (5.47), (5.48), (5.12) and (5.14) achieves dead-beat estimation of the vector θ^* , preserving the exponential convergence property for the closed-loop system.

We also tested the performance of the feedback law (5.31)-(5.37), (5.47), (5.48), (5.12) and (5.14) under the effect of periodic uncontrollable inflows with different

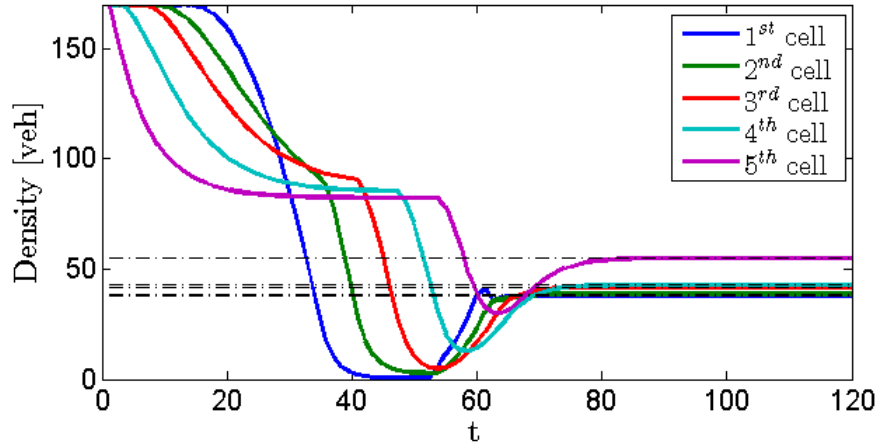


FIGURE 5.3: Time evolution of the states of the closed-loop system with a fully congested initial condition.

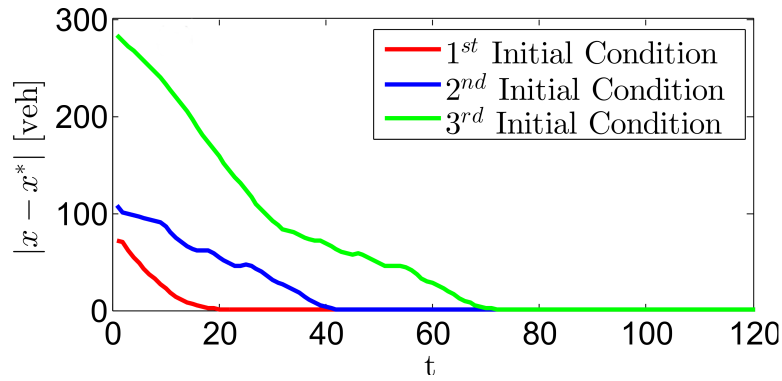


FIGURE 5.4: Time evolution of the Euclidean norm $|x - x^*|$ of the closed-loop system with three different initial conditions.

frequencies and different amplitudes, given by:

$$v_2^* = 1 + 0.3 \cos\left(\frac{3\pi t}{2}\right), v_4^* = 2 + 0.1 \cos(\pi t) \text{ and } v_5^* = 2.5 + 0.2 \cos\left(\frac{\pi t}{4}\right). \quad (5.49)$$

Figure 5.5 (a) and (b), depict the evolution of the Euclidean norm of the deviation $x(t) - x^*$ and the evolution of the weighted norm $\|\cdot\|_n$ of the deviation of the estimated parameters from the nominal parameters vector, defined by:

$$\|\hat{\theta}(t) - \theta^*\|_n = \left\| \left(\frac{1}{1-\epsilon}(\hat{p}(t) - p), \frac{\hat{v}_2^*(t) - v_2^*}{v_2^{max}}, \frac{\hat{v}_4^*(t) - v_4^*}{v_4^{max}}, \frac{\hat{v}_5^*(t) - v_5^*}{v_5^{max}}, \frac{1}{1-\epsilon}(\hat{v}_f(t) - v_f) \right) \right\|, \quad (5.50)$$

with respect to the unknown time-varying uncontrollable inflows (5.49) and under the proposed feedback regulator (5.31)-(5.37), (5.47), (5.48), (5.12) and (5.14). The initial conditions were the same as in the previous case. Again, the proposed regulator achieved to lead the system to the equilibrium state by performing only small deviations for the estimated parameters. Figure 5.5 shows that the proposed feedback stabilizer (5.31)-(5.37), (5.47), (5.48), (5.12) and (5.14) achieves the exponential

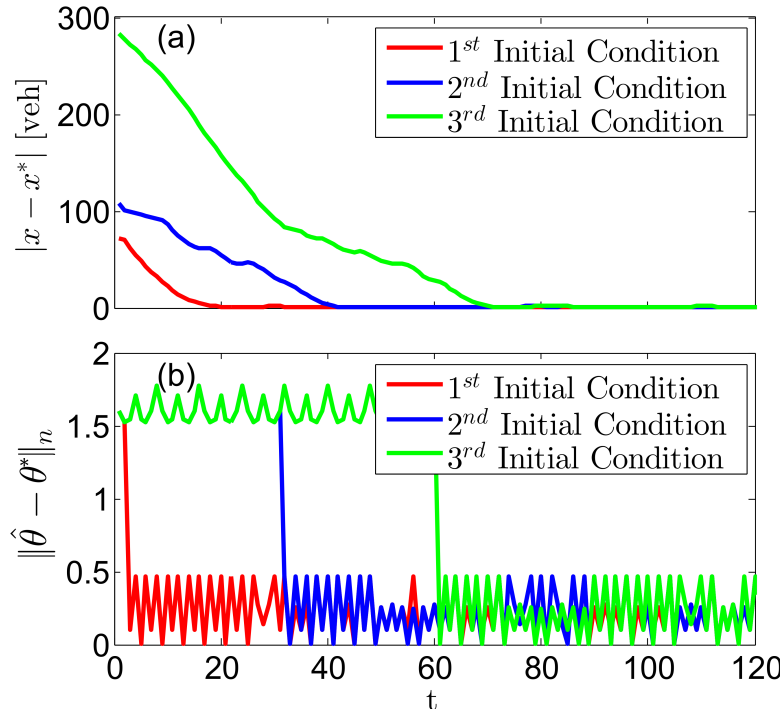


FIGURE 5.5: (a) The Euclidean norm $|x(t) - x^*|$, (b) the weighted norm $\|\hat{\theta}(t) - \theta^*\|_n$, for periodic uncontrollable inflows for the closed-loop system and three different initial conditions $x_0 = (10, 15, 10, 15, 10)'$ (red line), $x_0 = (70, 85, 64, 120, 100)'$ (blue line) and $x_0 = (170, 170, 170, 170, 170)'$ (green line).

convergence property of the densities to the desired UEP.

Furthermore, in order to illustrate the performance of the proposed feedback law under the presence of modeling errors, we considered the case where the demand functions do not satisfy Assumption 5.1. More specifically, we considered the piecewise quadratic demand functions:

$$f_{D,i}(z) = \begin{cases} 0.7z - \left(\frac{0.49}{110}\right)z^2 & , z \in [0, 55] \\ 25.025 - \left(\frac{7.025}{115}\right)(z - 55) & , z \in (55, 170] \end{cases}, i=1, \dots, 4, \quad (5.51)$$

$$f_{D,5}(z) = \begin{cases} 0.56z - \left(\frac{0.392}{110}\right)z^2 & , z \in [0, 55] \\ 20.02 - \left(\frac{3.02}{115}\right)(z - 55) & , z \in (55, 170] \end{cases}.$$

In this case the UEP is $x^* = [30.77, 31.5, 34.85, 36.1, 54.9997]$. Figure 5.7, shows the evolution of the Euclidean norm of the deviation $x(t) - x^*$ of the state from the UEP and for the closed-loop system with the proposed feedback regulator (5.31)-(5.37), (5.47), (5.48), (5.12) and (5.14) and three different initial conditions. Again, Figure 5.6 shows that the proposed feedback stabilizer (5.31)-(5.37), (5.47), (5.48), (5.12) and (5.14) achieves the exponential convergence property of the densities to the desired UEP, even under the presence of modeling errors.

In the same vein, Figure 5.7 shows the time evolution of the densities of every cell for the closed-loop system (5.10), (5.17) with (5.31)-(5.37), (5.47), (5.48), (5.12) and (5.14) with initial condition $x_0 = (60, 60, 60, 60, 60)'$ and under the presence of the same modeling errors. More specifically, in this figure the demand functions are

given by (5.44), which satisfy Assumption (5.1), for $t < 60$, while after that time modeling errors appear. This means that for $t \geq 60$ the demand functions are given by (5.51), which do not satisfy Assumption (5.1). Figure 5.7 shows that the exponential convergence property to the desired UEP is preserved even when modeling errors appear after an initial transient period.

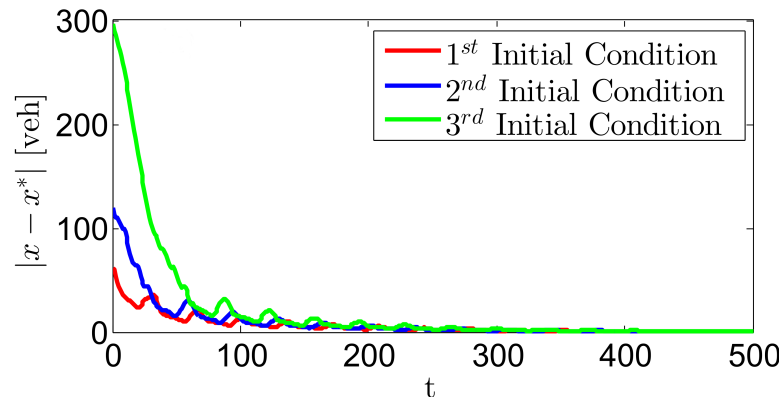


FIGURE 5.6: The Euclidean norm $|x(t) - x^*|$ for the closed-loop system and under the presence of modeling errors.

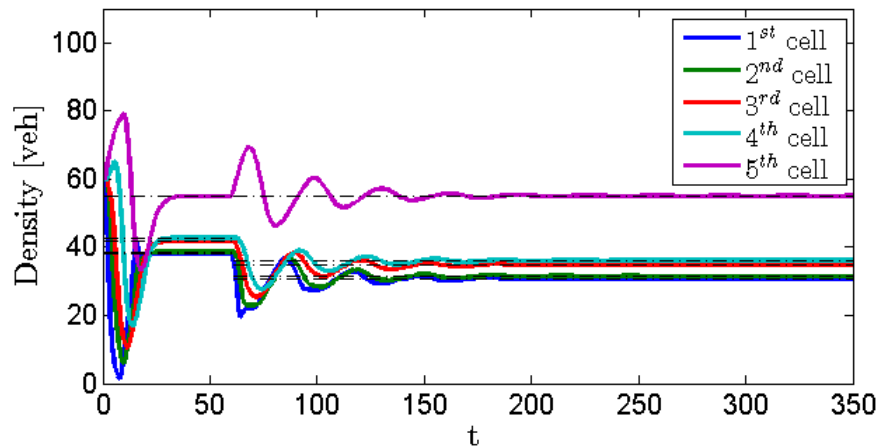


FIGURE 5.7: Time evolution of the density for the closed-loop system under modeling errors.

Chapter 6

Local and Coordinated Ramp Metering using Adaptive Control Scheme

6.1 Introduction

The ACS presented in the previous chapter (Chapter 5) can be used as a real-time ramp metering and mainline metering strategy either at local or coordinated levels. As shown in Chapter 5, the proposed ACS consists of two main components: a nominal feedback law (NFL) (derived from Chapter 4), in conjunction with a nonlinear dead-beat observer that estimates the unknown system parameters utilized by the NFL. It has been first rigorously shown that, for the freeway model (2.18)-(2.18), the NFL guarantees the RGES of any selected UEP when the model parameters are known and constant. Eventually, the designed nonlinear dead-beat observer performs the exact identification of the constant model parameters after a transient period. Using these two components (NFL and nonlinear observer), the proposed ACS was rigorously shown to guarantee the robust global exponential attractivity of a desired (partly unknown and moving) UEP.

However, Chapter 5 provides limited information on the practical implementation possibilities, implications and qualities of the proposed ACS. Motivated by the strong theoretical properties of the ACS, this chapter aims to provide insights into the practical properties and performance of the ACS under realistic and customary traffic scenarios occurring in freeway networks. Testing this strategy with sufficiently accurate traffic flow models, different than the ones used for ACS design, is deemed as an indispensable step towards potential application of the scheme in the field. In this study, the SOM METANET (Messmer and Papageorgiou, 1990) is utilized as a surrogate of ground truth for the application of the ACS. This choice is justified by the fact that METANET is able to reproduce with high accuracy the traffic dynamics as demonstrated in several model validation exercises using data from different freeway networks (see Section 2.4 and Frejo, Camacho, and Horowitz, 2012; Kotsialos, Papageorgiou, and Middelham, 2001; Papageorgiou, Blosseville, and Hadj-Salem, 1990; Spiliopoulou et al., 2014). For the simulation testing, realistic traffic scenarios are constructed, involving non-constant mainstream entrance and on-ramp demand flows. Particular attention is paid to two different aspects of the control action:

1. Firstly, the performance of the controller is investigated with respect to the stabilization of freeway traffic in case bottlenecks exist far downstream from a metered on-ramp; for this case, the application network and control scenario are the same as those utilized by Wang et al., 2014, in order to facilitate the

comparison of ACS with a previously developed local ramp metering strategy. Moreover, under the same framework, an extension of the basic ACS is proposed so as to handle the practically relevant RLB situation (Wang et al., 2010).

2. Secondly, by appropriately exploiting the application flexibility provided by ACS, the scheme is applied for coordinated ramp metering control, so as to balance the relative queue lengths created on the controllable on-ramps; for this case, the related network and control scenario share similar characteristics with those utilized in the work by Papamichail and Papageorgiou, 2008 for comparison reasons.

The structure of the present chapter is as follows: Section 6.2 is devoted to the description of ACS from an application-oriented point of view; some modifications of the original scheme are also proposed, mainly in the observer part, which simplify the estimation part of ACS. Section 6.3 presents the simulation set-up, while the results obtained from the application of the ACS as local and coordinated ramp metering strategy are presented in Sections 6.4 and 6.5, respectively.

6.2 The Adaptive Control Scheme

The proposed ACS is a real-time control strategy, which aims to delay, prevent or dissolve congestion phenomena caused by the presence of active bottlenecks within a freeway stretch. More often, recurrent congestion is created (spilling back several kilometers upstream) when the total arriving demand exceeds the bottleneck capacity. In order to apply any real-time control strategy, appropriate measurements, obtained from detectors installed at specific locations within the freeway, are required. The measurements reflect traffic flow variables such as flow, speed, density or occupancy, depending on the specific requirements of the employed real-time control strategy. If there is no availability of a specific type of measurement needed for the application of the control strategy or if there are no measurements available at specific locations, appropriate estimation schemes can be used so as to retrieve the required traffic flow information from available measurements (Seo et al., 2017; Sun, Muñoz, and Horowitz, 2004; Wang, Papageorgiou, and Messmer, 2006).

As mentioned above, the ACS consists of two main components, a NFL and a nonlinear observer. The first aims to steer the system towards a desired traffic state while the second aims to estimate the external traffic variables required for producing the desired traffic state. The following subsection presents the NFL component of the ACS under the assumption that all the required measurements or estimates are available.

6.2.1 Nominal Feedback Law

To enable the real-time operation of the NFL of the ACS, real-time information of traffic density should be available. Though direct density measurements are rarely provided, density estimates can be readily obtained from corresponding occupancy measurements (that are usually available) or can be provided by various estimation schemes proposed in the literature (see, for example, Bekiaris-Liberis, Roncoli, and Papageorgiou, 2015; Seo et al., 2017; Wang, Papageorgiou, and Messmer, 2006). In what follows, the measurements or estimates of density are in [veh/km].

Main features of the nominal feedback law

Although other configurations are also possible, we will consider a freeway traffic control setting that is compatible with the cases addressed by Wang et al., 2014 for isolated ramp metering, by Wang et al., 2010 for random-location bottleneck, and by Papamichail and Papageorgiou, 2008 for coordinated ramp metering. Specifically, we consider a freeway stretch under control, which extends from the most upstream controllable on-ramp (or mainline flow metering) until a recurrently activated bottleneck at its downstream boundary (Figure 6.1) in the aim of maximizing the bottleneck throughput. This freeway stretch may contain other controllable or uncontrollable on-ramps, as well as off-ramps. A space discretization of the considered freeway stretch is introduced with cells which are typically about 500 m in length. Let, here, n be the total number of cells emerging after discretizing the freeway; then each cell is denoted by the index $i \in \{1, \dots, n\}$ where the n^{th} (last) cell corresponds to the bottleneck cell. The on-ramps and the off-ramps are located at the upstream and downstream boundary of a cell, respectively, and are denoted by the index of the corresponding cell, as shown in Figure 6.1. A cell may have an on-ramp or an off-ramp or both or none of them. We denote by $O \subseteq \{1, \dots, n\}$ the index set of the on-ramps and $R \subseteq O$ the index set of the controllable on-ramps. Then, here, we denote by v_i the controllable inflow of on-ramp $i \in R$ and, in general, we denote by \bar{r}_i the actual inflow of on-ramp $i \in O$; in case $i \in R$, the actual inflow \bar{r}_i depends on the control decision and therefore becomes $\bar{r}_i(v_i)$ (see again Figure 6.1). Note here that all flows are measured in [veh/h]. The upstream-most boundary cell carries the index $i = 0$; in case mainline metering actions are to be considered, the index set of the controllable on-ramps becomes $R \cup \{0\}$.

The proposed control strategy is applied with control holding period T_c , which is an integer multiple of the measurements (or estimates) sampling period T (for simulation investigations, T denotes the simulation model's sampling period, see Section 6.3), i.e., $T_c = z_c T$ with constant $z_c \in \mathbb{N}$. With these definitions, the control action (at times $t = k_c T_c$ with $k_c = 1, 2, \dots$) ordered by the NFL (Theorem 4.1) of the ACS reads

$$v_i(k_c) = \max \left(v_i^{\min}, v_i^*(k_c) - \frac{v_i^*(k_c) - v_i^{\min}}{\tau} \sum_{j \in \{1, \dots, n\}} \sigma^j \max(0, x_j(k_c) - x_j^*(k_c)) \right), \quad (6.1)$$

for $i \in R$, where $v_i^{\min} > 0$ denotes the minimum admissible on-ramp flow, $\sigma \in (0, 1]$ (dimensionless) and $\tau > 0$ (in [veh/km]) are parameters of the regulator (same for every $i \in R$), and $x_j(k_c)$, for $j = 1, \dots, n$, correspond to (the average of the last z_c) density measurements or estimates. Moreover, (v_i^*, x_j^*) for $i \in R$ and $j = 1, \dots, n$, denotes the Desired Operating point (DOP), reflecting optimal non-congested conditions in the examined freeway stretch. It is again emphasized that, on the basis of the model (2.18)-(2.20), the NFL (6.1) (definition (4.7) in Chapter 4) guarantees the RGES of any selected UEP (x_1^*, \dots, x_n^*) when the external variables (such as exit rates, uncontrolled on-ramp flows) are known and constant (see Chapter 4). It is expected that these properties largely hold also if the equilibrium is slowly changing over time.

Specifically, v_i^* for $i \in R$ correspond to the (optimal) equilibrium inflows for the controllable on-ramps, which lead to the (optimal) uncongested equilibrium densities x_j^* for $j = 1, \dots, n$. Notice here that, due to the existence of on-ramps and off-ramps inside the considered freeway stretch, x_j^* may be different for each $j \in$

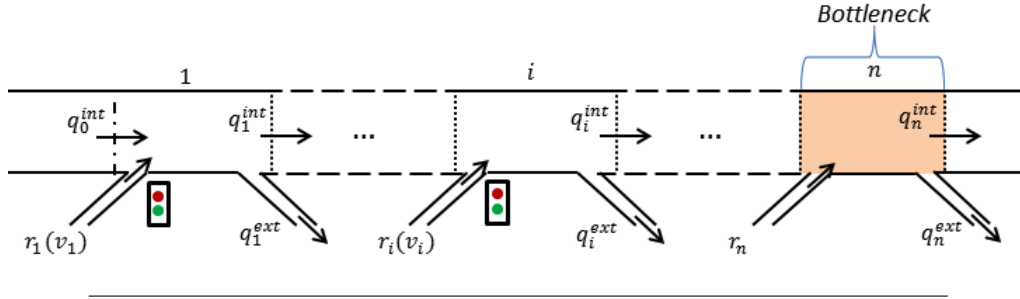


FIGURE 6.1: Space discretization of a freeway stretch.

$\{1, \dots, n\}$; and that, due to (possible) non-constant (uncontrollable) main-entrance and uncontrollable on-ramp flows, the DOP may be changing over time. Furthermore, the minimum admissible flow (v_i^{min}) is pre-specified and constant, while the maximum control value resulting from (6.1) is equal to the current optimal on-ramp inflow $v_i^*(k_c)$, for $i \in R$.

In simple terms, the feedback law (6.1) aims to steer the system towards the DOP ($v_i^*(k_c), x_j^*(k_c)$), for $i \in R$ and $j \in \{1, \dots, n\}$; in fact, if $x_j(k_c) = x_j^*(k_c)$ then (6.1) yields $v_i(k_c) = v_i^*(k_c)$, and the system operates at its optimal point; while, if $x_j(k_c) > x_j^*(k_c)$ for some j , then (6.1) leads to lower control flows $v_i(k_c) < v_i^*(k_c)$ in order to dissolve possible congestion and bring the cell densities back to their optimal values.

Apart from the proper determination of the (optimal) DOP (which is described in the following subsections), the efficient operation of the NFL (6.1) relies also on the proper determination of the regulator parameters σ and τ . In fact, the NFL (6.1) assigns a different control gain to each cell j of the considered freeway stretch which is equal to σ^j/τ (note that σ^j denotes σ to the power of j). However, simulation experiments indicate that the selection $\sigma = 1$ (yielding the same control gain, i.e. $\frac{1}{\tau}$, for each freeway cell) and appropriate determination of the parameter τ guarantees satisfactory control performance. Typical values for τ may be selected within the range $[1, 30]$; whereby smaller values of τ lead to more aggressive (even oscillating) control behavior, while larger values of τ lead to less aggressive (but possibly sluggish) control behavior. In any case, tuning of only one design parameter is sufficient to establish the desired dynamic characteristics of the control loop, and this is certainly a convenient feature for practical application of the method.

The determination of the DOP ($v_i^*(k_c), x_j^*(k_c)$) is crucial and is based on two aspects. It should guarantee: i) the maximization of throughput at the bottleneck location (cell n); and ii) the uncongested equilibrium flow along the considered freeway stretch.

Maximization of throughput at the bottleneck

Maximization of throughput requires knowledge of either the capacity flow of the bottleneck or its critical density (at which the flow reaches capacity). Control strategies that are based on capacity flow may be sensitive due to the stochastic and condition-dependent nature of the capacity flow value (Cassidy and Rudjanakanoknad, 2005; Eleftheriadou, Roess, and McShane, 1995; Lorenz and Eleftheriadou, 2001). In contrast, control strategies that target the critical density are preferable, because the critical density seems to be more consistent and stable under different traffic conditions (Cassidy and Rudjanakanoknad, 2005). Therefore, the proposed control scheme aims to maximize the throughput of a bottleneck by targeting its critical density, which is assumed to be known (as in other feedback control schemes as well).

The proper critical density value should be extracted from historical data or be specified after the control installation via fine-tuning; but it should be noted that the ultimate goal of throughput maximization is largely achieved by ACS, even if the employed critical density value is not exact, as will be demonstrated in the following sections (see Tables 6.3 and 6.4 in Sections 6.4 and 6.5, respectively). The target outflow q_n^* of the freeway stretch, which turns out to be the estimate of the capacity flow of the bottleneck location, is defined as:

$$q_n^*(k_c) = \rho_n^{ct} \bar{v}_{f,n}(k_c), \quad (6.2)$$

where, as previous, ρ_n^{ct} is the pre-specified value of the critical density of the bottleneck, while $\bar{v}_{f,n}(k_c)$ equals the (average of the last z_c) measured (if available) or real-time estimated mean speed at the bottleneck (in [km/h]) as long as the bottleneck density is undercritical; otherwise, $\bar{v}_{f,n}(k_c)$ is set equal to its previous value (see Corollary 5.3). The target outflow delivered by (6.2) may lead to unrealistically high estimated capacity values whenever the measured or estimated speed is near free speed. However, this is not harmful, as it implies that controllable inflows should be accordingly high; hence no control actions will be considered in this case, since the freeway operates under free flow conditions. On the other hand, when the real density approaches its critical value (and therefore the flow of the bottleneck approaches its capacity), the mean speed at the bottleneck location approaches the "critical speed" and the estimate (6.2) is close to the real capacity value.

Equilibrium flow

As mentioned earlier, the DOP (v_i^*, x_j^*) (for $i \in R$ and $j = 1, \dots, n$) reflects uncongested (and optimal) stationary conditions and therefore implies the balance between the total inflows and the total outflows (including the target outflow (6.2)) in the considered freeway stretch. More specifically, the total inflows comprise: i) the optimal inflows v_i^* of the controllable on-ramps ($i \in R$); ii) the measured or estimated uncontrollable on-ramp flows \bar{r}_i ($i \in O \setminus R$); and iii) the very upstream (measured or estimated) mainstream inflow q_0^{int} , i.e., the outflow from the cell $i = 0$ that becomes inflow for the cell $i = 1$. On the other hand, the total outflows comprise: i) the measured or estimated external (off-ramp) flows q_j^{ext} ($j = 1, \dots, n$), expressed as the product of the corresponding estimated exit rates p_j , $j \in \{1, \dots, n\}$, with the corresponding mainstream flows (in case cell j does not contain an off-ramp, $p_j = 0$); and ii) the target outflow of the bottleneck q_n^* . Then, the flow equilibrium for the uncongested freeway stretch (i.e. total inflows equal to total outflows) reads:

$$q_0^{int} \prod_{j=1}^n (1 - p_j) + \sum_{i \in R} v_i^* \prod_{j=i}^n (1 - p_j) + \sum_{i \in O \setminus R} r_i \prod_{j=i}^n (1 - p_j) = q_n^*, \quad (6.3)$$

where for $i = n$ we set $p_n = 0$. In case of mainline metering, q_0^{int} in (6.3) is substituted by q_0^* . Notice that the only unknown variables in (6.3) are the optimal inflows for the controllable on-ramps (v_i^* ; $i \in R$). Thus, (6.3) allows to specify these optimal inflows with $m - 1$ degrees of freedom, where m is the number of controllable on-ramps, i.e., the cardinality of the index set R . In case there is just one controllable inflow (local ramp metering case), relation (6.3) can be solved to retrieve the optimal inflow value $v_1^*(k_c)$. For more than one controllable on-ramps, the user has the freedom to specify the way that the optimal inflow values should be distributed among the controllable on-ramps (see for example Section 6.5). Thus, this control scheme allows to deal

with a variety of possible coordinated ramp-metering policies when more than one on-ramps are controllable. Note that the specified values of $(v_i^*; i \in R)$ should not be selected higher than the corresponding on-ramp capacities or demands or lower than the corresponding v_i^{min} .

Final determination of the (optimal) desired operating point

Having specified the optimal equilibrium inflows for the controllable on-ramps $(v_i^*(k_c); i \in R)$ as explained in the previous subsections, we proceed here to obtain also the corresponding equilibrium densities $(x_j^*(k_c); j \in \{1, \dots, n\})$ that are needed in the nonlinear feedback law (6.1). Notice that a similar relation as (6.3) can also be written for all cell (optimal) outflows q_j^* for $j = \{1, \dots, n-1\}$, which reads

$$q_1^* = q_0^{int} + v_1^*, \quad (6.4)$$

$$q_0^{int} \prod_{k=1}^{j-1} (1 - p_k) + \sum_{\substack{i \in R \\ i \leq j}} v_i^* \prod_{k=i}^{j-1} (1 - p_k) + \sum_{\substack{i \in O \setminus R \\ i \leq j}} r_i \prod_{k=i}^{j-1} (1 - p_k) = q_j^*, \quad (6.5)$$

for $j = 2, \dots, n-1$. Here, we define $\prod_{k=j}^{j-1} (\cdot) = 1$. Again, for mainline metering, q_0^{in} in (6.4) is substituted by q_0^* . Using the outflows q_j^* resulting from (6.4), (6.5), we may compute the target cell densities x_j^* from

$$x_n^* = \rho_n^{cr}, \quad x_j^* = \min \left(\frac{q_j^*}{v_j}, \rho_j^{cr} \right), \quad j \in \{1, \dots, n-1\}, \quad (6.6)$$

where v_j , for each $j \in \{1, \dots, n-1\}$, corresponds to the measured or real-time estimated mean speed of the j^{th} cell; and ρ_j^{cr} denotes the critical density of the j^{th} cell. Note that the min-operator in (6.6) guarantees that the target densities x_j^* will be uncongested, even if some cells are currently congested. Notice also that equations (6.6) correspond to definition (5.5) of Chapter 5.

To summarize, in order to apply the NFL, the following measurements or estimates are required:

1. All cell densities $(x_i; i = 1, \dots, n)$ to be used by the NFL (6.1).
2. External variables for deriving the equilibrium point, namely:
 - (a) Uncontrollable on-ramp flows $(\bar{r}_i; i \in O \setminus R)$,
 - (b) Cell speeds $(v_j; j = 1, \dots, n)$,
 - (c) Off-ramp flows or exit rates $(p_j; j = 1, \dots, n)$,
 - (d) Uncontrollable upstream mainstream inflow (q_0^{int}) .

All these quantities may be delivered by a general estimation scheme (Bekiaris-Liberis, Roncoli, and Papageorgiou, 2015; Seo et al., 2017; Sun, Muñoz, and Horowitz, 2004; Wang, Papageorgiou, and Messmer, 2006). However, in Chapter 5, a specific estimation scheme that is dedicated to the present traffic control problem and specifically concerns the real-time estimation of the external variables a, b and c above, has been proposed and is presented in the next section.

6.2.2 The Observer of the ACS

In this section, the specific nonlinear observer which is the second component of the ACS is appropriately modified and presented. A parameter vector to be estimated is defined, which includes the external variables a , b and c mentioned above. The mainline inflow q_0^{int} (if not controllable) is assumed to be known (measured). Moreover, the estimation scheme utilizes the density estimates x_j ($j = 1, \dots, n$), that are also used by NFL, as well as measurements of flow. More specifically, internal cell flow measurements (flow from one cell to the next, q_j^{int} , $j = 1, \dots, n$) and external flow measurements (exit flow from the off-ramps, q_j^{ext} , $j = 1, \dots, n$) are assumed to be available (as imposed also by the measured output (5.17) defined in Chapter 5). As illustrated in Chapter 5, the nonlinear observer achieves the precise knowledge of the (constant or slow-varying) parameter vector after a transient period when the system is under the action of the NFL. The estimated quantities are denoted, also in this chapter, by $(\hat{r}_i; i \in O \setminus R)$, $(\hat{v}_j; j = 1, \dots, n)$ and $(\hat{p}_j; j = 1, \dots, n)$, respectively. Each of these quantities is separately estimated.

Estimations of the uncontrollable on-ramp inflows

The inflow values for the uncontrollable (and unmeasured) on-ramps are estimated using the following rule (corresponding to (5.33)-(5.35) in Chapter 5):

$$\hat{r}_i(k_c) = \begin{cases} U_i(k_c) & \text{if } x_i(k_c) < \rho_i^{cr} \quad \text{and} \quad x_{i-1}(k_c) < \rho_{i-1}^{cr} \\ \hat{r}_i(k_c - 1) & \text{otherwise} \end{cases} \quad (6.7)$$

with

$$U_i(k_c) = \max\left(0, \min\left(r_i^{max}, \frac{L_i}{T_c}(x_i(k_c) - x_i(k_c - 1)) + q_i^{int}(k_c - 1) + q_i^{ext}(k_c - 1) - q_{i-1}^{int}(k_c - 1)\right)\right) \quad (6.8)$$

where L_i (in [km]) denotes the cell length. As it can be seen from (6.7), the value of each uncontrollable inflow is updated only if the density in the corresponding cell and in the upstream cell are undercritical; differently from (5.33)-(5.35), where the corresponding values update is performed when the entire density vector is undercritical. The estimation of the uncontrollable inflows is performed by means of a conservation equation, and the resulting values are truncated if they exceed a maximum value (r_i^{max}), corresponding to the on-ramp's capacity, or zero, as evidenced by (6.8).

Estimations of the mean speed

The mean speed of every cell is estimated using the following rule:

$$\hat{v}_i(k_c) = \begin{cases} V_i(k_c) & \text{if } 0 < x_i(k_c) < \rho_i^{cr} \quad \text{and} \quad 0 < x_{i+1}(k_c) < \rho_{i+1}^{cr} \\ \hat{v}_i(k_c - 1) & \text{otherwise} \end{cases}, \quad (6.9)$$

with

$$V_i(k_c) = \max\left(v_i^{min}, \min\left(v_i^{max}, \frac{q_i^{int}(k_c) + q_i^{ext}(k_c)}{x_i(k_c)}\right)\right) \quad (6.10)$$

where v_i^{min} and v_i^{max} are pre-specified constant speed bounds. As for the flow estimations of the uncontrollable on-ramps, (6.9) imposes that the speed estimations are updated only when the corresponding freeway cells are uncongested; again, differently from (5.36)-(5.37), where the corresponding values update is performed when the entire density vector is undercritical. Essentially, the estimates of mean speed correspond to the ratio of flow over density under non-congested conditions as evidenced by (6.10).

Estimations of the exit rates

The estimation of the exit rates is simply performed as follows:

$$\hat{p}_i(k_c) = \begin{cases} P_i(k_c) & \text{if } q_i^{int}(k_c) + q_i^{ext}(k_c) > 0 \\ \hat{p}_i(k_c - 1) & \text{otherwise} \end{cases}, \quad (6.11)$$

with

$$P_i(k_c) = \frac{q_i^{ext}(k_c)}{q_i^{int}(k_c) + q_i^{ext}(k_c)}. \quad (6.12)$$

The estimated values for the exit rates are updated only when the total exit flow from a cell is non-zero.

In the following sections, the performance of the ACS is investigated via appropriate simulation scenarios by use of a traffic flow model that is different than the FOM used to design the ACS and has been demonstrated in several validation exercises in the past to reproduce with satisfactory accuracy the real traffic flow dynamics.

6.2.3 The Random-Location Bottleneck Case

A concept that extends the fixed distant downstream bottleneck (denoted above with the index n) is required if one faces the Random-Location Bottleneck (RLB) situation, whereby the bottleneck may appear at several (unpredictable) locations within the considered freeway stretch. Some of the reasons for this phenomenon may be: i) traffic incidents, the exact location of which cannot be predicted, ii) long acceleration lanes, allowing ramp vehicles to merge into the mainstream anywhere along this stretch, iii) intense lane changing, e.g. due to the existence of a downstream off-ramp, iv) random impacts such as truck percentage, weather, lighting, or v) a sharp rise in the mainstream or ramp demand which may sometimes activate the merging bottleneck first, despite a stricter bottleneck farther downstream. Most of these situations have been actually encountered in the ramp metering practice and have motivated the work by Wang et al., 2010 to address them. That work involves the parallel application of a number of PI-type controllers, using multiple measurements from a specific freeway stretch downstream of the controlled ramp, as well as a decision policy which indicates the currently dominant downstream bottleneck that should be addressed by local ramp metering. The method has been in field-operational use successfully since its development.

To address the RLB situation with the ACS scheme, a data-driven decision policy is run first, aiming at identifying the currently dominating bottleneck cell in the considered freeway stretch. Eventually, ACS is applied assuming that cell to be the bottleneck cell in the sense of Figure 6.1. The decision is made by comparing the smoothed regulation error in each cell, i.e., the deviation of the current cell density from its critical value, and selecting the minimum one. More specifically, let \bar{n} be

the farthest downstream cell where a bottleneck may appear, and n the index of the currently dominating bottleneck cell at time k_c . Then, the following equations are executed before the application of ACS:

$$e_j(k_c) = \rho_j^{cr} - x_j(k_c), \text{ for } j = 1, \dots, \bar{n}, \quad (6.13)$$

$$e_j^{sm}(k_c) = \alpha e_j(k_c) + (1 - \alpha)e_j^{sm}(k_c - 1), \text{ for } j = 1, \dots, \bar{n}, \quad (6.14)$$

$$n = \arg \min_{j=1, \dots, \bar{n}} \{e_j^{sm}(k_c)\}, \quad (6.15)$$

where $e_j^{sm}(k_c)$ denotes the exponentially smoothed regulation error $e_j(k_c)$, and $\alpha \in [0, 1]$ is a constant. Thus, the decision policy selects for actual bottleneck implementation the cell n that features currently the minimum (smoothed) regulation error, and ACS is applied according to Figure 6.1.

6.3 Simulation Model and Set-Up

6.3.1 Simulation Model

The discrete SOM METANET (2.40)-(2.43), which consists of two interconnected dynamic equations for each cell, is utilized in the simulation tests of the following sections. The model describes the dynamic behavior of traffic flow along a freeway stretch, which has been divided into N cells. Notice here that the last freeway cell n considered as the bottleneck cell in the description of the ACS of the previous section, is not necessarily identical with the last cell of the simulation model, i.e., $n \leq N$. For the on-ramps as well as for the mainstream entrance flow, a simple queue model is used (Figure 6.2). The evolution of the origin queue ω_i (the queue created within the on-ramp i or the main entrance) is described by an additional state equation (conservation of vehicles in the queue):

$$\omega_i(k+1) = \omega_i(k) + T(\bar{D}_i(k) - r_i(k)), \quad (6.16)$$

where \bar{D}_i denotes external traffic demand.

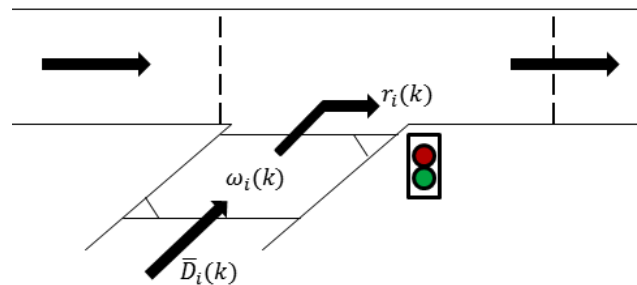


FIGURE 6.2: On-ramp cell: queue model.

The actual on-ramp flow \bar{r}_i , depends on the arriving demand \bar{D}_i and the ramp queue ω_i (if any), but also on the traffic conditions of the corresponding mainstream cell and the existence of ramp-metering control measures (Figure 6.2):

$$\bar{r}_i(k) = \min(r_i^{max}(k), v_i(k)), \quad (6.17)$$

TABLE 6.1: Parameters with common values for both scenarios of Sections 6.4 and 6.5.

T	T_c	T_{hor}	σ	v_i^{min}	$*D(\xi_i^d(k))$	$*D(\xi_i^v(k))$	$*D(\xi_i^q(k))$
5s	30s	1	10	300	400	5	100

where

$$r_i^{max}(k) = \min(\bar{D}_i(k) + T\omega_i(k), r_i^{poss}(k)), \quad (6.18)$$

$$r_i^{poss}(k) = \begin{cases} r_i^{cap} & \text{if } x_i(k) \leq \rho_i^{cr} \\ r_i^{cap} \frac{\rho_i^{max} - x_i(k)}{\rho_i^{max} - \rho_i^{cr}} & \text{if otherwise} \end{cases}, \quad (6.19)$$

where v_i is given by (6.1) for controllable on-ramps, otherwise it is set to a very high value; r_i^{cap} denotes the capacity of the i^{th} on-ramp and ρ_i^{max} denotes the maximum density on the mainstream. Thus in (6.19), the ramp-outflow capacity is linearly reduced if the density x_i of the corresponding merge cell increases beyond the critical density value, hence a ramp queue may appear even without ramp metering due to the mainstream congestion. If ramp metering is applied ($i \in R$), then the outflow that is allowed to leave the on-ramp i , during period $(kT, (k+1)T]$ is determined by the control law unless it exceeds the maximum possible ramp outflow r_i^{max} . Less important modeling details may be found by Messmer and Papageorgiou, 1990.

Simulation Set-Up

The ACS described in Section 6.2 can be used as a real-time ramp metering or mainline metering strategy either at local or coordinated levels. Therefore, two different control scenarios are considered in this chapter. First, Section 6.4 investigates the performance of the ACS as a local ramp metering strategy, in case bottlenecks exist at or far downstream of the metered ramp, including the RLB case. Second, Section 6.5 investigates the performance of the ACS as a coordinated control strategy, which aims at balancing the relative queue length on the controllable on-ramps. In the first case, the control scenario as well as the network topology and characteristics are precisely the same with those utilized by Wang et al., 2014; while for the second case, the network and the control scenario have common characteristics with those adopted by Papamichail and Papageorgiou, 2008. These specific choices have been considered for comparison purposes.

Due to the need to compare with previous works, most of the model parameters utilized for the two scenarios are different. Table 6.1 contains the parameter values that are common for both control scenarios of Sections 6.4 and 6.5; whereby $\tilde{d}(\cdot)$ denotes the standard deviation of the scalar random variables and T_{hor} denotes the time horizon for the simulation experiments. It is important to emphasise that, although different scenarios (Sections 6.4 and 6.5) and different cases for each scenario (subsections of Section 6.4) have been considered, the ACS regulator parameters σ and τ remain the same in all experiments conducted, indicating the low sensitivity of the ACS with respect to its control gains.

The control algorithm's interaction with the METANET simulator is illustrated in Figure 6.3. As may be seen, measurements of flow and density (specifically, $x_i(k)$,

$q_i^{int}(k)$, $q_i^{ext}(k)$ for each cell i of the considered freeway stretch), stemming from (2.40)-(2.43) and (6.16)-(6.19), are extracted from the simulator every $T = 5$ s. Then, the average of these measurements is fed to the observer (6.7)-(6.12) as well as the NFL (6.1) of the ACS every $T_c = 30$ sec. The observer estimates the unknown external variables (exit rates, mean speeds and uncontrollable on-ramp inflows) which are fed to (6.3) in order to obtain the optimal inflows for the controllable on-ramps, v_i^* , for $i \in R$. In case there are more than one controllable on-ramps, an additional decision policy (see Section 6.5) is required to exploit the additional degrees of freedom. The obtained optimal inflow values are subsequently utilized by (6.4)-(6.6) for the calculation of the equilibrium densities (x_j^* , $j = 1, \dots, n$) of the freeway stretch. Finally, the produced DOP (v_i^*, x_j^*) is fed to the NFL (6.1) which in turn feeds back the simulation model with the control decisions. This control loop is activated every $T_c = 30$ s.

We recall that in a real implementation, in case there are available measurements or estimates sufficient for the specification of the DOP, then one may drop the observer part and use the available traffic variables directly to obtain the DOP at each control time step (as illustrated by the dashed line in Figure 6.3). Lastly, we note that no maximum on-ramp queues have been considered in the investigated scenarios so as to focus on the impact of the ACS without additional constraints.

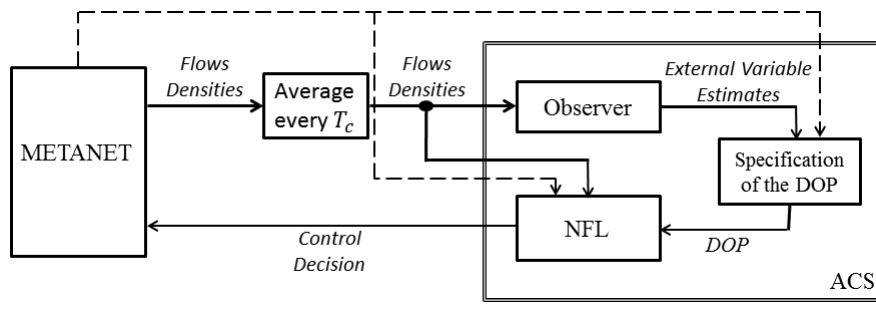


FIGURE 6.3: Control algorithm scheme.

6.4 Local Ramp Metering in Case of Distant Downstream Bottlenecks

In many practical cases, bottlenecks with smaller capacity than the merging area may exist further downstream for various reasons. In the work by Wang et al., 2014, the performance of the regulator ALINEA and its extension PI-ALINEA were investigated for such bottlenecks created by lane-drops, curvatures or uncontrolled on-ramps. Here, we intend to investigate the performance of the ACS in comparison with PI-ALINEA control strategy, which seems to respond very satisfactorily in such cases as shown by Wang et al., 2014, and which has been implemented in several field applications.

6.4.1 Network Description

For the simulation tests, three freeway networks of $N = 22$ cells have been considered (Figure 6.4). Each network has an on-ramp located at the upstream boundary of the 9th cell, which is 2 [km] downstream from the network entrance. Each cell is

$L_i = 0.25$ [km] long and has $l_i = 3$ [lanes]. The first network (Figure 6.4(a)) does not involve any downstream bottleneck; however, the on-ramp's merge area itself is a bottleneck. In order to distinguish this case from the others, it is referred hereafter as the non-bottleneck case. The other two networks have a 1 [km] bottleneck at locations 0.75 and 1.5 [km], respectively, downstream of the on-ramp (Figures 6.4 (b), (c)). A bottleneck cell differs from a non-bottleneck cell in its traffic flow characteristics. More specifically, the FD 1 (Figure 6.5) is included in the simulation model to emulate each non-bottleneck cell, whereas FD 2 is considered for each bottleneck cell. The model parameters related with FD as well as the rest of the model parameters are given in Table 6.2. The trapezoidal demand scenarios, shown in Figure 6.6, are used in the simulation investigations.

For each of these network scenarios, no control results and control results under the ACS are presented. Moreover, each case has been also tested under more realistic conditions involving stochastic demands and noise in the modelling equations.

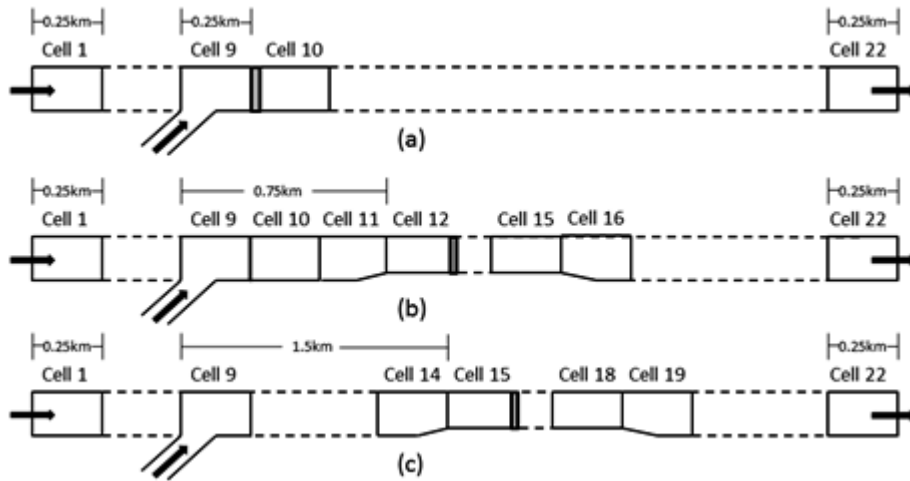


FIGURE 6.4: Hypothetical stretches (a) non-bottleneck case, (b) bottleneck case 1, (c) bottleneck case 2.

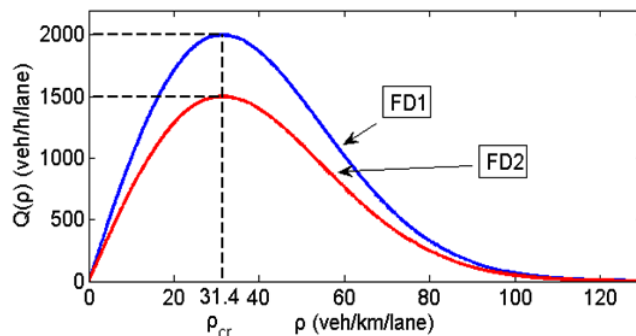


FIGURE 6.5: Considered FDs.

6.4.2 Simulation Investigations - Non bottleneck case

The non-bottleneck case is first considered for the application of the ACS. Due to the complex nonlinear dynamics of the macroscopic simulation model, the factual

TABLE 6.2: METANET Parameters.

ν	τ^m	δ	κ	v_{min}	ρ_{cr}	α	v_f	q_{cap}	
							FD1	FD2	
35s	20s	1.4	13	7	31.4	2	105	79	2000 1500

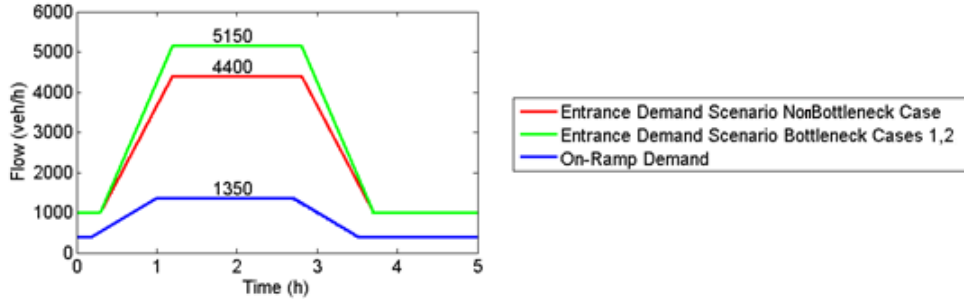


FIGURE 6.6: Mainstream and on-ramp traffic demand scenarios.

capacity and critical density of a simulated freeway stretch are not fully determined by the considered FD. Here, as also mentioned by Wang et al., 2014, the factual critical density is found to be around 38 [veh/km/lane].

In the following, no-control results (with the ramp metering actions deactivated) and control results under the impact of ACS are presented. The density and flow trajectories for the no-control case are shown in Figure 6.7(a) and Figure 6.7(b), respectively. The total demand entering the merging cell (mainstream and on-ramp demand) during the peak period (Figure 6.6) exceeds considerably the capacity level (around 6000 [veh/h]) of cell 9 and, in fact, of any other downstream cell. As shown by Figure 6.7(a), the density of cell 9 reaches the critical value of 38 [veh/km/lane] at about $t = 1.3$ h, while at the same time the traffic flow of cell 9 reaches the capacity level (Figure 6.7(b)). As the density continues to increase, congestion initially builds in cell 9 and spills back to the upstream cells. Consequently, the outflow from cell 9 and from the downstream cells drops to around 5800 [veh/h] (capacity drop). The congestion persists until the total demand decreases sufficiently. It is noted that: i) due to upstream propagation of the congestion shock wave, the cells downstream of cell 9 are not congested during the peak period (Figure 6.7(a)); ii) the outflows of all cells upstream of the on-ramp during the peak period are the same and lower than the mainstream demand, i.e. $4459 < 5150$ [veh/h], and therefore, in the no control case, the entrance demand cannot be adequately served. Note also that, during the peak period, the uncontrolled on-ramp inflow is equal to the on-ramp demand (1350 [veh/h]), which is exactly the observed flow difference at cells upstream and downstream from the on-ramp (Figure 6.7(b)).

The considered freeway stretch for the application of the ACS contains only the cell 9 which is the bottleneck cell. The ACS is fed with the density of cell 9 (x_9), the internal outflow from cell 8 (q_8^{int}) and the internal and external outflows of cell 9 (q_9^{int} and q_9^{ext}). Moreover, the ACS uses the critical density ρ_9^{cr} , which is called hereafter the set-point of the ACS. Under these settings, the observer of the ACS is employed only for the estimation of the mean speed at cell 9, i.e., \hat{v}_9 . Then, the optimal inflow

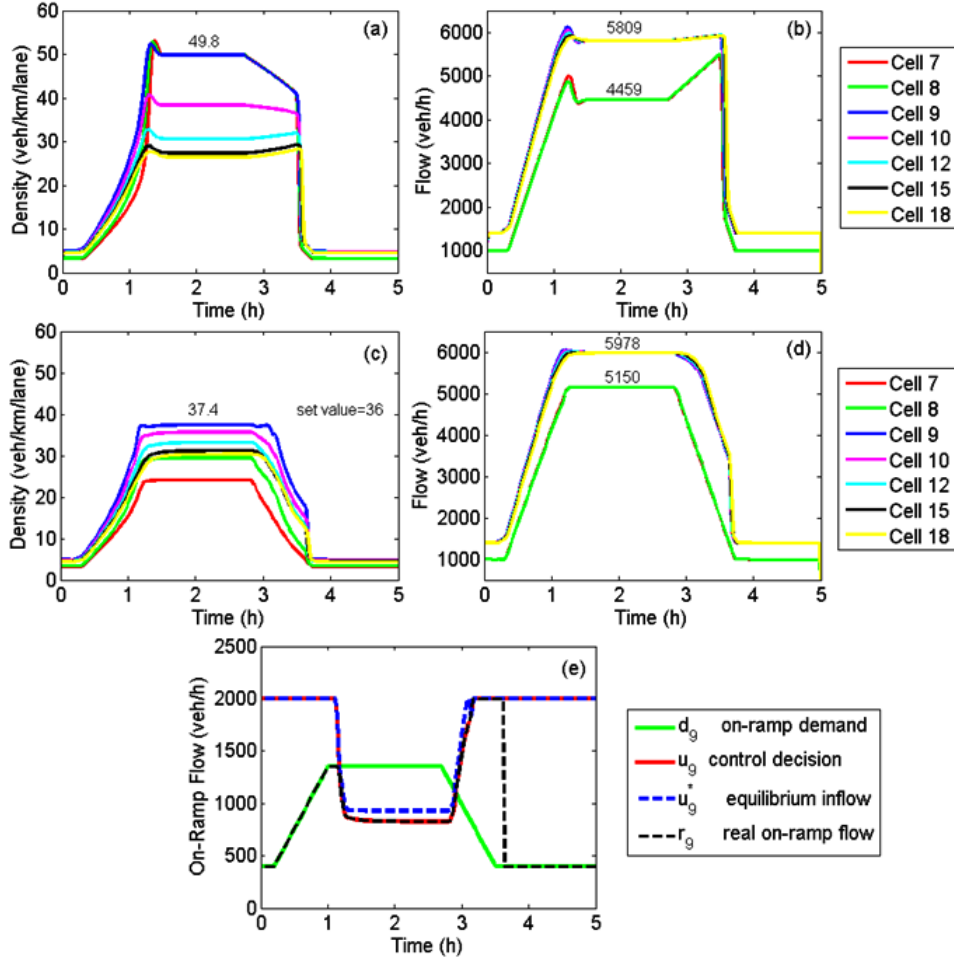


FIGURE 6.7: Non-bottleneck case: (a) density and (b) flow in the no-control case; (c) density and (d) flow with application of ACS; (e) time evolution of the variables related with the on-ramp flow.

v_9^* , according to (6.3), is obtained from:

$$v_9^*(k_c) = \rho_9^{cr} \hat{v}_9(k_c) \lambda_9 - q_8^{int}(k_c). \quad (6.20)$$

Figures 6.7 (c) and (d) illustrate the density and flow trajectories, respectively, under ACS and for set-point (utilized also in the observer and the determination of the DOP) equal to $\rho_9^{cr} = 36$ [veh/km/lane]. This set-point (instead of 38, which is the factual critical density of cell 9) was found to be the most efficient (resulting to maximum throughput), due to the offset between the set-point and the density resulting from the application of ACS. This offset is a natural consequence of the modeling mismatch (recall that the development of ACS has been based on FOMs). This implies that some fine-tuning may be also required for the set-point value in case of ACS field implementation for maximum efficiency.

Generally, ACS is seen to respond very satisfactorily. More specifically, Figure 6.7 (c) indicates that density trajectories are identical to those in the no-control case until the density of cell 9 reaches the factual critical value, after which all density trajectories are stabilized during the whole peak period. In particular, the density of the 9th cell is kept at 37.4, leading to: i) a stable capacity flow downstream of the on-ramp that accommodates all the entrance demand (Figure 6.7(d)); and ii) a

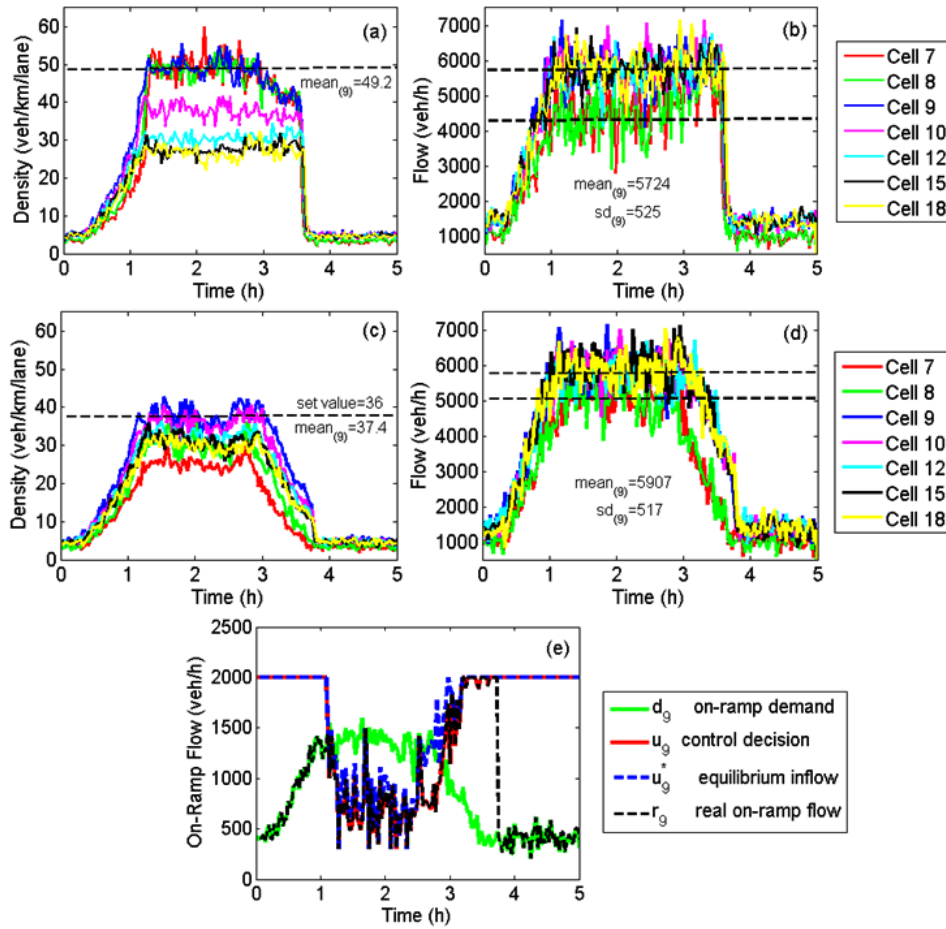


FIGURE 6.8: Non-bottleneck case under a stochastic demand and process noise: (a) density and (b) flow in the no-control case; (c) density and (d) flow with application of ACS; (e) time evolution of the variables related with the on-ramp flow.

controlled peak-period on-ramp flow (of almost 850 [veh/h], Figure 6.7(e)); which, in total, result to the desired freeway throughput (capacity flow). Clearly, the ramp metering action leads to the formation and, eventually, dissipation of a ramp queue, since the allowed on-ramp inflow is less than the on-ramp demand during the peak period (Figure 6.7(e)). Comparing the density trajectories of cells 7, 8 and 9 in Figures 6.7 (a) and (c), it is clear that, with the application of the ACS, no congestion is created in cell 9 or elsewhere. It is also noted that, due to the 3 % higher outflow from the merging cell (compare Figure 6.7(b) with Figure 6.7(d)), the density under the action of ACS, becomes undercritical much earlier than in the no-control case, i.e., the demand is served earlier. Furthermore, it is also interesting to see that no oscillations in the density trajectories at the cells close to the on-ramp are observed.

The application of the ACS has also been tested under different set-point values. This experiment aims to demonstrate that even a “sub-optimal” choice of set-point enables the freeway throughput to remain at satisfactory levels. Table 3 shows the resulting stationary density and flow emanated from a wide enough range of set-points. For example, for the “sub-optimal” choice $\rho_g^{cr} = 33$, the freeway throughput experiences a reduction of less than 0.3%.

The ACS was also tested with a more realistic stochastic scenario, whereby the

TABLE 6.3: Resulting stationary flow for all bottleneck cases and for different set values of the critical density.

Non-bottleneck		Bottleneck 1		Bottleneck 2	
Set-point / Stat.dens.	Stat.flow	Set-point / Stat.dens.	Stat.flow	Set-point / Stat.dens.	Stat.flow
33 / 33.34	5961	36 / 37.54	5229	38 / 38.7	5268
34 / 35.02	5975	37 / 38.63	5234	39 / 39.45	5268
35 / 36.03	5978	38 / 39.65	5236	40 / 40.02	5268
36 / 37.43	5978	39 / 40.62	5236	41 / 41.06	5268
37 / 38.46	5976	40 / 41.09	5236	42 / 42.12	5268
38 / 40.08	5971	41 / 42.05	5233	43 / 43.04	5266
39 / 41.48	5965	42 / 42.97	5227	44 / 44.45	5261

traffic demand is corrupted with noise and the model equations include noise terms (see (2.41), (2.42) and Table 6.1). This way, errors in the process modeling and high-frequency demand changes are taken into account. Also in this scenario, the density of cell 9 is kept near-critical (its mean during the peak period is equal to 37.4 [veh/km/lane], see Figure 6.8(c)), whereas in the corresponding no-control case (Figure 6.8(a)) the corresponding mean density value of cell 9 during the peak period is highly over-critical. The merge cell throughput remains high at the peak period (almost 3% higher than in the no-control case, see Figures 6.8 (b) and (d)), and the entrance flow demand is fully served. Figure 6.8(e) shows the trajectories of variables related with the control decision.

6.4.3 Simulation Investigations - Bottleneck Cases 1 and 2

For bottleneck cases 1 and 2, shown in Figures 6.4 (b) and (c), respectively, the factual critical density and the corresponding maximum throughput for the bottleneck section were found to be around 40 and 41 [veh/km/lane] and 5237 and 5268 [veh/h], respectively. In view of the lower bottleneck capacity, the demand scenario described by the red line in Figure 6.6 is considered for the following investigations. Note that the sum of the mainstream demand and the on-ramp demand during peak period is higher than the bottleneck capacity (else, there is no need to apply ramp-metering), but lower than the merge area capacity. In these cases, the congestion is expected to appear first in cells 12 and 15, respectively (Figures 6.4 (b), (c)), and the ramp metering target is to keep the bottleneck flow (rather than the merging cell flow) around its capacity level.

Figure 6.9(a) and Figure 6.11(a) show the density trajectories for the no-control case, where, indeed, the congestion occurs first in the corresponding bottleneck cells (12 and 15, respectively) and spills back upstream. During the whole peak period, the flow downstream of the on-ramp is lower (5165 and 5188 [veh/h], in Figure 6.9(b) and Figure 6.11(b), respectively) than the bottleneck capacity (5237 and 5268 [veh/h], respectively), due to capacity drop caused by the congestion. In addition, the flow upstream of the on-ramp is lower than the mainstream demand due to the uncontrolled on-ramp inflow.

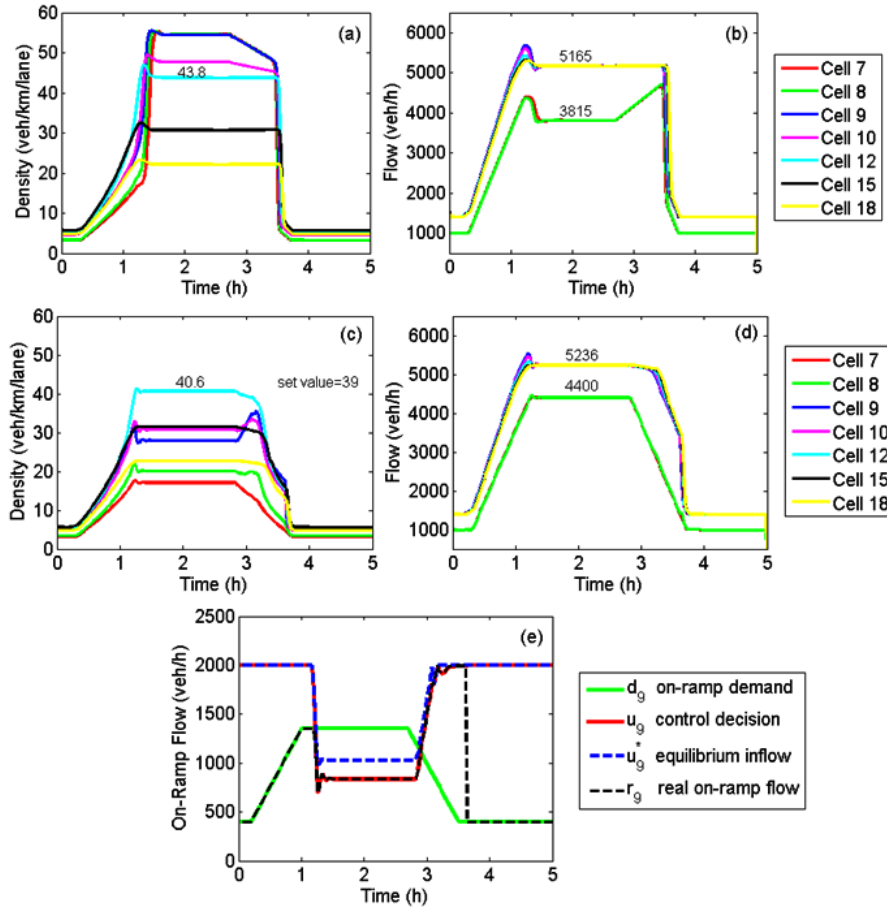


FIGURE 6.9: Bottleneck case 1: (a) density and (b) flow in the no-control case; (c) density and (d) flow with application of ACS; (e) time evolution of the variables related with the on-ramp flow.

The considered freeway stretch for application of the ACS extends from the controllable on-ramp to the first bottleneck cell. More specifically, for the bottleneck case 1, the considered freeway stretch extends from cell 9 to cell 12; while for the bottleneck case 2, the considered freeway stretch extends from cell 9 to cell 15. Due to the fact that there are no intermediate on-ramps and off-ramps, the observer of the ACS is called to estimate only the mean speeds of the cells of the considered freeway stretch. Then, the optimal inflow v_9^* utilized in the NFL of the ACS is obtained (using (6.3)) by:

$$v_9^*(k_c) = \rho_{12}^{cr} \hat{v}_{12}(k_c) l_{12} - q_8^{int}(k_c), \quad (6.21)$$

$$v_9^*(k_c) = \rho_{15}^{cr} \hat{v}_{15}(k_c) l_{15} - q_8^{int}(k_c), \quad (6.22)$$

for each respective bottleneck case.

The testing results of the ACS are presented in Figures 6.9 (c), (d), (e) and Figures 6.11 (c), (d), (e) for the bottleneck cases 1 and 2, respectively. The set-points used for each scenario are $\rho_{12}^{cr} = 39$ and $\rho_{15}^{cr} = 41$ [veh/km/lane], respectively. A small offset is seen to be present also here. Again, Table 6.3 shows, for different set-points, the resulting stationary density and flow for each bottleneck case.

The congestion formation and propagation from the bottleneck cells to upstream are suppressed. A small overshooting is observed at the initial phase of control

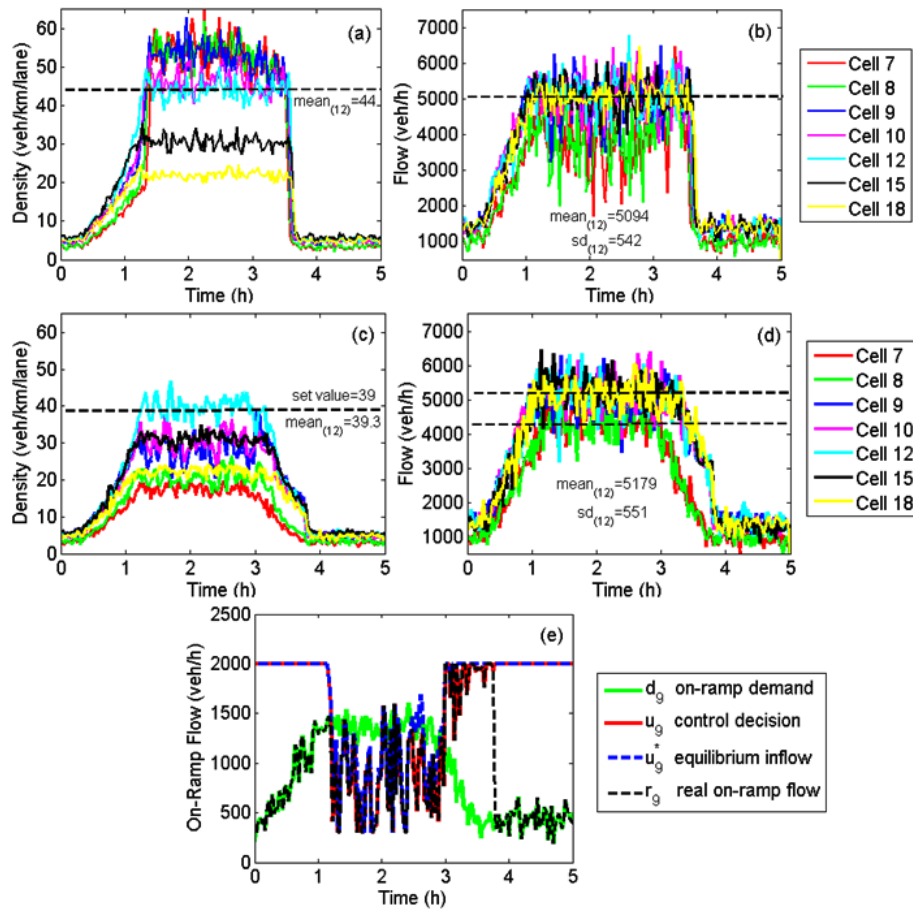


FIGURE 6.10: Bottleneck case 1 under a stochastic demand scenario and process noise: (a) density and (b) flow in the no-control case; (c) density and (d) flow with application of ACS; (e) time evolution of the variables related with the on-ramp flow.

activation, which, however, is deemed minor and is actually virtually masked by the noise in the stochastic versions of both scenarios. In fact, the trajectory of the density in cells 12 and 15 (Figure 6.9(c) and Figure 6.11(c), respectively) is smooth, and, in the steady state, the density of cells 12 and 15 is kept around the factual critical density, while the capacity level of the bottleneck cells is achieved, and the mainstream demand is well served. Except for cells 12 and 15, where the critical density prevails, all other cells are under free-flow conditions.

The ACS was also tested successfully for both bottleneck cases under the respective stochastic scenarios, see the respective Figures 6.10 and 6.12.

The investigations reported in this section demonstrate that ACS is efficient for local ramp metering where the bottleneck location may be either the on-ramp's merge area or another tighter bottleneck farther downstream. Three different cases of bottleneck locations have been addressed with equal design parameters for ACS. Since the same cases had also been considered by (Wang et al., 2014) by use of PI-ALINEA, a visual comparison with the results presented therein indicate similar performance, in fact with slightly better damped transient control period in the case of ACS.

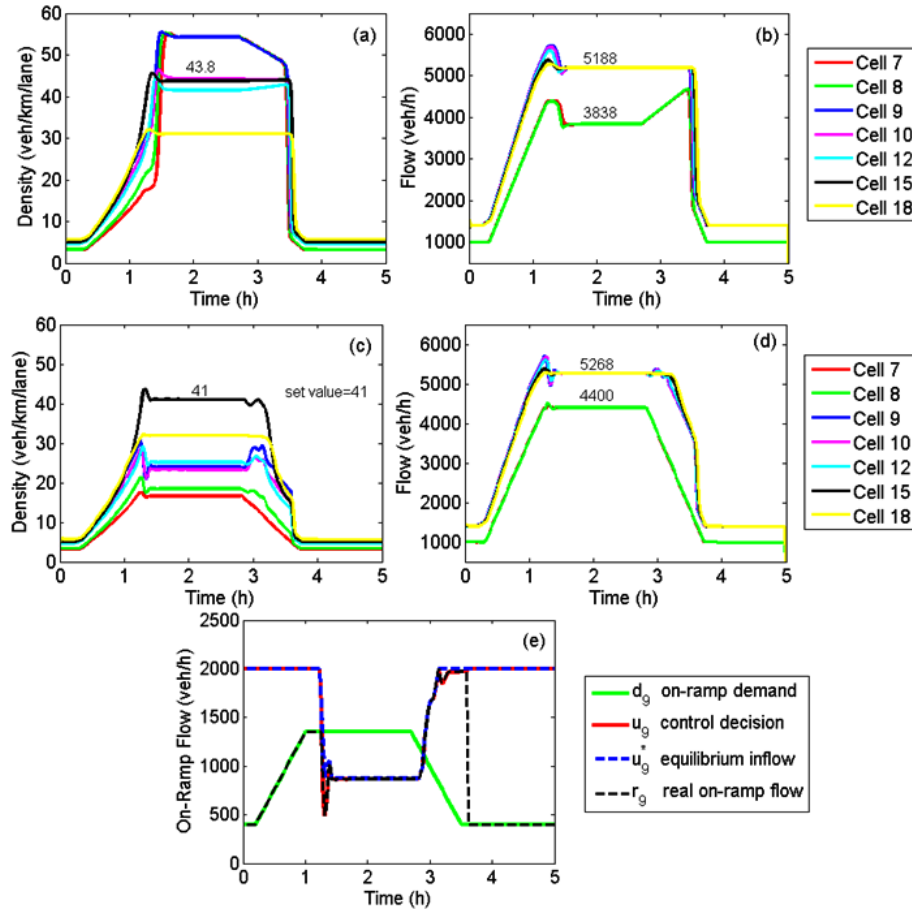


FIGURE 6.11: Bottleneck case 2: (a) density and (b) flow in the no-control case; (c) density and (d) flow with application of ACS; (e) time evolution of the variables related with the on-ramp flow.

6.4.4 Simulation Investigations - Random-Location Bottleneck Case

We now test the suitability and performance of ACS under the RLB situation using the control decision (6.13)-(6.15). Here, the aforementioned simulation settings are kept the same, but we assume that a bottleneck may randomly appear or disappear within the considered freeway stretch as well as that the bottlenecks may randomly change their spatial range. In order to have a better visualization of the control results, the demand scenario (red and green lines in Figure 6.6) is extended by one more hour for the peak period. For the simulation tests, we set $\bar{n} = 15$, $a = 0.5$ and we test the following (typical) scenario of random bottleneck switching:

[15 – 18]	→	No Bottleneck	→	[12 – 15]
$t = [0 - 2]h$		$t = [2 - 3]h$		$t = [0 - 2]h$

where [12-15] and [15-18] represent as previously a 1 [km] bottleneck at cells 12 to 15 (Figure 6.4(b)) and 15 to 18 (Figure 6.4(b)), respectively. In the non-bottleneck case (Figure 6.4(a)), the merging area is of course a candidate bottleneck. This scenario

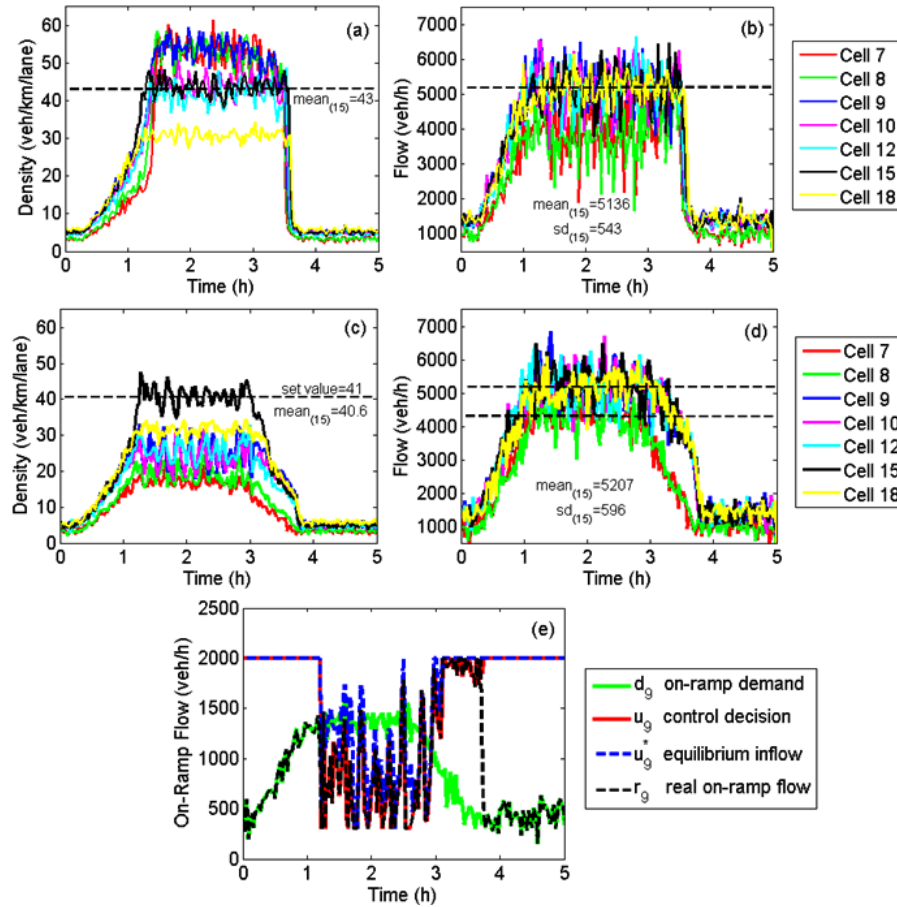


FIGURE 6.12: Bottleneck case 2 under a stochastic demand scenario and process noise: (a) density and (b) flow in the no-control case; (c) density and (d) flow with application of ACS; (e) time evolution of the variables related with the on-ramp flow.

addresses a situation in which originally the freeway stretch involves a far downstream bottleneck starting at cell 15, but, at a certain moment, this bottleneck disappears and the merge area becomes a candidate region for congestion; then again a bottleneck with different spatial range appears, starting at cell 12. All these changes are unknown to the ACS.

ACS in the simulation investigations aims to maintain the density of the selected bottleneck cell close to the critical density such that the corresponding throughput is maximized. The set-points for the ACS as well as for the decision policy (6.13)-(6.15) are set to $\rho_i^{cr} = 41$ for each $i = 9, \dots, 15$.

Figure 6.13 presents the density and flow trajectories for the above bottleneck scenario for the deterministic and stochastic scenarios. As shown with the dominating-bottleneck indicator in Figure 6.13(a), (c), when the demand levels are low (1st hour), cell 9 is dominating (with some switching in the stochastic scenario) for the control system outcome, although no control action is actually needed. As the demand increases, the impact of the bottleneck becomes visible and the regulation error of cell 15 dominates. Thus, as we also observed in the previous tests, the bottleneck density is kept around its critical value, leading to maximum outflow from cell 15 for the period from 1 to 2 hours. With the bottleneck removal at $t = 2h$, cell 9 becomes dominating again, and the total demand for the merge area includes the demand profiles

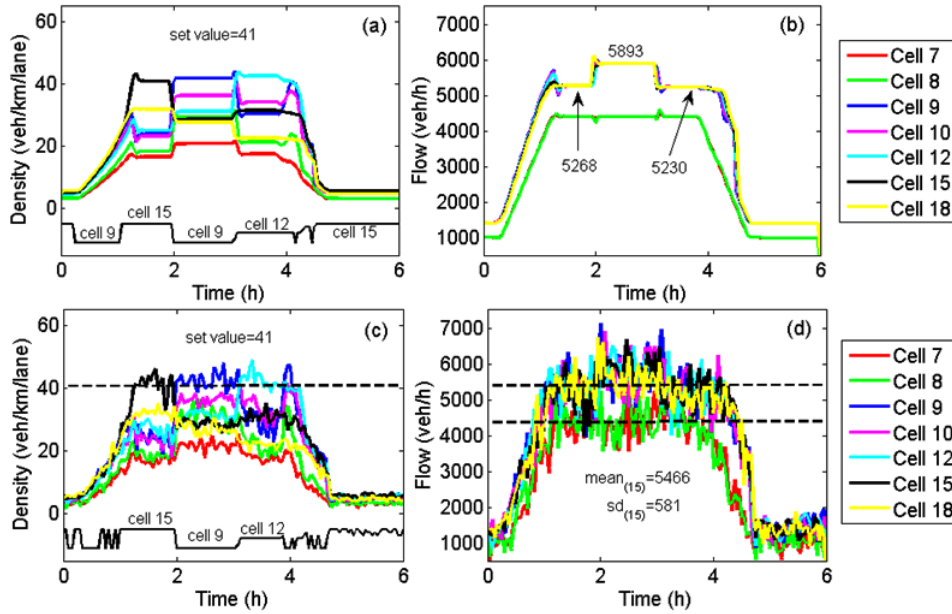


FIGURE 6.13: Application of the ACS for the RLB case: (a) density and (b) flow, under a deterministic scenario; (c) density and (d) flow, under a stochastic demand scenario and process noise.

of Figure 6.6 (i.e. 5750 [veh/h] in total) plus the accumulated on-ramp queue. As a result of ramp metering, the flows out of the merging area are maintained at the capacity level and the density of cell 9 is stabilized near its critical density (Figure 6.13(a)). Soon after the emergence of the bottleneck at cells 12 to 15, cell 12 takes over and ACS succeeds to stabilize it near its critical value.

To summarize, ACS complemented with the decision policy (6.13)-(6.15) behaves adequately in the RLB situation, switching promptly as appropriate to track the critical location along the freeway. The switching does not cause any noteworthy oscillations neither in the density nor the flow.

6.5 Application for Coordinated Ramp Metering Control

6.5.1 Network Description

In this section, ACS is tested as a control strategy for coordinated ramp metering. The adopted hypothetical network and control scenario share similar characteristics with those utilized in the work by Papamichail and Papageorgiou, 2008. More specifically, a 3-lane freeway stretch of 6.5 [km] is considered. The stretch is divided into $N = 13$ cells, each being 0.5 [km] long (Figure 6.13). There are two on-ramps on this freeway as well as an off-ramp in-between. The first and the second on-ramp are located at the upstream boundary of the 5th and the 9th cell, respectively, while the off-ramp is located at the downstream boundary of the 6th cell. The ACS is employed in order to simultaneously control both on-ramp flows, so as to maximize the throughput right after the second on-ramp (cell 9). The remaining degree of freedom shall be used to balance dynamically the relative lengths of the created queues (if any) on both controllable on-ramps. Let ω_5^{max} and ω_9^{max} be the maximum admissible on-ramp queues (in [veh]) for these two on-ramps.

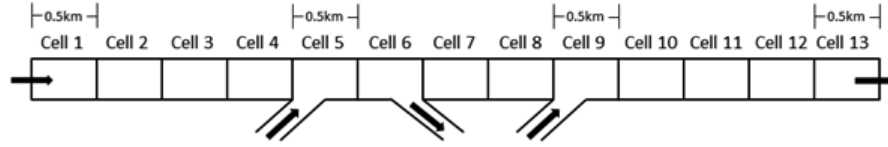


FIGURE 6.14: The utilized freeway for coordinated ramp metering.

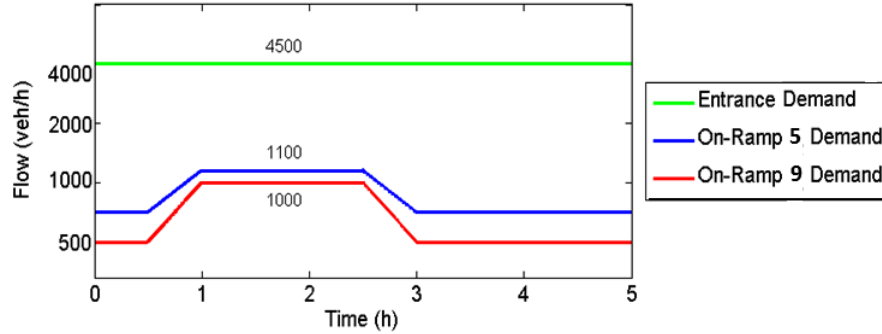


FIGURE 6.15: Mainstream and on-ramps traffic demand profiles.

The considered freeway stretch for the application of the ACS extends from cell 5 to cell 9. Due to the fact that there are no intermediate on-ramps within this stretch, the observer of the ACS is only employed in order to estimate the mean speeds of the cells of the considered freeway stretch as well as the exit rate from off-ramp 6. In order to balance the relative queue lengths on both controllable on-ramps, the optimal inflow values (here, v_5^* and v_9^*), utilized by the NFL of the ACS, must be appropriately determined. To this end, a second relationship, along with (6.3), that associates the optimal inflows is needed. This relationship may be directly derived from the target of balancing the relative ramp queues, i.e.,

$$\frac{\omega_5(k_c)}{\omega_5^{max}} = \frac{\omega_9(k_c)}{\omega_9^{max}}. \quad (6.23)$$

Substituting (6.16) into (6.23) and replacing r_5 and r_9 with v_5^* and v_9^* , respectively, a relationship between the optimal inflows is obtained. Using also relation (6.3), the optimal inflow values can be uniquely determined. More specifically, let us introduce, for convenience, the following notations:

$$A(k_c) = \rho_9^{cr} \hat{v}_9(k_c) l_9 - (1 - \hat{p}_6(k_c)) q_4^{int}(k_c), \quad (6.24)$$

$$A_1(k_c) = \omega_5(k_c) - T_c \bar{D}_5(k_c), \quad (6.25)$$

$$A_2(k_c) = \omega_9(k_c) - T_c (\bar{D}_9(k_c) - A(k_c)). \quad (6.26)$$

Then, the optimal inflows are given by:

$$v_5^*(k_c) = \frac{1}{T_c} \frac{\omega_9^{max} A_1(k_c) - \omega_5^{max} A_2(k_c)}{(1 - \hat{p}_6(k_c)) \omega_5^{max} + \omega_9^{max}}, \quad (6.27)$$

$$v_9^*(k_c) = A(k_c) - (1 - \hat{p}_6(k_c)) v_5^*(k_c). \quad (6.28)$$

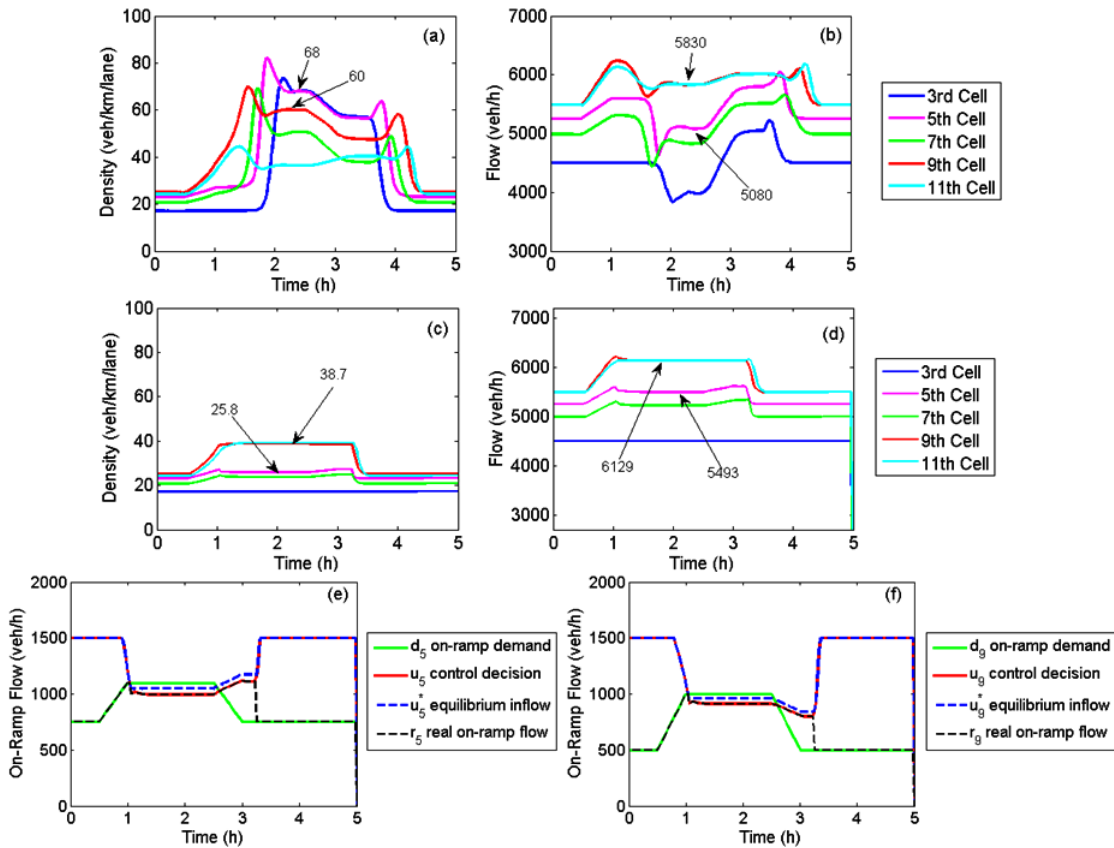


FIGURE 6.16: (a) Density and (b) flow trajectories for the no-control case; (c) density and (b) flow trajectories under ACS; and (e) and (f) trajectories of variables related with the on-ramp inflow for the two on-ramps.

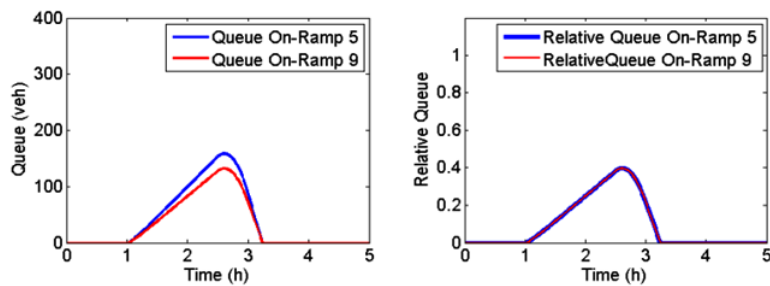


FIGURE 6.17: Queue lengths and relative queue lengths for the two onramps under ACS.

Each freeway cell is described by the same FD, and the corresponding model parameters are shown in Table 6.4. The trapezoidal demand profiles for the on-ramps and the constant demand profile for the entrance are shown in Figure 6.15. The exit rate at the off-ramp is set to $p_6 = 5\%$. Cell 9 is a potential bottleneck for the freeway due to the existence of high on-ramp and mainstream demands. After some simulation experiments, the factual critical density and the corresponding capacity flow are found to be 39 [veh/km/lane] and 6130 [veh/h], respectively. Notice that the total flow demand arriving at the upstream boundary of cell 9, during peak

TABLE 6.4: Simulation model and FD parameters (2^{nd} scenario).

ν	τ^m	δ	κ	v_{min}	ρ_{cr}	α	v_f	q_{cap}
24s	22s	1.7	13	7	36	1.5	110	2033

period, exceeds the capacity flow of the cell 9, i.e., $6320 > 6130$. The maximum ramp queue lengths considered for relative queue balancing are $\omega_5^{max} = 200$ [veh] and $\omega_9^{max} = 167$ [veh].

When no control is applied, the resulting density and flow profiles for both merge areas and also other cells of the freeway are shown in Figures 6.16 (a) and (b). Mainstream congestion appears after 1 [h] in the merge area of on-ramp 9 due to the high flows that arrive there; this leads to a visible mainstream flow decrease (capacity drop). The created congestion travels upstream and reaches the merge area of the on-ramp 5 at around 2 [h], also leading to a visible flow decrease. No queues are formed at the on-ramps, but a small queue is created at the far upstream entrance of the network.

Figures 6.16 (c) and (d) present the density and flow profiles under the application of ACS. For this test, the set-point value is equal to $\rho_9^{cr} = 38$ [veh/km/lane], though Table 5 presents different results for different set-points as well. It can be seen from Figure 6.16 (c) that congestion is avoided and the density of the cell 9 is around critical, resulting in maximization of throughput and near-capacity flow values from the same cell. Figures 6.16 (e) and (f) show the evolution of the variables related with the control decision. Regarding the balancing of on-ramp queues, Figure 6.17 shows the evolution both of the queue lengths and of the relative queue lengths for the two on-ramps. On-ramp 5 has larger capacity and therefore its queue is larger than at on-ramp 9. However, the relative queue lengths are equal during the whole simulation horizon as desired.

In order to test the performance of the proposed coordination scheme with respect to stochastic scenarios, appropriate simulations have been conducted which are presented in Figure 6.18. When no control measures are applied, the resulting density and flow trajectories are shown in Figures 6.18 (a) and (b), respectively, where a congestion in the mainstream is observed, starting again in the merge area of on-ramp 9 and propagating upstream. This congestion leads also to a decrease in the mainstream flow, the mean value of which, during the peak period, is equal to 5756 [veh/h]. However, also in this stochastic scenario, the application of ACS leads to noticeably better results, shown in Figures 6.18 (c) and (d). Apparently, the performance of the ACS is not affected by the presence of noise. Again, no congestion is formed along the freeway stretch (see Figure 6.18 (c)), while the outflow from cell 9 is kept near capacity (its mean is almost 6070 [veh/h], see Figure 6.18 (d)). Figures 6.18(e) and (f) show the evolution of the control decision variables, while Figure 6.19 shows the actual queue length (left) and the relative queue length (right) of each on-ramp, where the latter are equal during the whole simulation horizon.

The scenarios investigated in this section demonstrate that ACS is also efficient for coordinated ramp metering. As mentioned above, similar cases with the ones utilized in this study had also been considered in (Papamichail and Papageorgiou, 2008) by use of a linked control strategy. By comparing (again visually) the results therein with the reported results in this study, we conclude that no important differences in the performance of the two control strategies exist. However, ACS is

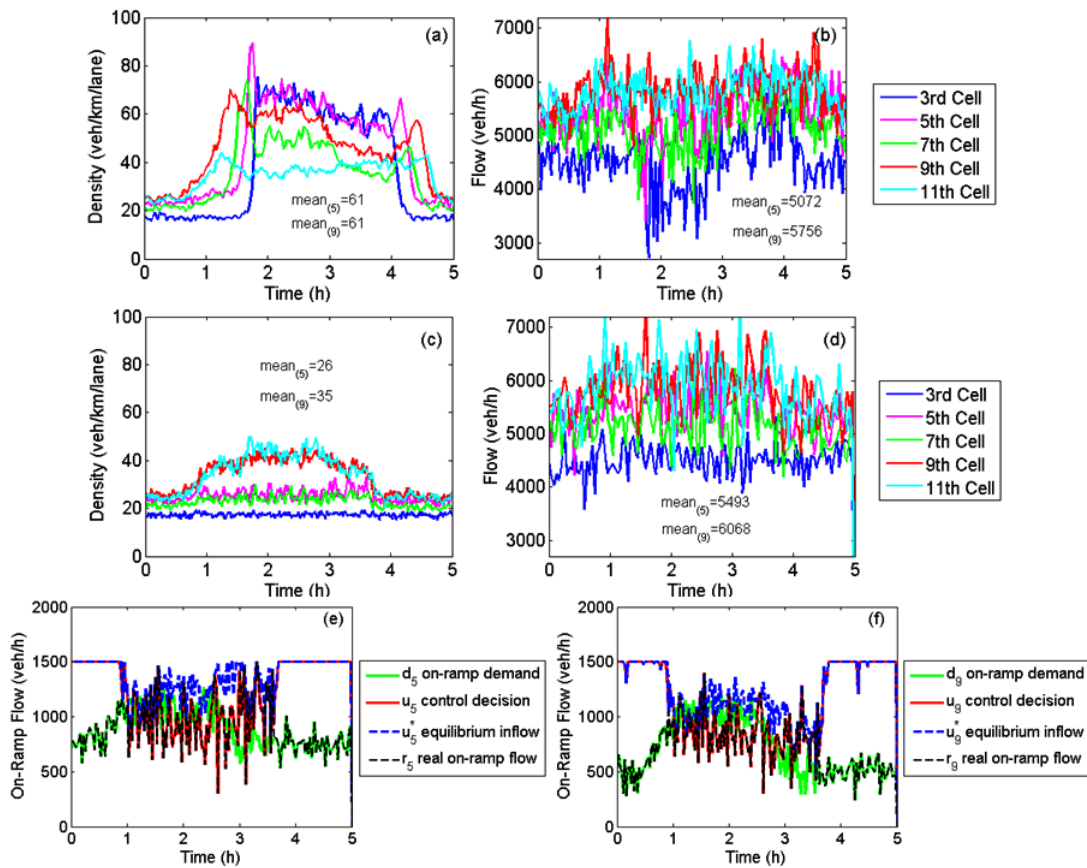


FIGURE 6.18: (a) Density and (b) flow trajectories for the no-control case; (c) density and (b) flow trajectories under ACS; and (e) and (f) trajectories of variables related with the on-ramp inflows for the two on-ramps under the stochastic scenario.

simpler in application than many existing coordination schemes, including the one presented by Papamichail and Papageorgiou, 2008.

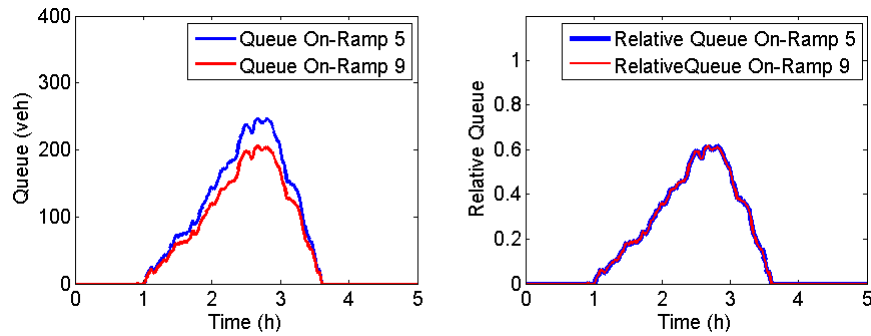


FIGURE 6.19: Queue lengths and relative queue lengths for the two onramps under ACS for the stochastic scenario.

TABLE 6.5: Resulting stationary density and flow for the coordinated ramp metering scenario and for different set-points.

Set-point / Stat.dens.	Stat.flow
35 / 35.42	6090
36 / 36.55	6109
37 / 37.63	6123
38 / 38.75	6129
39 / 39.95	6128
40 / 40.9	6122
41 / 42.15	6111

Chapter 7

Conclusions and Future Work

This final chapter summarizes the findings and results of this thesis. In particular, Section 7.1 gives a summary of the study and highlights the main results and contributions of this thesis, while Section 7.2 indicates future research aspects that could be considered to extend the investigation results.

7.1 Concluding Remarks

During the last decades, a large amount of research has been performed in the area of Mathematical Control Theory. This research resulted to the development of rigorous tools that can be used for Nonlinear Systems and Control and can be applied to many different engineering fields including Traffic Engineering. Therefore, it is essential to appropriately exploit these recent advances in order to deal with the increasing freeway traffic congestion problems. In particular, traffic control originated by rigorous Mathematical Control Theory methodologies will provide the community of Traffic Engineering with more robust and potentially more efficient control strategies. However, literature generally lacks, so far, of studies that provide rigorous model-based methods, which are characterized by strong theoretical properties, while, at the same time, can be easily applied for real traffic control. This thesis aims to commence such a promising approach focusing on the development of general control strategies for freeway networks.

First, in the modeling part of this thesis (Chapter 2), a general class of first-order discrete space-time models for acyclic traffic networks was developed and presented. Specific instances of the developed general modeling framework are well-known and established traffic flow models, which have been proposed in the literature, including CTM and its extensions. The proposed models are highly nonlinear and uncertain, while the related assumptions are, from a Traffic Engineering point of view, mild and reasonable. Due to their discrete nature, the developed models can be directly applied in a computer environment for simulations purposes and they are characterized by nice analytical properties (e.g., explicit state-space form, involvement of continuous and differential functions), short computation times and convenient discretization intervals.

Moreover, Chapter 2 presents an overview of modeling approaches to include capacity drop into LWR-type traffic flow models. Although LWR-type first-order freeway models are well-known effective tools, their inherent formulation do not allow the representation of capacity drop, which is a significant phenomenon observed in real traffic. The selected approaches were described and tested in terms of their ability to reproduce the right traffic pattern and the capacity drop phenomenon caused due to an on-ramp merging. First, the approaches are tested for a hypothetical network and traffic demand scenario, to highlight their principal behavior and qualitative properties; eventually, the models were rigorously calibrated

and validated using real data from a freeway in the U.K. The obtained results show that, although the tested models employ different mechanisms to reflect the capacity drop phenomenon, they all manage to produce a flow reduction at the merge area whenever traffic congestion is present. The obtained results were found to be quantitatively similar with respect to the achieved Performance Index values, which is mainly attributed to a traffic situation with limited complexity and few internal comparison data. Moreover, some of the approaches that incorporate the capacity drop into LWR-type models produced a lower flow error (better reproduction of capacity drop) than the one obtained by other than LWR-type FOMs. Most of the modifications performed in the basic discretized LWR model, so as to account with the capacity drop, are basically ad-hoc changes in the demand/supply functions. Therefore, a theoretical analysis (presented in Appendix C) was performed in order to prove the consistency of the proposed capacity drop model (Approach 5) with the original LWR model. The theoretical analysis indicated that the formal underlying PDE is still the LWR model, but with a source term present (i.e. a non-homogeneous PDE).

The second part of this thesis (Chapters 3 and 4) is devoted to the stabilization of the general models described in the first part. Specifically, a rigorous methodology for the construction of a parameterized family of explicit feedback laws that are able to guarantee the RGES of the UEP of the developed general traffic flow models was presented. In Chapter 3, the proposed methodology is based on the developed general acyclic traffic networks. The stability of the closed-loop system is checked in terms of Vector Lyapunov Function criteria and certain important properties of the acyclic traffic flow models. Appropriate propositions, lemmas and theorems are constructed, which gradually lead to the main stabilization results. The stabilization is achieved by regulating an appropriately selected set of inflows. In Chapter 4, the developed methodology concerns a class of freeway models; however, the construction of the global exponential feedback stabilizer utilizes a single Lyapunov function, which acts as a CLF for the open-loop system. The availability of a single Lyapunov function allowed the construction of sufficient conditions for the estimation of the set of the inflows that must be controlled in order to guarantee the RGES of the UEP of the freeway models. All the provided sufficient conditions can be easily checked and give to the traffic engineer the ability to design easily an opportune feedback controller. The applicability of the obtained results to real control problems was demonstrated by conducting related simulation studies. The simulation results demonstrated the efficacy of the proposed feedback control laws with respect to: i) the fast convergence to the UEP, ii) the existence of measurement and modeling errors, and iii) appropriate comparisons with other existing feedback laws proposed in the literature and employed in practice.

In case limited information is provided regarding the system parameters, this thesis also provided, in Chapter 5, a methodology for the construction of ACSs for general uncertain discrete-time systems. The developed ACS guarantee robust global exponential convergence to the desired UEP of the system, and consists of a nominal feedback law in conjunction with a nonlinear dead-beat observer. The proposed adaptive scheme did not require the knowledge of a Lyapunov function for the closed-loop system under the action of the nominal feedback stabilizer and is directly applicable to highly nonlinear, uncertain discrete-time systems with unknown constant parameters. The applicability of the general result to real control problems was demonstrated by the rigorous application of the proposed ACS to the developed uncertain freeway models. Simulation results showed the efficacy of the proposed adaptive control scheme even under the presence of modeling errors

and/or time-varying parameters.

In Chapter 6, the ACS, developed in Chapter 5, is tested under realistic and customary freeway traffic control scenarios in order to investigate its potential application to the real field. More specifically, the SOM METANET is used (rather than the developed first-order freeway model) as ground truth for the control application. Here, appropriate hypothetical scenarios are constructed and the developed scheme is tested with respect to its ability to stabilize the system when bottlenecks exist far downstream of a metered on-ramp. The reported investigations evidence that ACS is applicable, at will, as a local or coordinated ramp metering strategy, and that it acts efficiently in both cases. First, as a local ramp metering strategy, ACS succeeded to handle efficiently congestion phenomena caused by the presence of distant downstream bottlenecks, by regulating appropriately the inflow from an on-ramp. ACS, fed with measurements along the region extending from the controllable on-ramp to the downstream bottleneck, leads to damped and satisfactory control behavior. In addition, for cases where the bottleneck location is not exactly known or its spatial range may randomly change within a certain region, an extension of ACS was proposed in this paper. This extension imposes the prior execution of a decision procedure, which aims to detect (in real-time) the location where the congestion is likely to appear first; and that location is selected as the target location for maximizing freeway throughput by ACS. The corresponding simulation tests show that ACS, can satisfactorily handle the ramp metering task in various situations, including RLBs, within a freeway stretch. Second, as a coordinated ramp metering strategy, ACS succeeded to maintain the density of the freeway near-critical and to maximize throughput; while the additional degrees of freedom may be exploited to balance the relative queue lengths in the controllable on-ramps. The utilization of the same regulator parameters for various scenarios with different distances among the control actuator and the target bottleneck indicates that little fine-tuning will be necessary in potential field applications. Moreover, the observed performance of the ACS is not affected if there exists an additional disturbance, e.g. in form of an off-ramp between the controlled on-ramp and the downstream bottleneck. Some minor fine-tuning may be required for the selection of the set-point density due to the offset produced with the application of ACS. However, the new strategy is more flexible and simpler in application than many existing coordination schemes.

7.2 Further Research

There are various ways to extend the main results presented in this thesis. Few of them are listed below:

- First, the methodology presented in Chapter 5, for the class of freeway models presented in Section 2.2.3, can also be extended to account for the general acyclic traffic networks presented in Section 2.2.1.
- Additional research will also be performed in order to construct a CLF for the general acyclic traffic networks presented in Section 2.2.1; the knowledge of a CLF for the open-loop system can be exploited in order to address robustness issues in a rigorous way.
- The control approach, presented in Chapters 3 and 4, does not consider the impact of inflow control on upstream traffic flow conditions (e.g., queue forming at on-ramps); future extensions will address these issues appropriately.

- Testing the proposed feedback approach with more detail models, e.g., microscopic traffic simulation models, would also be of interest.
- An other important research direction could also be the extension of the proposed control results to continuous-time traffic flow models, either by developing continuous-time feedback or sample-data feedback control.
- As far as the calibration tests on capacity drop model are concerned, future investigations involving more complex traffic situations and richer data might shed more light on the comparative quantitative accuracy of different approaches. Moreover, it would be interesting to test and evaluate the behavior of the described models in case traffic control strategies are applied.

Appendix A

Mathematical Background

A.1 Nonlinear Systems and Control

This section presents some basic definitions and existed results that will be used throughout this thesis. Let $S \subseteq \mathbb{R}^n$ be a non-empty closed set, $D \subseteq \mathbb{R}^l$ be a non-empty compact set and consider the uncertain, discrete-time, dynamical system:

$$x^+ = F(d, x), \quad x \in S, \quad d \in D, \quad (\text{A.1})$$

where $F : D \times S \rightarrow S$ is a locally bounded mapping. The variable $x \in S$ denotes the state of (A.1) and $d \in D$ is an unknown, time-varying input. Here (and throughout the thesis) x^+ denotes the value of the state at the next time instant, i.e., (A.1) describes the recursive relation $x(t+1) = F(d(t), x(t))$. Given $x_0 \in S$, $\{d(t) \in D\}_{t=0}^{\infty}$ we are in a position to determine the solution $x(t)$ of (A.1), with $x(0) = x_0$ corresponding to input $\{d(t) \in D\}_{t=0}^{\infty}$, by means of the recursive relation $x(t+1) = F(d(t), x(t))$, for all $t \geq 0$. Let $x^* \in S$ be an equilibrium point of (A.1), i.e., $x^* \in S$ satisfies $x^* = F(d, x^*)$ for all $d \in D$. We also assume that $F : D \times S \rightarrow S$ is continuous on the set $D \times \{x^*\}$. Notice that the requirement $x^* = F(d, x^*)$, for all $d \in D$, implies that $d \in D$ denotes a vanishing perturbation, i.e., a disturbance that does not change the position of the equilibrium point of the system. In general, the decision of which variables are vanishing or non-vanishing perturbation depends on the equilibrium point that we have in mind: for example, a perturbation may change the position of other equilibria but not the position of the equilibrium point that we intend to study.

Here, we adopt the following RGES notion (see similar notions in Haddad and Chellaboina, 2008; Karafyllis and Papageorgiou, 2015; Lakshmikantham and Tripiante, 2002).

Definition A.1

We say that $x^* \in S$ is RGAS for system (A.1) if there exists a function $a \in KL$ such that for every $x_0 \in S$ and for every sequence $\{d(t) \in D\}_{t=0}^{\infty}$, the solution $x(t)$ of (A.1) with initial condition $x(0) = x_0$ corresponding to input $\{d(t) \in D\}_{t=0}^{\infty}$ (i.e., the solution that satisfies $x(t+1) = F(d(t), x(t))$ for all $t \geq 0$ and $x(0) = x_0$) satisfies the inequality $|x(t) - x^*| \leq a(|x_0 - x^*|, t)$ for all $t \geq 0$. We say that $x^* \in S$ is RGES if there exist constants $M, N > 0$ such that for every $x_0 \in S$ and for every sequence $\{d(t) \in D\}_{t=0}^{\infty}$ the solution $x(t)$ of (A.1) with initial condition $x(0) = x_0$ corresponding to input $\{d(t) \in D\}_{t=0}^{\infty}$ (i.e., the solution that satisfies $x(t+1) = F(d(t), x(t))$ for all $t \geq 0$ and $x(0) = x_0$) satisfies the inequality $|x(t) - x^*| \leq M \exp(-Nt)|x_0 - x^*|$ for all $t \geq 0$.

Lemma A.2

Consider system (A.1) and let $\Omega \subseteq S$ be a given set. Suppose that $F(D \times S)$ is bounded. Moreover, suppose that the following hold:

- i) There exist constants $M, N > 0$ such that for every $x_0 \in \Omega$, $\{d(t) \in D\}_{t=0}^{\infty}$ the solution $x(t)$ of (A.1) with initial condition $x(0) = x_0$ corresponding to input $\{d(t) \in D\}_{t=0}^{\infty}$ satisfies $|x(t) - x^*| \leq M|x_0 - x^*| \exp(-Nt)$, for all $t \geq 0$.
- ii) There exists an integer $\tilde{K} \geq 1$ such that for every $x_0 \in S$, $\{d(t) \in D\}_{t=0}^{\infty}$ and $t \geq \tilde{K}$ there exists $i(t) \in \{0, 1, \dots, \tilde{K}\}$ for which the solution $x(t)$ of (A.1) with initial condition $x(0) = x_0$ corresponding to input $\{d(t) \in D\}_{t=0}^{\infty}$ satisfies $x(t - i(t)) \in \Omega$.
- iii) There exists a constant $L \geq 1$, such that the inequality $|F(d, x) - x^*| \leq L|x - x^*|$ holds for all $d \in D$ and for all $x \in S$ in a neighborhood of x^* .

Then, $x^* \in S$ is RGES for the uncertain system (A.1).

It should be noticed that Lemma A.2 requires that the exponential stability estimate $|x(t) - x^*| \leq M|x_0 - x^*| \exp(-Nt)$ holds only for initial conditions x_0 that belong to the set Ω . Therefore, one can exploit this fact by selecting the set $\Omega \subseteq S$ in a convenient way. As always, there is a price to pay for this relaxation of requirements for RGES: one has to show that assumptions ii), iii) of Lemma A.2 hold as well.

Lyapunov functions are largely used in the study of Control Theory and they consist the basic tool for designing feedback control and for studying the qualitative behavior of dynamical systems (Sontag, 1998; Clarke, 2001; Anderson and Moore, 1990).

Definition A.3

A function $V : S \rightarrow \mathbb{R}_+$ for which there exist constants $K_2 \geq K_1 > 0$, $\kappa > 0$ and $\lambda \in [0, 1)$ such that the inequalities $K_1|x - x^*|^\kappa \leq V(x) \leq K_2|x - x^*|^\kappa$ and $V(F(d, x)) \leq \lambda V(x)$ hold for all $(d, x) \in D \times S$, is called a Lyapunov function with exponent $\kappa > 0$ for (A.1).

Remark A.1 If a Lyapunov function with exponent $\kappa > 0$ exists for (A.1), then $x^* \in S$ is RGES. Indeed, if the state space were \mathbb{R}^n and not $S \subseteq \mathbb{R}^n$ and if no disturbances were present, then we would be able to use Theorem 13.2 on pages 765-766 in (Haddad and Chellaboina, 2008) and conclude that the existence of a Lyapunov function with exponent $\kappa > 0$ for (A.1) is a sufficient condition for RGES of $x^* \in S$. However, since the uncertain dynamical system (A.1) is defined on $S \subseteq \mathbb{R}^n$ with disturbances $d \in D$, we cannot use the aforementioned theorem. On the other hand, we can use the inequality $V(F(d, x)) \leq \lambda V(x)$ inductively and obtain the estimate $V(x(t)) \leq \lambda^t V(x(0))$ for every solution of (A.1), for every sequence $\{d(t) \in D\}_{t=0}^{\infty}$ and for every integer $t \geq 0$. The required exponential estimate of the solution is obtained by combining the previous estimate with the inequality $K_1|x - x^*|^\kappa \leq V(x) \leq K_2|x - x^*|^\kappa$, which directly implies $K_1|x(t) - x^*|^\kappa \leq \lambda^t K_2|x(0) - x^*|^\kappa$, or $|x(t) - x^*| \leq M \exp(-Nt)|x_0 - x^*|$, where $M = (K_2/K_1)^{1/\kappa}$, $N := -\frac{\ln(\lambda)}{\kappa}$ for the case $\lambda > 0$ and arbitrary $N > 0$ for the case $\lambda = 0$.

Definition A.4

A *Trapping Region (TR)* for system (A.1) is a set $\Omega \subseteq S$ for which there exists an integer $m \geq 0$ such that for every $x_0 \in S$, $\{d(t) \in D\}_{t=0}^{\infty}$, the solution $x(t)$ of (A.1) with initial condition $x(0) = x_0$ corresponding to input $\{d(t) \in D\}_{t=0}^{\infty}$ satisfies $x(t) \in \Omega$, for all $t \geq m$.

A nonlinear system with a TR is a system for which all solutions enter a specific set after an initial transient period. A direct consequence of Definition A.4 is that every TR for (A.1) must contain all equilibrium points. The following theorem provides VLF stability criteria for the RGAS and RGES of the equilibrium of (A.1).

Theorem A.5

Consider system (A.1) and suppose that $\Omega \subseteq S$ is a TR for (A.1). Moreover suppose that there exists functions $\alpha_1, \alpha_2 \in K_{\infty}$ with $\alpha_1(s) \leq \alpha_2(s)$ for all $s \geq 0$, $V_i : \Omega \rightarrow \mathbb{R}_+$ ($i = 1, \dots, l$) and a matrix $\Gamma = \{\gamma_{i,j} \geq 0, i, j = 1, \dots, l\} \in \mathbb{R}_+^{l \times l}$ such that the following inequalities hold for all $x \in \Omega$, $d \in D$ and $i = 1, \dots, l$:

$$\alpha_1(|x - x^*|) \leq \max_{i=1, \dots, l} (V_i(x)) \leq \alpha_2(|x - x^*|), \quad (\text{A.2})$$

$$V_i(F(d, x)) \leq \sum_{j=1}^l \gamma_{i,j} V_j(x). \quad (\text{A.3})$$

Moreover, suppose that the spectral radius $\rho(\Gamma)$ of the matrix Γ is less than 1. Then, $x^* \in S$ is RGAS for (A.1). Moreover, if there exists constants $L \geq 0$, $0 < K_1 \leq K_2$, $\kappa > 0$ such that $\sup\{|F(d, x) - x^*| : d \in D\} \leq L|x - x^*|$ for all $x \in S \setminus \Omega$ and if $\alpha_i(s) = K_i s^{\kappa}$, ($i = 1, 2$) for all $s \geq 0$ then $x^* \in S$ is RGES for (A.1).

It should be emphasized that the novelty of Theorem A.5 with respect to existing results lies in the presence of deterministic uncertainty and the exploitation of the TR. The proof of Theorem A.5 can be found in (Karafyllis and Papageorgiou, 2015).

Next consider the uncertain, discrete-time, control system:

$$x^+ = F(x, u), x \in S, u \in U, \quad (\text{A.4})$$

where $F : S \times U \rightarrow S$ is a locally bounded mapping and $S \subseteq \mathbb{R}^n$, $U \subseteq \mathbb{R}^m$ are non-empty sets. Let $x^* \in S$ be an equilibrium point of (A.4), i.e., there exists $u^* \in U$ so that $x^* = F(x^*, u^*)$. We next define the notion of global asymptotic controllability for (A.4).

Definition A.6

We say that system (A.4) is *globally asymptotically controllable* to $x^* \in S$ if for every $x_0 \in S$ there exists $\{u(t) \in U\}_{t=0}^{\infty}$ such that the solution $x(t)$ of (A.4) corresponding to input $\{u(t) \in U\}_{t=0}^{\infty}$, with initial condition $x(0) = x_0$ satisfies $\lim_{t \rightarrow \infty} x(t) = x^*$.

Notice that global asymptotic controllability is a necessary condition for the existence of a globally stabilizing feedback for (A.4) (see Sontag, 1998).

A.2 Graph Theory

This section presents some results from *Graph Theory*, which will be used in the study of acyclic networks in Chapters 2 and 3.

From a graph-theoretic point of view, directed acyclic graphs are graphs whose vertices can admit a topological sorting. This means, that their vertices can be ordered in such a way, that the starting endpoint of every edge (joining two vertices) occurs earlier in the ordering than the ending endpoint of the edge. Assigning the vertices of the graph to the components or cells of the network, for any given acyclic network, and by using the previous definition, we are in a position to reorder the cells of the network into a topological sorting. The main consequence of this sorting is that the matrix $B = \{b_{i,j} : i, j = 1, \dots, n\} \in [0, 1]^{n \times n}$ containing the turning rates of the network becomes strictly upper triangular (Godsil and Royle, 2013; Kim, 1979; Kim, 1982).

The following technical lemmas are useful for the analysis of the networks. Their proofs are provided in the Appendix B.

Lemma A.7

For every non-negative, strictly upper triangular matrix B with $\sum_{j=1}^n b_{i,j} \leq 1$ for all $i = 1, \dots, n$, there exist positive constants $r_i > 0$ ($i = 1, \dots, n$), such that

$$r_i > \sum_{j=1}^n r_j b_{i,j}, \text{ for every } i = 1, \dots, n. \quad (\text{A.5})$$

Lemma A.8

Let $L_i \in (0, 1)$ and $G_i \in (0, 1]$ with $L_i \leq G_i$ for $i = 1, \dots, n$ be constants and let B be a non-negative, strictly upper triangular matrix with $\sum_{j=1}^n b_{i,j} \leq 1$, for $i = 1, \dots, n$. Then, there exist constants $\xi_i > 0$ ($i = 1, \dots, n$), such that

$$\sum_{j=1}^n b_{j,i} G_j \xi_j < L_i \xi_i, \text{ for every } i = 1, \dots, n. \quad (\text{A.6})$$

Using vector notation, inequality (A.6) becomes

$$(B' \text{diag}(G) - \text{diag}(L)) \xi \leq 0,$$

which is also equivalent to:

$$(I + B' \text{diag}(G) - \text{diag}(L)) \xi \leq \xi. \quad (\text{A.7})$$

Lemma A.9

Let $L_i \in (0, 1)$ and $G_i \in (0, 1]$ with $L_i \leq G_i$, for $i = 1, \dots, n$, be constants and let B be a non-negative, strictly upper triangular matrix with $\sum_{j=1}^n b_{i,j} \leq 1$, for $i = 1, \dots, n$. Then the matrix $I + B' \text{diag}(G) - \text{diag}(L)$ is a lower triangular matrix with $\rho(I + B' \text{diag}(G) - \text{diag}(L)) < 1$, where $G = (G_1, \dots, G_n)$ and $L = (L_1, \dots, L_n)$.

Appendix B

Proofs of Auxiliary Results

B.1 Proofs of Results of Appendix A

Proof of Lemma A.2: By virtue of assumption (iii), there exists $\delta > 0$ such that the inequality $|F(d, z) - z^*| \leq L|z - z^*|$ holds for all $d \in D$ and $z \in A := \{y \in X : |y - z^*| < \delta\}$. Since $F : D \times X \rightarrow X$ is a bounded mapping, there exists a constant $R > 0$ which satisfies:

$$\sup\{|F(d, z)| : z \in X, d \in D\} \leq R. \quad (\text{B.1})$$

It follows from (B.1) and the triangle inequality that the following inequality holds:

$$\begin{aligned} \sup \left\{ \frac{|F(d, z) - z^*|}{|z - z^*|} : d \in D, z \in X \setminus A \right\} &\leq \\ \delta^{-1} \sup\{|F(d, z) - z^*| : z \in X, d \in D\} &\leq \delta^{-1}(R + |z^*|). \end{aligned} \quad (\text{B.2})$$

Combining (B.2) and the fact that $|F(d, z) - z^*| \leq L|z - z^*|$ holds for all $d \in D$ and for all $z \in A$, we get:

$$|F(d, z) - z^*| \leq \max(L, \rho^{cr-1}(R + |z^*|))|z - z^*|, \text{ for all } (d, z) \in D \times X. \quad (\text{B.3})$$

Let $z_0 \in X$ be an arbitrary vector and let $\{d(t) \in D\}_{t=0}^\infty$ be an arbitrary sequence. Consider the solution $z(t)$ of $\dot{z} = F(d, z)$ with initial condition $z(0) = z_0$ corresponding to input $\{d(t) \in D\}_{t=0}^\infty$. By virtue of assumption (ii), there exists $i(N) \in \{0, 1, \dots, N\}$ with $z(N - i(N)) \in \Omega$. By virtue of assumption (i), we get:

$$|z(t) - z^*| \leq M|z(k) - z^*| \exp(-\sigma(t - k)), \quad (\text{B.4})$$

for all $t \geq k$, where $k = N - i(N)$. Notice that $k \in \{0, 1, \dots, N\}$. Using induction and (B.3), we get

$$|z(t) - z^*| \leq \tilde{L}^t |z_0 - z^*|, \text{ for all } t \geq 0, \quad (\text{B.5})$$

where $\tilde{L} := \max(L, \rho^{cr-1}(R + |z^*|)) \geq 1$. Combining (B.4), (B.5) and the fact that $k \in \{0, 1, \dots, N\}$, we obtain:

$$|z(t) - z^*| \leq M\tilde{L}^N \exp(\sigma N) |z_0 - z^*| \exp(-\sigma t) \quad (\text{B.6})$$

for all $t \geq 0$. Noticing that assumption (iii) guarantees that $z^* = F(d, z^*)$, we conclude that estimate (B.6) implies that $z^* \in X$ is RGES for the uncertain system (A.1). The proof is complete. \triangleleft

Proof of Lemma A.7: Due to the fact that B is strictly upper triangular, it holds that $b_{i,j} = 0$ for every $j \leq i$ and $b_{i,j} \in [0, 1]$ otherwise. Therefore, in order to prove inequalities (A.5), it suffices to show that for every $r_n > 0$ there exist $r_i > 0$ ($i =$

$1, \dots, n-1$), such that $r_i > \sum_{j=i+1}^n r_j$, for $i = 1, \dots, n-1$. By choosing $r_i = 2^{n-i}$ we obtain:

$$2^{n-i} > \sum_{j=i+1}^n 2^{n-j} = \sum_{j=0}^{n-(i+1)} 2^j = 2^{n-i} - 1,$$

which holds for every $i = 1, \dots, n-1$. The proof is complete. \triangleleft

Proof of Lemma A.8: Due to the fact that B is strictly upper triangular, it holds that $b_{i,j} = 0$ for every $j \leq i$ and $b_{i,j} \in [0, 1]$ otherwise. Therefore, in order to prove inequalities (A.6), it suffices to show that there exist $\xi_i > 0$ ($i = 1, \dots, n$), such that the inequalities $\sum_{j=1}^{i-1} G_j \xi_j < L_i \xi_i$ hold for $i = 2, \dots, n$. For arbitrary $\xi_1 > 0$, we generate recursively the constants $\xi_i > 0$, $i = 2, \dots, n$, by using the following formula:

$$\xi_i = \frac{2}{L_i} \sum_{j=1}^{i-1} G_j \xi_j \quad (\text{B.7})$$

The proof is complete. \triangleleft

Proof of Lemma A.9: We prove this lemma by using the following Fact.

Fact: The product of a strictly lower triangular matrix A and a diagonal matrix D is a strictly lower triangular matrix $\hat{C} = AB$.

Proof of the Fact: From the definition of matrix product, we have that $\hat{c}_{i,j} = \sum_{k=1}^n a_{i,k} d_{k,j}$ for every $i, j \in \{1, \dots, n\}$. Due to the fact that D is diagonal, it follows that $\hat{c}_{i,j} = a_{i,j} d_{j,j}$. Due to the fact that A is strictly lower triangular, it follows that $a_{i,j} = 0$ for $i \leq j$, which implies $\hat{c}_{i,j} = 0$ for $i \leq j$. \triangleleft

Since the matrix B is a strictly upper triangular matrix, it holds that B' is a strictly lower triangular matrix. Then, the product $B' \text{diag}(G)$ is a strictly lower triangular matrix from the above fact. The matrix $I - \text{diag}(L)$ is a diagonal matrix. Then, the matrix $I + B' \text{diag}(G) - \text{diag}(L)$ is a lower triangular matrix with its diagonal elements being $(1 - L_1, \dots, 1 - L_n)$ corresponding to its eigenvalues. Due to the fact that $L_i \in (0, 1)$, we have that $\rho(I + B' \text{diag}(G) - \text{diag}(L)) = \max_i (|1 - L_i|) = \max_i (1 - L_i) < 1$. The proof is complete. \triangleleft

B.2 Proofs of Results of Chapter 2

Proof of Proposition 2.1: Using (2.9) we obtain:

$$\begin{aligned} \sum_{i=1}^n r_i x_i^+ &= \sum_{i=1}^n r_i x_i + \sum_{i=1}^n r_i \bar{s}_i(d, x, v) v_i - \sum_{i=1}^n r_i s_i(d, x, v) f_{D,i}(d, x_i) + \\ &\sum_{i=1}^n \sum_{j=1}^n r_i b_{j,i} s_j(d, x, v) f_{D,j}(d, x_j) = \\ &\sum_{i=1}^n r_i x_i + \sum_{i=1}^n r_i \bar{s}_i(d, x, v) v_i - \sum_{i=1}^n \left(1 - \sum_{j=1}^n r_i^{-1} r_j b_{i,j} \right) r_i s_i(d, x, v) f_{D,i}(d, x_i). \end{aligned} \quad (\text{B.8})$$

Define

$$\hat{Q} := \min_{i=1, \dots, n} \left(1 - \sum_{j=1}^n r_i^{-1} r_j b_{i,j} \right). \quad (\text{B.9})$$

Notice that Lemma A.7 guarantees that $\hat{Q} > 0$. Using (B.8), (B.9) and the fact that $\bar{s}_i(d, x, v) \in [0, 1]$, we obtain:

$$\left(\sum_{i=1}^n r_i x_i \right)^+ \leq \sum_{i=1}^n r_i x_i + \sum_{i=1}^n r_i v_i - \hat{Q} \sum_{i=1}^n r_i s_i(d, x, v) f_{D,i}(d, x_i). \quad (\text{B.10})$$

Then, we obtain from (B.10) and Consequence (C3):

$$\left(\sum_{i=1}^n r_i x_i \right)^+ \leq \sum_{i=1}^n r_i x_i + \sum_{i=1}^n r_i v_i - \hat{Q} \Theta \sum_{i=1}^n r_i s_i(d, x, v) x_i. \quad (\text{B.11})$$

Since the set $D \times S$ is compact, it follows from continuity of the functions $f_{S,i} : D \times S \rightarrow \mathfrak{R}_+$ ($i = 1, \dots, n$) that there exists $\delta > 0$ such that $|f_{S,i}(d, x) - f_{S,i}(\tilde{d}, 0)| < \frac{1}{2} \min_{i=1, \dots, n} (\tilde{\epsilon}_i)$ for all $i = 1, \dots, n$, $(d, x) \in D \times S$, $\tilde{d} \in D$ with $|d - \tilde{d}| + |x| < \delta$. Since $b_{i,j} \in [0, 1]$, for $i, j = 1, \dots, n$, $v_i \leq \min \{f_{S,i}(d, 0) : d \in D\} - \tilde{\epsilon}_i$ for $i = 1, \dots, n$, and since $0 < f_i(d, z) < z$ for all $z \in (0, \rho_i^{max}]$ and $i = 1, \dots, n$ (see Assumption (H 2.1)), we get for all $i = 1, \dots, n$, $(d, x) \in D \times S$ with $|x| < \min(\delta, \frac{1}{2n} \min_{i=1, \dots, n} (\tilde{\epsilon}_i))$:

$$\begin{aligned} v_i + \sum_{j=1}^n b_{j,i} f_{D,j}(d, x_j) &\leq \min \{f_{S,i}(d, 0) : d \in D\} - \tilde{\epsilon}_i + \sum_{j=1}^n x_j \\ &\leq \min \{f_{S,i}(d, 0) : d \in D\} - \frac{\tilde{\epsilon}_i}{2} \leq f_{S,i}(d, x). \end{aligned}$$

It follows from the above inequality, (2.8) and (B.11) that the following inequality holds for all $(d, x) \in D \times S$ with $|x| < \min(\delta, \frac{1}{2n} \min_{i=1, \dots, n} (\tilde{\epsilon}_i))$:

$$\left(\sum_{i=1}^n r_i x_i \right)^+ \leq (1 - \hat{Q} \Theta) \sum_{i=1}^n r_i x_i + \sum_{i=1}^n r_i v_i. \quad (\text{B.12})$$

Define $V = \{v = (v_1, \dots, v_n)' \in \mathfrak{R}_+^n : v_i \leq \min(v_i^{max}, \min \{f_{S,i}(d, 0) : d \in D\}) - \tilde{\epsilon}_i, i = 1, \dots, n\}$. We next claim that there exists a constant $\gamma > 0$ such that:

$$\sum_{i=1}^n r_i \tilde{s}_i(d, x, v) x_i \geq \gamma \sum_{i=1}^n r_i x_i, \quad (\text{B.13})$$

for all $(d, x, v) \in D \times S \times V$ with $|x| \geq \min\left(\delta, \frac{1}{2n} \min_{i=1, \dots, n} (\tilde{\epsilon}_i)\right)$.

Indeed, we define

$$\gamma := \inf \left\{ \frac{\sum_{i=1}^n r_i \tilde{s}_i(d, x, v) x_i}{\sum_{i=1}^n r_i x_i} : (d, x, v) \in D \times S \times V, |x| \geq \min\left(\delta, \frac{1}{2n} \min_{i=1, \dots, n} (\tilde{\epsilon}_i)\right) \right\}. \quad (\text{B.14})$$

In order to show (B.13), it suffices to show that $\gamma \geq 0$ as defined by (B.14) is positive. Continuity of the functions $\tilde{s}_i : D \times S \times \mathfrak{R}_+^n \rightarrow [0, 1]$ ($i = 1, \dots, n$) and compactness of the set $\{(d, x, v) \in D \times S \times V : |x| \geq \min(\delta, \frac{1}{2n} \min_{i=1, \dots, n} (\tilde{\epsilon}_i))\}$ imply that there

exists $(d^*, x^*, v^*) \in D \times S \times V$ with $|x^*| \geq \min\left(\delta, \frac{1}{2n} \min_{i=1, \dots, n} (\tilde{\varepsilon}_i)\right)$ and

$$\sum_{i=1}^n r_i \tilde{s}_i(d^*, x^*, v^*) x_i^* = \gamma \sum_{i=1}^n r_i x_i^*. \quad (\text{B.15})$$

We proceed by using a contradiction argument. Suppose that $\gamma = 0$. It follows from (B.15) that $x_i^* \tilde{s}_i(d^*, x^*, v^*) = 0$, for $i = 1, \dots, n$. However, (H 2.3) and (2.10) imply that $x^* = 0$, which contradicts the fact that $|x^*| \geq \min\left(\delta, \frac{1}{2n} \min_{i=1, \dots, n} (\tilde{\varepsilon}_i)\right)$.

It follows from (B.11), (B.12), (B.13) and the fact that $s_i(d, x, v) \geq \tilde{s}_i(d, x, v)$ for all $(d, x, v) \in D \times S \times \mathfrak{H}_+^n$, $i = 1, \dots, n$, that inequality (2.13) holds with $C := \hat{Q}\Theta \min(1, \gamma)$. The proof is complete. \triangleleft

B.3 Proofs of Results of Chapter 3

Proof of Lemma 3.5: Proposition 3.4 guarantees that there exist constants $\beta_i \in (x_i^*, \mu_i]$ ($i = 1, \dots, n$) such that (3.6) holds. Using (3.14), (3.16), (3.2), we obtain for all $x \in \Omega$ and $i = 1, \dots, n$:

$$\begin{aligned} x_i^+ - x_i^* &\leq -(v_i^* - v_i^{\min}) \min\left(1, \tau^{-1} \sum_{j=1}^n K_{i,j} \max(0, x_j - x_j^*)\right) \\ &\quad + (1 - L_i) \max(0, x_i - x_i^*) + \sum_{j=1}^n b_{j,i} G_j \max(0, x_j - x_j^*). \end{aligned} \quad (\text{B.16})$$

Inequality (3.7) is a direct consequence of inequalities (B.16). Using Assumption (H 2.1), we get $G_i(x_i - x_i^*) \leq f_{D,i}(d, x_i) - f_{D,i}(d, x_i^*) \leq L_i(x_i - x_i^*)$ for $i = 1, \dots, n$ and $x_i \leq x_i^*$. Using the above inequality and Consequence (C2) it follows that:

$$\begin{aligned} f_{D,i}(d, x_i) - f_{D,i}(d, x_i^*) &\geq -G_i \max(0, x_i^* - x_i) \\ x_i - x_i^* + f_{D,i}(d, x_i^*) - f_{D,i}(d, x_i) &\geq -(1 - L_i) \max(0, x_i^* - x_i) \\ &\text{for } x_i \in [0, \beta_i], i = 1, \dots, n. \end{aligned} \quad (\text{B.17})$$

Using (3.14), (3.2), we obtain for all $x \in \Omega$, $i = 1, \dots, n$:

$$\begin{aligned} x_i^+ - x_i^* &\geq -(1 - L_i) \max(0, x_i^* - x_i) - \\ &\quad (v_i^* - v_i^{\min}) \min\left(1, \tau^{-1} \sum_{j=1}^n K_{i,j} \max(0, x_j - x_j^*)\right) - \sum_{j=1}^n b_{j,i} G_j \max(0, x_j^* - x_j). \end{aligned} \quad (\text{B.18})$$

Inequalities (B.18) imply the following inequalities for all $x \in \Omega$ and $i = 1, \dots, n$:

$$\begin{aligned} x_i^* - x_i^+ &\leq (1 - L_i) \max(0, x_i^* - x_i) + \\ &\quad (v_i^* - v_i^{\min}) \min\left(1, \tau^{-1} \sum_{j=1}^n K_{i,j} \max(0, x_j - x_j^*)\right) + \sum_{j=1}^n b_{j,i} G_j \max(0, x_j^* - x_j). \end{aligned} \quad (\text{B.19})$$

Inequality (3.8) is a direct consequence of inequalities (B.19) and the fact that $\min(1, \tau^{-1} \sum_{j=1}^n K_{i,j} \max(0, x_j - x_j^*)) \leq \tau^{-1} \sum_{j=1}^n K_{i,j} \max(0, x_j - x_j^*)$ for all $x \in \Omega$ and $i = 1, \dots, n$. The proof is complete. \triangleleft

Proof of Lemma 3.6: Lemma 3.5 guarantees that there exist constants $\beta_i \in (x_i^*, \mu_i]$ ($i = 1, \dots, n$) such that (3.6), (3.7), (3.8) hold. Using (3.7), (3.8) in conjunction with the following inequalities

$$1'_n h(x - x^*) + 1'_n h(x^* - x) = \sum_{i=1}^n |x_i - x_i^*| \geq |x - x^*|, \quad (\text{B.20})$$

$$h(x - x^*) \leq |x - x^*| 1_n, h(x^* - x) \leq |x - x^*| 1_n, \quad (\text{B.21})$$

which hold for all $x \in \mathfrak{R}^n$, and the facts that $(I + B' \text{diag}(G) - \text{diag}(L))$, $K \in \mathfrak{R}_+^{n \times n}$, $\text{diag}(v^* - b)$ are non-negative matrices and $\tau > 0$, we are in a position to guarantee the existence of $\hat{\delta} > 0$ such that:

$$\begin{aligned} |x^+ - x^*| &\leq 1'_n (2I + 2B' \text{diag}(G) - 2\text{diag}(L) + \text{diag}(v^* - b) \tau^{-1} K) 1_n |x - x^*| \\ &\text{for all } x \in S, d \in D, \text{ with } |x - x^*| < \hat{\delta} \text{ and} \\ v &= v^* - \text{diag}(v^* - b) (1_n - h(1_n - \tau^{-1} K h(x - x^*))). \end{aligned} \quad (\text{B.22})$$

Since $x^+ \in S$ for $x \in S$, $d \in D$, $v = (v_1, \dots, v_n)' \in \mathfrak{R}_+^n$ and since $S = [0, \rho_1^{max}] \times \dots \times [0, \rho_n^{max}]$, it follows that:

$$\begin{aligned} |x^+ - x^*| &\leq 2\sqrt{n} \max_{i=1, \dots, n} (\rho_i^{max}), \text{ for all } x \in S, d \in D \text{ and} \\ v &= v^* - \text{diag}(v^* - v^{min}) (1_n - h(1_n - \tau^{-1} K h(x - x^*))). \end{aligned} \quad (\text{B.23})$$

Estimates (B.22), (B.23) imply that (3.9) holds with $M := 1'_n (2I + 2B' \text{diag}(G) - 2\text{diag}(L) + \text{diag}(v^* - v^{min}) \tau^{-1} K) 1_n + 2\sqrt{n} \hat{\delta}^{-1} \max_{i=1, \dots, n} (\rho_i^{max})$. The proof is complete. \triangleleft

Proof of Lemma 3.7: Lemma 3.5 guarantees that there exist constants $\beta_i \in (x_i^*, \mu_i]$ ($i = 1, \dots, n$) such that (3.6), (3.7), (3.8) hold. Let $K \in \mathfrak{R}_+^{n \times n}$ be a matrix so that

$$K_{i,j} \geq \frac{1}{\min_k (\beta_k - x_k^*)}, \text{ for every } i, j = 1, \dots, n. \quad (\text{B.24})$$

It follows from (B.24) that for every $\tau \in (0, 1)$ we have

$$\tau^{-1} K_{i,j} (\beta_j - x_j^*) \geq 1, \text{ for every } i, j = 1, \dots, n. \quad (\text{B.25})$$

Using the fact that $x_i^* < \beta_i$ for every $i = 1, \dots, n$, it follows from (B.25) and the fact that $\max(0, x_i - x_i^*) = x_i - x_i^*$ for $x \in S \setminus \Omega$ (recall that $\Omega = [0, \beta_1] \times \dots \times [0, \beta_n]$), that

$$\tau^{-1} \sum_{j=1}^n K_{i,j} \max(0, x_j - x_j^*) \geq 1 \text{ for every } i, j = 1, \dots, n \text{ and } x \in S \setminus \Omega. \quad (\text{B.26})$$

and consequently, since $v = v^* - \text{diag}(v^* - v^{min}) (1_n - h(1_n - \tau^{-1} K h(x - x^*)))$, we get

$$v = v^{min}, \text{ for } x \in S \setminus \Omega. \quad (\text{B.27})$$

In order to show that the set $\Omega = [0, \beta_1] \times \cdots \times [0, \beta_n]$ is a TR for the closed-loop system (2.9) with (3.4), it suffices to show that for every $x_0 \in S$, $\{d(t) \in D\}_{t=0}^\infty$ the solution $x(t)$ of the closed-loop system (2.9) with (3.4) and initial condition $x(0) = x_0$ corresponding to input $\{d(t) \in D\}_{t=0}^\infty$ satisfies $x(t) \in \Omega$ for all $t \geq m$, where

$$m := \left\lceil \frac{\ln(C \min_{i=1, \dots, n}(r_i \beta_i) - r'b) - \ln(Cr'\rho^{max})}{\ln(1-C)} \right\rceil + 1 \quad (\text{B.28})$$

where $\rho^{max} = (\rho_1^{max}, \dots, \rho_n^{max})' \in \text{int}(\mathfrak{R}_+^n)$. We proceed by contradiction. Suppose that there exist $x_0 \in S$, $\{d(t) \in D\}_{t=0}^\infty$ such that the solution $x(t)$ of the closed-loop system (2.9) with (3.4) and initial condition $x(0) = x_0$ corresponding to input $\{d(t) \in D\}_{t=0}^\infty$ satisfies $x(t) \notin \Omega$ for certain $t \geq m$. Since the set $\Omega = [0, \beta_1] \times \cdots \times [0, \beta_n]$ is positively invariant (a direct consequence of (3.6)), it follows that $x(q) \notin \Omega$ for all $q = 0, 1, \dots, m$. Define

$$\tilde{I}(q) := r'x(q) \quad (\text{B.29})$$

and notice that (2.13), (B.27) imply the following estimate for all $q = 0, 1, \dots, m$:

$$\tilde{I}(q+1) \leq (1-C)\tilde{I}(q) + r'v^{min}. \quad (\text{B.30})$$

Estimate (B.30) implies the following estimate for all $q = 0, 1, \dots, m+1$:

$$\tilde{I}(q) \leq (1-C)^q \tilde{I}(0) + C^{-1}r'v^{min} (1 - (1-C)^q). \quad (\text{B.31})$$

Since $\tilde{I}(0) = r'x(0) = r'x_0 \leq r'\rho^{max}$ for all $x_0 \in S$, we obtain from (B.31) for all $q = 0, 1, \dots, m+1$:

$$\tilde{I}(q) \leq (1-C)^q r'\rho^{max} + C^{-1}r'v^{min}. \quad (\text{B.32})$$

Estimate (B.32) in conjunction with definition (B.28) implies that $\tilde{I}(m) \leq \min_{i=1, \dots, n}(r_i \beta_i)$, which combined with definition (B.29) shows that $x(m) \in \Omega$, a contradiction. The proof is complete. \triangleleft

B.4 Proofs of Results of Chapter 4

In order to prove the claims involved in the proof of Theorem 4.1 we need first to prove the following facts:

Fact 1: The following equality holds for all $x \in S$, $v = (v_1, \dots, v_n)' \in (0, +\infty) \times \mathfrak{R}_+^{n-1}$, $d = (d_1, \dots, d_{n-1}) \in [0, 1]^{n-1}$ with $p_n = 1 = s_n$

$$\sum_{i=1}^n I_i(x^+) = \sum_{i=1}^n I_i(x) + \sum_{i=1}^n (n+1-i) \bar{s}_i v_i - \sum_{i=1}^n (1+p_i(n-i)) s_i f_{D,i}(x_i). \quad (\text{B.33})$$

Proof of Fact 1: The following equations holds for all $x \in S$, $v = (v_1, \dots, v_n)' \in (0, +\infty) \times \mathfrak{R}_+^{n-1}$, $d = (d_1, \dots, d_{n-1}) \in [0, 1]^{n-1}$ with $p_n = 1 = s_n$ and are direct consequences of (2.18)-(2.20) and definitions $I_j(x) := \sum_{i=1}^j x_i$, for $j = 1, \dots, n$:

$$I_j(x^+) = I_j(x) + \sum_{i=1}^j \bar{s}_i v_i - \sum_{i=1}^{j-1} s_i p_i f_{D,i}(x_i) - s_j f_{D,j}(x_j), j = 2, \dots, n-1 \quad (\text{B.34})$$

$$I_n(x^+) = I_n(x) + \sum_{i=1}^n \bar{s}_i v_i - \sum_{i=1}^{n-1} s_i p_i f_{D,i}(x_i) - f_{D,n}(x_n). \quad (\text{B.35})$$

Equality (B.33) is a consequence of (2.18), (B.34), (B.35) and definitions $p_n = 1 = s_n$.

Fact 2: The following inequality holds for all $x \in S$, $v \in \mathfrak{R}_+ \times [0, v_2^{max}] \times \dots \times [0, v_n^{max}]$, $d \in [0, 1]^{n-1}$ with $p_n = 1 = s_n$:

$$\sum_{i=1}^n (1 + p_i(n-i)) s_i f_{D,i}(x_i) \geq C \sum_{i=1}^n (n+1-i)x_i. \quad (\text{B.36})$$

Proof of Fact 2: By virtue of definition (B.9) and Consequence (C3), inequality (B.36) can be directly obtained by choosing $r_i = n+1-i$, for $i = 1, \dots, n$. Notice that this selection for r_i satisfies Lemma A.7.

Proof of the Claim 1 (Theorem 4.1): We distinguish two cases:

Case 1: $x \in \tilde{\Omega} = (0, mu_1] \times \dots \times (0, mu_n]$, $d \in [0, 1]^{n-1}$.

Definition (4.9) and equations (B.33), (4.11) with $v_i = k_i(x) \leq v_i^*$ give:

$$\begin{aligned} V(x^+) &= \sigma |x_1 - f_{D,1}(x_1) + v_1 - x_1^*| + \\ &\sum_{i=2}^n \sigma^i |x_i - f_{D,i}(x_i) + (1 - p_{i-1})f_{D,i-1}(x_{i-1}) + v_i - x_i^*| + A\Xi(x^+) + \\ &K \max \left(0, \sum_{i=1}^n I_i(x) - \sum_{i=1}^n (1 + (n-i)p_i) f_{D,i}(x_i) + \sum_{i=1}^n (n+1-i)v_i - P(x^+) \right) \end{aligned} \quad (\text{B.37})$$

with $p_n = 1$. Using (4.15), Consequence (C2), the fact that $mu_i \leq \tilde{\rho}_i^{cr}$, for $i = 1, \dots, n$ and definition (4.12), we get from (B.37):

$$\begin{aligned} V(x^+) &\leq L \sum_{i=1}^n \sigma^i |x_i - x_i^*| + \sum_{i=1}^n \sigma^i |v_i - v_i^*| + LA\Xi(x) + \\ &K \max \left(0, \sum_{i=1}^n I_i(x) - \sum_{i=1}^n (1 + (n-i)p_i) f_{D,i}(x_i) + \sum_{i=1}^n (n+1-i)v_i - P(x^+) \right) \end{aligned} \quad (\text{B.38})$$

It follows from the combination of (4.7) and inequality (B.38) that the following inequality holds for all $x \in \tilde{\Omega}$:

$$\begin{aligned} V(x^+) &\leq L \sum_{i=1}^n \sigma^i |x_i - x_i^*| + \sum_{i \in R} \sigma^i \min(\gamma_i \Xi(x), v_i^* - v_i^{min}) + LA\Xi(x) + \\ &K \max \left(0, \sum_{i=1}^n I_i(x) - \sum_{i=1}^n (1 + (n-i)p_i) f_{D,i}(x_i) + \sum_{i=1}^n (n+1-i)v_i - P(x^+) \right). \end{aligned} \quad (\text{B.39})$$

Inequality (B.36) and the fact that $s_i = \bar{s}_i = 1$ for $x \in \tilde{\Omega}$ imply that:

$$\sum_{i=1}^n (1 + (n-i)p_i) f_{D,i}(x_i) \geq C \sum_{i=1}^n I_i(x). \quad (\text{B.40})$$

Using (B.38) and (B.40), we get:

$$\begin{aligned} V(x^+) &\leq L \sum_{i=1}^n \sigma^i |x_i - x_i^*| + \sum_{i \in R} \sigma^i \min(\gamma_i \Xi(x), v_i^* - v_i^{min}) + LA\Xi(x) \\ &+ K \max(0, (1-C) \sum_{i=1}^n I_i(x) + \sum_{i=1}^n (n+1-i)v_i - P(x^+)) \end{aligned} \quad (\text{B.41})$$

We next distinguish two cases:

Case 1(i): $\Xi(x) \leq \tau$.

In this case we have $\gamma_i \Xi(x) \leq v_i^* - v_i^{\min}$ for all $i \in R$. Since $\Xi(x) \leq h$ (a consequence of $\tau < \tau^* \leq h$), we get from (4.15) and definition (4.7) that $v_i = k_i(x) = v_i^* - \gamma_i \Xi(x) \geq v_i^{\min}$ for all $i \in R$ and $\min(h, \Xi(x^+)) \leq L \min(h, \Xi(x))$. Using the definitions $I_j(x) := \sum_{i=1}^j x_i$ for $j = 1, \dots, n$, $P(x) := \tilde{M} - \bar{\theta} \min(h, \Xi(x))$ and the facts

- $\tilde{M} \geq (1-C) \sum_{i=1}^n I_i(x^*) + (1-C)h \max_{i=1, \dots, n} ((n+1-i)\sigma^{-i}) + \sum_{i=1}^n (n+1-i) v_i^*$
- $\sum_{i \in R} (n+1-i) \gamma_i = \tau^{-1} \sum_{i \in R} (n+1-i) (u_i^* - v_i^{\min}) \geq (\tau^*)^{-1} \sum_{i \in R} (n+1-i) (v_i^* - v_i^{\min}) \geq \bar{\theta} L$ (a consequence of $\tau \leq \tau^* \leq (\bar{\theta} L)^{-1} \sum_{i \in R} (n+1-i) (u_i^* - v_i^{\min})$),
- $\sum_{i=1}^n (n+1-i) (x_i - x_i^*) \leq \sum_{i=1}^n ((n+1-i)\sigma^{-i}) \sigma^i \max(0, x_i - x_i^*) \leq \max_{i=1, \dots, n} ((n+1-i)\sigma^{-i}) \Xi(x)$ for $i = 1, \dots, n$ (a consequence of definition (4.8)),

we get:

$$\begin{aligned} \tilde{M} &\geq (1-C) \sum_{i=1}^n I_i(x^*) + (1-C)h \max_{i=1, \dots, n} ((n+1-i)\sigma^{-i}) + \sum_{i=1}^n (n+1-i) v_i^* \Rightarrow \\ \tilde{M} &\geq (1-C) \sum_{i=1}^n I_i(x^*) + (1-C)\Xi(x) \max_{i=1, \dots, n} ((n+1-i)\sigma^{-i}) + \sum_{i=1}^n (n+1-i) v_i^* \Rightarrow \\ \tilde{M} &\geq \bar{\theta} L \Xi(x) - \sum_{i \in R} (n+1-i) \gamma_i \Xi(x) + (1-C) \sum_{i=1}^n I_i(x^*) + \\ &\quad (1-C) \sum_{i=1}^n (n+1-i) (x_i - x_i^*) + \sum_{i=1}^n (n+1-i) v_i^* \Rightarrow \\ \tilde{M} &\geq \bar{\theta} \min(h, \Xi(x^+)) + (1-C) \sum_{i=1}^n I_i(x) + \sum_{i \in R} (n+1-i) (v_i^* - \gamma_i \Xi(x)) + \\ &\quad \sum_{i \notin R} (n+1-i) v_i^* \Rightarrow \\ 0 &\geq \sum_{i=1}^n (n+1-i) v_i + (1-C) \sum_{i=1}^n I_i(x) - P(x^+) \end{aligned}$$

Combining (B.41) with the above inequality, we obtain:

$$V(x^+) \leq L \sum_{i=1}^n \sigma^i |x_i - x_i^*| + \sum_{i \in R} \sigma^i \gamma_i \Xi(x) + LA \Xi(x) \quad (\text{B.42})$$

It follows from (B.42) and the fact that $A \geq (1-L)^{-1} \sum_{i \in R} \sigma^i \gamma_i$ that (4.19) holds when $\Xi(x) \leq \tau$.

Case 1(ii): $\Xi(x) > \tau$.

In this case $\gamma_i \Xi(x) > v_i^* - v_i^{\min}$ for all $i \in R$. Definition (4.7) implies that $K_i(x) = v_i^{\min}$ for all $i \in R$. Moreover, in this case there exists at least one $i \in \{1, \dots, n\}$ for which $x_i > x_i^*$. Since $f_{D,i}$ is increasing on $[0, \mu_i]$ for $i = 1, \dots, n$ (a consequence of Assumption (H 2.1*)) and the fact that $\mu_i \leq \bar{\rho}_i^{cr}$, we conclude that there exists at least one $i \in \{1, \dots, n\}$ for which $f_{D,i}(x_i) > f_{D,i}(x_i^*)$. Consequently, we get from

(4.14) and the fact that $v_i = K_i(x) = v_i^{min}$ for all $i \in R$:

$$\sum_{i=1}^n (n+1-i)v_i = \sum_{i \in R} (n+1-i)v_i^{min} + \sum_{i \notin R} (n+1-i)v_i^* \leq$$

$$\min_{i=1, \dots, n} (((n-i)p_i + 1)f_{D,i}(x_i^*)) \leq \sum_{i=1}^n ((n-i)p_i + 1)f_{D,i}(x_i).$$

Combining (4.18), (B.39) with the above inequality and using the fact $A \geq (1-L)^{-1} \sum_{i \in R} \sigma^i \gamma_i$, we conclude that (4.19) holds when $\Xi(x) > \tau$.

Case 2: $x \in S \setminus \tilde{\Omega}$, $d \in [0, 1]^{n-1}$.

In this case, there exists at least one $i \in \{1, \dots, n\}$ for which $x_i > \mu_i$. Therefore, definition (4.8) implies $\Xi(x) > h = \min_{i=1, \dots, n} (\sigma^i (\mu_i - x_i^*))$, and consequently definition (4.10) gives $P(x) = \tilde{M} - \bar{\theta}h$. Moreover, definition (4.7) gives $K_i(x) = v_i^{min}$, for all $i \in R$ (a direct consequence of the facts that $\tau < \tau^* \leq h$ and $\gamma_i = \tau^{-1}(v_i^* - v_i^{min}) \geq h^{-1}(v_i^* - v_i^{min})$). Combining, we get from definition (4.9) and (4.18):

$$V(x^+) = \sum_{i=1}^n \sigma^i |x_i^+ - x_i^*| + A\Xi(x^+) + K \max(0, \sum_{i=1}^n I_i(x^+) - P(x^+))$$

$$\leq \sum_{i=1}^n \sigma^i |x_i^+ - x_i^*| + K \max(0, \sum_{i=1}^n I_i(x^+) - \tilde{M} + \bar{\theta}h) + A\Xi(x^+) \quad (\text{B.43})$$

Using (2.13), the facts that $v_i = K_i(x) = v_i^{min}$, for all $i \in R$, $\tilde{M} - \bar{\theta}h = \epsilon \min_{i=1, \dots, n} ((n+1-i)\mu_i)$ and $\sum_{i \in R} (n+1-i)v_i^{min} + \sum_{i \notin R} (n+1-i)v_i^* \leq \epsilon C \min_{i=1, \dots, n} ((n+1-i)\mu_i)$ (which both imply that $\sum_{i \in R} (n+1-i)v_i^{min} + \sum_{i \notin R} (n+1-i)v_i^* \leq C(\tilde{M} - \bar{\theta}h)$), we get:

$$\max(0, \sum_{i=1}^n I_i(x^+) - \tilde{M} + \bar{\theta}h) \leq (1-C) \max(0, \sum_{i=1}^n I_i(x) - \tilde{M} + \bar{\theta}h). \quad (\text{B.44})$$

Combining (B.43) and (B.44), we get:

$$V(x^+) \leq \sum_{i=1}^n \sigma^i |x_i^+ - x_i^*| + K(1-C) \max(0, \sum_{i=1}^n I_i(x) - \tilde{M} + \bar{\theta}h) + A\Xi(x^+). \quad (\text{B.45})$$

Definition (4.8) in conjunction with (B.45) implies that the following inequality holds:

$$V(x^+) \leq \sum_{i=1}^n \sigma^i \max(\rho_i^{max} - x_i^*, x_i^*) + K(1-C) \max(0, \sum_{i=1}^n I_i(x) - \tilde{M} + \bar{\theta}h)$$

$$+ A \sum_{i=1}^n \sigma^i (\rho_i^{max} - x_i^*) \quad (\text{B.46})$$

The fact that there exists at least one $i \in \{1, \dots, n\}$ for which $x_i > \mu_i$, implies that

$$\sum_{i=1}^n I_i(x) = \sum_{i=1}^n (n+1-i)x_i \geq \min_{i=1, \dots, n} ((n+1-i)\mu_i). \quad (\text{B.47})$$

Using (B.46), (B.47) and the fact that $\tilde{M} - \bar{\theta}h = \epsilon \min_{i=1, \dots, n} ((n+1-i)\mu_i)$, we obtain:

$$V(x^+) \leq \sum_{i=1}^n \sigma^i \max(\rho_i^{max} - x_i^*, x_i^*) + K \max\left(0, \sum_{i=1}^n I_i(x) - \tilde{M} + \bar{\theta}h\right) \quad (\text{B.48})$$

$$+ A \sum_{i=1}^n \sigma^i (\rho_i^{max} - x_i^*) - KC(1-\epsilon) \min_{i=1, \dots, n} ((n+1-i)\mu_i)$$

Since $K \geq \frac{\sum_{i=1}^n \sigma^i \max(\rho_i^{max} - x_i^*, x_i^*) + A \sum_{i=1}^n \sigma^i (\rho_i^{max} - x_i^*) - (A+L)h}{(1-\epsilon)C \min_{i=1, \dots, n} ((n+1-i)\beta_i)}$, $\sum_{i=1}^n \sigma^i |x_i - x_i^*| \geq \Xi(x) > h$, we conclude from (B.48) and definition (4.9) that (4.19) holds. The proof is complete. \triangleleft

Proof of the Claim 2 (Theorem 4.1) Since $\sigma \in (0, 1]$, we get for all $x \in S$:

$$\sigma^n |x - x^*| \leq \sum_{i=1}^n \sigma^i |x_i - x_i^*| \leq |x - x^*| \sum_{i=1}^n \sigma^i \quad (\text{B.49})$$

Similarly, using definition (4.8), we get for all $x \in S$:

$$0 \leq \Xi(x) \leq \sum_{i=1}^n \sigma^i |x_i - x_i^*| \leq |x - x^*| \sum_{i=1}^n \sigma^i. \quad (\text{B.50})$$

Using (B.50), the fact that $I_j(x) := \sum_{i=1}^j x_i$, for $j = 1, \dots, n$, definition (4.10) and the fact that $\tilde{M} \geq \sum_{i=1}^n I_i(x^*)$ (a consequence of (2.13) and the fact that $\tilde{M} \geq (1-C) \sum_{i=1}^n I_i(x^*) + \sum_{i=1}^n (n+1-i)v_i^*$), we get for all $x \in S$:

$$\begin{aligned} & \max\left(0, \sum_{i=1}^n I_i(x) - P(x)\right) \leq \\ & \max\left(0, \sum_{i=1}^n I_i(x) - \sum_{i=1}^n I_i(x^*)\right) + \max\left(0, \sum_{i=1}^n I_i(x^*) - P(x)\right) \leq \\ & \max\left(0, \sum_{i=1}^n (n+1-i)(x_i - x_i^*)\right) + \max\left(0, \sum_{i=1}^n I_i(x^*) - \tilde{M} + \bar{\theta} \min(h, \Xi(x))\right) \leq \\ & \sum_{i=1}^n (n+1-i)|x_i - x_i^*| + \max\left(0, \sum_{i=1}^n I_i(x^*) - \tilde{M}\right) + \bar{\theta} \min(h, \Xi(x)) \leq \\ & \sum_{i=1}^n (n+1-i)|x_i - x_i^*| + \bar{\theta} \Xi(x) \leq |x - x^*| \sum_{i=1}^n (n+1-i) + \bar{\theta} |x - x^*| \sum_{i=1}^n \sigma^i \end{aligned} \quad (\text{B.51})$$

It follows from definition (4.9) and (B.49), (B.50), (B.51) that there exist constants $K_2 \geq K_1 > 0$ such that inequality (4.20) holds. The proof is complete. \triangleleft

B.5 Proofs of Results of Chapter 5

Proof of Theorem 5.1: The proof of Theorem 5.1 relies on Lemma A.2. Let $\Phi(x)$ be the (possibly empty) set of all $w = (w_1, \dots, w_\kappa) \in Y^\kappa$ for which there exist $\xi \in S$, $(d(i), \hat{\theta}(i)) \in D \times \Theta$, $i = 0, \dots, \kappa - 1$ such that the vectors $\bar{x}(i)$, $i = 0, \dots, \kappa$, defined by

the recursive formula

$$\begin{aligned}\bar{x}(0) &= \xi \\ \bar{x}(i+1) &= f(d(i), \theta^*, \bar{x}(i), K(\hat{\theta}(i), h(d(i), \theta^*, \bar{x}(i))))\end{aligned}\tag{B.52}$$

for $i = 0, \dots, \kappa - 1$, satisfy $\bar{x}(\kappa) = x$ and $w_{\kappa-i} = h(d(i), \theta^*, \bar{x}(i))$ for $i = 0, \dots, \kappa - 1$. Notice that $\Phi(x^*) \neq \emptyset$ since by selecting $\xi = x^* \in S$, $\hat{\theta}(i) = \theta^* \in \Theta$ and arbitrary $d(i) \in D$ for $i = 0, \dots, \kappa - 1$, the recursive formula (B.52) gives $\bar{x}(\kappa) = x^*$ and $w_{\kappa-i} = y^*$ for $i = 0, \dots, \kappa - 1$.

All assumptions of Lemma A.2 hold with $X = S \times Y^\kappa \times \Theta$, $z = (x, w, \hat{\theta})$, $\Omega = \cup_{x \in S} \{(x, w, \theta^*) : w \in \Phi(x)\}$, $N = m + \kappa + 1$, $z^* = (x^*, y^*, \dots, y^*, \theta^*)$ and

$$F(d, z) := \begin{bmatrix} f(d, \theta^*, x, K(\hat{\theta}, h(d, \theta^*, x))) \\ h(d, \theta^*, x) \\ w_1 \\ \vdots \\ w_{\kappa-1} \\ g(h(d, \theta^*, x), w, \hat{\theta}) \end{bmatrix},$$

where

$$g(h(d, \theta^*, x), w, \hat{\theta}) := \begin{cases} \hat{\theta} & \text{if } w \notin A \\ \Psi(h(d, \theta^*, x), w) & \text{if } w \in A \end{cases}.$$

Notice again that $\Omega \neq \emptyset$ since $\Phi(x^*) \neq \emptyset$. We show next that assumptions (i), (ii) of Lemma A.2 are direct consequences of Assumptions (J1), (J2), (J3).

Let $\{d(t) \in D\}_{t=0}^\infty$ be an arbitrary sequence and let $(x_0, w_0, \hat{\theta}_0) \in \Omega$ be an arbitrary vector with $\hat{\theta}_0 = \theta^*$. Consider the solution $(x(t), w(t), \hat{\theta}(t))$ of the closed-loop system (5.1), (5.2) with (5.3), initial condition $(x(0), w(0), \hat{\theta}(0)) = (x_0, w_0, \hat{\theta}_0)$ corresponding to input $\{d(t) \in D\}_{t=0}^\infty$. By virtue of (B.52), the component $x(t)$ of the solution satisfies $x(t) = \bar{x}(t + \kappa)$ for all $t \geq 0$, for certain solution $\bar{x}(i)$ of the system $\bar{x}^+ = f(\rho^{cr}, \theta^*, \bar{x}, K(\nu, h(d, \theta^*, \bar{x})))$ (that corresponds to certain inputs $\{(\delta(t), \nu(t)) \in D \times \Theta\}_{i=0}^\infty$ with $\delta(t + \kappa) = d(t)$, $\nu(t + \kappa) = \hat{\theta}(t)$ for all $t \geq 0$ and appropriate initial condition $\xi \in S$). Moreover, $w(t) = \bar{y}^{(\kappa)}(t + \kappa) \in \Phi(x(t))$ for all $t \geq 0$, where $\bar{y}(t) = h(\delta(t), \theta^*, \bar{x}(t))$. Notice that if $w(0) = w_0 \in A$ then $\bar{y}^{(\kappa)}(\kappa) \in A$, and, consequently, Assumption (J2) guarantees that $\hat{\theta}(1) = \theta^*$. If $w(0) = w_0 \notin A$ then $\hat{\theta}(1) = \hat{\theta}(0) = \theta^*$. Using induction and the previous argument, it follows that $\hat{\theta}(t) = \theta^*$ for all $t \geq 0$. Therefore, assumption (i) of Lemma A.2 is a consequence of Assumption (J1).

Assumption (ii) of Lemma A.2 follows from the fact that $w(t) = y^{(\kappa)}(t) \in \Phi(x(t))$ for all $t \geq \kappa$. Assumption (J3) guarantees that $w(t - i(t)) = y^{(\kappa)}(t - i(t)) \in A$ for some $i(t) \in \{0, 1, \dots, m\}$ and for all $t \geq m + \kappa$. It follows from (5.3) that $\hat{\theta}(t - i(t) + 1) = \theta^*$. Since $t - i(t) + 1 \geq p + 1$, we also get $w(t - i(t) + 1) \in \Phi(x(t))$ and thus $z(t - i(t) + 1) \in \Omega$. Therefore, assumption (ii) of Lemma A.2 holds with $N = m + \kappa + 1$. Since $A \subseteq Y^\kappa$ contains all $w \in Y^\kappa$ in a neighborhood of (y^*, \dots, y^*) and since there exist neighborhoods $N_1 \subseteq \mathfrak{R}^n$ of x^* , $N_2 \subseteq \mathfrak{R}^k$ of y^* , $N_3 \subseteq \mathfrak{R}^q$ of θ^* , such that:

$$\begin{aligned}|f(d, \theta^*, x, K(\hat{\theta}, x)) - x^*| + |h(d, \theta^*, x) - y^*| \leq \\ L|x - x^*| - L|\hat{\theta} - \theta^*|,\end{aligned}$$

$$|\Psi(h(d, \theta^*, x), w) - \theta^*| \leq L|x - x^*| + L \sum_{i=1}^{\kappa} |w_i - y^*|$$

hold for all $x \in N_1 \cap S$, $d \in D$, $\hat{\theta} \in N_3 \cap \Theta$, $w_i \in N_2 \cap Y$ ($i = 1, \dots, \kappa$) with $w = (w_1, \dots, w_\kappa)$, it follows that assumption (iii) of Lemma A.2 holds. \triangleleft

Proof of Proposition 5.2: Assume that $v_i^{min} > 0$ ($i \in R$) and v_i^{max} ($i \notin R$) are sufficiently small so that

$$\sum_{i \in R} (n+1-i)v_i^{min} + \sum_{i \notin R} (n+1-i)v_i^{max} < C \min_{i=1, \dots, n} ((n+1-i)\mu_i). \quad (\text{B.53})$$

Since $\tau \leq \epsilon^2 \sigma^n \min_{i \in R} ((v_i^{max} - v_i^{min})^{-1})$ and $\hat{v}_i^* \in [v_i^{min} + \epsilon, v_i^{max}]$ for $i \in R$, it follows that

$$\tau^{-1}(\hat{v}_i^* - v_i^{min}) \geq \epsilon^{-1}(v_i^{max} - v_i^{min})\sigma^{-n} \text{ for all } i \in R. \quad (\text{B.54})$$

Let $m \geq 1$ be an integer that satisfies:

$$m \geq 2 + [\Lambda] \quad (\text{B.55})$$

where $\Lambda = (\ln(\min_{i=1, \dots, n} ((n+1-i)\mu_i) - C^{-1}\kappa) - \ln(\sum_{i=1}^n (n+1-i)\rho_i^{max})) / \ln(1-C)$.

Next, we show the following claim.

Claim: if $x \notin \Omega$ then for every $(\hat{\theta}, d) \in \Theta \times [0, 1]^{n-1}$ it holds that:

$$\sum_{i=1}^n I_i(x^+) \leq (1-C) \sum_{i=1}^n I_i(x) + \kappa \quad (\text{B.56})$$

where $C \in (0, 1)$ is the constant involved in (??), $\kappa := \sum_{i \in R} (n+1-i)v_i^{min} + \sum_{i \notin R} (n+1-i)v_i^{max}$ and x^+ is given by (5.10) with $u = K(\hat{\theta}, x)$.

Proof of Claim: if $x \notin \Omega = \prod_{i=1}^n (0, \mu_i)$, then there exists $i \in \{1, \dots, n\}$ such that $x_i \geq \mu_i$. Since $\hat{x}^* = (\hat{x}_1^*, \dots, \hat{x}_n^*) \in \prod_{i=1}^n [0, \mu_i - \epsilon]$ (recall (5.12)), it follows from (5.14) and Property (C5) that $\sigma \in (0, 1]$ that $\Xi(\hat{\theta}, x) \geq \sigma^n (x_i - \hat{x}_i^*) \geq \epsilon \sigma^n$. Since (B.54) holds, it follows from (5.13) that $v_i = v_i^{min}$ for all $i \in R$. Inequality (B.56) is a consequence of (??) and the fact that $v_i^* \in [0, v_i^{max}]$ for all $i \notin R$. The proof of the claim is complete.

We show next, by means of a contradiction, that for every sequence $\{d(t), \hat{\theta}(t) \in D \times \Theta\}_{t=0}^\infty$ and for every $x_0 \in S$, the solution $x(t)$ of (5.10), (5.17) with $u = K(\hat{\theta}, y)$, initial condition $x(0) = x_0$ corresponding to inputs $\{d(t), \hat{\theta}(t) \in D \times \Theta\}_{t=0}^\infty$ satisfies $y(t-1-i(t)) \in A$ for some $i(t) \in \{0, 1, \dots, m\}$ and for all $t \geq m+1$. Suppose that, on the contrary, there exists a sequence $\{d(t), \hat{\theta}(t) \in D \times \Theta\}_{t=0}^\infty$, a vector $x_0 \in S$ and an integer $t \geq m+1$, such that the solution $x(t)$ of (5.10), (5.17) with $u = K(\hat{\theta}, y)$, initial condition $x(0) = x_0$ corresponding to inputs $\{d(t), \hat{\theta}(t) \in D \times \Theta\}_{t=0}^\infty$ satisfies $y(t-1-i(t)) \notin A$ for all $i(t) \in \{0, 1, \dots, m\}$. By virtue of (5.23), this implies that $x(t-1-i(t)) \notin \Omega$ for all $i(t) \in \{0, 1, \dots, m\}$ (notice that (5.7), (5.8), (5.15), (5.16), (5.17) and (5.23) guarantee that $x \in \Omega$ implies that $y \in A$). It follows from the Claim, that:

$$\sum_{i=1}^n I_i(x(l+1)) \leq (1-C) \sum_{i=1}^n I_i(x(l)) + \kappa \quad (\text{B.57})$$

for $l = t-1-m, \dots, t-1$

Using (B.57) repeatedly, we get:

$$\begin{aligned} \sum_{i=1}^n I_i(x(t-1)) &\leq \\ (1-C)^m \sum_{i=1}^n I_i(x(t-1-m)) + \kappa \frac{1-(1-C)^m}{C} \end{aligned} \quad (\text{B.58})$$

Using the definition $I_j(x) := \sum_{i=1}^j x_i$ for $j = 1, \dots, n$ and the fact that $x \in S = \prod_{i=1}^n (0, \rho_i^{max}]$, we get from (B.58):

$$\begin{aligned} (n+1-j)x_j(t-1) &\leq (1-C)^m \sum_{i=1}^n (n+1-i)\rho_i^{max} + C^{-1}\kappa \\ &\text{for all } j = 1, \dots, n \end{aligned} \quad (\text{B.59})$$

Using (B.59), (B.6) and (B.55), we get:

$$(n+1-j)x_j(t-1) \leq \min_{i=1, \dots, n} ((n+1-i)\mu_i)$$

for all $j = 1, \dots, n$ which implies that $x(t-1) \in \Omega = \prod_{i=1}^n (0, \mu_i)$, a contradiction. The proof is complete. \triangleleft

Appendix C

Consistency Analysis

The analysis of the proposed new discretized model (Approach 5) with respect to its relation with the continuous space-time PDE of the LWR is presented here. More specifically, it is investigated how the introduced parameters of Approach 5 affect the solution of the discretized model when the discretization parameters (cell length and simulation time step) tend to zero. However, in order to conduct such an analysis, it is important to determine the way the on-ramp flow term is treated. There are two main ways to treat the on-ramp: first by assuming that the on-ramp flow term is treated as a distributed flow within specific space bounds; second by assuming that the on-ramp flow is treated as a concentrated (Dirac function) flow at a given space point of the freeway. Sections C.1 and C.2 present the analysis for the two respective cases.

In any case, we consider the difference-equation state-space model described by equations (2.24), (2.36), (2.37) and (2.27), which describe the proposed model (Approach 5) for which this analysis is performed. Notice that, in case $\theta_r = 1$ (in (2.36)) and $f_{D,i}(\rho_i) = Q_i$ for $\rho_i \geq \rho_{cr}$ (in (2.37)), the basic discretized LWR model is obtained. Additionally, if $g(\rho_i) = v_{f,i}\rho_i l_i$ (in (2.37)), then we end up with the CTM. The discretization time step is denoted as previously with T_h . In order to simplify the present analysis, we consider that the above equations describe a single-lane homogeneous freeway cell with no off-ramps (which are not considered important in the present analysis). Thus, we assume that $p_i = 0$, $L_i = L$, $f_{D,i} = f_D$, $f_{S,i} = f_S$ and $f_i = f$, for $i = 1, \dots, n$. Let A_{km} and B_{km} be the starting and ending points of the freeway stretch, respectively. Then the total freeway length is $B - A_{km}$, and the proposed model is described by (where in this section we consider for convenience a different notation for the density, i.e., instead of x (which here denotes the space argument), here we use ρ):

$$\rho_i(k+1) = \rho_i(k) + \frac{T}{L} (-f(\rho_i(k), \rho_{i+1}(k), r_{i+1}(k)) + f(\rho_{i-1}(k), \rho_i(k), v_i(k)) + v_i(k)), \quad (\text{C.1})$$

where

$$f(\rho_i(k), \rho_{i+1}(k), v_{i+1}(k)) = \min \{f_D(\rho_i(k)), f_S(\rho_{i+1}(k)) - \theta_r v_{i+1}(k)\}, \quad (\text{C.2})$$

and f_D , f_S are given by (2.37), (2.27) and $0 < \theta \leq 1$.

C.1 Distributed on-ramp flow

In this case we assume that each on-ramp has an acceleration lane of length equal to L_{rmp} km. We consider the following definitions:

$$\rho_i(k) := \frac{1}{L} \int_{iL}^{iL+L} \rho(kT, z) dz, \quad (\text{C.3})$$

$$v_i(k) = v_i(kT) := \int_{iL}^{iL+L} u(kT, z) dz, \quad (\text{C.4})$$

where $\rho \in C^1$ ([veh/km]) corresponds to the density and $u \in C^0$ ([veh/time/space]) corresponds to the inflow per unit space at a given time instant. Notice that, by definitions (C.3) and (C.4), we have considered average density and inflow values, respectively, for every cell. Since a uniform distribution of the entering flow from the on-ramp to a number of cells is assumed, we have for each such cell

$$u(kT, z) = \frac{v_{rmp}(kT)}{L_{rmp}}, \quad (\text{C.5})$$

where $v_{rmp}(kT)$ is the total on-ramp inflow. Moreover, we consider arbitrary C^1 functions $f_D(\rho)$ and $f_S(\rho)$ that satisfy $f_D(\rho) = f_S(\rho)$, for $\rho = \rho^{cr}$, $f_D(\rho) < f_S(\rho)$, for $\rho < \rho^{cr}$, $f_D(\rho) > f_S(\rho)$, for $\rho > \rho^{cr}$, $f_D(0) = 0$ and $f_S(\rho^{max}) = 0$. Notice that the above requirements are satisfied for the demand and supply functions considered in (2.37) and (2.27) respectively. Substituting (C.3) and (C.4) in (C.1) we obtain:

$$\begin{aligned} & \frac{1}{T} \left(\int_{iL}^{iL+L} (\rho(kT, z) - \rho(kT + T, z)) dz \right) = \\ & -f \left(\frac{1}{L} \int_{iL}^{iL+L} \rho(kT, z) dz, \frac{1}{L} \int_{iL+L}^{iL+2L} \rho(kT, z) dz, \int_{iL+L}^{iL+2L} u(kT, z) dz \right) \\ & +f \left(\frac{1}{L} \int_{iL-L}^{iL} \rho(kT, z) dz, \frac{1}{L} \int_{iL}^{iL+L} \rho(kT, z) dz, \int_{iL}^{iL+L} u(kT, z) dz \right) \\ & + \int_{iL}^{iL+L} u(kT, z) dz \end{aligned} \quad (\text{C.6})$$

Set $t = kT$ and $iL = x$. Then, using the Mean Value Theorem (MVT) for $T \rightarrow 0$, it follows from (C.6) that:

$$\begin{aligned} & \int_x^{x+L} \frac{\partial \rho}{\partial t}(t, z) dz = \\ & -f \left(\frac{1}{L} \int_x^{x+L} \rho(t, z) dz, \frac{1}{L} \int_{x+L}^{x+2L} \rho(t, z) dz, \int_{x+L}^{x+2L} u(t, z) dz \right) \\ & +f \left(\frac{1}{L} \int_{x-L}^x \rho(t, z) dz, \frac{1}{L} \int_x^{x+L} \rho(t, z) dz, \int_x^{x+L} u(t, z) dz \right) + \int_x^{x+L} u(t, z) dz \end{aligned} \quad (\text{C.7})$$

We use the following definition:

$$\begin{aligned} & F(t, x, L) := \\ & f \left(\frac{1}{L} \int_x^{x+L} \rho(t, z) dz, \frac{1}{L} \int_{x+L}^{x+2L} \rho(t, z) dz, \int_{x+L}^{x+2L} u(t, z) dz \right) = f(a_1, a_2, a_3) \end{aligned} \quad (\text{C.8})$$

where a_1, a_2, a_3 have been introduced as auxiliary variables to ease the analysis corresponding to the arguments of the flux function f . Combining (C.7) and (C.8) we obtain

$$\int_x^{x+L} \left(\frac{\partial \rho}{\partial t}(t, z) - u(t, z) \right) dz = -F(t, x, L) + F(t, x - L, L). \quad (\text{C.9})$$

Then, we make the following substitution:

$$-F(t, x, L) + F(t, x - L, L) = - \int_{x-L}^x \frac{\partial F}{\partial z}(t, z, L) dz,$$

which combining with (C.9) yields the following relation, which holds for every $L > 0$:

$$\int_x^{x+L} \left(\frac{\partial \rho}{\partial t}(t, z) - u(t, z) + \frac{\partial F}{\partial z}(t, z - L, L) \right) dz = 0. \quad (\text{C.10})$$

Then, using the fact that (C.10) holds for every $L > 0$ and the MVT for $L \rightarrow 0$ we have that:

$$\frac{\partial \rho}{\partial t}(t, x) = - \frac{\partial F}{\partial x}(t, x, 0) + u(t, x). \quad (\text{C.11})$$

Now, in order to obtain the flux function F in terms of the demand and supply functions, we follow the next steps. For constant $L > 0$ we have that:

$$\begin{aligned} \frac{\partial F}{\partial x}(t, x, L) = & \frac{\partial f}{\partial a_1} \left(\frac{1}{L} \int_x^{x+L} \rho(kT, z) dz, \frac{1}{L} \int_{x+L}^{x+2L} \rho(kT, z) dz, \int_{x+L}^{x+2L} u(kT, z) dz \right) \\ & \left(\frac{1}{L} (\rho(t, x+L) - \rho(t, x)) \right) + \\ & \frac{\partial f}{\partial a_2} \left(\frac{1}{L} \int_x^{x+L} \rho(kT, z) dz, \frac{1}{L} \int_{x+L}^{x+2L} \rho(kT, z) dz, \int_{x+L}^{x+2L} u(kT, z) dz \right) \\ & \left(\frac{1}{L} (\rho(t, x+2L) - \rho(t, x+L)) \right) + \\ & \frac{\partial f}{\partial a_3} \left(\frac{1}{L} \int_x^{x+L} \rho(kT, z) dz, \frac{1}{L} \int_{x+L}^{x+2L} \rho(kT, z) dz, \int_{x+L}^{x+2L} u(kT, z) dz \right) \\ & (u(t, x+2L) - u(t, x+L)). \end{aligned} \quad (\text{C.12})$$

Thus, using the Mean Value Theorem (MVT) for $L \rightarrow 0$ and using (C.2) we obtain:

$$\begin{aligned} \frac{\partial F}{\partial x}(t, x, 0) = & \left(\left\{ \begin{array}{ll} f'_D(\rho(t, x)) & \text{if } \rho(t, x) \leq \rho^{cr} \\ 0 & \text{if } \rho(t, x) > \rho^{cr} \end{array} \right\} + \left\{ \begin{array}{ll} 0 & \text{if } \rho(t, x) \leq \rho^{cr} \\ f'_S(\rho(t, x)) & \text{if } \rho(t, x) > \rho^{cr} \end{array} \right\} \right) \frac{\partial \rho}{\partial x}(t, x), \end{aligned} \quad (\text{C.13})$$

which in turn corresponds to the following PDE:

$$\frac{\partial \rho}{\partial t}(t, x) + \frac{\partial}{\partial x} q(\rho(t, x)) = u(t, x) \text{ for } t > 0 \text{ and } A < x < B \quad (\text{C.14})$$

with

$$q(\rho) = \int_0^\rho \left(\frac{\partial f}{\partial a_1}(z, z, 0) + \frac{\partial f}{\partial a_2}(z, z, 0) \right) dz = \begin{cases} f_D(\rho) & \text{if } \rho \leq \rho^{cr} \\ f_S(\rho) & \text{if } \rho > \rho^{cr} \end{cases}. \quad (\text{C.15})$$

The above analysis proves the consistency of the discretized model (C.1), (C.2) with the LWR model (C.14). The result has been obtained by considering smooth functions f_D , f_S , f , as well as the fact that $\rho(t, x)$ lies within appropriate intervals. However, a similar analysis as above can be made even for piecewise differentiable functions. In such cases the solution converges to generalized (weak) solutions of (C.14). Therefore, the discrete-time model is consistent to the LWR model (C.14).

This result is supported by some conducted numerical experiments (Figure C.1(a), (b), (c)). The simulation results depicted in these figures have been obtained using the same illustrative scenario of Section 3.3. More specifically, density and flow for the complete freeway stretch at the same time instant (i.e., $t = 1.9\text{h}$) are depicted for

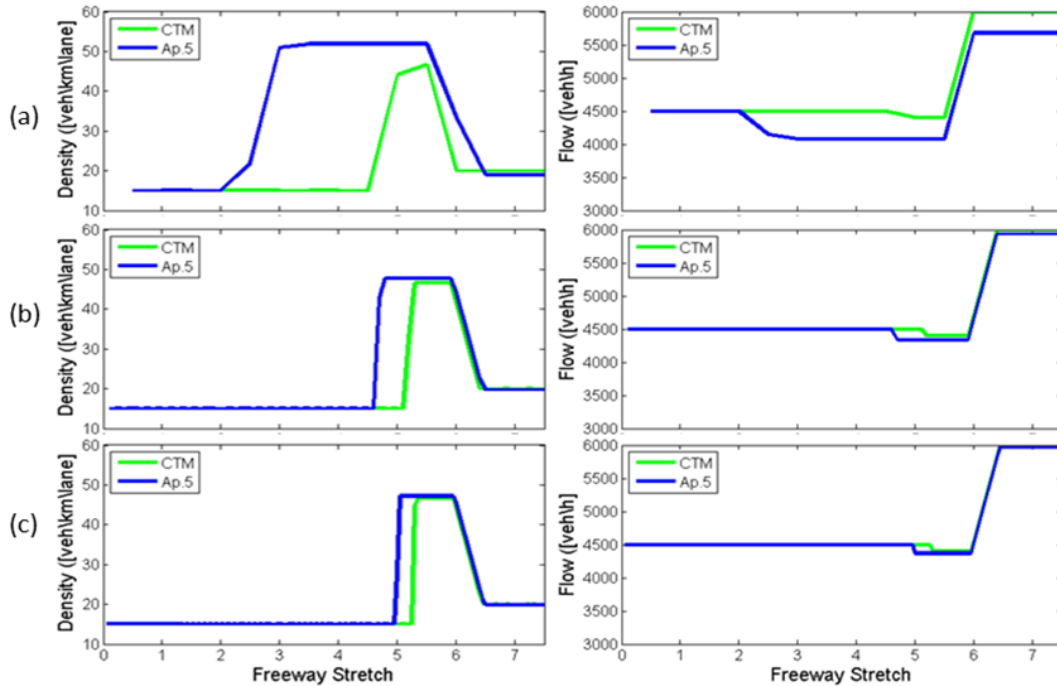


FIGURE C.1: (Distributed on-ramp flow) The density (left) and the flow (right) at $t = 1.9h$ in the freeway stretch for (a) $L = 0.5$ km, (b) $L = 0.1$ km and (c) $L = 0.05$ km.

the two different schemes (CTM and A5) and for three different spatial discretizations ($L = 0.5, L = 0.1, L = 0.05$ km). The numerical results indicate that, as L tends to zero, both schemes converge to the same solution.

C.2 Concentrated on-ramp flow as a singular source

Here we show that, when the on-ramp is incorporated as a singular source (for both CTM and Approach 5 model), the effect of the on-ramp contribution is more pronounced, independently of the spatial discretization, and a modified shock speed is derived for the model described by Approach 5 in comparison with CTM. We point out here that, in the case where the on-ramp contribution is incorporated as a singular source (i.e., as a Dirac function), the differential form of the conservation law is not valid in the position where the on-ramp is implemented; only the integral form of the conservation law is valid there. Consequently, the comparison between the CTM and Approach 5 is materialized on this base.

Referring again to the model (C.1) - (C.2), we use the compact forms $\rho_i^k = \rho_i(k)$, $v_i^k = v_i(k)$, $f_D(\rho_i(k)) = f_{D,i}^k$ and $f_S(\rho_i(k)) = f_{S,i}^k$. Assuming that the on-ramp is implemented only at a distinct point of the i^{th} computational cell, and there are no other similar sources within the freeway (i.e., $v_j = 0$, for $j \neq i$), we obtain from (C.1) with (C.2) that:

$$\rho_i^{k+1} = \rho_i^k + \frac{T}{L} \left(-\min \left(f_{D,i}^k, f_{S,i+1}^k - 0 \right) + \min \left(f_{D,i-1}^k, f_{S,i}^k - \theta_r v_i^k \right) + v_i^k \right) \quad (\text{C.16})$$

where $v_i^k = v_{rmp}^k(t) = v_{rmp}(kT)$. We recall again here that the differences between the CTM and Approach 5 lie on the parameter θ_r and the right part of the demand

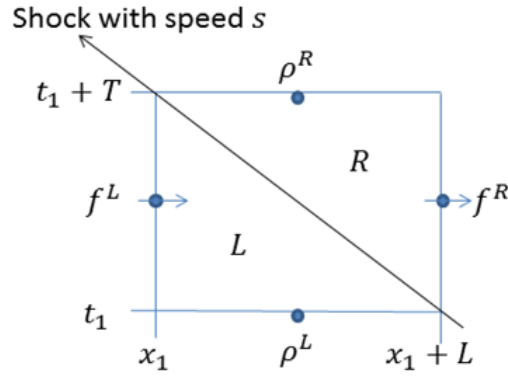


FIGURE C.2: The Rankine-Hugoniot jump conditions are determined by integrating over an infinitesimal rectangular region on the $x - t$ plane.

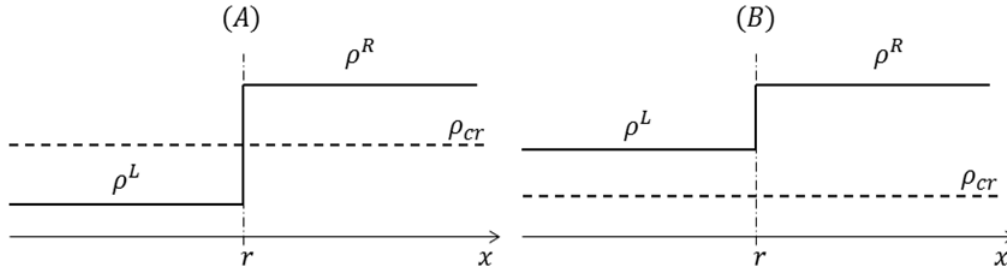


FIGURE C.3: Characteristic Riemann problems.

function. Thus, referring to Figure C.2 and by denoting with s the speed of the left moving shock, we have that $L = -sT$. Then, we obtain from (C.16) that:

$$s(\rho_i^{k+1} - \rho_i^k) = \min(f_{D,i}^k, f_{S,i+1}^k) - \min(f_{D,i-1}^k, f_{S,i}^k - \theta_r v_i^k) - v_i^k \quad (\text{C.17})$$

We will compute jump conditions at the location of the on-ramp using the procedure proposed by (LeVeque, 2002). Figure C.2 depicts a small rectangular region in which a shock wave is present. The Rankine-Hugoniot jump conditions will be derived using this illustrative example. In this case, (C.17) becomes:

$$s(\rho^R - \rho^L) = \min(f_D^R, f_S^R) - \min(f_D^L, f_S^L - \theta_r v_i) - v_i \quad (\text{C.18})$$

We assume that the on-ramp flow cannot exceed the capacity of the network and therefore $Q > v_i$. Moreover, in order to simplify the present analysis, we consider $g(\rho_i) = v_f \rho_i$. Thus, we have that $\rho_{cr} = Q/v_f$, $Q = w(\rho_{max} - \rho_{cr})$ and, therefore, $\rho_{max} = (v_f/w + 1)\rho_{cr}$. The two considered illustrative cases, which we intend to examine here, are shown in Figure C.3. Then, (C.18) imposes that the resulting speed of the shock wave depends on the intervals in which ρ^R and ρ^L lie. Therefore, we distinguish points $\rho_1 = (Q - v_i)/v_f$, $\rho_2 = (Q - \theta_r v_i)/v_f$ and $\rho_3 = \rho_{max} - v_i/w$. Notice that $0 < \rho_1 < \rho_2 < \rho_{cr} < \rho_3 < \rho_{max}$.

Tables C.1 and C.2 show the resulting speed and sign of the shock for case (A), for CTM and Approach 5, respectively. As it can be clearly seen, the intensity of the shock clearly depends on the magnitude of the on-ramp flow. For that reason, there are cases ($\rho_2 < \rho^L < \rho_{cr}$) where the intensity of the shock is larger for Approach 5

TABLE C.1: Speed and sign of the shock for CTM for case (A).

(A)		CTM	
$0 < \rho^L < \rho_1$	$\rho_{cr} < \rho^R < \rho_3$ $\rho_3 < \rho^R < \rho_{max}$	+ or - -	$s = \frac{w(\rho_{max}-\rho^R)-v_f\rho^L-v_i}{\rho^R-\rho^L}$
$\rho_1 < \rho^L < \rho_2$	$\rho_{cr} < \rho^R < \rho_3$ $\rho_3 < \rho^R < \rho_{max}$	- -	$s = \frac{w(\rho_{max}-\rho^R)-Q}{\rho^R-\rho^L}$
$\rho_2 < \rho^L < \rho_{cr}$	$\rho_{cr} < \rho^R < \rho_3$ $\rho_3 < \rho^R < \rho_{max}$	- -	$s = \frac{w(\rho_{max}-\rho^R)-Q}{\rho^R-\rho^L}$

TABLE C.2: Speed and sign of the shock for Approach 5 for case (A).

(A)		Approach 5	
$0 < \rho^L < \rho_1$	$\rho_{cr} < \rho^R < \rho_3$ $\rho_3 < \rho^R < \rho_{max}$	+ or - -	$s = \frac{w(\rho_{max}-\rho^R)-v_f\rho^L-v_i}{\rho^R-\rho^L}$
$\rho_1 < \rho^L < \rho_2$	$\rho_{cr} < \rho^R < \rho_3$ $\rho_3 < \rho^R < \rho_{max}$	+ or - -	$s = \frac{w(\rho_{max}-\rho^R)-v_f\rho^L-v_i}{\rho^R-\rho^L}$
$\rho_2 < \rho^L < \rho_{cr}$	$\rho_{cr} < \rho^R < \rho_3$ $\rho_3 < \rho^R < \rho_{max}$	- -	$s = \frac{w(\rho_{max}-\rho^R)-Q-(1-\theta_r)v_i}{\rho^R-\rho^L}$

due to the effect of the parameter θ_r . For the case (B) the shock speed is negative (the shock wave moves to the left), no matter what are the values of ρ^R and ρ^L . However, as it is shown in Table C.3, the intensity of the shock is higher for Approach 5, depending again on the selection of the parameter θ .

The previous theoretical observations are illustrated by the numerical experiments shown in Figure C.4 using the same illustrative scenario of the previous section. More specifically, density and flow for the complete freeway stretch at the same time instant (i.e., $t = 1.9$ h) are depicted for the two different schemes (CTM and Approach 5) and for three different spatial discretizations ($L = 0.5, L = 0.1, L = 0.05$ km). The numerical results indicate that, as L tends to zero, the two schemes converge to a different solution; the scheme of Approach 5 results in a higher (negative) shock speed and a higher density at the congested region compared to the shock generated by CTM.

Following from the previous analysis, it is clear that the proposed scheme (Approach 5) with its modified supply and demand functions introduces a modified

TABLE C.3: Sign and intensity of the shock for CTM and Approach 5 for case (B).

(A)	CTM	Approach 5
$\rho_{cr} < \rho^L < \rho^R < \rho_{max}$	$-w$	$-w - \frac{(1-\theta_r)v_i}{\rho^R-\rho^L}$

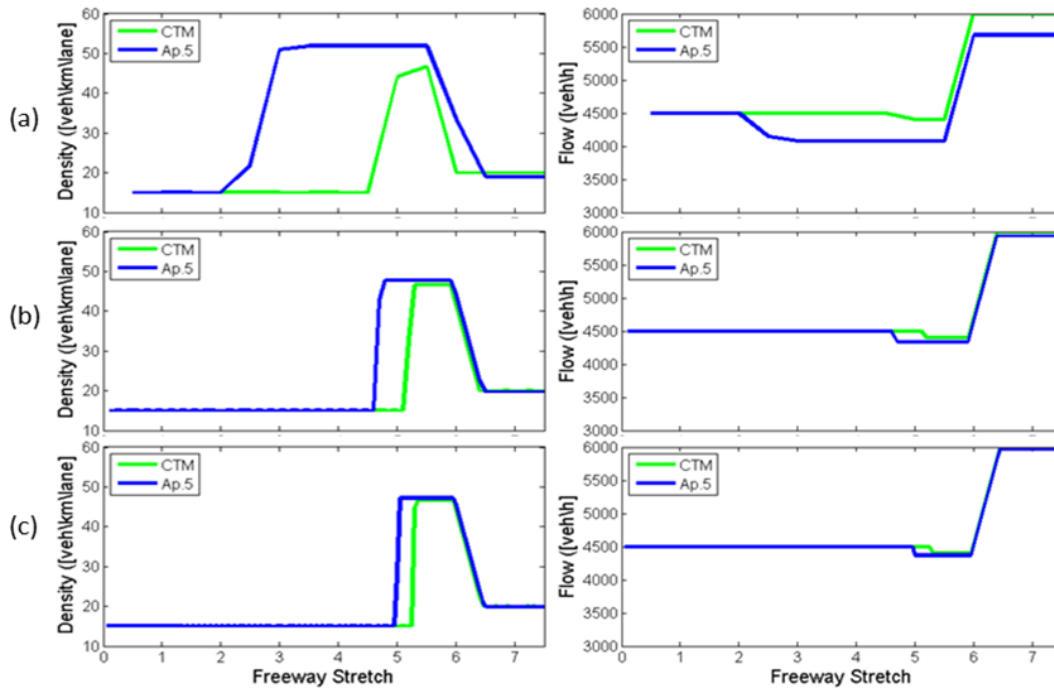


FIGURE C.4: (Concentrated on-ramp flow) The density (left) and the flow (right) at $t = 1.9h$ in the freeway stretch for (a) $L = 0.5$ km, (b) $L = 0.1$ km and (c) $L = 0.05$ km.

jump condition in the Riemann problems depicted previously, when the on-ramp flow is considered as a concentrated singular source term in a single cell. In this case, the proposed modifications to the supply and demand functions are always present as L tends to zero. These modifications can be viewed as imposed inhomogeneities in the on-ramp cell which result in a generalized Riemann problem solved by a modified Godunov scheme similar to those presented by (Jin et al., 2009; Lebacque, 1996). On the contrary, when a distributed on-ramp entering flow is considered (as in Section A.1), the corresponding modifications to the supply and demand functions vanish as L tends to zero.

Bibliography

- Aboudolas, K. and N. Geroliminis (2013). "Perimeter and boundary flow control in multi-reservoir heterogeneous networks". In: *Transportation Research Part B: Methodological* 55, pp. 265–281.
- Aboudolas, K., M. Papageorgiou, and E. Kosmatopoulos (2009). "Store-and-forward based methods for the signal control problem in large-scale congested urban road networks". In: *Transportation Research Part C: Emerging Technologies* 17.2, pp. 163–174.
- Ahmed, A., I. Akhtar, and I. Aziz (2015). "Analysis of stable and unstable manifolds in fluid flows using Lagrangian Coherent Structures". In: *Proceedings of the 12th International Bhurban Conference on Applied Sciences and Technology*, pp. 375–384.
- Ahmed-Ali, T., F. Giri, and M. Krstic (2017). "Observer design for triangular nonlinear systems in the presence of arbitrarily large output delay - a PDE based approach". In: *Proceedings of the American Control Conference*. IEEE, pp. 481–486.
- Alecsandru, C. et al. (2011). "An assessment of the cell-transmission traffic flow paradigm: development and applications". In: *Proceedings of the 90th Annual Meeting of Transportation Research Board*. paper no. 11-1152.
- Alvarez-Icaza, L. and G.J. Islas (2013). "Hysteretic cell transmission model". In: *Proceeding of the 16th International IEEE Conference on Intelligent Transportation Systems (ITSC-2013)*, pp. 578–583.
- Anderson, B. and J. Moore (1990). *Optimal control: linear quadratic methods*. Prentice-Hall.
- Artstein, Z. (1983). "Stabilization with relaxed controls". In: *Nonlinear Analysis, Theory and Methods* 7, pp. 1163–1173.
- Aw, A. and M. Rascole (2000). "Resurrection of "second order" models of traffic flow". In: *SIAM Journal on Applied Mathematics* 60.3, pp. 916–938.
- Bekiaris-Liberis, N., C. Roncoli, and M. Papageorgiou (2015). "Highway traffic state estimation with mixed connected and conventional vehicles using speed measurements". In: *Proceedings of the 18th International Conference on Intelligent Transportation Systems*. IEEE, pp. 2806–2811.
- Bellemans, T., B. De Schutter, and B. De Moor (2002). "Model predictive control with repeated model fitting for ramp metering". In: *Proceeding of the 5th International Conference on Intelligent Transportation Systems*. IEEE, pp. 236–241.
- Buisson, C., J.-P. Lebacque, and J.B. Lesort (1996). "STRADA, a discretized macroscopic model of vehicular traffic flow in complex networks based on the Godunov scheme". In: *CESA'96 IMACS Multiconference: Computational Engineering in Systems Applications*, pp. 976–981.
- Burger, M. et al. (2013). "Considerations for model-based traffic control". In: *Transportation Research Part C: Emerging Technologies* 35, pp. 1–19.
- Burghout, W., H. Koutsopoulos, and A. Ingmar (2005). "Hybrid mesoscopic - microscopic traffic simulation". In: *Transportation Research Record: Journal of the Transportation Research Board* 1934, pp. 218–255.
- Calugi, F. (2002). *Observer-based adaptive control*. Master thesis.

- Carlson, R.C., I. Papamichail, and M. Papageorgiou (2011). "Local feedback-based mainstream traffic flow control on motorways using variable speed limits". In: *IEEE Transactions on Intelligent Transportation Systems* 12.4, pp. 1261–1276.
- Carlson, R.C. et al. (2010a). "Optimal motorway traffic flow control involving variable speed limits and ramp metering". In: *Transportation Science* 44.2, pp. 238–253.
- (2010b). "Variable speed limits as a mainline metering device for freeways". In: *Proceedings of the 89th Annual Meeting of Transportation Research Board*. paper no. 10-1529.
- Cassidy, M. and S. Ahn (2005). "Driver turn-taking behavior in congested freeway merges". In: *Transportation Research Record: Journal of the Transportation Research Board* 1934, pp. 140–147.
- Cassidy, M.J. (1998). "Bivariate relations in nearly stationary highway traffic". In: *Transportation Research Part B: Methodological* 32.1, pp. 49–59.
- Cassidy, M.J. and J. Rudjanakanoknad (2005). "Increasing the capacity of an isolated merge by metering its on-ramp". In: *Transportation Research Part B: Methodological* 39.10, pp. 896–913.
- Chen, O.J., A.F. Hotz, and M.E. Ben-Akiva (1997). "Development and evaluation of a dynamic ramp metering control model". In: *IFAC Proceedings Volumes*. Vol. 30, pp. 1089–1095.
- Clarke, F.H. (2001). "Nonsmooth analysis in control theory: a survey". In: *European Journal of Control* 7, pp. 145–159.
- Colombo, R. (2003). "Hyperbolic phase transitions in traffic flow". In: *SIAM Journal on Applied Mathematics* 1, pp. 708–721.
- Coogan, S. and M. Arcaç (2014). "Dynamical properties of a compartmental model for traffic networks". In: *Proceedings of the American Control Conference*. IEEE, pp. 2511–2516.
- Coron, J.-M. and L. Praly (1991). "Adding an integrator for the stabilization problem". In: *Systems and Control Letters* 17, pp. 89–104.
- Coron, J.-M. and L. Rosier (1994). "A relation between continuous time-varying and discontinuous feedback stabilization". In: *Journal of Mathematical Systems, Estimation, and Control* 4, pp. 67–84.
- Daganzo, C.F. (1994). "The cell transmission model: a dynamic representation of highway traffic consistent with the hydrodynamic theory". In: *Transportation Research Part B: Methodological* 28.4, pp. 269–287.
- (1995a). "Requiem for second-order fluid approximations of traffic flow". In: *Transportation Research Part B: Methodological* 29.4, pp. 277–286.
- (1995b). "The cell transmission model, part II: network traffic". In: *Transportation Research Part B: Methodological* 29.2, pp. 79–93.
- Delis, A.I., I.K. Nikolos, and M. Papageorgiou (2014). "High-resolution numerical relaxation approximations to second-order macroscopic traffic flow models". In: *Transportation Research Part C: Emerging Technologies* 44, pp. 318–349.
- Diakaki, C. and M. Papageorgiou (1994). "Design and simulation test of coordinated ramp metering control (METALINE) for A10-west in Amsterdam". In: *Dynamic Systems and Simulation Laboratory, Technical University of Crete, Chania, Greece, Internal Report 2*.
- Eddie, L.C. (1961). "Car-following and steady-state theory for noncongested traffic". In: *Operations Research* 9.1, pp. 66–76.
- Elefteriadou, L., R.P. Roess, and W.R. McShane (1995). "Probabilistic nature of breakdown at freeway merge junctions". In: *Transportation Research Record: Journal of the Transportation Research Board* 1484, pp. 80–89.

- Fermo, L. and A. Tosin (2013). "A fully-discrete-state kinetic theory approach to modeling vehicular traffic". In: *SIAM Journal on Applied Mathematics* 73.4, pp. 1533–1556.
- Ferrara, A., S. Sacone, and S. Siri (2015). "Event-triggered model predictive schemes for freeway traffic control". In: *Transportation Research Part C: Emerging Technologies* 58, pp. 554–567.
- Frejo, José Ramón Domínguez, Eduardo Fernández Camacho, and Roberto Horowitz (2012). "A parameter identification algorithm for the METANET model with a limited number of loop detectors". In: *Proceedings of the 51st Annual Conference on Decision and Control*. IEEE, pp. 6983–6988.
- Gauthier, J.-P. and I. Kupka (1994). "Observability and observers for nonlinear systems". In: *SIAM Journal on Control and Optimization* 32, pp. 975–994.
- (2001). *Deterministic observation theory and applications*. Cambridge university press.
- Godsil, C. and G.F. Royle (2013). *Algebraic graph theory*. Vol. 207. Springer Science & Business Media.
- Godunov, S.K. (1959). "A difference method for numerical calculation of discontinuous solutions of the equations of hydrodynamics". In: *Matematicheskii Sbornik* 89.3, pp. 271–306.
- Gomes, G. and R. Horowitz (2006). "Optimal freeway ramp metering using the asymmetric cell transmission model". In: *Transportation Research Part C: Emerging Technologies* 14.4, pp. 244–262.
- Gomes, G. et al. (2008). "Behavior of the cell transmission model and effectiveness of ramp metering". In: *Transportation Research Part C: Emerging Technologies* 16.4, pp. 485–513.
- Haddad, J. and N. Geroliminis (2012). "On the stability of traffic perimeter control in two-region urban cities". In: *Transportation Research Part B: Methodological* 46.9, pp. 1159–1176.
- Haddad, W.M. and V. Chellaboina (2008). *Nonlinear dynamical systems and control: a Lyapunov-based approach*. Princeton University Press.
- Han, Y. et al. (2016). "A new variant of discretized LWR model to reproduce capacity drop". In: *Proceedings of the 95th Annual Meeting of the Transportation Research Board*. paper no. 16-3482, pp. 96–96.
- Hayakawa, T., W.M. Haddad, and A. Leonessa (2004). "A Lyapunov-based adaptive control framework for discrete-time nonlinear systems with exogenous disturbances". In: *International Journal of Control* 77.3, pp. 250–263.
- Hegyi, A., B. De Schutter, and J. Heelendoorn (2003). "MPC-based optimal coordination of variable speed limits to suppress shock waves in freeway traffic". In: *Proceedings of the American Control Conference*. Vol. 5. IEEE, pp. 4083–4088.
- Hegyi, A., B. De Schutter, and H. Hellendoorn (2005). "Model predictive control for optimal coordination of ramp metering and variable speed limits". In: *Transportation Research Part C: Emerging Technologies* 13.3, pp. 185–209.
- Helbing, D. and A.F. Johansson (2009). "On the controversy around Daganzo's requiem for and Aw-Rasclé's resurrection of second-order traffic flow models". In: *The European Physical Journal B-Condensed Matter and Complex Systems* 69.4, pp. 549–562.
- Hou, Z., J.-X. Xu, and J. Yan (2008). "An iterative learning approach for density control of freeway traffic flow via ramp metering". In: *Transportation Research Part C: Emerging Technologies* 16.1, pp. 71–97.
- Hourdakis, J. and P. Michalopoulos (2002). "Evaluation of ramp control effectiveness in two twin cities freeways". In: *Transportation Research Record: Journal of the Transportation Research Board* 1811, pp. 21–29.

- Ioannou, P. and E. Kosmatopoulos (2006). *Adaptive control*. John Wiley & Sons, Inc.
- Iordanidou, G.R. et al. (2015). "Feedback-based mainstream traffic flow control for multiple bottlenecks on motorways". In: *IEEE Transactions on Intelligent Transportation Systems* 16.2, pp. 610–621.
- Jacobson, L.N., K.C. Henry, and O. Mehryar (1989). *Real-time metering algorithm for centralized control*. 1232. Transportation Research Board.
- Jiang, Z.-P., A. Teel, and L. Praly (1994). "Small-gain theorem for ISS systems and applications". In: *Mathematics of Control, Signals, and Systems (MCSS)* 7, pp. 95–120.
- Jin, W.-L. (2010). "A kinematic wave theory of lane-changing traffic flow". In: *Transportation Research Part B: Methodological* 44.8, pp. 1001–1021.
- Jin, W.-L., Q.-J. Gan, and J.-P. Lebacque (2015). "A kinematic wave theory of capacity drop". In: *Transportation Research Part B: Methodological* 81, pp. 316–329.
- Jurdevic, V. and J.P. Quinn (1978). "Controllability and stability". In: *Journal of Difference Equations* 28, pp. 381–389.
- Kachroo, P. and K.M.A. Ozbay (2011). *Feedback ramp metering in intelligent transportation systems*. Springer Science & Business Media.
- Karafyllis, I., N. Bekiari-Liberis, and M. Papageorgiou (2017). "Analysis and control of a non-standard hyperbolic PDE traffic flow model". In: *arXiv:1707.02209*.
- Karafyllis, I. and Z.-P. Jiang (2011). *Stability and stabilization of nonlinear systems*. Springer Science & Business Media.
- Karafyllis, I. and C. Kravaris (2007). "On the observer problem for discrete-time control systems". In: *IEEE Transactions on Automatic Control* 52.1, pp. 12–25.
- Karafyllis, I. and M. Krstic (2016). "Adaptive certainty-equivalence control with regulation-triggered finite-time least-squares identification, part I: design". In: *arXiv:1609.03016 [math.OC]*.
- Karafyllis, I. and M. Papageorgiou (2014). "Stability results for simple traffic models under PI-regulator control". In: *IMA Journal of Mathematical Control and Information*, dnu040.
- (2015). "Global exponential stability for discrete-time networks with applications to traffic networks". In: *IEEE Transactions on Control of Network Systems* 2.1, pp. 68–77.
- Kesting, A., M. Treiber, and D. Helbing (2007). "General lane-changing model MOBIL for car-following models". In: *Transportation Research Record: Journal of the Transportation Research Board* 1999, pp. 86–94.
- Khalil, H. and L. Praly (2014). "High-gain observers in nonlinear feedback control". In: *International Journal of Robust and Nonlinear Control* 24, pp. 993–1015.
- Kim, K.-H. (1979). "An extension of the Dulmage-Mendelsohn theorem". In: *Linear Algebra and its Applications* 27, pp. 187–197.
- Kim, K.H. (1982). *Boolean matrix theory and applications*. Vol. 70. Dekker.
- Kontorinaki, M. et al. (2016). "Capacity drop in first-order traffic flow models: overview and real-data validation". In: *Proceedings of the 95th Annual Meeting of the Transportation Research Board*. papaer no. 16-3541.
- Koshi, M., M. Iwasaki, and I. Ohkura (1983). "Some findings and an overview on vehicular flow characteristics". In: *Proceedings of the 8th International Symposium on Transportation and Traffic Flow Theory*. Vol. 198. 1, pp. 403–426.
- Kotsialos, A. and M. Papageorgiou (2004). "Nonlinear optimal control applied to coordinated ramp metering". In: *IEEE Transactions on Control Systems Technology* 12.6, pp. 920–933.

- Kotsialos, A., M. Papageorgiou, and F. Middelham (2001). "Optimal coordinated ramp metering with AMOC". In: *Preprints of the 80th Annual Transportation Research Board Meeting*. paper no. 3125.
- Krstic, M., I. Kanellakopoulos, and P. Kokotovic (1995). *Nonlinear and adaptive control design*. Wiley Series on Adaptive, Learning Systems for Signal Processing, Communications, and Control.
- Krstic, M., P.V. Kokotovic, and I. Kanellakopoulos (1995). *Nonlinear and adaptive control design*. John Wiley & Sons, Inc.
- Lakshmikantham, V. and Donato Trigiante (2002). *Theory of difference equations numerical methods and applications*. CRC Press.
- Landman, R.L., A. Hegyi, and S.P. Hoogendoorn (2015). "Coordinated ramp metering based on on-ramp saturation time synchronization". In: *Transportation Research Record: Journal of the Transportation Research Board* 2484, pp. 50–59.
- Laval, J.A. and C.F. Daganzo (2006). "Lane-changing in traffic streams". In: *Transportation Research Part B: Methodological* 40.3, pp. 251–264.
- Lebacque, J.-P. (1996). "The Godunov scheme and what it means for first order traffic flow models". In: *Proceedings of the International Symposium on Transportation and Traffic Theory*, pp. 647–677.
- (2003). "Two-phase bounded-acceleration traffic flow model: analytical solutions and applications". In: *Transportation Research Record: Journal of the Transportation Research Board* 1852, pp. 220–230.
- Lebacque, J. P. and M. M. Khoshyaran (2002). "First-order macroscopic traffic flow models for networks in the context of dynamic assignment". In: *Transportation Planning*. Applied Optimization 64. Springer US, pp. 119–140.
- Lebacque, J.-P. et al. (1996). "The STRADA model for dynamic assignment". In: *Intelligent Transportation: Realizing the Future. Abstracts of the Third World Congress on Intelligent Transport Systems*.
- Leclercq, Ludovic, Jorge A Laval, and Nicolas Chiabaut (2011). "Capacity drops at merges: an endogenous model". In: *Transportation Research Part B: Methodological* 45.9, pp. 1302–1313.
- LeVeque, R.J. (2002). *Finite volume methods for hyperbolic problems*. Vol. 31. Cambridge university press.
- Li, P.Y. et al. (1997). "An automated highway system link layer controller for traffic flow stabilization". In: *Transportation Research Part C: Emerging Technologies* 5.1, pp. 11–37.
- Li, Z. et al. (2015). "Optimal mainline variable speed limit control to improve safety on large-scale freeway segments". In: *Computer-Aided Civil and Infrastructure Engineering*.
- Lighthill, M.J. and G.B. Whitham (1955a). "On kinematic waves I: flood movement in long rivers". In: *Proceedings of the Royal Society of London A: Mathematical, Physical and Engineering Sciences*. Vol. 229. 1178, pp. 281–316.
- (1955b). "On kinematic waves II: a theory of traffic flow on long crowded roads". In: *Proceedings of the Royal Society of London A: Mathematical, Physical and Engineering Sciences*. Vol. 229. 1178, pp. 317–345.
- Liu, T., D.J. Hill, and Z.-P. Jiang (2012). "Lyapunov formulation of the large-scale, ISS cyclic-small-gain theorem: the discrete-time case". In: *Systems & Control Letters* 61.1, pp. 266–272.
- Lo, H.K. (2001). "A cell-based traffic control formulation: strategies and benefits of dynamic timing plans". In: *Transportation Science* 35.2, pp. 148–164.

- Lorenz, M. and L. Elefteriadou (2001). "Defining freeway capacity as function of breakdown probability". In: *Transportation Research Record: Journal of the Transportation Research Board* 1776, pp. 43–51.
- Marinaki, M. and M. Papageorgiou (2005). *Optimal real-time control of sewer networks*. Springer Science & Business Media.
- Masher, D.P. et al. (1975). "Guidelines for design and operation of ramp control systems". In:
- Messmer, A. and M. Papageorgiou (1990). "METANET: a macroscopic simulation program for motorway networks". In: *Traffic Engineering & Control* 31.8-9, pp. 466–470.
- Moarref, M. and L. Rodrigues (2016). "Piecewise affine networked control systems". In: *IEEE Transactions on Control of Network Systems* 3.2, pp. 173–181.
- Monamy, T., H. Haj-Salem, and J.-P. Lebacque (2012). "A macroscopic node model related to capacity drop". In: *Procedia-Social and Behavioral Sciences* 54, pp. 1388–1396.
- Muñoz, L. et al. (2004). "Methodological calibration of the cell transmission model". In: *Proceedings of the American Control Conference*. Vol. 1. IEEE, pp. 798–803.
- Muralidharan, A. and R. Horowitz (2015). "Computationally efficient model predictive control of freeway networks". In: *Transportation Research Part C: Emerging Technologies* 58, pp. 532–553.
- Muralidharan, A., R. Horowitz, and P. Varaiya (2012). "Model predictive control of a freeway network with capacity drops". In: *ASME 2012 5th Annual Dynamic Systems and Control Conference joint with the JSME 2012 11th Motion and Vibration Conference*. American Society of Mechanical Engineers, pp. 303–312.
- Nagel, K. and M. Schreckenberg (1992). "A cellular automation model for freeway traffic". In: *Journal de Physique* 2, pp. 2221–2229.
- Newell, C. (1982). *Applications of queueing theory*. Vol. 2nd Edition. Chapman & Hall, New York.
- Papageorgiou, M. (1995). "An integrated control approach for traffic corridors". In: *Transportation Research Part C: Emerging Technologies* 3.1, pp. 19–30.
- Papageorgiou, M., J.-M. Blosseville, and H. Hadj-Salem (1989). "Macroscopic modelling of traffic flow on the Boulevard Peripherique in Paris". In: *Transportation Research Part B: Methodological* 23.1, pp. 29–47.
- (1990). "Modelling and real-time control of traffic flow on the southern part of Boulevard Peripherique in Paris: part I: modelling". In: *Transportation Research Part A: General* 24.5, pp. 345–359.
- Papageorgiou, M., H. Hadj-Salem, and J.-M. Blosseville (1991). "ALINEA: a local feedback control law for on-ramp metering". In: *Transportation Research Record: Journal of the Transportation Research Board* 1320.
- Papageorgiou, M., H. Hadj-Salem, and F. Middelham (1997). "ALINEA local ramp metering: summary of field results". In: *Transportation Research Record: Journal of the Transportation Research Board* 1603, pp. 90–98.
- Papageorgiou, M. and A. Kotsialos (2000). "Freeway ramp metering: An overview". In: *Proceedings of the Intelligent Transportation Systems*. IEEE, pp. 228–239.
- Papageorgiou, M. and R. Mayr (1982). "Optimal decomposition methods applied to motorway traffic control". In: *International Journal of Control* 35.2, pp. 269–280.
- Papageorgiou, M. et al. (2003). "Review of road traffic control strategies". In: *Proceedings of the IEEE* 91.12, pp. 2043–2067.
- Papamichail, I. and M. Papageorgiou (2008). "Traffic-responsive linked ramp-metering control". In: *IEEE Transactions on Intelligent Transportation Systems* 9.1, pp. 111–121.

- Papamichail, I. et al. (2010). "Heuristic ramp-metering coordination strategy implemented at Monash freeway, Australia". In: *Transportation Research Record: Journal of the Transportation Research Board* 2178, pp. 10–20.
- Payne, H.J. (1971). "Models of freeway traffic and control." In: *Mathematical models of public systems*.
- Pipes, L.A. (1953). "An operational analysis of traffic dynamics". In: *Journal of Applied Physics* 24, pp. 274–281.
- Pisarski, D. and C. Canudas-de Wit (2012). "Analysis and design of equilibrium points for the cell-transmission traffic model". In: *Proceedings of the American Control Conference*, pp. 5763–5768.
- Reuschel, R. (1950). "Fahrzeugbewegungen in der Kolonne bei gleichformig". In: *Z. Osterr. Ing. Arch. Ver.* 95, pp. 52–62.
- Richards, P.I. (1956). "Shock waves on the highway". In: *Operations research* 4.1, pp. 42–51.
- Roncoli, C., M. Papageorgiou, and I. Papamichail (2015a). "An optimisation-oriented first-order multi-lane model for motorway traffic". In: *Proceedings of the 94th Annual Meeting of the Transportation Research Board*. paper no. 15-2905.
- (2015b). "Traffic flow optimisation in presence of vehicle automation and communication systems—part I: a first-order multi-lane model for motorway traffic". In: *Transportation Research Part C: Emerging Technologies* 57, pp. 241–259.
- (2015c). "Traffic flow optimisation in presence of vehicle automation and communication systems—part II: optimal control for multi-lane motorways". In: *Transportation Research Part C: Emerging Technologies* 57, pp. 260–275.
- Seo, T. et al. (2017). "Traffic state estimation on highway: a comprehensive survey". In: *Annual Reviews in Control*.
- Sepulchre, R., M. Jankovic, and P. Kokotovic (1997). *Constructive nonlinear control*. London: Springer.
- Shahid, A. (2016). "Event based reduction of power fluctuation using cyber-physical control-communication network in smart grids". In: *Power Systems Conference (PSC), 2016 Clemson University*, pp. 1–5.
- Shlayan, N. and P. Kachroo (2013). "Feedback ramp metering using Godunov method based hybrid model". In: *Journal of Dynamic Systems, Measurement, and Control* 135.5, pp. 051010–051010.
- Smith, M.J. (1984). "The stability of a dynamic model of traffic assignment— an application of a method of Lyapunov". In: *Transportation Science* 18.3, pp. 245–252.
- Sontag, E.D. (1998). *Mathematical control theory: deterministic finite dimensional systems*. Vol. 6. Springer Science & Business Media.
- Spiliopoulou, A. et al. (2014). "Macroscopic traffic flow model validation at congested freeway off-ramp areas". In: *Transportation Research Part C: Emerging Technologies* 41, pp. 18–29.
- Srivastava, A. and N. Geroliminis (2013). "Empirical observations of capacity drop in freeway merges with ramp control and integration in a first-order model". In: *Transportation Research Part C: Emerging Technologies* 30, pp. 161–177.
- Sun, X. and R. Horowitz (2005). "A localized switching ramp-metering controller with a queue length regulator for congested freeways". In: *Proceedings of the American Control Conference*, pp. 2141–2146.
- (2006). "Set of new traffic-responsive ramp-metering algorithms and microscopic simulation results". In: *Transportation Research Record: Journal of the Transportation Research Board* 1959, pp. 9–18.

- Sun, X., L. Muñoz, and R. Horowitz (2004). "Mixture Kalman filter based highway congestion mode and vehicle density estimator and its application". In: *Proceedings of the American Control Conference*. Vol. 3, pp. 2098–2103.
- Torné, J.M., F. Soriguera, and N. Geroliminis (2014). "Coordinated active traffic management freeway strategies using capacity-lagged cell transmission model". In: *Proceedings of the 93rd Annual Meeting Transportation Research Board*.
- Treiber, M., A. Hennecke, and D. Helbing (2000). "Congested traffic states in empirical observations and microscopic simulations". In: *Physical Review E* 62, pp. 1805–1824.
- Treiber, M., A. Kesting, and D. Helbing (2006). "Understanding widely scattered traffic flows, the capacity drop, and platoons as effects of variance-driven time gaps". In: *Physical Review E* 74.1, p. 016123.
- Treiterer, J. and J. Myers (1974). "The hysteresis phenomenon in traffic flow". In: *Transportation and Traffic Theory* 6, pp. 13–38.
- Tsinias, J. (1989). "Sufficient Lyapunov-like conditions for stabilization". In: *Mathematics of Control, Signals, and Systems (MCSS)* 2, pp. 343–357.
- (2000). "Backstepping design for time-varying nonlinear systems with unknown parameters". In: *Systems and Control Letters* 39, pp. 219–227.
- Van Lint, J., S. Hoogendoorn, and M. Schreuder (2008). "Fastlane: New multiclass first-order traffic flow model". In: *Transportation Research Record: Journal of the Transportation Research Board* 2088, pp. 177–187.
- Vukanovic, D.I.S. and D.I.O. Ernhofer (2006). "Field evaluation of the fuzzy logic based ramp metering algorithm ACCEZZ". In: *IFAC Proceedings Volumes* 39.12, pp. 119–123.
- Wang, Y. and M. Papageorgiou (2006). "Local ramp metering in the case of distant downstream bottlenecks". In: *Proceedings of the IEEE Intelligent Transportation Systems Conference*, pp. 426–431.
- Wang, Y., M. Papageorgiou, and A. Messmer (2006). "RENAISSANCE—A unified macroscopic model-based approach to real-time freeway network traffic surveillance". In: *Transportation Research Part C: Emerging Technologies* 14.3, pp. 190–212.
- Wang, Y. et al. (2010). "Local ramp metering in random-location bottlenecks downstream of metered on-ramp". In: *Transportation Research Record: Journal of the Transportation Research Board* 2178, pp. 90–100.
- Wang, Y. et al. (2014). "Local ramp metering in the presence of a distant downstream bottleneck: theoretical analysis and simulation study". In: *IEEE Transactions on Intelligent Transportation Systems* 15.5, pp. 2024–2039.
- Whitham, G.B. (2011). *Linear and nonlinear waves*. Vol. 42. John Wiley & Sons.
- Xie, L.-L. and L. Guo (1999). "Fundamental limitations of discrete-time adaptive nonlinear control". In: *IEEE Transactions on Automatic Control* 44.9, pp. 1777–1782.
- Yuan, K. et al. (2015). "A hybrid kinematic wave model incorporating capacity drops". In: *Proceedings of the 18th International Conference on Intelligent Transportation Systems*, pp. 471–476.
- Zhang, H., S.G. Ritchie, and W.W. Recker (1996). "Some general results on the optimal ramp control problem". In: *Transportation Research Part C: Emerging Technologies* 4.2, pp. 51–69.
- Zhang, H.M. (1998). "A theory of nonequilibrium traffic flow". In: *Transportation Research Part B: Methodological* 32, pp. 485–498.
- (2001). "New perspectives on continuum traffic flow models". In: *Networks and Spatial Economics* 36, pp. 9–33.
- (2002). "A non-equilibrium traffic model devoid of gas-like behavior". In: *Transportation Research Part B: Methodological* 36, pp. 275–290.

- Zhang, H.M. and W.W. Recker (1999). "On optimal freeway ramp control policies for congested traffic corridors". In: *Transportation Research Part B: Methodological* 33.6, pp. 417–436.
- Zhang, H.M. and S.G. Ritchie (1997). "Freeway ramp metering using artificial neural networks". In: *Transportation Research Part C: Emerging Technologies* 5.5, pp. 273–286.
- Zhang, L. and D. Levinson (2004). "Optimal freeway ramp control without origin–destination information". In: *Transportation Research Part B: Methodological* 38.10, pp. 869–887.
- Zhang, L. and C. Prieur (2017). "Necessary and sufficient conditions on the exponential stability of positive hyperbolic systems". In: *IEEE Transactions on Automatic Control*.
- Zhang, Y., C. Wen, and Y.C. Soh (1999). "Robust adaptive control of uncertain discrete-time systems". In: *Automatica* 35.2, pp. 321–329.
- (2001). "Robust adaptive control of nonlinear discrete-time systems by backstepping without overparameterization". In: *Automatica* 37.4, pp. 551–558.
- Zhao, J. and I. Kanellakopoulos (1997). "Adaptive control of discrete-time strict-feedback nonlinear systems". In: *Proceedings of the American Control Conference*. Vol. 1, pp. 828–832.
- Ziliaskopoulos, A.K. (2000). "A linear programming model for the single destination system optimum dynamic traffic assignment problem". In: *Transportation science* 34.1, pp. 37–49.